DAMAGE IDENTIFICATION IN RAILWAY BRIDGES BASED ON TRAIN INDUCED DYNAMIC RESPONSES

Andreia Gomes Meixedo
2021

A dissertation presented to the Faculty of Engineering of the University of Porto
for the degree of Doctor of Philosophy in Civil Engineering

"Para ser grande, sê inteiro: nada
Teu exagera ou exclui.

Sê todo em cada coisa. Põe quanto és
No mínimo que fazes.

Assim em cada lago a lua toda
Brilha, porque alta vive."

(in "Odes", Ricardo Reis
Heterónimo de Fernando Pessoa)

Aos meus Pais e à minha Irmã

THESIS EXAMINING COMMITTEE

The present thesis has been examined on May 14, 2021, at the Faculty of Engineering of the University of Porto by the following committee:

President:

- Doctor Rui Manuel Carvalho Marques de Faria (by delegation of the Dean of the Faculty of Engineering of the University of Porto), Full Professor of the Civil Engineering Department of the Faculty of Engineering of the University of Porto, Portugal.

Examiners:

- Doctor Raid Karoumi, Full Professor of the Civil Engineering Department of the KTH Royal Institute of Technology, Sweden.

- Doctor Luís Oliveira Santos, Senior Researcher of the Structural Engineering Department of the Laboratório Nacional de Engenharia Civil (LNEC), Portugal.

- Doctor Filipe Manuel Rodrigues Leite Magalhães, Associate Professor of the Civil Engineering Department of the Faculty of Engineering of the University of Porto, Portugal.

- Doctor Alexandre Abrahão Cury, Associate Professor of the Department of Applied and Computational Mechanics of the Federal University of Juiz de Fora, Brazil.

- Doctor Rui Artur Bártolo Calçada, Full Professor of the Civil Engineering Department of the Faculty of Engineering of the University of Porto, Portugal (Supervisor).

GENERAL CONTENTS

ABSTRACT

Bridge maintenance is vital to the safety, integrity and cost-effectiveness of any transportation system, and, therefore, the detection of early structural changes or damage plays a central role in any maintenance programme. Although the condition of the large majority of bridges is assessed through periodical visual inspections, these are expensive, scattered in time and prone to error, which motivated the wide application of Structural Health Monitoring (SHM), especially in large newly built bridges. Hence, the need to define warning strategies and systems to minimize the disruption of the network.

Despite widespread research in this field, up to this date the large majority of applications is either based on static responses or ambient vibration. Measuring static responses to generate health data cannot characterize the dynamic response, which often has its own unique and sensitive correlations to some kinds of damage. On the other hand, ambient vibration analyses are typically based on small-magnitude responses that do not provide local damage-sensitive information or fail to excite nonlinearities where the damage might be more observable. Transient signals generated by traffic have not been used efficiently and robustly for damage identification in railway infrastructures. While such large responses induced by trains might create more damage-sensitive information in the measured response, it also amplifies the effects on those measurements from the environment. The unique combination of moving-loads imposed to these structures during short periods can thus be considered an advantage if appropriate analyses are undertaken.

In this context, this thesis exploits unsupervised data-driven SHM in order to propose a continuous online procedure for damage identification based on train-induced dynamic bridge responses, taking advantage of the large-magnitude loading for enhancing sensitivity to small-scale structural changes. The focus is placed on ensuring robustness and efficiency implementing a hybrid combination of time series analysis methods and multivariate statistical techniques. The novelty lies in the automatic extraction of compact, meaningful information related to the bridge condition under a moving window machine learning methodology that allows real-time damage detection with a negligible number of false positive detections. Furthermore, the unsupervised character of the procedure proposed herein includes the ability of

detecting damage in bridges that already exhibit changed structural conditions, through an original definition of a confidence boundary that can adapt to new changes detected over time and be ready for the detection of additional ones observed in the near future.

The strategy analysis and validation allowed concluding that the ability to identify early damage, imperceptible in the original signals, while avoiding observable changes induced by variations in train speed or temperature, was achieved by carefully defining the modelling and fusion sequence of the information. In fact, the strategy proved to be efficient and robust even when implementing a latent-variable method, which proved effective in removing the operational and environmental effects without the need to measure them.

The effectiveness of the proposed methodology was tested and validated, using a reliable digital twin of the complex bowstring-arch railway bridge over the Sado River tuned with experimental data acquired from a SHM system installed on site. The methodology proved robust to false detections for a comprehensive set of damage scenarios, as well as sensitivity to smaller damage levels (earlier in the structure's life), even when it consists of small stiffness reductions that do not impair structural safety.

Keywords: Railway bridges; Structural Health Monitoring; damage identification; online assessment; unsupervised learning; data-driven approach; traffic induced dynamic responses; time series analysis; multivariate statistical techniques.

RESUMO

A manutenção de pontes é vital para a segurança, integridade estrutural e rentabilidade de qualquer sistema de transportes. Neste sentido, a deteção precoce de alterações estruturais ou danos desempenha um papel central em qualquer programa de manutenção. Embora a grande maioria das pontes seja avaliada através de inspeções visuais periódicas, estas são dispendiosas, espaçadas no tempo e sujeitas a erros, o que tem motivado a ampla aplicação de sistemas de Monitorização da Integridade Estrutural (MIE), especialmente em pontes de grande vão construídas recentemente. Existe, portanto, a necessidade de definir estratégias e sistemas de alerta para minimizar a interrupção deste tipo de infraestruturas de transporte.

Apesar da vasta investigação realizada nesta área, a maioria das metodologias desenvolvidas são baseadas em respostas estáticas ou de vibração ambiental. A medição de respostas estáticas não permite caracterizar a resposta dinâmica da estrutura, que muitas vezes tem correlações únicas e sensíveis a alguns tipos de dano. Por outro lado, análises de vibração ambiental são tipicamente baseadas em respostas de baixa magnitude que não permitem extrair informação relacionada com danos locais, ou, falham a excitar não linearidades onde o dano pode ser mais facilmente observado. Por sua vez, os sinais transientes gerados por tráfego não têm sido utilizados de forma eficiente e robusta para identificação de dano em infraestruturas ferroviárias. Apesar destas respostas de elevada magnitude induzidas pelos comboios poderem gerar informação sensível ao dano, também amplificam os efeitos ambientais nas medições. A combinação única e conhecida a priori das cargas-móveis impostas a este tipo de estrutura durante curtos períodos de tempo pode, portanto, ser considerada uma vantagem se análises adequadas forem implementadas.

A presente dissertação estuda a MIE não supervisionada utilizando uma abordagem direta com base em técnicas de inteligência artificial. O principal objetivo centra-se no desenvolvimento de um procedimento online e contínuo para identificação de danos, tendo por base as respostas dinâmicas da ponte induzidas pela passagem dos comboios. Pretende-se, deste modo, aproveitar o carregamento de elevada magnitude para aumentar a sensibilidade a alterações estruturais. A estratégia aqui proposta foca-se em garantir robustez e eficiência utilizando uma combinação híbrida de métodos de análise de séries temporais e técnicas de

análise estatística multivariada. A inovação deste procedimento está na extração automática de informação relevante acerca da condição estrutural das pontes, através da implementação de uma metodologia de inteligência artificial aplicada em janelas móveis e que permite a deteção de danos em tempo real e com um número residual de falsos alertas. O carácter não supervisionado do procedimento aqui proposto inclui a capacidade de detetar danos em pontes que já apresentem alterações estruturais, através de uma definição inovadora do limite de confiança. Este limite tem a aptidão de se adaptar às alterações estruturais detetadas ao longo do tempo, mantendo-se operacional para a deteção de novos danos que apareçam num futuro próximo.

A análise e validação da metodologia permite concluir que a capacidade de, por um lado, identificar danos precoces impercetíveis nos sinais em bruto, e por outro, suprimir a influência predominante das alterações induzidas pela variação da temperatura ou da velocidade do comboio, é alcançada definindo criteriosamente a sequência de modelação dos dados e fusão da informação. A metodologia mostra-se eficiente e robusta mesmo com métodos de variável latente que garantem a remoção dos efeitos ambientais e operacionais sem ser necessário medi-los.

A eficácia da metodologia proposta foi testada e validada através da criação de uma réplica digital fidedigna da complexa ponte ferroviária sobre o rio Sado, ajustada com recurso a dados experimentais adquiridos por um sistema de monitorização instalado no local. A metodologia provou ser robusta a falsos alertas para um conjunto alargado de cenários de dano, assim como, sensível a danos de pequena escala, mesmo quando estes resultam de reduções de rigidez muito baixas que não colocam em causa a segurança estrutural.

Palavras-chave: Pontes ferroviárias; Monitorização da Integridade Estrutural; identificação de danos; avaliação em tempo real; aprendizagem estatística não supervisionada; respostas dinâmicas de pontes induzidas por comboios; análise de séries temporais; análise estatística multivariada.

LIST OF PUBLICATIONS

The following publications have been derived from the development of the present thesis.

International scientific journals

- <u>Meixedo, A.</u>, Santos, J., Ribeiro, D., Calçada, R., Todd, M. (2021). *Online unsupervised detection of structural changes using train-induced dynamic responses*, Mechanical Systems and Signal Processing, [submitted and revised].

- <u>Meixedo, A.</u>, Santos, J., Ribeiro, D., Calçada, R., Todd, M. (2021). *Damage detection in railway bridges using traffic-induced dynamic responses*, Engineering Structures, 238(112189), DOI: 10.1016/j.engstruct.2021.112189.

- <u>Meixedo, A.</u>, Ribeiro, D., Santos, J., Calçada, R., Todd, M. (2021). *Progressive numerical model validation of a bowstring-arch railway bridge based on a structural health monitoring system,* Journal of Civil Structural Health Monitoring, 11(2): 421–449, DOI: 10.1007/s13349-020-00461-w.

- Ribeiro, D., Leite, J., <u>Meixedo, A.</u>, Pinto, N., Calçada, R., Todd, M. (2021) *Statistical methodologies for removing the operational effects from the dynamic responses of a high-rise telecommunications tower*, Structural Control and Health Monitoring, 28(4):e2700, DOI: 10.1002/stc.2700.

Book Chapters

- <u>Meixedo, A.</u>, Ribeiro, D., Santos, J., Calçada, R., Todd, M. (2021). *Real-time unsupervised detection of early damage in railway bridges using traffic induced responses*, Chapter 8, Structural Health Monitoring Based on Data Science Techniques, Springer (Book chapter in Press).

- <u>Meixedo, A.</u>, Ribeiro, D., Santos, J., Calçada, R., Todd, M. (2021). *Structural health monitoring strategy for novelty detection in railway bridges using traffic induced*

dynamic responses, Best-Practices Handbook on Rail Infrastructure Resilience, Elsevier (submitted).

E-Books

- Cury, A., <u>Meixedo, A.</u>, Ribeiro, D., Branco, L. (2019). *Curso Avançado de Monitorização de estruturas para deteção de danos*, Instituto Superior de Engenharia do Porto, Porto, Portugal, ISBN: 978-989-54236-7-5, 163 pp.

International conference proceedings

- Mosleh, A., <u>Meixedo, A.</u>, Ribeiro, D., Montenegro, P., Calçada, R. (2021). *Feature extraction and normalization for wheel flat detection on railway vehicles*, SHMII10 (online).

- <u>Meixedo, A.</u>, Santos, J., Ribeiro, D., Calçada, R., Todd, M. (2021). *Data-driven approach for detection of structural changes using train-induced dynamic responses*, SHMII10 (online).

- Ribeiro, D., Leite, J., <u>Meixedo, A.</u>, Pinto, N., Calçada, R. (2019). *Metodologia estatística para remoção dos efeitos operacionais das respostas dinâmicas de uma torre de telecomunicações,* CILAMCE 2019, Natal, Brasil.

- <u>Meixedo, A.</u>, Santos, J., Ribeiro, D., Calçada, R. (2019). *Assessment of the dynamic behavior of the railway bridge over the Sado River based on a monitoring system*, Proceedings of the 7th International Conference on Structural Engineering, Mechanics and Computation, Cape Town; South Africa, pp. 1805-1809, ISBN: 978-113838696-9.

- <u>Meixedo, A.</u>, Alves, V., Ribeiro, D., Cury, A., Calçada, R. (2016). *Damage identification of a railway bridge based on genetic algorithms*, Proceedings of the 8th International Conference on Bridge Maintenance, Safety and Management, IABMAS, Foz do Iguaçu, Brazil, pp. 998-1005, ISBN: 978-113802851-7.

- <u>Meixedo, A.</u>, Alves, V., Ribeiro, D., Calçada, R. (2016). *Selection of sensitive features for damage identification in a railway bridge*, Railways 2016 – 3rd International Conference on Railway Technology: Research, Development and Maintenance, Cagliari,

Sardinia, Italy, Civil-Comp Proceedings, J. Pombo (Ed), Civil-Comp Proceedings, vol. 110, ISSN: 17593433.

- Alves, V., <u>Meixedo, A.,</u> Ribeiro, D., Calçada, R., Cury, A. (2015). *Evaluation of the Performance of Different Damage Indicators in Railway Bridges*, 1st International Conference on Structural Integrity, ICSI, Funchal, Madeira, Portugal, Procedia Engineering, vol. 114, pp. 746-753, ISSN: 18777058.

National conference proceedings

- <u>Meixedo, A.,</u> Ribeiro, D., Santos, J., Calçada, R. (2019). *Damage identification based on dynamic indicators of the train-bridge system*, 3rd Doctoral Congress in Engineering - DCE2019, Faculty of Engineering – University of Porto, Porto, pp. 16, ISBN. 978-972-752-218-7.

- <u>Meixedo, A.,</u> Ribeiro, D., Santos, J., Calçada, R. (2019). *Avaliação do comportamento dinâmico da ponte ferroviária sobre o rio Sado*, TEST&E – Monitorizar e Preservar, 2º Congresso de Ensaios e Experimentação em Engenharia Civil, Porto, Portugal.

- <u>Meixedo, A.,</u> Ribeiro, D., Santos, J., Calçada, R. (2017). *Damage identification in railway bridges based on dynamic performance indicators of the train-bridge system.* Symposium on Civil and Environmental Engineering of DCE17, 2nd Doctoral Congress in Engineering, FEUP, Porto, Portugal, 8-9 June 2017.

- <u>Meixedo, A.;</u> Ribeiro, D.; Calçada, R. e Delgado, R. (2015) – *Damage identification in railway bridges based on dynamic performance indicators of the train-bridge system.* Symposium on Civil and Environmental Engineering of DCE15, 1st Doctoral Congress in Engineering, FEUP, Porto, Portugal, 11-12 June 2015.

ACKNOWLEDGMENTS / AGRADECIMENTOS

The development of this dissertation was a challenging journey, longer than expected, filled with both thrilling and difficult moments. However, the accomplishment feeling, the professional and personal knowledge earned, as well as, the new friendships made, end up compensating the drawbacks experienced during the last years. Therefore, I would like to take this opportunity to express my gratitude to everyone who supported me throughout this academic achievement. To all of them I convey my sincere thanks:

- To my supervisor, Prof. Rui Calçada, to whom I am grateful for the unconditional support throughout this research work. His enthusiasm about railways, his huge knowledge about the dynamic behavior of structures, as well as his encouraging words given in the most difficult times were crucial to the success of this dissertation. Hence, I would like to thank him, not only for all the support, scientific knowledge and guidance provided during this journey, but also for the friendship established between us;

- To my co-supervisor, Prof. Diogo Ribeiro, for all the scientific discussions and for the willingness, availability and dedication to help me and teach me, even on weekends, vacations or during my internship in the University of California San Diego. I am aware that his contribution, encouragement, positivism and guidance were undoubtedly essential to accomplish this academic achievement. Our friendship that started almost ten years ago, still during my graduation, will always be kept in the future;

- To my co-supervisor, Dr. João Santos, the one who most promoted my curiosity, knowledge, and expertise about damage identification and structural health monitoring research topics. His contribution for a better understanding of these topics, as well as his completely dedication to help me throughout this journey, were of the utmost importance for the fruitful development of this thesis. I also would like to thank him for promoting my internship in LNEC and for his daily availability during that period. His friendship was the most pleasant surprise that this Ph.D. gave me;

- To Prof. Michael Todd, for granting me the opportunity of doing an internship in the University of California San Diego. I would like to thank him for the warm welcome in his institution and for his unconditional scientific and personal support during my stay in San Diego. I also would like to show my appreciation for the ongoing research collaboration, specifically for the help and support given in the articles submitted to scientific journals;

- To the Portuguese Foundation for Science and Technology (FCT), for the funding of this work through the research grant SFRH/BD/93201/2013;

- To LESE, the Structural and Seismic Engineering Laboratory research group of CONSTRUCT - Institute of R&D in Structures and Construction, for providing me all the equipment and human resources that I needed in the experimental campaigns;

- To LNEC – Laboratório Nacional de Engenharia Civil, in particular to my co-supervisor Dr. João Santos, to Dr. Manuel Pipa and to Dr. Luís Oliveira Santos, for granting me the opportunity of doing an internship in the LNEC installations and for providing me all the equipment and human resources that I needed in the experimental campaigns to the bridge over the Sado River;

- To IP – Infraestruturas de Portugal, for giving me the opportunity and conditions to carry out all the experimental tests;

- To Nuno Pinto for all his knowledge, availability and patience during the development and implementation of the experimental campaigns. His help and dedication will never be forgotten;

- To Carlos Albuquerque, for the availability and knowledge shared regarding the numerical model of the bridge over the Sado River and the numerical analyses implemented during this work.

- To Vinicius Alves, for the availability in sharing with me his knowledge regarding damage identification in the beginning of this dissertation, and for the collaboration in scientific publications.

- To Prof. Alexandre Cury, for providing me raw data regarding a railway bridge in France, which was extremely helpful for the initial tests concerning the development of the methodology.

- To Marta Lima, to whom I am grateful for all the help that she gave me regarding all the bureaucracies that needed to be carried out, since I initiated my research journey.

- To my friends and colleagues Pedro Oliveira and Tiago Coelho from LNEC, for the invaluable help in all experimental campaigns, for all the technical support regarding the acquisition system of the SHM installed in the bridge over the Sado River and, last but not least, for making room for me in their office and being so welcoming during my internship in LNEC.

- To my other friends and colleagues from LNEC, for receiving me warmly and making my internship in LNEC and stay in Lisbon even better: Catarina Oliveira, Cláudia Santos, and Emily Sanches;

- To Andy Chong and his wife Shien Teo, for all the support and friendship demonstrated during my stay in San Diego;

- To my friends and colleagues from the railway research group of FEUP, for their availability to share their knowledge and experience when I needed the most, and for all the wonderful moments spent together: Aires Colaço, Alejandro de Miguel, André Paixão, Araliya Mosleh, Artur Silva, Carolina Magalhães, Cláudio Horas, Cristiana Bonifácio, Cristina Ribeiro, Joana Delgado, João Francisco Rocha, João Rocha, Joel Malveiro, José Neto, Ladislao Melo, Lígia Monteiro, Luís de Matos, Nuno Santos, Pedro Jorge, Pedro Montenegro, Rúben Silva and Sérgio Neves;

- To the other friends and colleagues whom I had the great pleasure to meet and spent time, during the last years in FEUP: António Silva, Aurélio Sine, Inês Sousa, Luís Macedo, Mário Marques, Miriam López, Nuno Pereira and Rui Barros.

- To my closest friends, that have been always by my side giving me encouragement and motivation: Ana Teresa Pereira, Luís Santos, Ricardo Araújo and Rosa Palma Alves;

- À minha família mais chegada, em particular aos meus tios, Armanda, Teresa e José, aos meus primos Liliana e Noé e aos meus afilhados Eva e Gabriel, por todo o apoio dado ao longo desta jornada.

- Aos meus queridos avós, Cândida, Deolinda, Gaspar e José, que, embora já não estejam fisicamente comigo, ao longo da minha vida, sempre me acompanharam com imenso carinho e preocupação e, demonstraram ser os meus maiores fãs.

- Ao Frederico, por se revelar um dos principais pilares da minha vida ao longo destes últimos anos, acompanhando-me nesta jornada de forma dedicada e atenta e, demonstrando o seu amor e carinho diariamente. Quero agradecer ainda a paciência, o alento e a motivação extra que me transmitiu sobretudo nos dias mais frustrantes. O seu apoio incondicional e companheirismo foram fulcrais na realização e finalização desta tese.

- Finalmente, mas de todo menos importante, aos meus pais, Estrela e Gaspar, e à minha irmã, Vera, pelo amor incondicional, pelo apoio incessante e pela dedicação diária. As suas demonstrações contínuas de força, motivação e confiança foram imprescindíveis para levar esta tese a bom porto. São sem dúvida os principais impulsionadores dos meus sonhos e do que já conquistei até hoje, em particular esta dissertação, e por esse motivo lhes dedico este documento.

TABLE OF CONTENTS

Chapter 3 – Structural monitoring system of a bowstring-arch railway bridge

LIST OF SYMBOLS

For clarity purposes, all the abbreviations, notations and symbols presented in this list are defined in the text when first used. Generally, the use of the same symbol for different entities is avoided. However, in situations in which such procedure proved to be inadequate, the risk of misunderstanding is minimized by preventing the simultaneous use of the same symbol for different entities in the same context. The following list is ordered alphabetically.

ABBREVIATIONS

3D	Three-dimensional
AANN	Auto Associative Neural Network
AIC	Akaike Information Criterion
AP	Alfa Pendular
AR	Autoregressive
ARX	Autoregressive with exogenous input
AVT	Ambient Vibration Test
CDF	Cumulative Distribution Function
DI	Damage Index
EFDD	Enhanced Frequency Domain Decomposition
EOV	Environmental and Operational Variation
FA	Factor Analysis
FE	Finite Element
IC	Intercity train
ICDF	Inverse Cumulative Distribution Function
IP	Infraestruturas de Portugal (Portuguese road and railway infrastructures manager)

LNEC	Laboratório Nacional de Engenharia Civil
MAC	Modal Assurance Criterion
MD	Mahalanobis Distance
MLP	Multi-Layer Perceptron
MLR	Multivariate Linear Regression
MSD	Mahalanobis Squared Distance
NLPCA	Nonlinear Principal Component Analysis
NRMSE	Normalized Root Mean Square Error
OMA	Operational Modal Analysis
PAC	Programmable Automate Controller
PCA	Principal Component Analysis
SHM	Structural Health Monitoring
SPT	Standard Penetration Test
SIL	Global silhouette index
SSR	Sum-of-Square Residual errors
SVD	Singular Value Decomposition
VPN	Virtual Private Network

LATIN SYMBOLS

a_i	AR/ARX parameter of the output data
$B(P_k)$	Overall between-cluster distance of partition P_k
B_i	Pile group width
b_k	ARX parameter of the input data
C	Damping matrix
c_1	Mass proportional damping coefficient
c_2	Stiffness proportional damping coefficient

CB	Confidence boundary
D	Pile diameter
d	Distance
DC	Average dissimilarity between clusters
d_{ck}	Dissimilarity between clusters' centroids
E	Modulus of Elasticity
$E_p I_p$	Flexural rigidity of pile foundation
E_s	Soil elasticity modulus
F	Force
f	Frequency
FN	Normal force
F_{PCA}	Prediction of X
FS	Tangential force
G	Shear modulus
g	Acceleration of gravity
γ	Weight/volume
G_0	Small-strain shear modulus
I	Moment of Inertia
K	Stiffness matrix (Chapter 4) Number of clusters (Chapter 5 & 6)
K_s	Coefficient of Subgrade Reaction of the soil
L_i	Pile length
M	Mass matrix
N	Total number of features
n_a	AR/ARX model order of the output data
n_b	ARX model order of the input data
N_p	Number of estimated parameters

N_t	Number of predicted data points
OD	Overall distance of a symbolic data set
p	Number of principal components to discard
P_k	Static load of the axle
R^2	Coefficient of determination
S_0	Dynamic Signature of the train
S_x	Covariance matrix (MD)
t	Time
T	Transformation matrix
V	Vehicle speed
V_s	Shear wave velocity of soil
$\hat{w}$	*(s+1)-by-m* matrix with the estimated coefficients of the MLR model
$W(P_k)$	Overall within-cluster distance of partition P_k
X	*n-by-m* matrix of the dependent/original variables (PCA) *n-by-(s+1)* input matrix of the predictor variables (MLR)
x	Input term of the AR/ARX model
x_k	Distance between axle k and the first axle of the train
y	Output term of the AR/ARX model Measured data (NRMSE)
$\hat{y}$	Simulated data through the ARX model
$\bar{y}$	Mean of the measured dataset
Y	*n-by-m* matrix of the principal component scores (PCA) *n-by-m* output matrix of predicted variables (MLR)

GREEK SYMBOLS

Λ	Singular values of the covariance matrix
α	Level of significance

Δt	Integration time step
ε	Residual error
$\hat{\varepsilon}_{MLR}$	MLR residual error matrix
λ	Wavelength of excitation
μ	Friction coefficient
$\bar{\mu}$	Mean value
ν	Poisson's ratio
ξ	Damping coefficient
σ	Standard deviation
Σ	Covariance matrix
ω	Angular frequency

Chapter 1

INTRODUCTION

1.1 SCOPE

The critical dependency of modern societies upon transport infrastructure such as roadway or railway bridges and tunnels has motivated active research that aims to reduce the costs of inspection and maintenance. A large number of bridges are nearing the end of their original design life, and since these infrastructure cannot be economically replaced, techniques for damage identification are being developed and implemented so that their safe operation may be extended beyond the design basis for service life. Structural health monitoring (SHM) represents a promising strategy in this ongoing challenge of achieving sustainable infrastructural systems since it has the potential to identify structural damage before it becomes critical, enabling early preventive actions to be taken to minimize costs (Farrar & Worden, 2013). The main goal of SHM should not be to replace the traditional inspection techniques, but to complement them with quantitative information. Proactive conservation strategies based on long-term monitoring are increasingly recommended for special structures such as long-span bridges. In fact, disruption or even the collapse of a bridge can lead to important and irreversible negative consequences for society and the economy. In short, SHM offers economical, efficient and intelligent technologies to manage the operation and maintenance of infrastructure, thereby improving safety, increasing longevity and reducing maintenance (Figure 1.1).
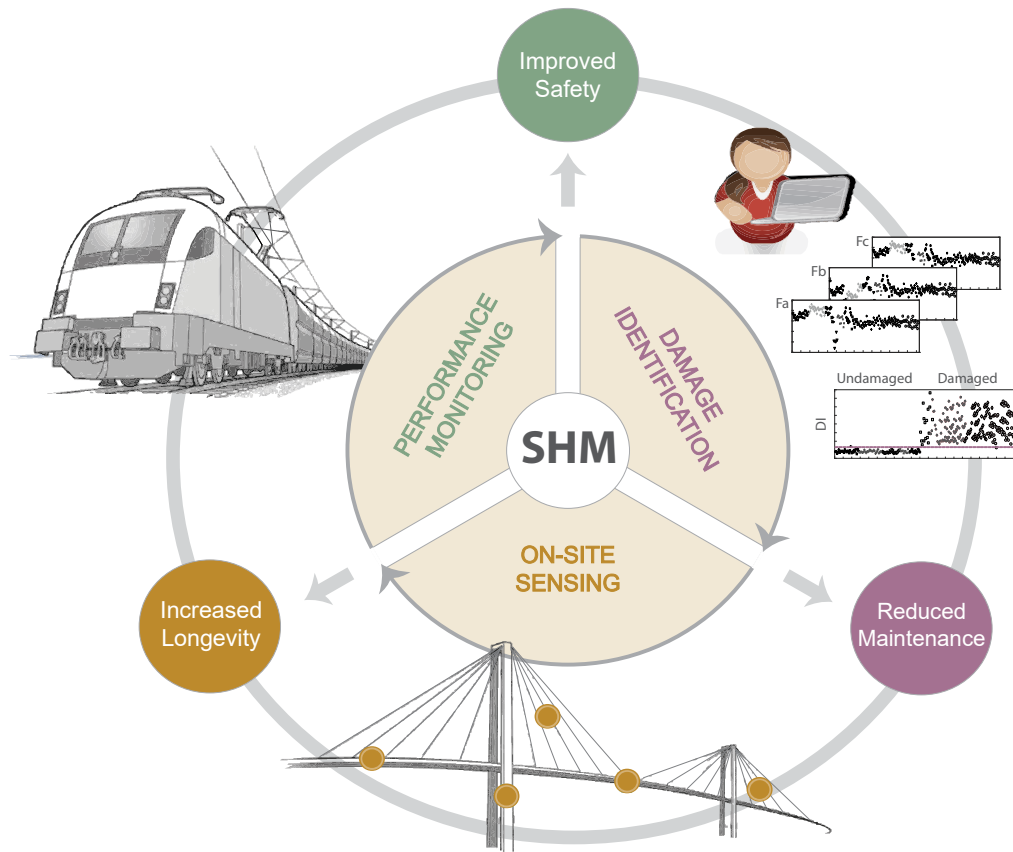
Figure 1.1 – Structural Health Monitoring cycle and its advantages.

The major challenges and limitations related with structural health monitoring techniques for damage identification are mentioned throughout this chapter and identified as important motivations for the present dissertation. Along with these limitations, the last sections of the present chapter point out the main objectives and original contributions, and sets the outline of this thesis.

1.2   MOTIVATION

Bridge maintenance is vital to the structural integrity and cost-effectiveness of any transportation system, and, therefore, the detection of early structural changes or damage plays a central role in any maintenance programme (Carey et al., 2013). With specific regard to railway bridges, the moving loads imposed to these structures, typically for short periods of time, may be undesirable for fatigue or wear life, but can be considered an advantage for observing the full range of structural response behaviour, due to the high amplitude of traffic-induced vibrations. Additionally, although the large majority of bridges are assessed through periodic visual inspections, these are expensive, temporally inconsistent, and prone to human errors in judgment and interpretation, which ultimately led to the increasing development and deployment of

structural health monitoring (SHM) systems, particularly for large newly built bridges (Cantero & González, 2015). Hence, the need to define warning strategies and systems to minimize the disruption of the network (Huang et al., 2012).

In Portugal alone there are approximately 2.200 railway bridges, 700 of them with more than a century. A combination of damage assessment technologies is necessary, and new developments in SHM aim at covering as many structures as possible at a reasonable cost. Although some bridges are already monitored using sophisticated measurement systems employing several sensors, there is a lack of useful and efficient interpretation of the results provided, with frequent difficulty in detecting early damage (Magalhães et al., 2012; Cavadas et al., 2013; Zhang et al., 2017; Neves et al., 2020). Thus, there is a need for data interpretation techniques that provide reliable information to assist engineers in structural management. It is crucial to devise robust online continuous SHM systems that allow structures to be designed and operated safely, without extended downtime periods associated with additional inspection or maintenance. Also, it is important to develop unsupervised data-driven SHM systems that can be used in any geometry and that can identify damage in old structures, which already have a changed structural condition, in order to support the decision making process related to maintenance and conservation strategies.

Many of the existing damage identification and monitoring algorithms have originally been developed in the field of aerospace and mechanical industries. However, these algorithms do not fully address the issues that arise in the monitoring of civil structures such as bridges. The main challenges for the development of a robust damage detection and monitoring system in case of bridges are the following (Sohn & Law, 2000):

- Bridges involve a significant amount of uncertainties caused by environmental effects such as temperature, loading or humidity. Additionally, the uncertainty to estimate the strength and stiffness of structural components is significantly higher than for example that of truss members commonly used for space structures;

- Bridges typically display more complicated and unique geometry; consist of many different materials; and involve more redundancy in the design than space or mechanical structures. These issues make the accurate modelling very difficult even with the possibility of model updating and refinement techniques be employed prior to damage identification;

- ▪ The dimension of the bridges requires the instrumentation of a large number of sensors and actuators, and the excitation of higher modes, which demands a big economical investment. Moreover, the application of forced vibration tests, which are commonly used for system identification, can be difficult for bridges in service because of the economic and social impact caused by service interruption due to road or railway closure. Ambient vibration tests are more suitable since the test can be conducted under normal operation of structures and can be easily repeated to collect additional modal data sets. One difficulty with ambient tests is related with the excitation of higher modes. Therefore, most damage identification for civil structures can suffer from lack of data: only a small number of measurement points and a few fundamental modes would be available.

There is no single solution for the correct monitoring and assessment of bridges because of the variety of structures, materials, loads, and environmental conditions to consider for a particular site. Damage identification techniques in civil engineering structures, including bridges, have consistently focused on monitoring modal-based damage-sensitive features, as these are directly related to intrinsic parameters of the structure such as stiffness, which is expected to change in the presence of damage (Yan et al., 2005; Alvandi & Cremona, 2006; Alves et al., 2015; Meixedo et al., 2016; Neves et al., 2020). In addition, modal quantities also have the advantage of being used for structural design and for assessing the vulnerability of the structures to actions and hazards (Santos et al., 2015). Regardless of these advantages, Operational Modal Analysis (OMA)-based information can also be considered insensitive to early damage due to the need of identifying high order modes shapes, as mentioned before, which is particularly challenging for any real structure's complex loading combinations and environmental variability (Santos et al., 2013).

Recent works have been using the structural responses generated by traffic on bridges to take advantage of the repeatability of these actions, their known behaviour, and their great magnitude (Entezami et al., 2019, Nie et al., 2020). Cavadas et al. (2013), gathered data on the displacement and rotation along a beam frame subjected to an unknown moving load. Principal component and Robust regression analysis were used to reduce dimensionality. Afterwards, data collected during a baseline period were used to characterize the natural variation of the parameters, so that subsequent variation beyond this baseline range could be flagged as damage. The method successfully detected stiffness reductions of 20 % in a beam element 30 cm long. However, only

a single load was considered, as well as a controlled load speed and a quasi-static behaviour, which are seldom the case in real bridges. Gonzalez & Karoumi (2015) proposed a model-free damage detection method that uses deck accelerations and bridge weigh-in-motion data to train a machine learning setup based on ANN and a Gaussian process to classify the data into healthy or damaged. The method was further developed by Neves et al. (2017), however, the limitations found for the proposed strategy were the limited number of damage scenarios and the non-consideration of environmental effects. Nie et al. (2020) proposed a data-driven damage detection method based on fixed moving principal component analysis to examine structural dynamic responses and monitor the damage occurrence. A beam bridge model subjected to stochastic loads was used in numerical simulation and experimental tests. The authors mentioned that further studies were necessary to determine the optimal number of sensors required for a reliable structural condition detection with respect to the sensor locations, structural types, size of structures, and quality of recorded data. Azim & Gül (2019) presented a sensor-clustering-based time-series analysis method for continuous global monitoring of girder-type railway bridges using operational data. The main limitations pointed out by the authors were the linear nature of the methods used and the influence of environmental condition changes, which was not considered in their study. Moreover, the validation of the methodology was carried out with a numerical model that was not experimentally validated.

Despite the research made in this field, effective implementations of SHM in bridges based on traffic-induced dynamic responses that allow for an online and continuous damage identification are still scarce. In the majority of these methodologies, their validation is performed using numerical simulations on simple structural elements, the type of damage studied is limited, the loading scenarios are very specific, the influence of environmental and operational variations (EOVs) on the structural response is often underestimated, and/or the online and unsupervised character is not fully addressed. All these constraints limit the usefulness of SHM for real complex bridges, especially in those where it is expected to be most useful, such as older and underperforming structures.

1.3   OBJECTIVES AND MAIN CONTRIBUTIONS

In line with the motivation described in the previous section, the major goal of this dissertation is to develop a reliable and robust, fully autonomous and online, unsupervised data-driven methodology for early damage identification based on train-induced dynamic

responses and supported by machine learning. The idea is to take advantage of the fact that identical known vehicles cross the bridge regularly, that normally only one train is on the bridge at a time and that the positioning of the loads does not change.

The global objective is achieved through a set of intermediate goals:

- Test and implement a hybrid combination of advanced techniques found in literature to develop a novelty approach for damage identification in railway bridges using traffic induced dynamic responses;

- Design and implement an online monitoring system in a real complex bridge;

- Develop and experimentally validate a numerical model of the bridge;

- Apply and validate the methodology in order to detect a comprehensive set of damage scenarios in the case study bridge;

- Test the robustness and efficiency of the methodology;

- Propose a generic continuous SHM methodology of the railway bridges condition.

The signals resulting from train crossings correspond to a large mass traveling at significant speeds, thus generating features that can obscure information associated with damage. The set of techniques studied herein will allow removing all the train-related features in order to expose, with high sensitivity, those generated by damage. This approach takes advantage of the signals' large amplitudes and the small influence of temperature and other time dependent structural effects. These effects generally produce bias and reduce the sensitivity of the majority of the damage identification techniques that rely on long-term trends.

The following milestones are to be achieved with this research work:

- the development and implementation of an original online unsupervised data-driven damage identification methodology for bridges, based on dynamic responses induced by trains;

- the reduction of the influence of slow environmental actions, such as temperature and humidity, as well as material properties, such as shrinkage, creep and relaxation, by acquiring signal in short periods of time, as opposed to continuous monitoring;

- the development of a methodology capable of detecting damage based on responses that can be measured without interfering with the normal service condition of the structure;

- the improvement of the sensitivity of the damage-sensitive features by using larger magnitude signals resulting from the passage of trains during short periods of time, when compared to ambient vibration or static loads;

- to prove the importance of feature modelling by showing the supremacy of the environmental and operational effects when compared to damage;

- to show the importance of multi-sensor data fusion to enhance the detection of early-damages;

- the development of a novel approach to define an adaptive confidence boundary that successfully detects new damage in bridges already showing structural changes;

- the validation of the methodology using a reliable digital twin of a complex railway bridge.

In short, the focus is placed on ensuring robustness and efficiency using a hybrid combination of time-series models and multivariate statistical techniques. The novelty lies in automatically extracting compact, meaningful information sets related to the bridge condition with a moving window data-driven methodology that allows an online and real-time damage detection with a negligible number of false detections. Furthermore, the unsupervised character of the procedure proposed herein includes the ability to detect damage in bridges that already exhibit changed structural conditions. This is achieved through an original definition of a confidence boundary that can adapt to new changes detected over time, and be ready for the detection of additional ones observed in the near future.

1.4 OUTLINE

The objectives described in the previous section conducted to an outline of the present dissertation divided in seven chapters, being this first one devoted to present the scope, motivation and major goals of the thesis. This chapter also aims at giving an overview of the limitations of SHM, which are then used to set the original milestones to be reached in the present dissertation.

During Chapter 2, the reader is introduced to the key concepts, definitions and steps to address SHM techniques and to follow this dissertation. An historical overview is conducted, as well as a literature review on damage identification. The strategy implemented and followed in this thesis for structural health monitoring and to develop a damage identification methodology is also presented.

This dissertation intends to implement an entire SHM process, from the identification of the structural vulnerabilities and SHM constraints to the detection, modelling and classification of structural changes. In this context, Chapter 3 introduces the case study that will be used throughout this work, which consists of the long-span bowstring-arch railway bridge over the Sado River. A progressively phased monitoring system, which provided a diverse set of data streams ranging from static and dynamic responses to the measurement of environmental and operational traffic loads, is described in detail. A data analysis of the measurements obtained during different phases of the monitoring system is also presented during this chapter.

In line with the previous, Chapter 4 addresses a progressive numerical model validation of the case study based on the analysis of experimental data from different structural response measurements, namely, static deformations under environmental actions, modal vibrations, and transient dynamic responses under traffic loads. This chapter also exploits an integrated approach that uses structural monitoring measurements in combination with FE modelling to understand the structural behaviour of a long-span complex bridge. This progressive validation increases the reliability of the numerical model, envisaging further uses such as condition assessment or evaluation of safety, capabilities that ultimately begin to realize the concept of a digital twin for the structure.

Chapter 5 is divided according to four main tasks: i) feature extraction, focusing on the extraction of damage-sensitive feature from the dynamic responses measured by the monitoring system using time-series models, ii) feature modelling, addressing regression-based and latent variable-based algorithms capable of distinguishing between the effects provided by "regular" actions and novel behaviour, iii) data fusion, for compacting information and enhancing the features sensitivity, and iv) feature discrimination, proposing a set of strategies, comprising statistical learning, to allow identifying structural changes in real-time and without requiring previous knowledge of the structural condition. Different techniques are tested within each task in order to select the most promising and best performing combination. To implement the

previous mentioned tasks, a comprehensive set of realistic scenarios, healthy and damaged, were simulated in different locations along the bridge and with increasing severities.

Chapter 6, entitled after the ultimate goal of the present dissertation - "Online unsupervised procedure for early damage identification based on train induced dynamic responses", proposes and validates a continuous procedure combining time-series techniques and machine learning algorithms sequentially applied to the monitoring data, in a moving window process. To assess whether the online procedure was reliable for different damage scenarios, a sensitivity analysis to damages in different locations and with increasing severities is performed. To study the trade-off between robustness and detection swiftness, a parametric analysis is conducted on the window lengths and on the number of sensors used by the SHM system. Using several train-induced responses from the bridge comprising different types of damage simulated with progressively increasing magnitudes, an original adaptive confidence boundary for detecting new structural changes is implemented, tested and validated.

Finally, in Chapter 7, overall conclusions are drawn and the perspectives for future research in the field of SHM and damage identification as a consequence of this work are suggested.

Chapter 2

STRUCTURAL HEALTH MONITORING FOR DAMAGE IDENTIFICATION

2.1 SCOPE

The present chapter starts by describing the main background, motivations and approaches to Structural Health Monitoring for civil structures. The review is not intended to be exhaustive; instead, it is focused in framing the main topics comprising the broad subject of SHM, and in providing an overview of the most important trends and innovations. Hereafter, focus is made on SHM techniques developed and applied for the purpose of identifying damage in bridges. The major challenges and limitations related with these techniques are mentioned throughout this chapter. It also aims at reviewing the most important steps for implementing a damage identification strategy, which is usually carried out in the context of SHM. In the last section, the SHM procedure developed and implemented during this thesis is presented.

2.2 SHM BACKGROUND

The SHM emerges as the process of implementing a damage identification strategy for aerospace, civil and mechanical engineering infrastructure (Farrar & Worden, 2007). The basic idea of SHM is to build up a system similar to the human nervous system, where the brain (computer) processes the information and determines actions (maintenance activities), and the

nerves (sensors) feel the pain (damage), as shown in Figure 2.1 (Figueiredo et al., 2013). Thus, the goal of SHM is to improve the observation of a structural or mechanical system over time using periodically spaced measurements to determine the current state of the system health.
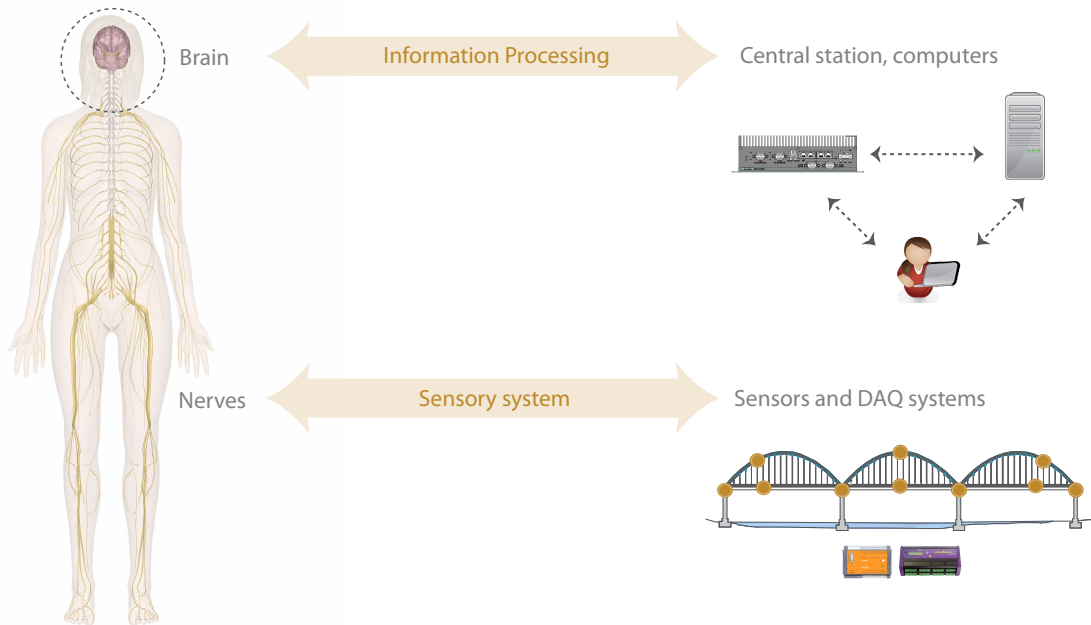

Figure 2.1 - SHM analogy with the human nervous system.

For long-term SHM, the output of this process is periodically updated, providing information regarding the ability of the structure to perform its intended function in light of the inevitable aging and degradation resulting from operational environments. After extreme events, such as earthquakes, vehicle collisions or unanticipated blast loadings, SHM is used for rapid condition screening and aims to provide, in nearly real time, reliable information regarding the integrity of the structure (Farrar et al., 2001).

SHM can be divided into two main typologies: static and vibration-based (Posenato et al., 2010). A review of the historical evolution using vibration-based SHM is presented in the following section.

2.2.1 Historical overview

The basic premise of vibration-based damage detection is that the damage will alter the stiffness, mass or energy dissipation properties of a system, which, in turn, will alter the measured dynamic response of the system. Although the basis for vibration-based damage detection appears intuitive, its actual application poses many significant technical challenges. The most fundamental challenge is the fact that damage is typically a local phenomenon and

may not significantly influence the lower-frequency global response of a structure that is typically measured during vibration tests. This challenge is supplemented by many practical issues associated with making accurate and repeatable vibration measurements at a limited number of locations on structures, often operating in adverse environments (Farrar et al., 2001; Kong et al., 2015).

The civil engineering community has studied vibration-based damage detection methods for bridges since the early 1980s. Initial studies examined changes in conventional modal properties such as frequencies and mode shapes, but the lower frequency global modes of the structure, which are the ones that tend to be identified in ambient vibration tests, were found to be insensitive to local damage (Farrar & Worden, 2013). In addition, these low-frequency global modal properties have been shown to be sensitive to changing operational and environmental conditions, which further confound their use as damage indicators (Farrar & James, 1997).

During the last 20 years, more sophisticated methods of damage identification that extract features from the modal parameters such as modal strain energy, uniform load flexibility shapes, and finite element model updating similar to that developed for aerospace applications have been implemented to bridges with success but also with limitations and challenges yet to be tackled.

With the objective of reducing errors in the modal extraction, researchers have studied damage identification methods using the frequency response functions (FRFs). The FRF-based method is very promising because FRF data can be directly obtained without any further data extraction and processing (Kong et al., 2015). However, the estimation of mode shapes and FRFs require either a single excitation point with many sensors or a roving exciter with one or more fixed sensors. In this sense, researchers have started to consider the vehicle response very useful in system identification and damage detection. The fact is that in a vehicle-bridge-coupled system with time-variant features, the vehicle can serve as both a force transducer and a mobile sensor of the system (Kong et al., 2015). Moreover, vehicle dynamic responses such as accelerations have similar features as modal shapes but are easy to measure.

Researchers have also started to develop local active inspection techniques based on pattern recognition that monitor very specific portions of the bridge structure such as loss of preload in a bolted connection (Park et al., 2008). To account for variability in ambient loading conditions and environmental variability, it is imperative that the statistical pattern classifiers and associated data modelling procedures be adapted for these SHM applications. Without this

technology, it will be difficult to determine if changes in the identified features are caused by damage or by varying operational and environmental conditions.

Unfortunately, bridge design modifications and inspection programme changes are often made only in response to catastrophic failures. The collapses of certain bridges around the world have pressured authorities to develop solutions to periodically inspect their bridges and to support maintenance activities. A very recent example is the collapse of a 200-metre section of the Morandi bridge in Italy in 2018, including one of its three supporting towers (Figure 2.2). The tragedy killed 43 people and left 600 homeless. In Portugal, on 4 March of 2001, the Entre-os-Rios tragedy showed the deficiencies of the bridge management and marked the shift to a new era in this field. The disaster occurred after many days of intense rain and consequent increase of the river stream, when one of the piers of the Hintze Ribeiro Bridge, over the Douro River, collapsed resulting in the partial fall of the deck (Figure 2.3). The collapse dragged together a bus and three cars, killing 59 people.

Figure 2.2 - Morandi bridge collapse, Italy, in 2018 (Zennaro, 2019).

Figure 2.3 - Hintze Ribeiro bridge collapse, Portugal, in 2001 (Silva, 2016).

At present, bridges in Portugal are generally monitored through annual routine inspections, as well through principal inspection carried out at each two to six year periods, largely based on visual inspection techniques. This procedure is slow, systematic but not based on quantitative

measurements and prone to leave portions of the bridge uninspected due to its inaccessibility. There is the possibility that damage can go undetected at inspection or that cracks in load-carrying members can grow to critical levels between inspection intervals, as happened with the I-35 Bridge that collapsed in Minneapolis during the summer of 2007 (National Transportation Safety Board, 2008); see Figure 2.4. In addition to these more gradual damage accumulation mechanisms, sudden damage leading to bridge collapse also occurs as a result of extraordinary events such as collisions.

Figure 2.4 - Collapsed north section of the Minneapolis I-35W Bridge, USA, in 2007 (WordPress, 2016).

Even though there is still a long way to go for a successful real-world SHM application in civil engineering structures, regulatory requirements are driving current research and development of vibration-based bridge monitoring systems. In the USA, the long-term bridge performance program was included in the highway legislation. This program attempts to provide quantitative data for network and bridge level management and, ultimately, to improve the safety assessment of the nation's bridges (Figueiredo et al., 2010). In Asian countries, regulatory requirements, which mandate the companies that construct the bridges to certify their structural health periodically, are driving current research and commercial development of vibration-based bridge monitoring systems. In Portugal, there are already several bridges with long-term monitoring systems. Some examples of bridges incorporated with those systems are: the 25 de Abril Bridge in Lisbon (Figure 2.5a), the Lezíria Bridge in Carregado (Figure 2.5b) and the São João Bridge in Porto (Figure 2.5c). However, the demand of new processing strategies to efficiently extract useful information from data collected by dynamic monitoring systems is evidenced by the lack of clear and useful interpretation of the results provided by the monitoring systems installed in these bridges (Magalhães et al., 2011). Experience gained by analysing data from in situ structures will be crucial in developing new damage-sensitive features as well as defining new and improved hardware for the vibration measurements and robust approaches to data modelling and classification (Farrar & Worden, 2013).

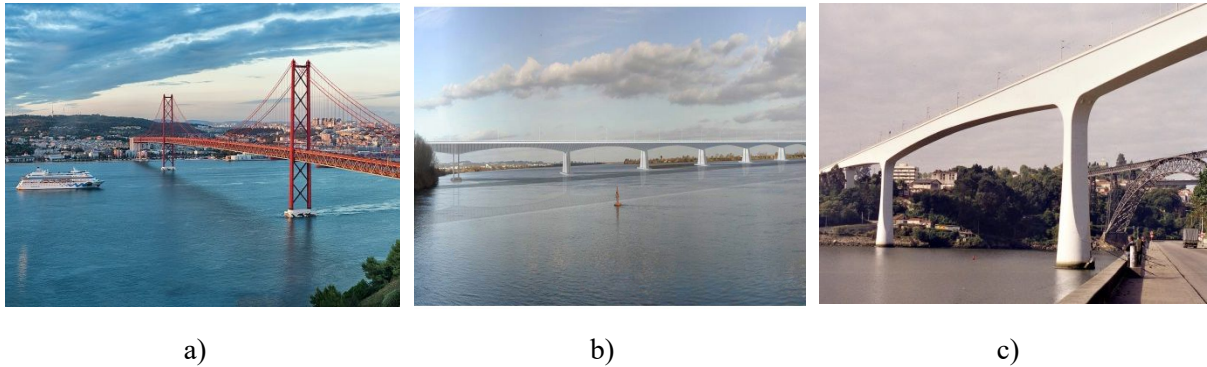<div align="center">a)   b)   c)</div>

Figure 2.5 - Portuguese bridges with long-term monitoring systems: a) 25 de Abril Bridge in Lisbon, b) Lezíria Bridge in Carregado and c) São João Bridge in Porto.

2.2.2   Most common damage scenarios

In devising an intelligent fault detection system, the primary consideration is an unambiguous definition of damage as a prerequisite to providing a unified approach to damage evaluation across all the engineering disciplines (Worden & Dulieu-Barton, 2004).

It is important to distinguish between two different concepts: failure and damage. Failure occurs when the structure can no longer operate satisfactorily, while damage can be defined as a change in a structural system which affects its present or future performance concerning both structural safety and serviceability (Worden & Dulieu-Barton, 2004). Such changes can be generated by variations in the material or geometric properties of structural systems, including boundary conditions. Implicit in this definition is the concept that damage is not meaningful without a comparison between two different states of the system, one of which is assumed to represent the initial and often undamaged state. In this sense, failure can be seen as a direct consequence of damage occurrence (Farrar et al., 2001).

On the other hand, a damage occurrence can be classified according to two distinct factors: its location and its duration (Cury & Cremona, 2010; Santos, 2014). Regarding its location, damage usually starts at a single element, and, considering different scenarios and loads, can spread up to partial or entire collapse of a structural system. Concerning its duration, damage can be classified as progressive, such as fatigue, corrosion or deformation; or sudden, in case of those generated by earthquakes, storms, vehicle collisions or construction accidents.

Unfortunately, a great number of bridges continues to fail nowadays due to: i) floods (through scour effect), ii) train and vehicle collisions, iii) overload, iv) deficiencies in design and detail, v) earthquake, vi) exceptional wind, vii) fire occurrences, viii) fatigue, cracking and corrosion

of steel elements, ix) insufficient resistance or stiffness, mainly in steel elements or steel reinforcement, x) corrosion of pins, hangers, reinforcement and prestress tendons, xi) design deficiency of structural bearings under the actions of creep, shrinkage and temperature, xii) fire, and xiii) lack of maintenance (Santos, 2014).

Considering specifically the cases of Portuguese bridges, the most common damage scenarios observed are: i) corrosion in metallic components, ii) generalized concrete degradation (cracking, delamination, and corrosion of the reinforcement bars), iii) degradation of corrugated metal culverts, iv) degradation of the expansion joints, v) degradation of the bearing devices and vi) construction defects. The corrosion in metal elements is normally observed in beams, bearings, and railings, derived from defects of painting or protective coating. The concrete deterioration is mainly caused by debris (traps moisture), deficient drainage or leakage (Figueiredo et al., 2013). The degradation of the bearing devices may result in the full restraint of its movements or even in the loss of a bearing. Figure 2.6 to Figure 2.9 illustrate some damages scenarios commonly observed in Portuguese bridges.
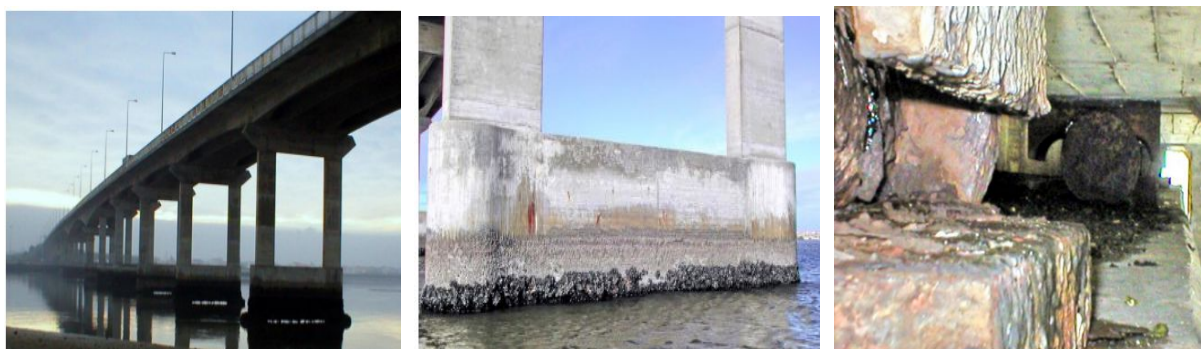

Figure 2.6 - Cracks and corrosion observed at the foundation and in the simple supported beam bearings of Barra bridge (Armando Rito Engenharia, 2016).

Figure 2.7 - Corrosion of the reinforcement bars in Edgar Cardoso bridge (Armando Rito Engenharia, 2016).

Figure 2.8 - Observed corrosion on the top flange of Eiffel bridge, Viana do Castelo (Cavadas, 2008).

Figure 2.9 - Deterioration of the connections and corrosion of the metal elements in Soure bridge (Appleton, 2005).

2.2.3   Hierarchical structure of damage identification

Damage identification strategies have been widely classified according to Rytter's four-level hierarchy (Rytter, 1993) based on the amount of damage related knowledge that can be extracted. More recently (Worden & Dulieu-Barton, 2004) proposed an additional level which sets up the hierarchical classification into five. SHM techniques can thus be classified into one of the following levels, according to their ability to answer the following questions:

- Level 1: Is the damage present in the structural system (detection)?

- Level 2: Where is the damage located (localization)?

- Level 3: What kind of damage is present (type)?

- Level 4: What is the extent of damage (severity)?

- Level 5: What is the residual lifetime (prediction)?

The answers to the questions above can be made only in a sequential way, e.g., the answer to the severity of damage can only be made with a priori knowledge of the type of damage. Level 1 is distinguished in the sense that can be accomplished with no prior knowledge of how the

system will behave when damaged (Worden & Dulieu-Barton, 2004). While the answers to the questions about localization, type and severity of the damage can be regarded as diagnosis, the fifth question can be seen as prognosis and its fulfilment typically requires addressing topics adjacent to SHM such as fatigue and fracture analysis (Doebling et al., 1996, Farrar et al., 2001, Cury & Cremona, 2010, Santos et al., 2013); see Figure 2.10. Identifying the level of damage is a key decision to be made when seeking to apply SHM methods and will have a major bearing on the approach adopted (Barthorpe, 2011).
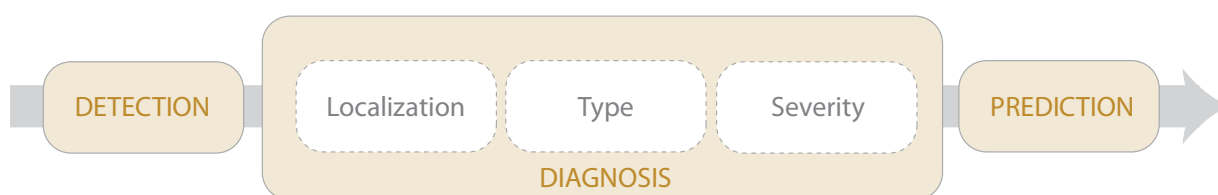

Figure 2.10 - Hierarchical structure of damage identification.

2.3 LITERATURE REVIEW ON DAMAGE IDENTIFICATION

2.3.1 Overview

The process of implementing a damage identification strategy involves the observation of a structure over a period of time using periodically spaced measurements, the extraction of features from these measurements, and the analysis of these features to determine the current state of health of the system (Farrar et al., 2001).

Figure 2.11 shows a flowchart summarizing the main four steps to implement a SHM solution. Each of these steps is detailed during the present chapter. Inherent in the data acquisition, feature extraction, and feature discrimination for damage identification portions of the SHM procedure are data modelling, cleansing, fusion, and compression. These four processes are described throughout sections 2.3.6 and 2.3.7.
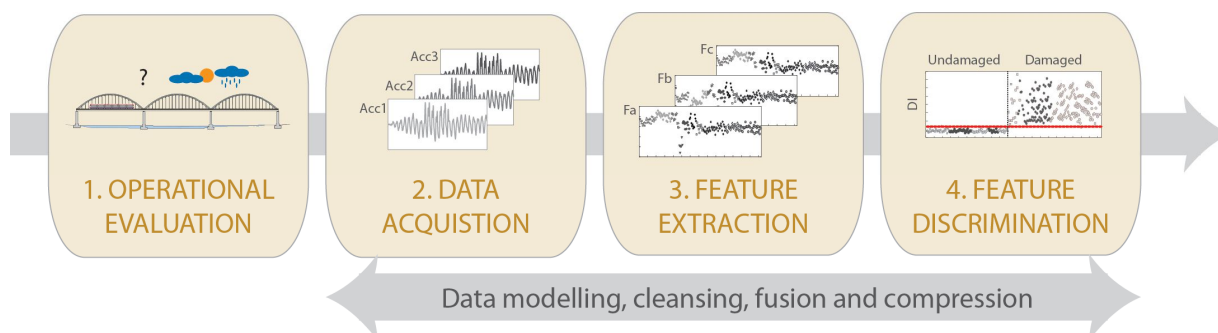

Figure 2.11 - Flowchart for implementing a SHM strategy.

2.3.2   Operational Evaluation

The first step to developing a SHM strategy is to perform an operational evaluation. This phase attempts to provide answers to four questions, which are mentioned in Figure 2.12, regarding the implementation of a damage identification investigation (Farrar & Worden, 2007; Sohn et al., 2004).
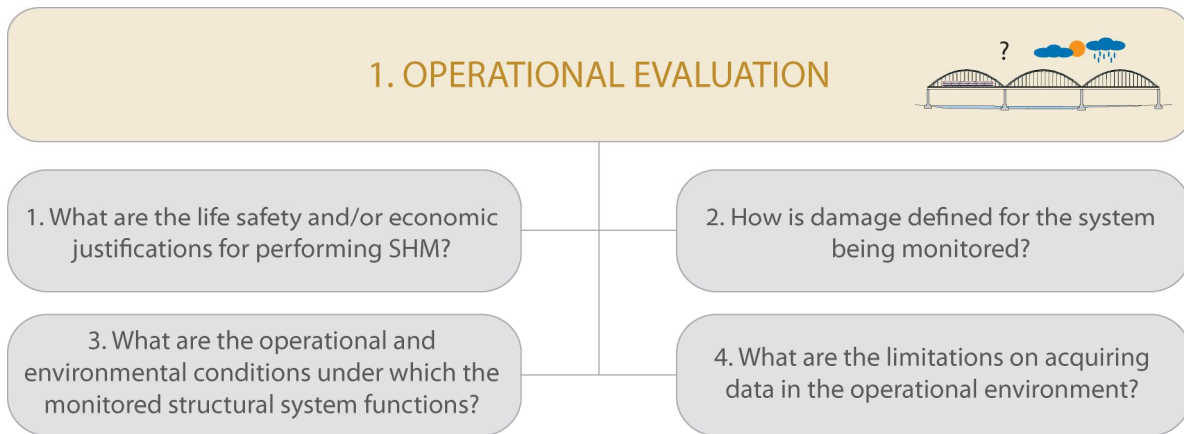

Figure 2.12 - Flowchart with the four main questions to be answered during operational evaluation.

By providing answers to the above questions, the operational evaluation process begins to set limitations on what will be monitored and how the monitoring will be accomplished.

Safety, economic, operational and social constraints, which must be defined in conjunction with designers, owners and authorities, play an important role in operational evaluation, and their definition allows answering the first of the four questions (Santos et al., 2013).

On the other hand, the success of any damage identification technique is directly related to the ability to define that damage that has to be detected in as much detail as possible and in as quantifiable terms as possible. Here the definition of damage can include issues such as i) the type of damage to be detected, ii) the threshold level of damage that must be detected, iii) the critical level of damage that produces failure or that will no longer allow for a planned safe shut down of the system, iv) locations where the particular type of damage accumulates in the structure and v) the tolerable or anticipated rate of damage growth. By taking advantage of each structural systems' unique features, the most convenient sensorial solution can be defined and the damage identification process can be tailored in a more efficient way (Farrar et al., 2001; Figueiredo et al., 2010; Santos, 2014).

Additionally, the damage identification process will have to deal with structures that experience changing operational and environmental conditions, which will alter the measured

system response. It is imperative that these changes are not interpreted as indications of damage. Varying temperature is one common environmental condition that must be accounted for during the damage identification process. Running equipment or vehicles at varying speeds are other operational parameters that can significantly influence dynamic quantities that are being measured as part of the damage identification process. Defining and quantifying the operational and environmental conditions acting on the structure will help to define the required data acquisition system capabilities better, and will also impact other portions of SHM process including the data modelling procedures, feature selection and feature discrimination (Farrar & Worden, 2013).

2.3.3 Data Acquisition

Obtaining accurate measurements of a system's dynamic response is essential to SHM. There are many different sensors and data acquisition systems that can be applied to SHM problem and the one employed will be application specific. In this sense, Figure 2.13 details the several considerations that one should make during this step.

2. DATA ACQUISITION
a. Define data to be acquired.
b. Define data to be used (or not) in the feature extraction process.

Acc3
Acc2
Acc1
t
t
t

Types and amount of data to be collected
a. Sensors placement,
b. Data acquisition, storage and transmittal system.

Periodicity in data acquisition
a. Only after extreme events,
b. Periodic intervals,
c. Continuous.

Monitoring typologies
a. Static-based,
b. Vibration-based,
c. Both.

Sources of variability
Changing environmental/testing/data reduction conditions.

Data modelling procedures

Data cleansing procedures

Feedback from feature extraction

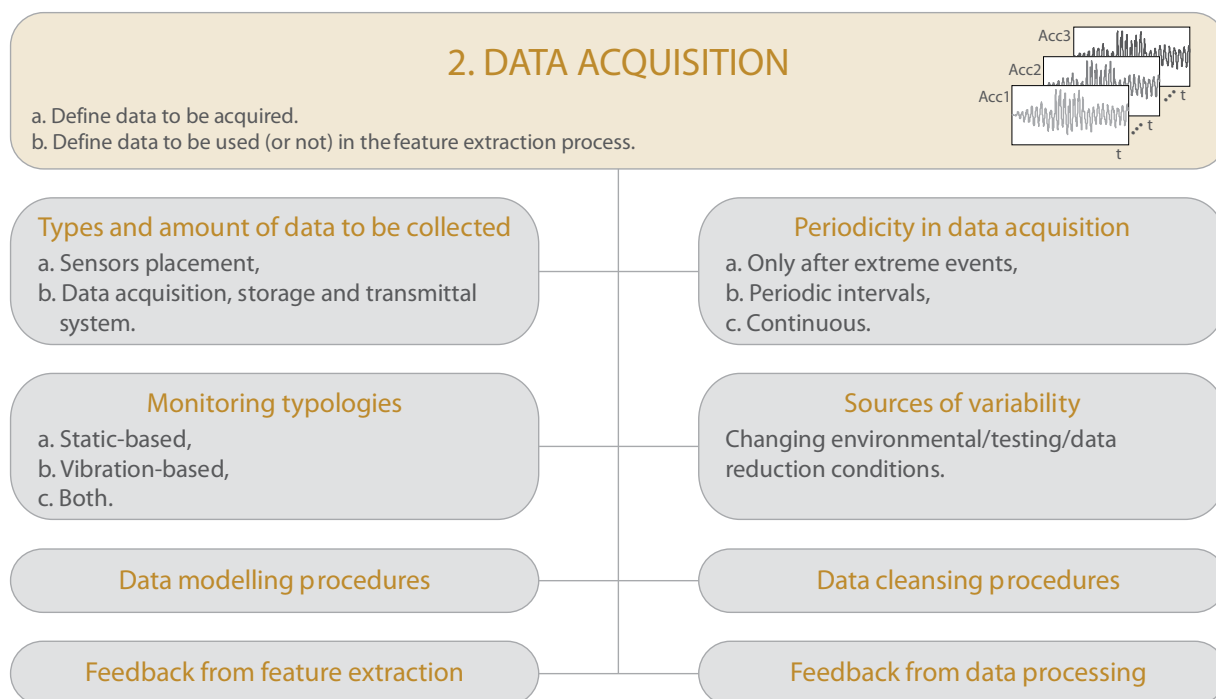**Feedback from data processing**

Figure 2.13 - Flowchart detailing the step two of SHM strategy.

The data acquisition portion of the SHM strategy requires selecting the excitation methods; the sensor types, numbers, and locations; and the data acquisition/storage/processing/transmittal hardware. Economic considerations play a major role in making these decisions.

Another consideration regarding data acquisition is how often the data should be collected. In some cases, it may be adequate to collect data immediately before and at periodic intervals after a severe event. However, in another cases, it may be necessary to collect data almost continuously at relatively short time intervals.

The greatest constraint for the implementation of the data acquisition process is, perhaps, the SHM typology. Depending on the outcome of the operational evaluation, SHM can be divided into three main typologies: static, vibration-based or both (Posenato et al., 2008; Santos, 2014).

A fundamental premise regarding data acquisition and sensing is that these systems do not measure damage. Rather, they measure the response of a system to its operational and environmental loading or the response to inputs from actuators embedded with the sensing system. Depending on the sensing technology deployed and the type of damage to be identified, the sensor readings may be more or less directly correlated to the presence and location of damage. In fact, feature extraction and feature discrimination for damage identification procedures are the necessary components of a SHM system that convert the sensor data into information related to the structural condition (Farrar & Worden, 2013).

Because data can be measured under varying conditions, the ability to model the data becomes very important to the damage-detection process. Additionally, data cleansing is applied by selectively choosing data to accept for, or reject from, the feature selection process (Farrar et al., 2001). These two procedures, data modelling and data cleansing, are explain in detail in sections 2.3.6 and 2.3.7.

Finally, it should be noted that the data acquisition portion of a SHM process should not be static. Insight gained from the feature extraction process and the damage discrimination process will provide information regarding changes that can improve the data acquisition process.

2.3.4   Feature Extraction

Identifying features that can accurately distinguish a damaged structure from an undamaged one is the focus of most SHM technical literature. Figure 2.14 summarizes the main ideas that support the feature extraction (and selection) process.
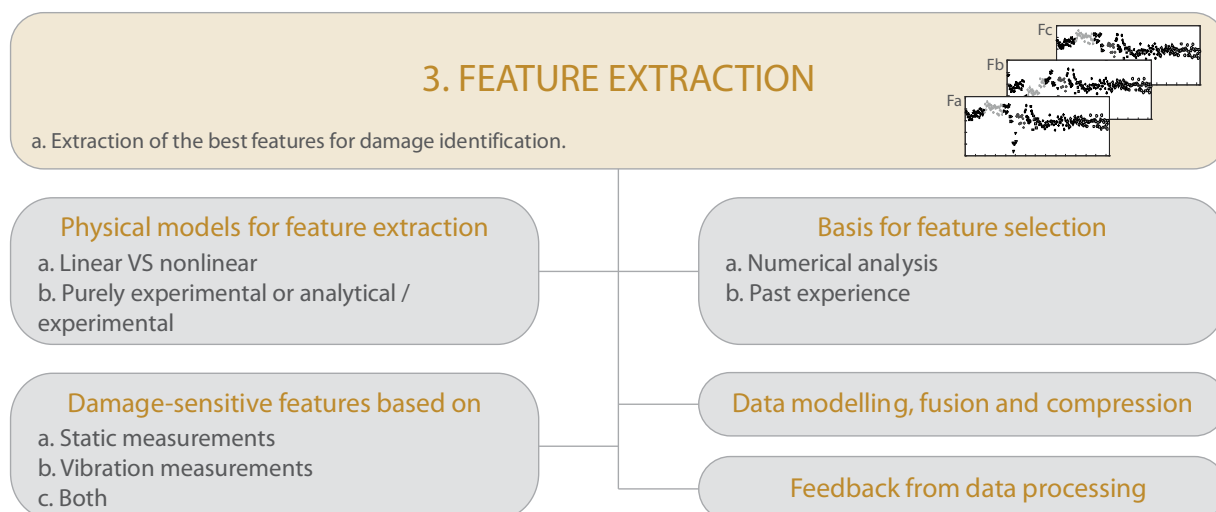
Figure 2.14 - Flowchart detailing the step three of SHM strategy.

Fundamentally, feature extraction refers to the process of transforming the measured data into some alternative form where the correlation with the damage is more readily observed (Worden & Dulieu-Barton, 2004). Often in SHM, the feature extraction process is based on fitting some model, either physics-based or data-based, to the measured response data. The parameters of these models, quantities derived from the parameters or the predictive errors associated with these models, become then the damage-sensitive features (Farrar et al., 2001). These processes usually output multivariate data sets, generally named as feature vectors, whose length and dimensionality must be as low as possible. In an effort to obtain a low-dimensional feature vector, procedures are developed to fuse and compress data from multiple sensors. A common example of data fusion is the extraction of mode shapes from the relative amplitude and phase information contained in data from a sensor array. Similarly, the extraction of frequencies from measured acceleration time histories can be thought of as a data compression process (Santos, 2014; Meixedo et al., 2016).

One of the tasks of feature extraction is to eliminate as far as possible, fluctuations on the normal condition data. In this sense, various forms of data modelling are employed during the feature extraction process in an effort to separate changes in the measured response caused by varying operational and environmental conditions from changes caused by damage.

After the feature extraction comes the feature selection, the process of determining which feature to use in the damage detection process (Farrar & Worden, 2013). Ideally, one should select a feature that is sensitive to the presence of the damage in the structure and insensitive to all forms of operational and environmental variability, which in most real-world applications is very difficult to achieve. Past experience with measured data from a system, particularly if

damaging events have been previously observed for that system, is often the basis for feature selection. Numerical simulation of the damaged system's response to simulated inputs is another mean of identifying features for damage identification (Worden & Dulieu-Barton, 2004).

It is important to distinguish the concept of feature extraction from feature selection, because while the former is almost always done through some mathematically rigorous process, the latter can be done by a wide range of techniques ranging from equally mathematically rigorous processes to very heuristic or intuitive selection processes.

Modal or modal-based features are the most common in the literature (Yan et al., 2005a; Alvandi & Cremona, 2006; Alves et al., 2015; Meixedo et al., 2016) due to the advantage of being directly associated with the mass and, more importantly, with structural stiffness, which is expected to change in the presence of damage. Regardless of these advantages, OMA-based information can also be considered not sensitive to early damage due to the need of identifying high order modes shapes, which proved to be very challenging for real structure monitoring (Santos et al., 2013). Symbolic data (Cury & Cremona, 2012), wavelet components (Posenato et al., 2010) and basic signal statistics are also examples of techniques successfully applied as extractors of damage-sensitive features for both static and dynamic monitoring.

However, in applications comprising acceleration measurements, autoregressive (AR) models have been widely reported for several reasons (Figueiredo et al., 2010; Lautour & Omenzetter, 2010; Datteo et al., 2018; Azim & Gül, 2019). One of them is their ability to extract features that are sensitive to damage, as the variation in physical parameters (e.g. stiffness) indicating the existence of damage manifests itself by a variation in the coefficients of the fitted AR models. Moreover, AR models depend solely on the response of the structure, and its parameters reflect the inherent structural properties regardless of the excitation sources and their respective variations (Entezami & Shariatmadar, 2017). In addition, the computational implementation of these models is fairly simple.

2.3.5 Feature Discrimination

2.3.5.1 Damage identification approaches

Once an operational evaluation stage has passed and a sensor network has been designed, the SHM system can begin to deliver data. At this stage, one is now faced with the challenge of making an accurate assessment of the damage condition of a given structure based on any

extracted features. The choice and implementation of algorithms to process the data and carry out the identification is arguably the most crucial component of an intelligent damage identification strategy.

Before even choosing the algorithm, it is necessary to choose between two complementary approaches to the problem, as described in Figure 2.15.
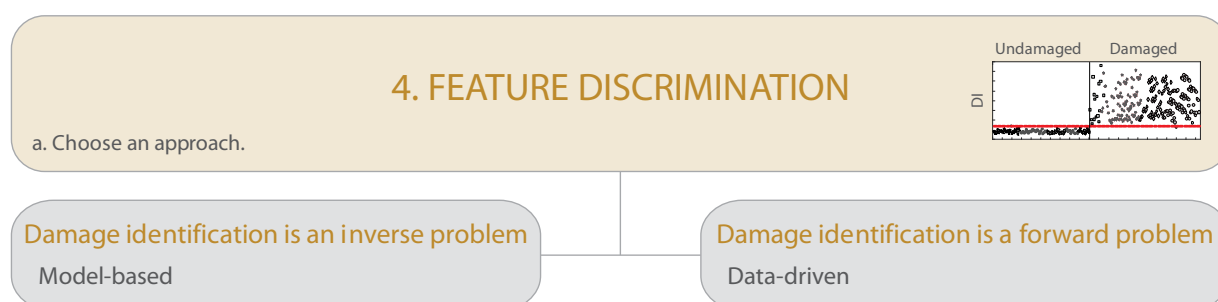

Figure 2.15 - Flowchart indicating the two possible approaches to the damage identification problem.

The inverse approach combines an initial model of the structure and measured data to improve the model or test a hypothesis. In practice, the model is commonly based on finite element analysis. Once the model is built, it is updated based on measured data from the real structure, such as acceleration and force responses, often in the form of a modal database, although frequency response function data may also be directly used (Friswell, 2008; Colombo et al., 2019). The goal is to adjust the built model in such a way as to make it conform better with data from the real structure. Although, it is important to be aware that the updating step brings up an important point; it is very difficult to build an accurate model of a structure since the information will be lacking in many areas. For example, the exact nature of bonds or joints on can be difficult to specify. Another issue is that material properties may not be known with great accuracy. After updating, as far as possible, an accurate model of the structure of interest in its actual condition can be obtained. When data from a subsequent monitoring phase become available, if any deviations from the normal condition are observed (e.g. the natural frequencies of the structure change), a further update of the model will indicate the location and extent of where structural changes have occurred, and this provides a damage diagnosis (Doebling et al., 1996).

Figure 2.16 shows an example of a three-dimensional calibrated numerical model of a railway bridge.
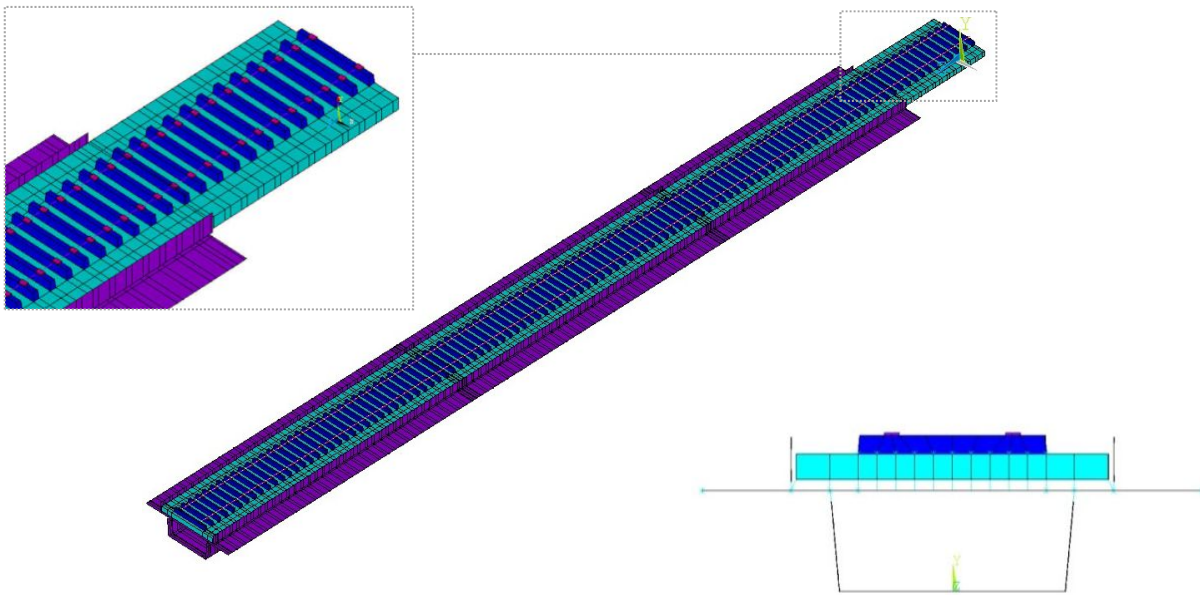
Figure 2.16 - Three-dimensional numerical model of Alverca railway viaduct (Meixedo et al., 2014).

Meruane & Heylen (2011) proposed a damage detection method based on an inverse approach, which is able to deal with temperature variations. The objective function correlates mode shapes and natural frequencies, and a parallel genetic algorithm handles the inverse problem. The numerical model of the structure assumes that the elasticity modulus of the materials is temperature-dependent. The algorithm updates the temperature and damage parameters together. Therefore, it is possible to distinguish between temperature effects and real damage events. Simulated data of a three-span bridge and experimental one of the I-40 Bridge validate the proposed methodology. Results show that the proposed algorithm is able to assess the experimental damage despite of temperature variations.

In turn, the forward approach does not require the development of numerical or analytical models to be fitted with in situ data; instead, it is based on the discipline of machine learning or, often more specifically, the pattern recognition aspects of machine learning. The idea is that one can learn relationships from data. In the context of SHM, this means that one can learn to assign a damage state or class to a given measurement vector from the structure or system of interest. The measurement vectors must be formed from measurements that are sensitive to the damage; in the normal terminology of pattern recognition, they are referred to as features, as discussed in the last section. Once features have been defined, the mapping between the features and the diagnosis can be constructed. In the forward approach one can still make effective use of law-based models as a means of establishing good features for damage identification (Doebling et al., 1996).

Posenato et al. (2010) present two statistical-based methodologies for model-free data interpretation to identify and localize anomalous behavior in civil engineering structures: i) moving principal component analysis and ii) robust regression analysis are demonstrated to be useful for damage detection during continuous static monitoring of civil structures. The methodologies are tested on numerically simulated elements with sensors for a range of noise in measurements. A comparative study with other statistical analyses demonstrates superior performance of these methods for damage detection. Methodologies are then validated on two full-scale structures. The results show the ability of the methodology to identify abrupt permanent changes in behavior.

There are pros and cons for both approaches; in any case, the distinction between the two philosophies is not as clear-cut as one might wish. The model-based approach depends critically on the availability of training data for the initial update step; the data-driven approach also establishes a model, but a statistical one.

2.3.5.2 Statistical modelling

The portion of the SHM process that is less documented in the technical literature is the development of statistical models for discrimination between features from the undamaged and damaged structures. Statistical model development is concerned with the implementation of algorithms that operate on the extracted features to quantify the damage state of the structure. The functional relationship between the selected features and the damage state of the structure is often difficult to define. Therefore, the statistical models are derived using machine learning techniques. The machine learning algorithms used in statistical model development usually fall into two categories i) supervised learning and ii) unsupervised learning, see Figure 2.17.

When training data is available from both undamaged and damaged structures, supervised learning algorithms can be used; group classification and regression analysis are primary examples of such algorithms. In the case of group classification, the output of the algorithm is a discrete class label. In its most basic form, this algorithm might simply assign a "damage" or "not damage" label to features. This type of algorithm is useful in the sense that the algorithms can be trained to give the probability of class membership. Using a regression algorithm, the outputs are one or more continuous variables. This problem is often nonlinear and is particularly suited to neural networks or other machine learning algorithms (Farrar & Worden, 2007).
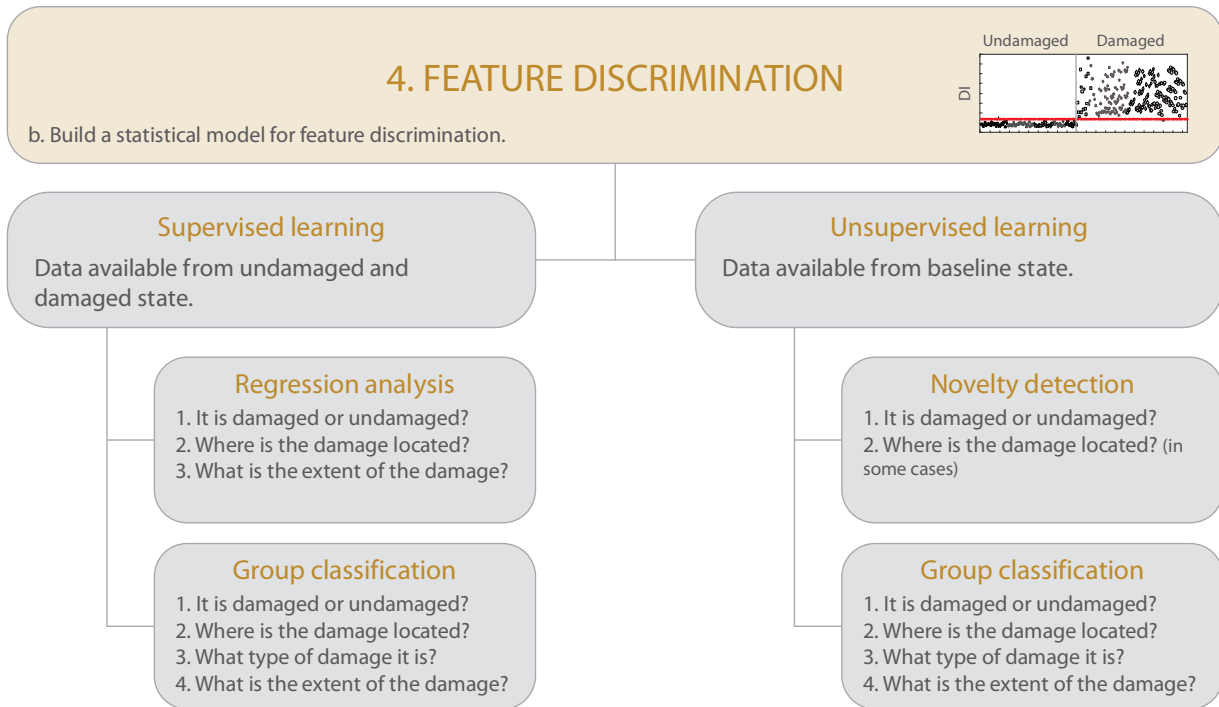
Figure 2.17 - Flowchart of statistical model building for feature discrimination.

Since data obtained from damaged civil engineering structures is rare or inexistent, unsupervised learning algorithms have been increasingly observed in the literature. Novelty detection methods are the primary class of algorithms used in this situation. This type of algorithm is a two-class problem that indicates if the acquired data comes from normal operating conditions or not (Farrar & Worden, 2007). There are many novelty detection techniques, e.g. outlier analysis, kernel density estimation and auto-associative neural networks (Posenato et al., 2008; Gonzalez & Karoumi, 2015). All techniques fit a probability distribution to the normal condition data then assess the probability of the test data having been generated by the same mechanism. As illustrated in Figure 2.18, an outlier is a data point that belongs to a distribution that is different from the remaining points of a certain sample, and therefore believed to be generated by an alternate mechanism. In damage identification, the data point is different to the data acquired from the normal operating condition of the structure and this is assumed to be due to the presence of damage. In this case, a normal operating condition means a state of the system when there is some assurance, statistical or otherwise, that the system is fit-for-purpose. In some cases, there may be macroscopic damage, like a fatigue crack; however, if it is known that the crack will not grow under the standard loadings on the system, this state qualifies as a normal operating condition. Novelty detection will then look for new cracks or unexpected growth of the old crack. Note that for high capital expenditure structures, such as most civil infrastructure,

the unsupervised learning algorithms are often required because only data from the undamaged condition (baseline) are available (Worden & Dulieu-Barton, 2004).
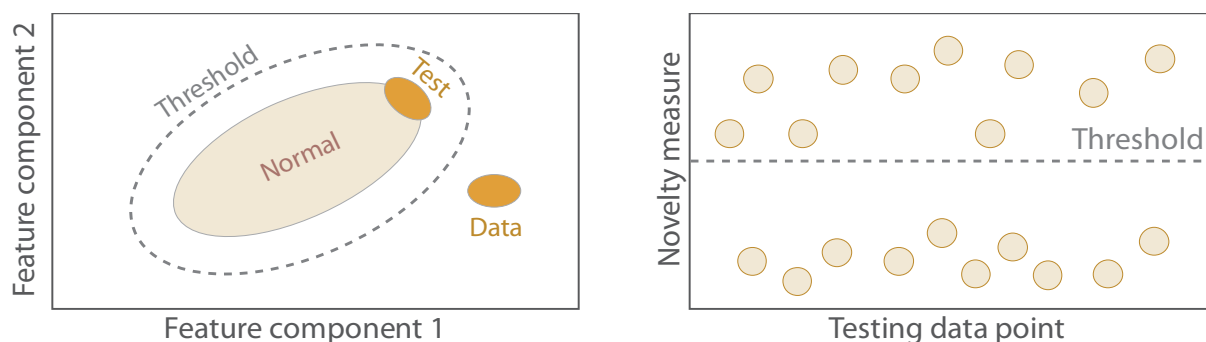

Figure 2.18 - Schemes illustrating novelty detection.

In spite of the SHM feature discrimination resorting to clustering methods has been reported mainly following the supervised strategy of pre-defining cluster partitions to describe one or more known structural behaviours, and subsequently compare them with new ones (Cury & Cremona, 2010; Silva et al., 2008), this type of techniques have an unsupervised nature (Santos, 2014). The major advantage of cluster-based strategies, over those previously described consists of the greater sensitivity exhibited by these algorithms, which is related to their capacity to analyse data compactness and separation instead of defining boundaries between or around data objects (Koutroumbas, 2009; Rendón et al., 2011; Santos, 2014). The works describing cluster-based classification for novelty identification refer its high sensitivity to structural changes, and associate it with the ability of these methods to analyse compactness and separation within feature sets (Santos et al., 2015).

Regarding the hierarchy discussed in Rytter (1993) and mentioned in section 2.2.3, when applied in an unsupervised learning mode, statistical models can typically be used to answer questions regarding the existence (and sometimes, but not always, the location) of damage. When applied in a supervised learning mode and coupled with analytical models, the statistical procedures can, in theory, be used to determine the existence, the location of damage, the type of damage, the extent of damage and the remaining useful life of the structure (Farrar et al., 2001).

If supervised learning is required, there will be serious demands associated with it; data from every important damage situation must be available. The two possible sources of such data are physics-based modelling (i.e. from finite element analysis) and experiment. Modelling presents problems if the structure or system of interest is geometrically or materially complex; for

example, finite element analysis of structures requiring a fine mesh can be extremely time consuming even if the material is well understood. The damage itself may be difficult to model and it may make the structure dynamically nonlinear. Finally, it might be difficult to anticipate the future loading for the system or structure. Unfortunately, the situation is no better for experiment. In order to accumulate enough training data, it would be necessary to make copies of the system of interest and damage it in all the ways that might occur naturally. For high-value structures like bridges, this is simply not possible (Farrar & Worden, 2007).

In case of unsupervised learning, often referred to as novelty detection, a model of the normal condition is created. Later, during monitoring, newly acquired data are compared with the model. If there are any significant deviations, the algorithm indicates novelty. The implication is that the system has departed from the normal condition, that is, acquired damage. The advantage of such an approach is clear; if the training data is generated from a model, only the baseline condition is required and this will simplify matters considerably. From an experimental point of view, there is no need to damage the structure of interest. Although novelty identification is only a level 1 (or sometimes level 2) approach, there are many situations where this is sufficient, for example safety-critical systems where any fault on the system would require it to be taken out of service (Sohn & Law, 2000).

It is important to notice that supervised and unsupervised learning come usually associated with a forward damage identification approach.

Statistical models can also be applied to avoid incorrect diagnosis of damage. False diagnoses fall into two categories: i) false-positive damage indication (indication of damage when none is present) and ii) false-negative damage indication (no indication of damage when damage is present). The false-positives are known as Type I and are the primary motivator for economic SHM concerns. On the other hand, false-negatives are known as Type II and are the primary motivator for life-safety as SHM concerns. Unless the measured features for a given problem completely separate the undamaged and damaged condition, there will be Type I and Type II errors and the placing of the threshold will mediate their relative frequency.

Finally, statistical models are used to implement two types of SHM: i) protective and ii) predictive (Farrar & Worden, 2013). Protective monitoring refers to the case when damage-sensitive features are used to identify impending failure and shut the system down or alter its use in some other manner before catastrophic failure results. In this case, the statistical models are used to establish thresholds on acceptable levels of feature change. Predictive

monitoring refers to the case where one identifies trends in data features that are then used to predict when the damage will reach a critical level. This type of monitoring is necessary to develop cost-effective maintenance planning.

2.3.6 Data Modelling

The ability to perform robust data modelling is one of the biggest challenges facing SHM when attempting to transition this technology from research to field deployment and practice on in situ structures (Farrar & Worden, 2013). This process can be applied during data acquisition, feature extraction or feature discrimination portions of the SHM process.

As it applies to SHM, data modelling is the process of separating changes in sensor reading caused by damage from those caused by varying operational and environmental conditions (Farrar et al., 2001). Concerning data modelling issue, the two different situations shown in Figure 2.19 can happen.
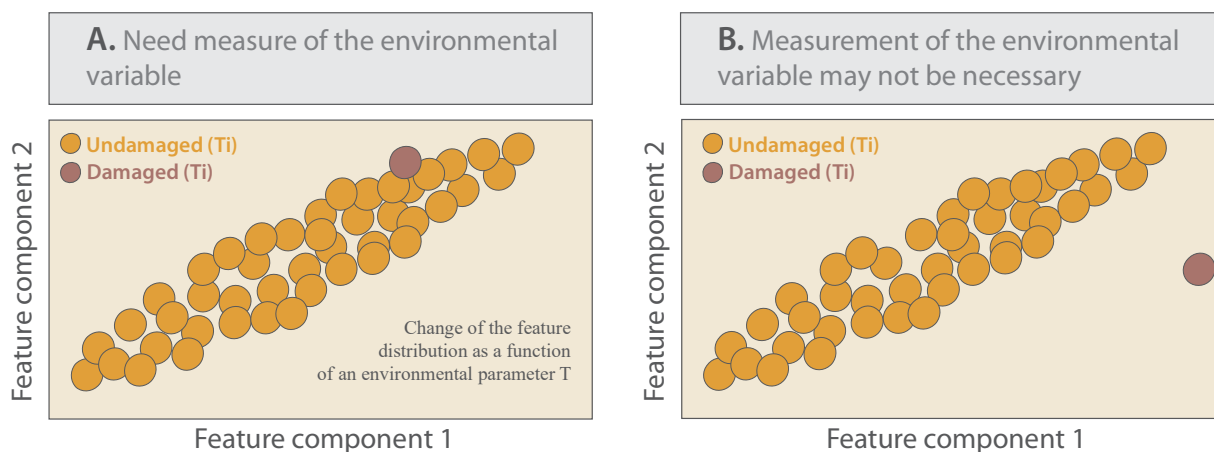

Figure 2.19 – Schematic representation of two type of situations that can happen regarding data modelling.

In real-world cases, situation A is the most common, since the changes in features distribution produced by severe damage are of the same order of magnitude as changes that can be expected by varying environmental or operational conditions. In this sense, the ability to normalize the data becomes very important to the damage identification process; otherwise, changes in the measured response caused by operational and environmental conditions may be mistaken as an effect of damage. Additional measurements may be required to provide the information necessary to model the measured data and the need for this should be considered in the operational evaluation stage (Cury et al., 2012).

Among the operational and environmental effects generating changes in structural responses, temperature is reported as the most significant (Li et al., 2010; Cury et al., 2012). Figueiredo (2010) performed several dynamical tests in the Alamosa Canyon Bridge to examine the variability of the deck modal parameters. As shown in Figure 2.20, taking the difference between the extreme values and dividing by the maximum value, variations of 5% in the first natural frequency and 26% on damping ratio were observed on a single day cycle. This can occur mainly due to changes in structural stiffness and boundary conditions.
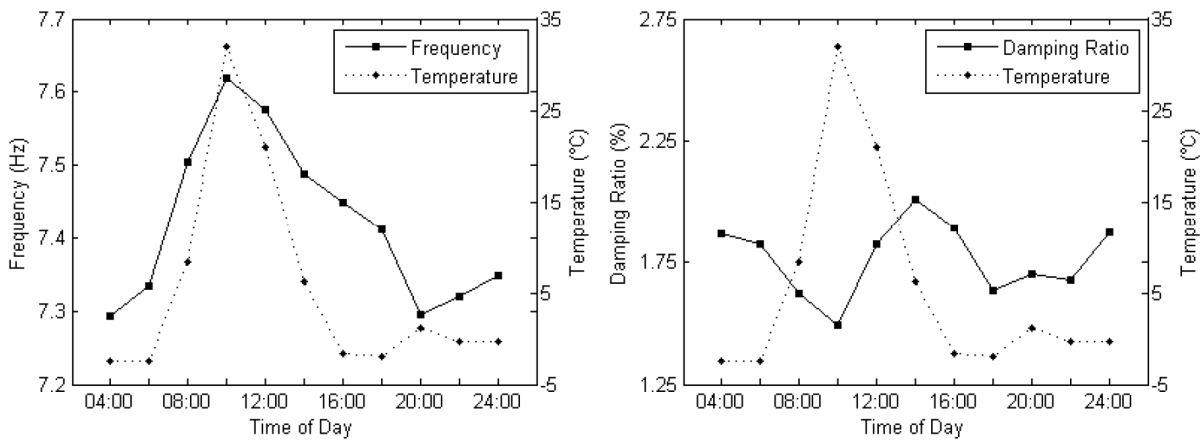

Figure 2.20 - Variability in the modal parameters along with the differential temperature across the deck during a 24-hour test: (a) first natural frequency; and (b) first damping ratio (Figueiredo, 2010).

As described in Santos (2014), non-modal measurements such as displacements and strain, are even more influenced by temperature. As shown in Figure 2.21, the strain time-series acquired in the Salgueiro Maia Bridge revealed high correlation with temperature action.

As expected, the influence of the wind speed can be important for some specific civil structures such as high buildings and long-span bridges. In Fujino & Siringoringo (2008), it is referred that the vertical amplitude of the bridge response decreases according to a quadratic function of wind speed.

Structural measurements can also suffer important variations caused by traffic, especially in the case of heavy loads such as trains. Tests performed with and without traffic on the I-40 bridge showed a 4% change in the first-mode frequency (Farrar & Worden, 2013).

The influence of humidity on structural response seems to be of minor importance when compared to temperature. In Peeters & Roeck (2001) the authors concluded that the humidity had no relation with natural frequencies of the Z24 overpass.

From the literature review, it can be concluded that the effects generated by traffic, temperature and wind must be considered when aiming at identifying structural changes in civil structures. Humidity, however, was reported as an environmental change with low influence (Santos, 2014).
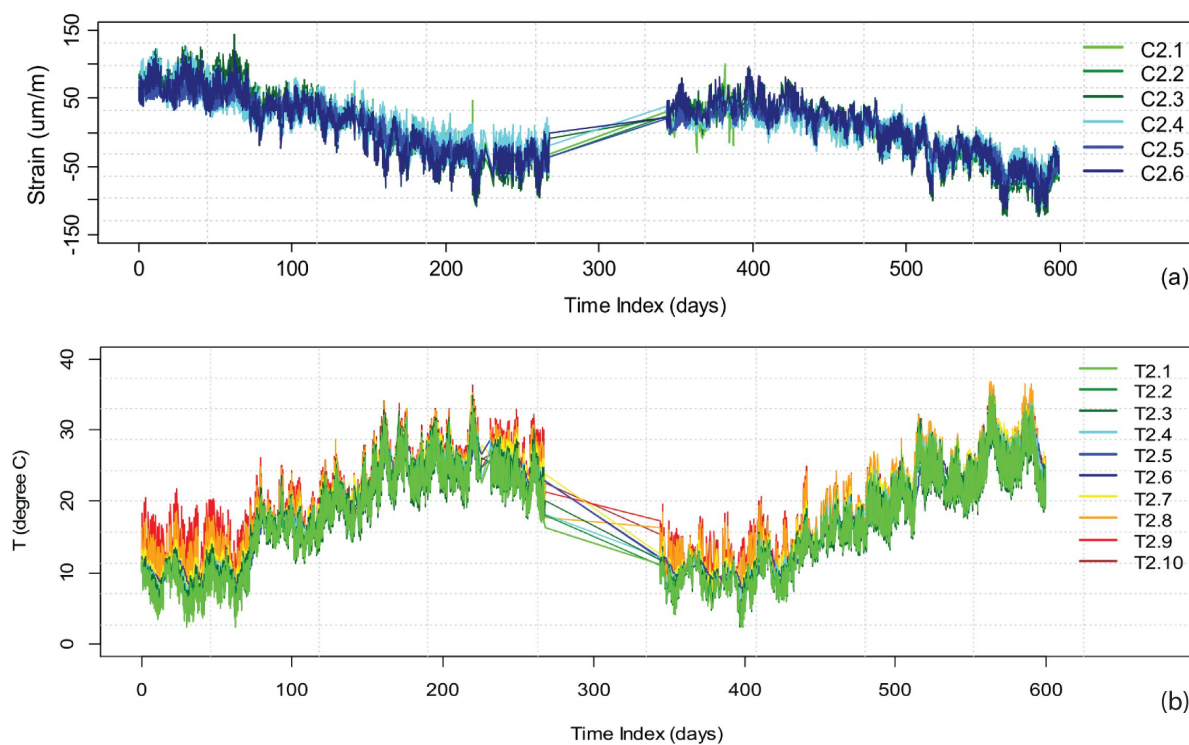

Figure 2.21 - Measurements obtained from the Salgueiro Maia Bridge: (a) strain time-series and (b) temperatures (Santos, 2014).

Regarding data modelling methods, two approaches are generally found in the literature to separate changes in damage-sensitive features caused by operational and environmental conditions from those caused by damage: i) input-output, based on regression methods (Cavadas et al., 2013; Peeters & Roeck, 2001) or ii) output-only, based on latent variable methods (Alvandi & Cremona, 2006; Santos et al., 2013). The first removes the effects of the environmental and operational effects, establishing relationships between measured actions (e.g. temperature, traffic, wind) and measured structural responses (Cury, 2010). When monitoring systems do not include the measurement of EOVs, latent variable statistical algorithms that "learn" the influence of the operational and environmental conditions from the response data can be employed (Santos et al., 2013). This approach has the important advantage of being able to suppress independent actions using only structural measurements(Zhou et al., 2010). Also, it paves the way for studying complex structural systems whose actions can be of difficult and expensive characterization.

33

In this work, some of the most effective methods for each approach are summarized in Figure 2.22.
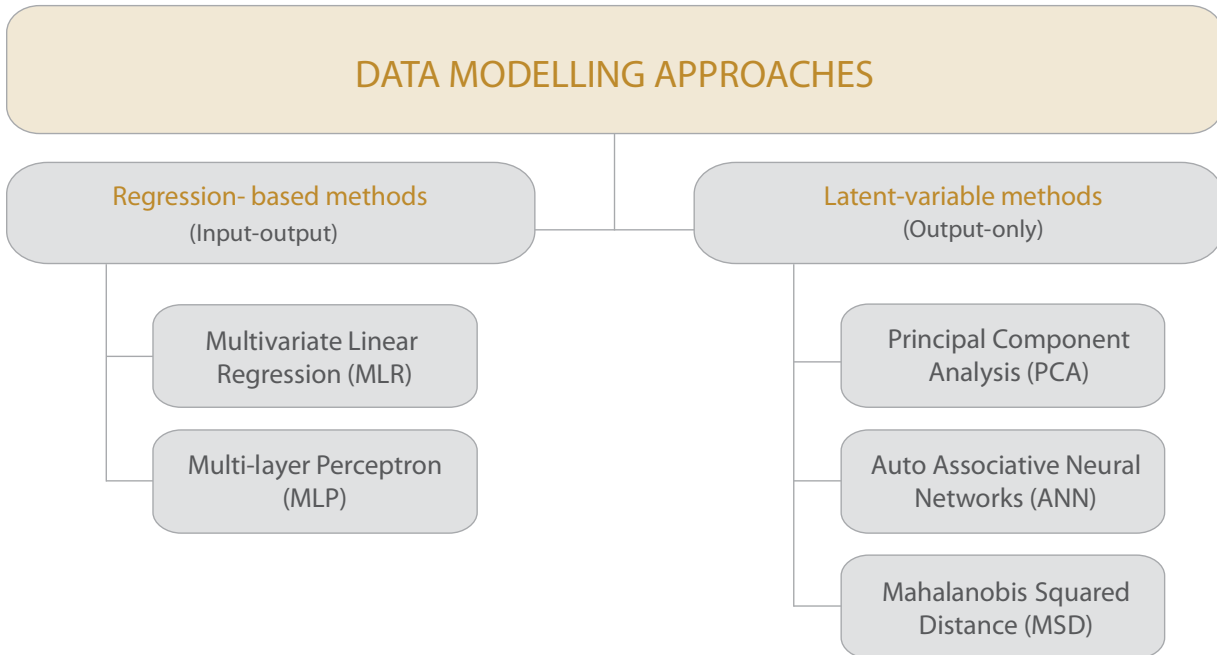

Figure 2.22 - Data modelling approaches.

2.3.6.1 *Regression-based methods*

One of the most direct regression methods used for data modelling is the multivariate linear regression (MLR). Its theoretical and computational simplicity along with the fact that most physical relations between environmental and operational actions and structural measurements have a linear nature, make it appealing for normalization (Santos, 2014). In Cury (2010), a multivariate linear regression model was used to find the relation between each modal frequency and the sets of temperatures measured in two bridges. Figueiredo (2010), use 24 hours' modal and temperature data from Alamosa Canyon bridge to develop a regression model that predicts the first two natural frequencies as a function of the temperature differential across the deck including one-time delay.

However, numerous SHM applications refer the need for using nonlinear methods to appropriately model relations between the structural data and the actions. Among nonlinear statistical-learning regression algorithms, the Artificial Neural Networks named Multi-Layer Perceptron (MLP), have been the most used (Bishop, 1995; Worden et al., 2011). Ni et al. (2009) assess the generalization capacity of MLP for describing the relation between temperature and modal frequencies. In Cury et al. (2012), MLP was used for modelling the temperature effect in

modal frequency data and its better performance over linear regression proved important for accurately detecting the effects of retrofitting processes in two bridges.

In sum, the computational simplicity and the fact that most structural responses are linearly correlated with the actions makes the MLR a very appealing normalization method. However, the literature review shows that it is less accurate than the nonlinear and nonparametric MLP (Santos, 2014).

2.3.6.2 Latent-variable methods

Latent-variable methods develop a functional relationship that models how changing operational and environmental conditions influence the underlying distribution of the damage-sensitive features. When subsequent features are analysed with these algorithms and the new set of features are shown not to fit into an appropriate distribution, they might be more confidently classified as outliers or, potentially, features from a damaged structure, because the varying operational and environmental conditions have been incorporated into the classification procedure (Worden et al., 2011).

Principal Component Analysis (PCA) is one example of this type of method and is considered the simplest in terms of computational application (Jolliffe, 2002). In Yan et al. (2005), one of the first PCA-based modelling applied to civil SHM works is performed on frequencies obtained from numerical and laboratorial case studies, as well as from one year monitoring of the Z24 overpass. The authors selected the first two principal components with higher deviations related to temperature. In Hu et al. (2012), the efficiency of PCA-based modelling approach was verified using 3 years of measurements at Pedro e Inês footbridge, in Coimbra, under operational and environmental conditions and simulating several realistic damage scenarios. It was considered only the largest principal component as related to temperature effect, a choice which is justified by the high variance explained by that principal component. Santos et al. (2013) applied PCA-based modelling to data acquired from a cable-stayed bridge, but instead of an empirical choice of the number of principal components, the authors proposed a successfully systematic statistical approach based on randomness hypothesis. Besides the benefit of data normalization reduction, PCA is also a powerful tool for compressing data and can be used in the context of feature extraction.

Auto Associative Neural networks (AANN), also known as Nonlinear Principal Component Analysis (NLPCA) is very similar in concept to PCA. While PCA is restricted to mapping only

linear correlations among variables, NLPCA can reveal the nonlinear correlations present in data (Sohn, 2007).

Several studies have used the AANN to remove the effects of the operational and environmental variability and to detect damage. The first reference to the use of AANN in civil SHM data normalization was in 2002 by Sohn et al. (2002). The authors used it to normalize regression coefficients and concluded about the effectiveness of the method in outlining damage under normal environmental conditions. Li et al. (2010) applied the AANN as a signal pre-processing tool to distinguish temperature and wind effects on the modal parameters from other environmental factors.

Another method for performing data normalization when direct measures of the environmental and operational parameters that are causing variability in the damage-sensitive features are not available is based on the Mahalanobis squared-distance (MSD). The MSD has been extensively applied in SHM for data modelling (Farrar & Worden, 2013). For instance, Worden et al. (2003) applied the Mahalanobis distance algorithm to vibration data obtained from a simplified model of a metallic aircraft wingbox to detect damage in the stringer. Figueiredo et al. (2011) addressed the implementation and comparison of four data modelling algorithms, AANN, MSD, SVD (Singular Value Decomposition) and FA (Factor Analysis). Tests were performed in laboratory considering a base-excited three-story frame structure and varying stiffness and mass conditions with the assumption that these sources of variability are representative of changing operational and environmental conditions. The authors concluded that the MSD seems to be the best data modelling approach in terms of the classification performance, the reduced computational efforts (during both training and test), and the fact that no assumptions are required regarding its architecture.

In sum, all three latent-variable methods offer some advantages over regression-based normalization techniques because the operational and environmental variables (e.g. traffic loading and temperature) do not need to be measured to reveal their influence on the structural responses. However, these algorithms have potential problems if the training data are only characteristic of a limited range of operational and environmental variability. Hence, all sources of variability must be well characterized by the training data so that the algorithms can accurately learn their influence on the system's response.

2.3.7   Data cleansing, compression and fusion

Inherent in the data acquisition, feature extraction, and feature discrimination portions of the SHM strategy are data cleansing, fusion, and compression procedures, as well as data modelling, detailed in the previous section.

Data cleansing is the process of selectively choosing data to pass on to, or reject from, the feature selection process. This process is usually based on knowledge gained by individuals directly involved with the data acquisition (Farrar et al., 2001). As an example, an inspection of the test setup may reveal that a sensor was loosely mounted and, hence, based on the judgement of the individuals performing the measurement, this set of data or the data from that particular sensor may be selectively deleted from the feature selection process. Signal processing techniques such as i) filtering to remove noise, ii) resampling, iii) spike removal by median filtering, iv) removal of outliers (care is needed here as the presence of outliers is one indication that the data is not from normal condition), and v) treatment of missing data values, can also be thought of as data cleansing procedures (Worden & Dulieu-Barton, 2004).

Data compression is the process of reducing the dimensionality of the data, or the features extracted from the data, in an effort to facilitate efficient storage of information and to enhance the statistical quantification of these parameters. The operational implementation of the measurement technologies needed to perform SHM inherently produces large amounts of data. A condensation of the data is advantageous and necessary when comparisons of many feature sets obtained over the lifetime of the structure are planned (Farrar & Worden, 2013).

Regarding the data fusion, there are many definitions of this process, but one of the first came from the North American Joint Directors of Laboratories, and says that data fusion is "a multilevel, multifaceted process dealing with the automatic detection, association, correlation, estimation and combination of data from single and multiple sources" (White, 1990).

The fusion process may combine data from spatially distributed sensors of the same type such as an array of strain gauges mounted on a structure. Alternatively, heterogeneous data types including kinematic response measurements (e.g. acceleration) along with environmental parameter measurements (e.g. temperature) and measures of operational parameters (e.g. traffic volume on a bridge) can be combined to determine more easily if damage is present.

Clearly, data fusion is closely related to the data modelling, cleansing and compression processes. In general, fusion models allow information to be combined at the feature extraction,

the pattern level or the decision level. The objective at all times is to reach a decision with higher confidence than can be reached using any of the information sources alone.

One of the most famous fusion paradigms is the Omnibus model (Bedworth & O'Brien, 1991) illustrated in Figure 2.23. It includes the possibility of action. In the context of SHM, this could be repair; in the context of feature discrimination, this could be control. In the event of a sensor failure, this could entail the reallocation of sensors or the switching in of redundant sensors. The model has a loop structure that makes clear the fact that action need not interrupt the monitoring process, but may enhance it. The generality of the model makes it excellent to use when one is planning a sensor and data fusion process (Worden & Dulieu-Barton, 2004).
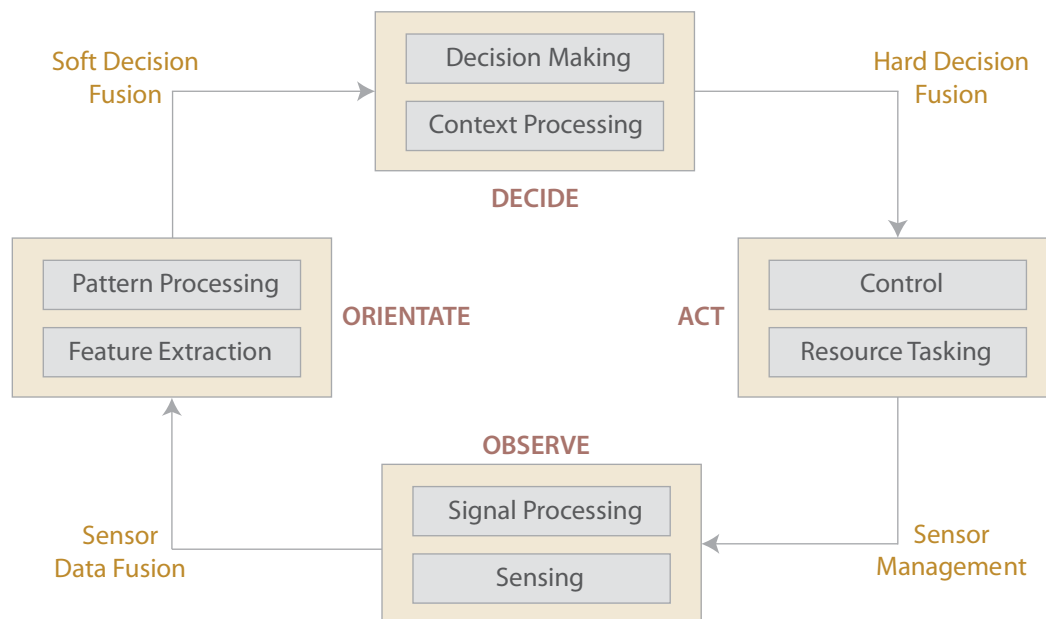

Figure 2.23 - The Omnibus model for data fusion (adapted from Worden & Dulieu-Barton, (2004)).

In the context of feature extraction, data fusion techniques can be classified, according to their location within the work-flow of SHM techniques as: centralized strategies (Figure 2.24a), pattern-level strategies (Figure 2.24b), or combinations of both (Figure 2.24c) (Worden & Dulieu-Barton, 2004; Santos, 2014). In case of vibration-based monitoring, the centralized-level is required for converting the large amounts of acceleration data into sets of meaningful vibration features such as modal frequencies (Cury, 2010; Hu et al., 2012). Pattern-level data fusion is required to convert either these vibration features or static-based measurements in compact information that can be statistically classified as "known" or "novel" with high accuracy (Santos, 2014). PCA (Cavadas et al., 2013) and Symbolic Data (Cury & Cremona, 2010; Santos et al., 2016) are good examples of such techniques.
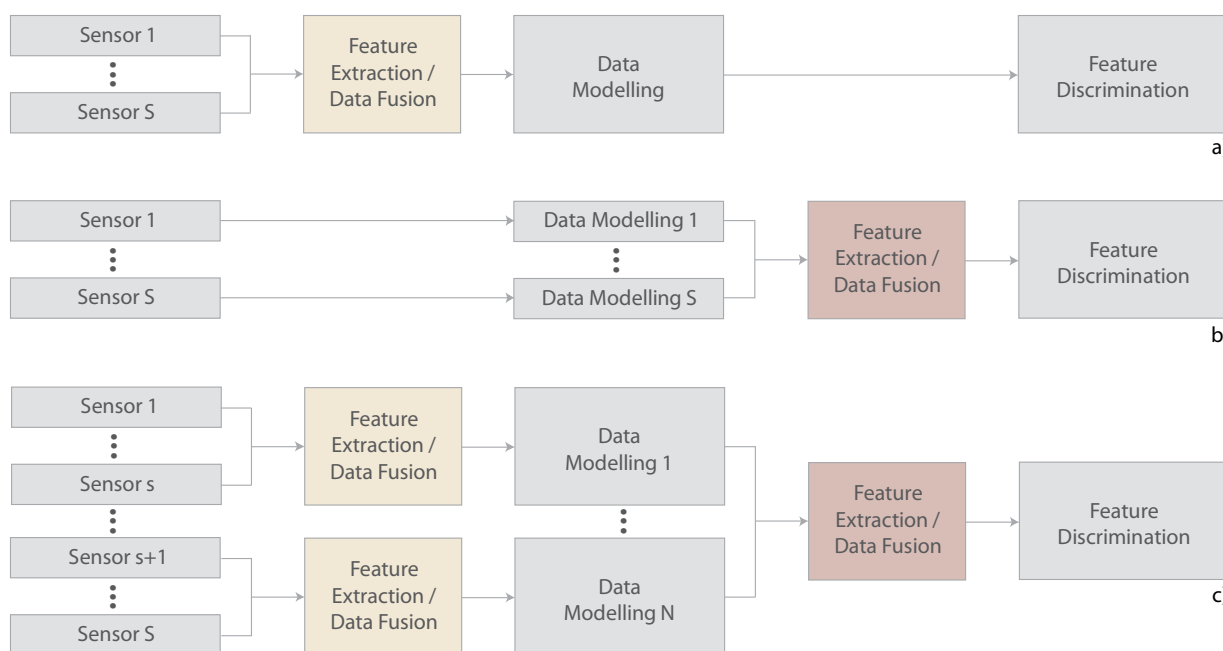
Figure 2.24 - Classification of data fusion according to its location within the SHM data-flow: a) centralized, b) pattern-level and c) both (adapted from Santos, 2014).

The Mahalanobis distance has been thoroughly used in the context of data fusion due to its capacity to describe the variability in multivariate data sets. In fact, a larger number of Mahalanobis distance's applications is performed on estimations' errors obtained from PCA, as it can be observed in Yan et al. (2005a) and Hu et al. (2012). Distinct strategies also comprise the extraction of Mahalanobis distances directly from AR coefficients (Figueiredo et al., 2010).

2.4   SHM PROCEDURE IMPLEMENTED

A schematic representation of the proposed SHM for early damage identification followed in this dissertation is depicted in Figure 2.25, where all the steps from Figure 2.11 are implemented.

A long-span bowstring-arch railway bridge was selected as case study, and the first two steps of the SHM strategy – Operational Evaluation and Data Acquisition – were applied, as will be presented in Chapter 3. In order to accomplish a fully autonomous and real-time monitoring system, a process involving moving windows was implemented. Within each window, the following four main steps regarding damage identification are performed: 1) feature extraction, 2) feature modelling, 3) data fusion and 4) feature discrimination. The feature extraction is accomplish implementing time-series analysis to the vibration-based measurements acquired by the monitoring system installed in the railway bridge. During this step, data compression is achieved by transforming the thousands of points from each dynamic response of the structure

into a few dozens of features. Subsequently, feature modelling is performed to reduce the influence of operational and environmental conditions. Both regression-based and latent-variable methods are implemented in order to select the one that better suits the features. To enhance sensitivity a pattern-level data fusion is performed afterwards by implementing a Mahalanobis distance to merge the features and/or to merge the information from several sensors. Finally, feature discrimination is performed as a data-driven approach and implementing unsupervised machine learning algorithms, namely, outlier and cluster analyses. Chapters 5 and 6 describe, respectively, the strategy and the online procedure based on moving windows in detail.
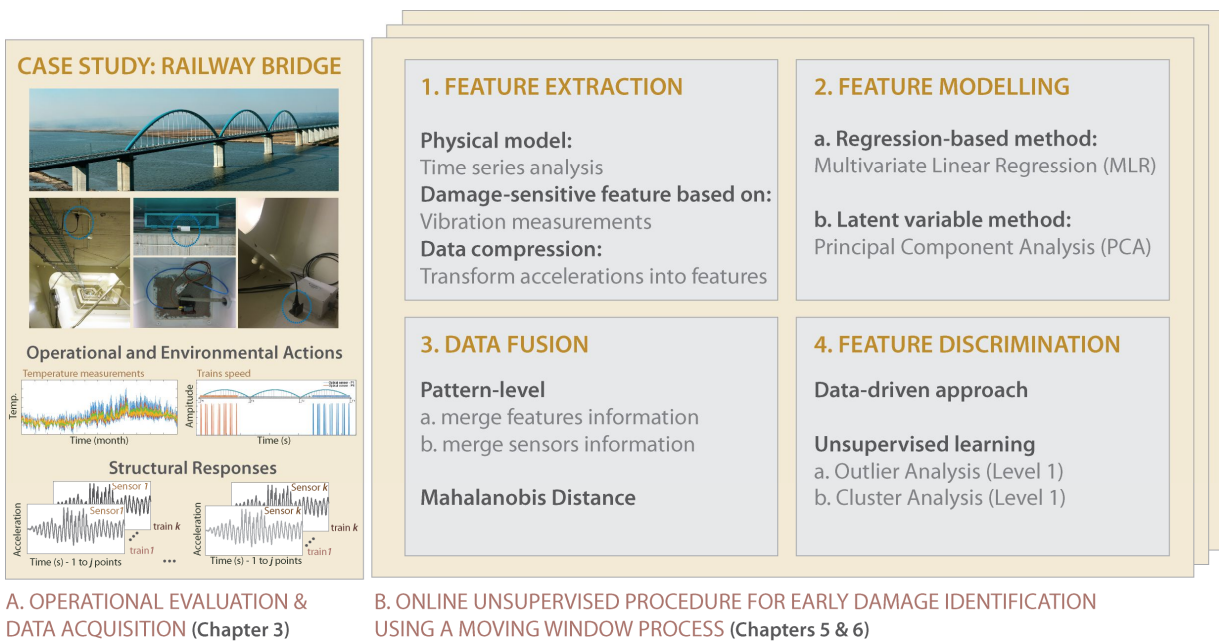

Figure 2.25 - Schematic representation of the SHM implemented for early damage identification.

As data-driven approaches are usually less computationally complex, they are better suited for early damage identification. Moreover, in civil engineering structures the most important question to answer is if there is or not a damage. The questions about location and severity are usually less important in this type of structures since the simple existence of damage will trigger other management procedures (Wenzel, 2009). For those reasons, data-driven approaches are followed in the present thesis with the aim of detecting damage (level 1). However, finite element models can be used to simulate damage scenarios that are not possible to obtain in any other way. These data can be then used to test the validity and robustness of the methodologies proposed for damage identification. This approach is followed in Chapter 4, where a progressive numerical model validation of the railway bridge over the Sado River is performed, in order to,

afterwards, simulate damage scenarios and demonstrate the efficiency of the developed methodology.

Chapter 3

STRUCTURAL MONITORING SYSTEM OF A BOWSTRING-ARCH RAILWAY BRIDGE[*]

3.1 INTRODUCTION

A bowstring-arch railway bridge over the Sado River was selected as the case study used throughout this work, since it is a recent, long-span complex structure that has been monitored by LNEC (Laboratório Nacional de Engenharia Civil) from the beginning of its life-cycle. In the context of this thesis and with LNEC's collaboration, an optimized online monitoring system with different types of sensors was set up. The present chapter aims at presenting the railway bridge over the Sado River, as well as the evolution of the monitoring system installed over the years. An analysis of the data acquired is performed and it is shown that dynamic traffic-based monitoring system will provide greater sensitivity in detecting the non-linear behaviour of the components of the bridge, possibly related to structural changes, due to the effects of high amplitude actions induced by regular train loading schemes (axle configuration and loads) (Meixedo et al., 2019).

After the introduction, sections 3.2 and 3.3, respectively, show the case study and the installed monitoring system as well as a discussion regarding the main data acquired. Finally, section 3.4 lists the concluding remarks of this chapter.

3.2 BRIDGE OVER THE SADO RIVER

The composite bowstring-arch bridge over the Sado River is located on the southern line of the Portuguese railway network that establishes the connection between Lisbon and Algarve (Figure 3.1). The structure was built from November 2008 to August 2010, when it entered in operation phase. It is prepared for conventional and tilting passenger trains with speeds up to 250 km/h, as well as for freight trains with a maximum axle load of 25 t.

Figure 3.1 Bridge over the Sado River: a) overview, b) general view of the deck with the Alfa Pendular train crossing.

This bridge is part of a 28.98 km long railway stretch called the Alcácer bypass, located between the Pinheiro Station and km 94 of the above-mentioned Lisbon-Algarve line (Figure 3.2). This line allows a reduction of travel time in the Lisbon-Algarve connection and increases the transfer of passengers from road to railways. Additionally, it improves the capacity of the

seaport of Sines, by making faster its connection to the logistic hubs of Poceirão and Elvas and to the seaports of Setúbal and Lisbon.

Figure 3.2 - Geographical location of the bypass and schematic representation (adapted from REFER (2010)).

The bridge has a total length of 480 m, divided into 3 continuous spans each 160 m long, and it is part of a longer structure that includes the North access viaduct at 1115 m length and the South access viaduct with a length of 1140 m. As shown in Figure 3.3, the deck is suspended from three parabolic arches connected by 18 hangers distributed over a single plane on the axis of the structure. The hangers have a circular cross-section with a diameter of 200 mm and a spacing of 8 m in the longitudinal direction. The superstructure is composed of a steel-concrete composite deck, while the substructure, which includes the piers, the abutments and the pile foundations, is built in reinforced concrete. As illustrated in Figure 3.3, the deck is fixed on pier P1, whereas on piers P2, P3 and P4 only the transverse movements of the deck are restrained, while the longitudinal movements are constrained by seismic dampers. The ballasted railway track confirms with the Iberian gauge (1.668 m) and is composed of continuously welded rails (type UIC60E1) resting on mono-block concrete sleepers. Even though the bridge accommodates two rail tracks, only the upstream track is currently in operation, as it can be observed in Figure 3.1b.

The bridge deck consists of a concrete slab laid over a steel box girder (Figure 3.4). The concrete slab has a total width of 15.85 m and a cross-section thickness ranging from 200 mm at the edge to 430 mm at the bridge's symmetry plane. The U-shaped steel box girder has a total height of 2.6 m and two inclined lateral webs, a 6.20 m wide bottom flange and three top flanges – two outer ones connected to the lateral webs and one in the middle connected to the cross-section diagonals and hangers. The top outer flanges are 1.50 m wide, the middle one is

1.20 m, and their thickness varies between 30 mm and 60 mm. The inclined webs are 30 mm thick across the entire length of the deck.
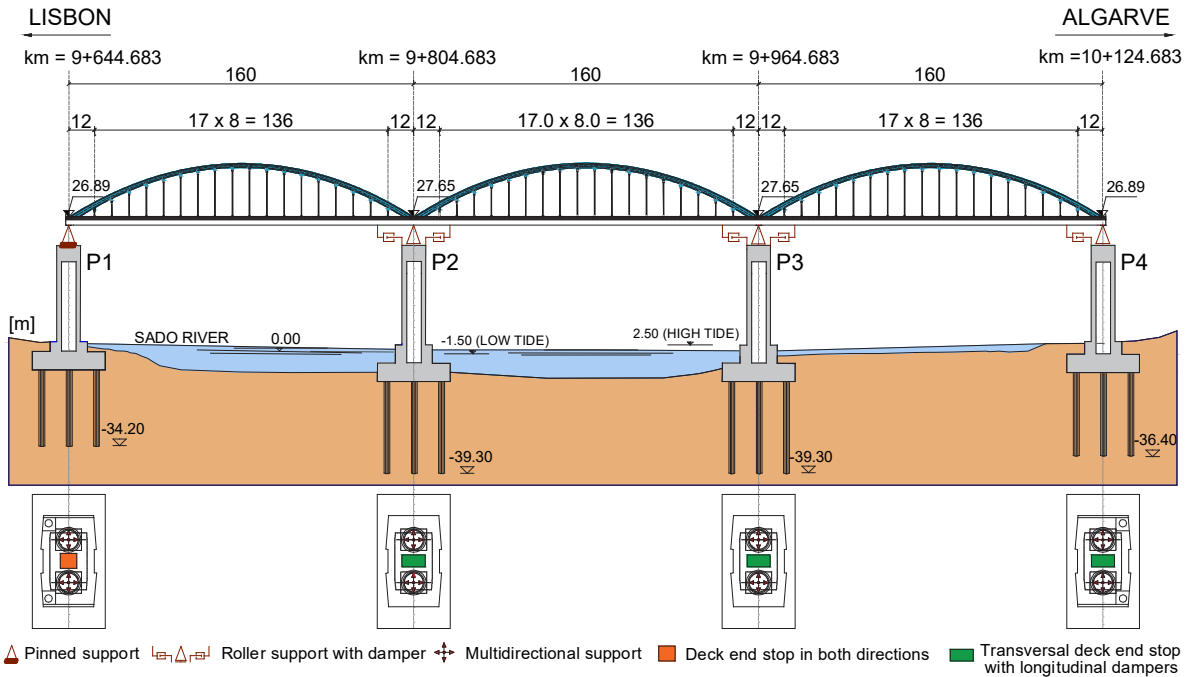

Figure 3.3 - Lateral view of the bridge detailing the bearing devices (adapted from GRID et al. (2006)).

Figure 3.4 - Cross-section of the deck (adapted from GRID et al. (2006)).
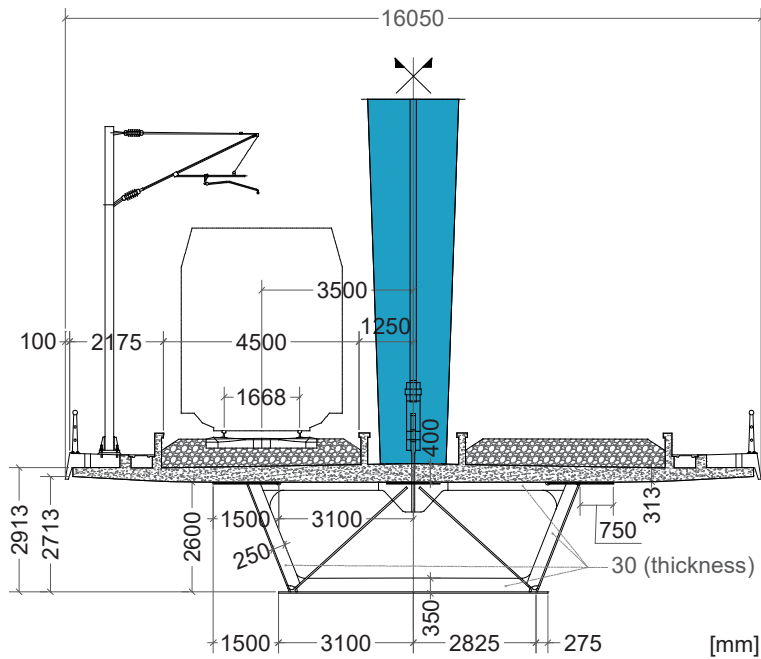
The three parabolic arches have a hexagonal hollow cross-section, with a variable width increasing towards the top, as illustrated in Figure 3.5. The maximum rise of the arches is 25.4 m. The arches' webs are 80 mm to 120 mm thick. On the other side, the thickness of the arches' flanges varies between 60 mm in the top section and 120 mm in the bottom section.
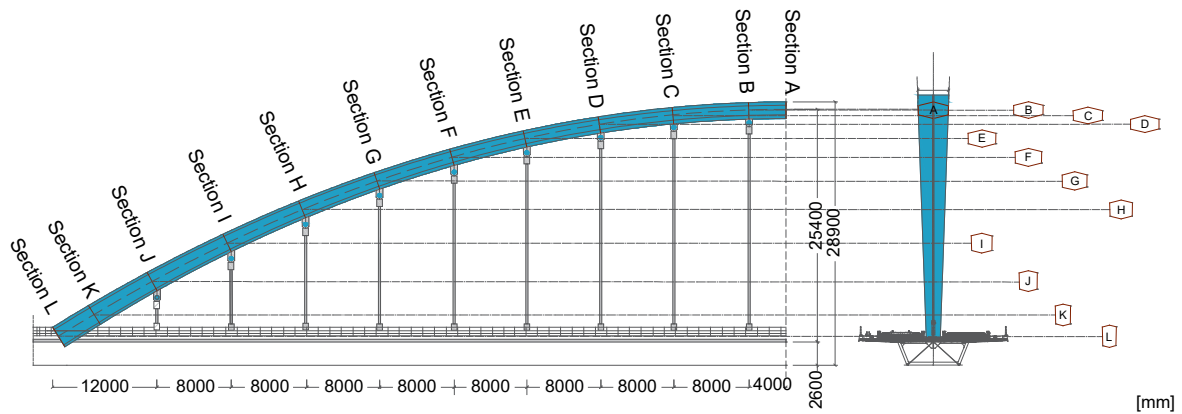
Figure 3.5 - Section variation in arch cross-section (adapted from GRID et al. (2006)).

The connection between the deck and the hanger is performed through spherical hinges that allow the torsional rotation of the deck and prevent fatigue phenomena. The suspension of the deck loads is carried out through the hangers by means of steel diaphragms and two diagonal strings at each connection. The bridge deck is supported by four reinforced concrete piers with a hexagonal hollow cross-section. Each pier rests on heads of reinforced concrete piles with lengths up to 50 m and 2 m diameters. Piers P1 and P4 are supported by nine piles, while piers P2 and P3 by twelve piles. Figure 3.6 details the deck, piers P2/P3 and their foundations through a side elevation and a front elevation.
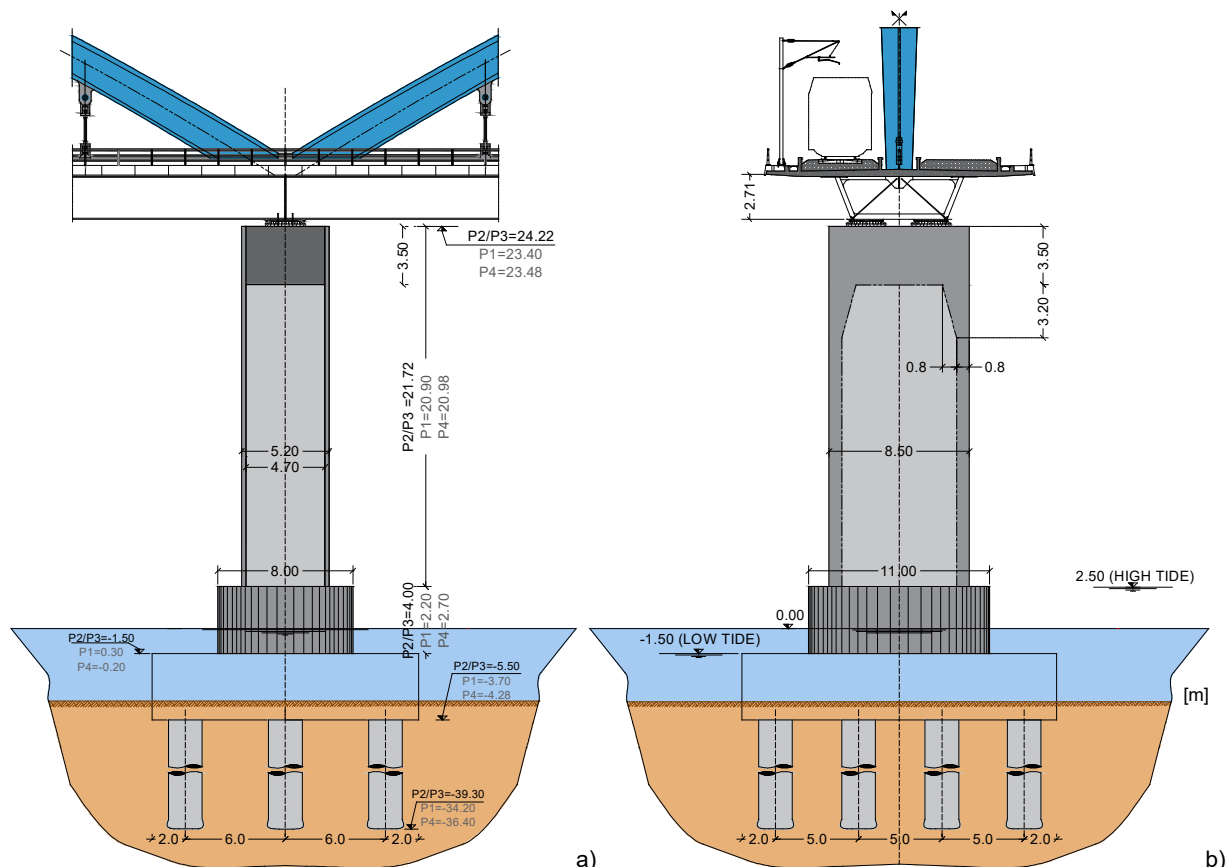

Figure 3.6 - Bridge details: a) side elevation, b) front view (adapted from GRID et al. (2006)).

At the top of each pier there are two spherical and multidirectional steel sliding bearing devices, 4 m apart. The bearing devices have a circular contact surface, with a 910 mm diameter on piers P1 and P4, and a 1300 mm diameter on piers P2 and P3, and include an antifriction layer in XLIDE material. Figure 3.7 shows the design drawings of the bearings on piers P2 and P3, as well as the description of the components and materials of each layer.

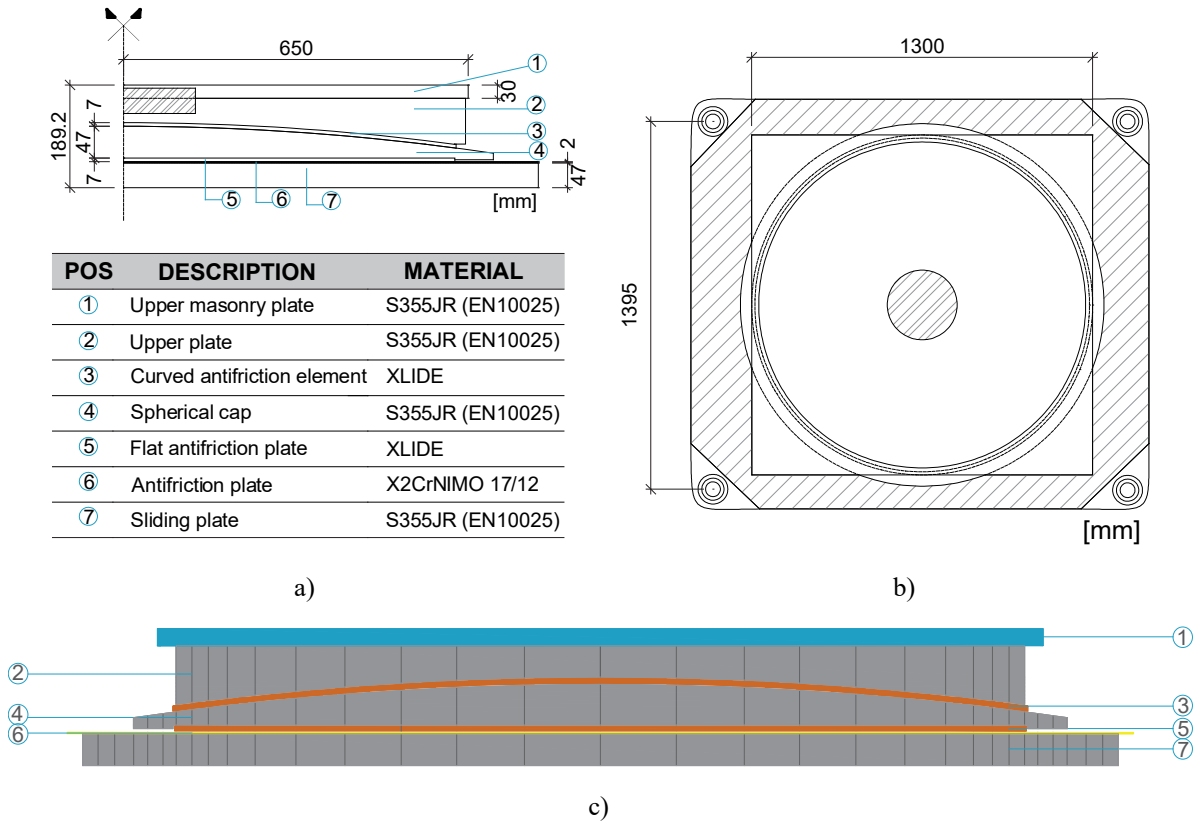| POS	DESCRIPTION	MATERIAL
①	Upper masonry plate	S355JR (EN10025)
②	Upper plate	S355JR (EN10025)
③	Curved antifriction element	XLIDE
④	Spherical cap	S355JR (EN10025)
⑤	Flat antifriction plate	XLIDE
⑥	Antifriction plate	X2CrNIMO 17/12
⑦	Sliding plate	S355JR (EN10025)

a) b)

c)

Figure 3.7 - Design drawings of piers P2/P3: a) half of the bearing lateral view, b) floor plan of the bearing, c) schematic representation of the bearing (adapted from GRID et al. (2006)).

3.3   MONITORING SYSTEM

Immediately after construction, the modal properties of the bridge, namely its natural frequencies, mode shapes and damping coefficients, were assessed through an Ambient Vibration Test (AVT). In addition, the structural condition of the railway bridge over the Sado River was monitored through periodic visual inspections, and using a monitoring system defined with the objective of controlling the global stiffness of the bridge and the global longitudinal internal forces, as well as the behaviour of its special devices, such as the bearings, to the important actions of temperature and railway traffic. As this is a single-plane bowstring-arch structure, the important torsional effect resulting from train loading on only one side of the girder, was also taken into account, insofar as the sensors were eccentrically positioned in order

to monitor not only the effects due to bending but also the torsion of the structure. Between 2011 and 2016, the system consisted of static measurements of strain, temperature, and displacement, whose responses were evaluated every hour. In 2017 an upgrade of the monitoring system was implemented to allow for a better characterization of the dynamic response of the bridge. This upgrade consisted of additional dynamic measurements using accelerometers located on the top of each pier and along the deck, to take advantage of the excitation induced by the several trains that cross the bridge every day.

The following subsections describe the different phases of the structural monitoring of the bridge, including the system's architecture, the sensors' network and the analysis of data acquired over the years.

3.3.1 Architecture

3.3.1.1 Software components

The architecture of the monitoring system followed the aim of a real-time SHM with permanent availability of data. As shown in Figure 3.8, the acquisition and management system of the bridge over the Sado River is highly distributed, being located in four distinct hardware components. First, the signals from the transducers are acquired through local data acquisition units, which then transfer the data to an industrial computer located on the bridge. In turn, this component sends the data to the management server using a VPN (Virtual Private Network) protocol. Once the data is stored on the database server, it can be accessed by the users.
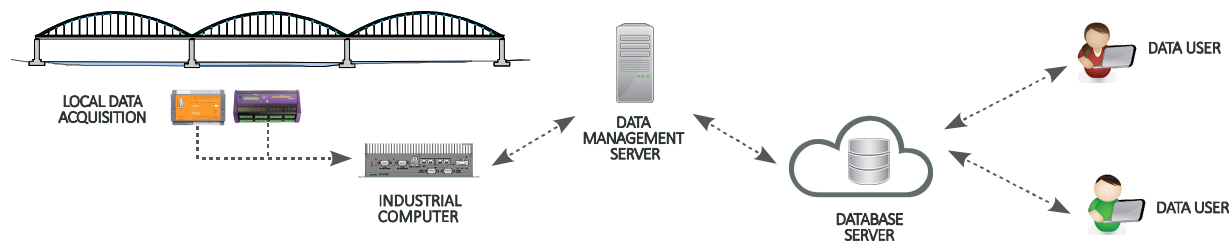
Figure 3.8 - Architecture of the monitoring system.

3.3.1.2 Hardware components

The hardware of the online structural monitoring system is defined bearing in mind the sensor's location and the acquisition of the data with minimum ambient noise. Figure 3.9 shows examples of the main hardware components installed on site and Figure 3.10a summarizes the sparse distribution of the acquisition units and the programmable automate controllers (PAC).

As it is possible to observe, the network of acquisition units tries to maximize the length of digital signal transport and minimize the analogue, resulting in high measuring sensitivity. The electrical supply is ensured by IP (Infraestruturas de Portugal, S.A. – the road and railway infrastructure manager) at the main points needed, as outlined in Figure 3.10b.

The communication between the several units installed in the bridge over the Sado River is based on Ethernet and RS-485 networks. The first one enables the communication between each PAC unit and the industrial computer, while the second one establishes the connection between the "fast" PAC units and their input boards. Nine PAC are deployed on the main acquisition points of the bridge. The four "slow" PAC units are located in the central span, as the five "fast" PAC are in the central span and at mid of the first and third spans.

To allow overcoming the long distances between the sensors and PAC units without loss of information, and to guarantee better protection against electromagnetic interference, an eight optical fibres cable connects the several PAC units.
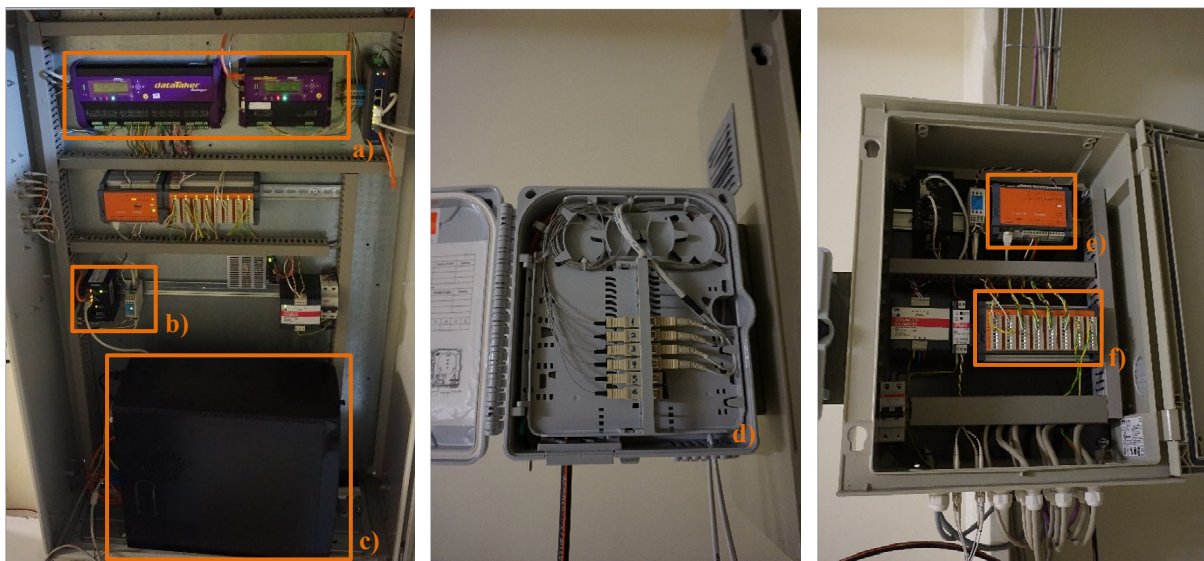

Figure 3.9 - Data acquisition hardware installed in the bridge over the Sado River: a) "slow" PAC, b) Ethernet / fibre converter, c) industrial computer, d) optical fibre connection box, e) "fast" PAC, f) "fast" input board.
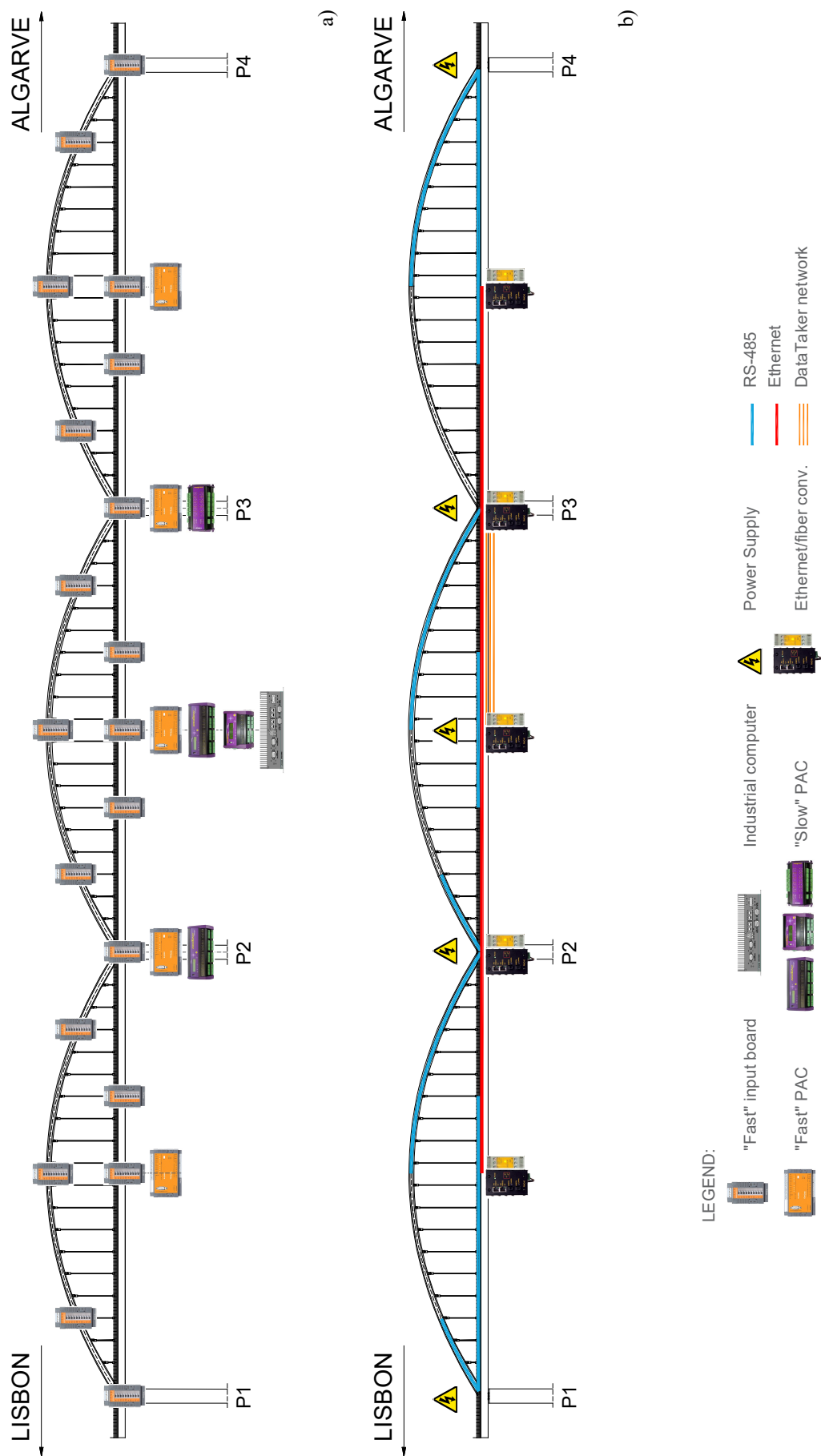
Figure 3.10 - Hardware components installed in the bridge over the Sado River: a) acquisition and processing, b) communication and supply.

3.3.2 Ambient vibration test

3.3.2.1 Description

The AVT was held immediately before the structure entering into operation and covered 25 sections of the deck and 12 sections of the arches, as indicated in Figure 3.11. The measurements were performed by means of fixed references and mobile measuring points, with a total of 15 uniaxial EpiSensor (ES-U) force balance accelerometers, from Kinemetrics. The ambient vibration response was evaluated in 8 successive setups by measuring: i) vertical accelerations on the downstream side of the slab; ii) vertical and transverse accelerations on the upstream side of the slab; iii) longitudinal accelerations at locations 2, 3, 17, 18, 32 and 33; iv) vertical and transverse accelerations in the arches, and v) vertical and longitudinal accelerations over the bearings. The ambient vibration data was continuously acquired at 500 Hz for approximately 30 minutes during each setup. The measurements were made with a precision of ± 2 µg (Min & Santos, 2011).
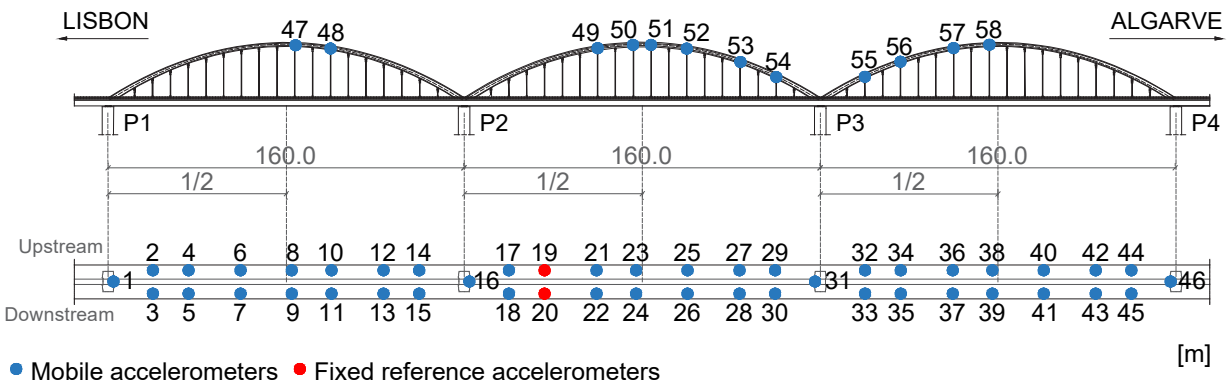
Figure 3.11 - Measuring points of the ambient vibration test.

3.3.2.2 Results

The AVT allowed the identification of the modal properties of the bridge to establish a baseline condition, comprising 22 vibration modes, characterized by their frequencies, mode shapes and damping coefficients. This identification was performed by applying the Enhanced Frequency Domain Decomposition method (EFDD), available in the ARTeMIS software (SVS, 2005) (Min & Santos, 2011). Figure 3.12 shows the curves of the average normalized singular values of the spectral density matrices. Five lateral modes of the arches are outlined on the first curve (Figure 3.12a), as well as sixteen vertical vibration modes associated with the deck and arches on the second curve (Figure 3.12b), and one longitudinal mode of the deck on the third

curve (Figure 3.12c). The first 10 of the 22 mode shapes, frequencies and damping coefficients experimentally identified are plotted in Figure 3.13.
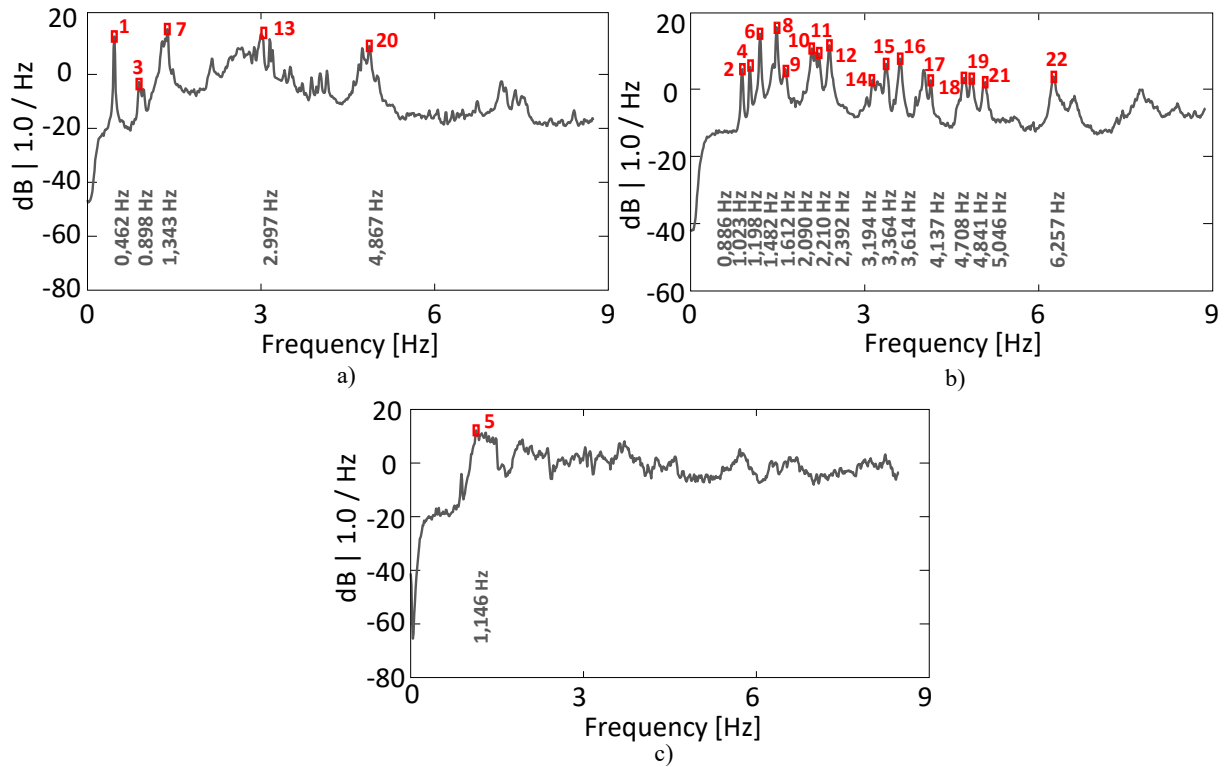
Figure 3.12 - EFDD method: average normalized singular values of the spectral density matrices: a) lateral modes of the arches, b) vertical modes of the deck and the arches, c) longitudinal mode of the deck (Min & Santos, 2011).

Mode 1 | 1st Lateral – Arches | f = 0.462 Hz | ξ = 1.45 %

Mode 2 | 1st Vertical | f = 0.886 Hz | ξ = 1.18 %

Mode 3 | 1st Lateral - Arch & Deck coupled | f = 0.898 Hz | ξ = 1.12 %

Mode 4 | 2nd Vertical | f = 1.023 Hz | ξ = 1.02 %

Mode 5 | 1st Longitudinal | f = 1.146 Hz | ξ = 2.52 %

Mode 6 | 3rd Vertical | f = 1.198 Hz | ξ = 0.78 %

Mode 7 | 2nd Lateral - Arches | f = 1.343 Hz | ξ = 1.09 %

Mode 8 | 4th Vertical | f = 1.482 Hz | ξ = 0.62 %

Mode 9 | 5th Vertical | f = 1.612 Hz | ξ = 1.31 %

Mode 10 | 6th Vertical | f = 2.09 Hz | ξ = 0.77 %

Figure 3.13 - Experimental mode shapes, natural frequencies and damping coefficients (Min & Santos, 2011).

3.3.3   Static monitoring

3.3.3.1 Description of the sensors network

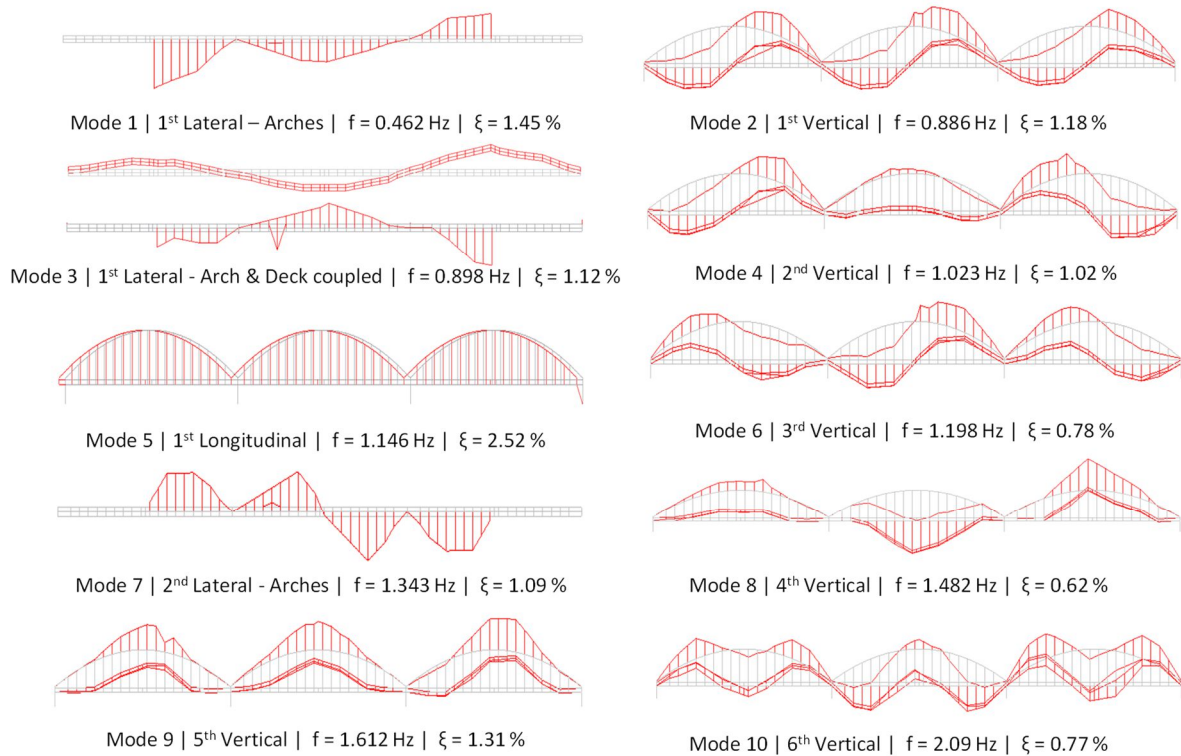The first phase of the bridge monitoring, carried out between 2011 and 2016, consisted of the installation of a system that is mainly concerned with monitoring the stress on the arches and on the deck, as shown in Figure 3.14. Figure 3.15 to Figure 3.17 show the scheme and details of the instrumented sections. The structural temperature action was measured using NTC thermistors and PT100 thermometers. Twelve NTC thermistors were installed in three sections of each arch, as outlined in Figure 3.15a,b. Additionally, measurements were also taken from four NTC thermistors fixed to the steel box girder and three PT100 sensors embedded in the concrete slab, as illustrated in the cross-section of Figure 3.16a. Regarding the stress measurements, responses were obtained from the electrical resistance strain gauges installed as a full Wheatstone bridge in the arches (Figure 3.15c) and fixed to the steel box (Figure 3.16b,c). To control the increased friction in the bearings, the responses measured by a longitudinal displacement transducer installed at pier P4 (Figure 3.17) were evaluated.
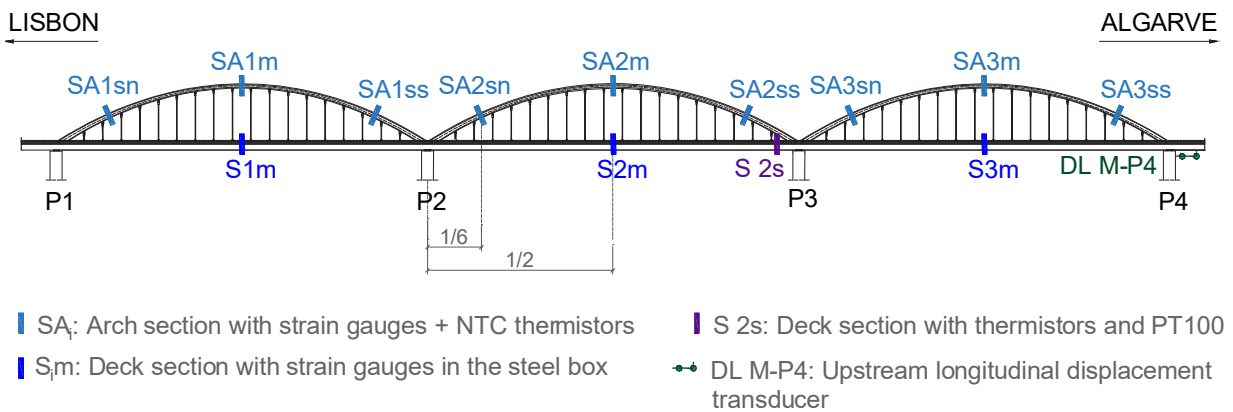

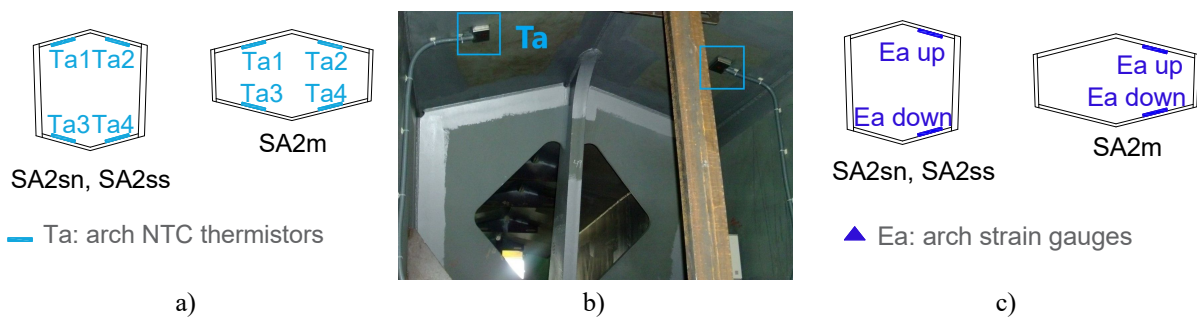Figure 3.14 - Sensors installed for static measurements.

Figure 3.15 - Arch sections: a) NTC thermistors (Ta) location, b) NTC thermistors (Ta) installation, c) strain gauges (Ea) location.
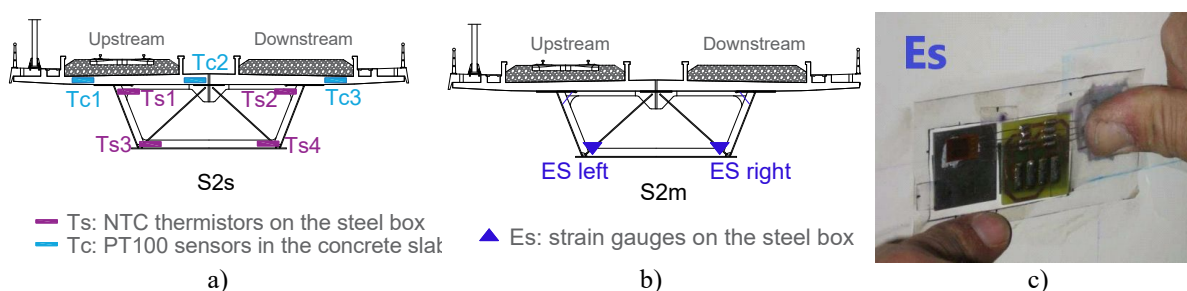
Figure 3.16 - Bridge cross section: NTC thermistors in the steel box (Ts) and PT100 sensors in the concrete slab (Tc), b) strain gauges on the steel box (Es), c) electric strain gauge (Es) installation.

Figure 3.17 - Longitudinal displacement transducer (DL): a) cross section location, b) sensor installation.

3.3.3.2 Data analysis

Between 2011 and 2016, visual inspections allowed observing, for the bearing devices located on piers P2 and P3, excessive deformations of the spherical cup (Figure 3.18a), excessive relative displacements between the upper plate and the spherical cup (Figure 3.18b) and an apparently insufficient thickness of the sliding element (XLIDE) located between the upper plate and the spherical cup (Figure 3.18c). These findings suggested that the bearings were not fully unrestrained and could result in increased friction between the piers and the deck.

Figure 3.18 - Information obtained from visual inspections carried out on the bearings of piers P2 and P3 of the bridge over the Sado River.

However, as observed in Figure 3.19, the static-based global monitoring was not specifically tailored to capture these slight changes in the behaviour of the bridge. This figure shows the evolution of the longitudinal displacements of the bearings on pier P4, the only one comprising

dedicated sensors at that time, along with the temperatures measured on the arch (upper fiber – Ta1, and bottom fiber – Ta2), steel box (Ts3) and concrete slab (Tc2), between November 2011 and November 2016. Comparing the two plots, it is possible to observe that the longitudinal displacement is characterized by a long-period cycle directly related with the annual temperature variation. Therefore, there is a direct correlation between the expansion and contraction of the bridge and the seasonal variation of the temperature. Moreover, no deviations or unexpected variations are identified, suggesting that the changes on the bearings of piers P2 and P3 did not influence the overall response of the bridge measured between the deck and pier P4.

a)

b)
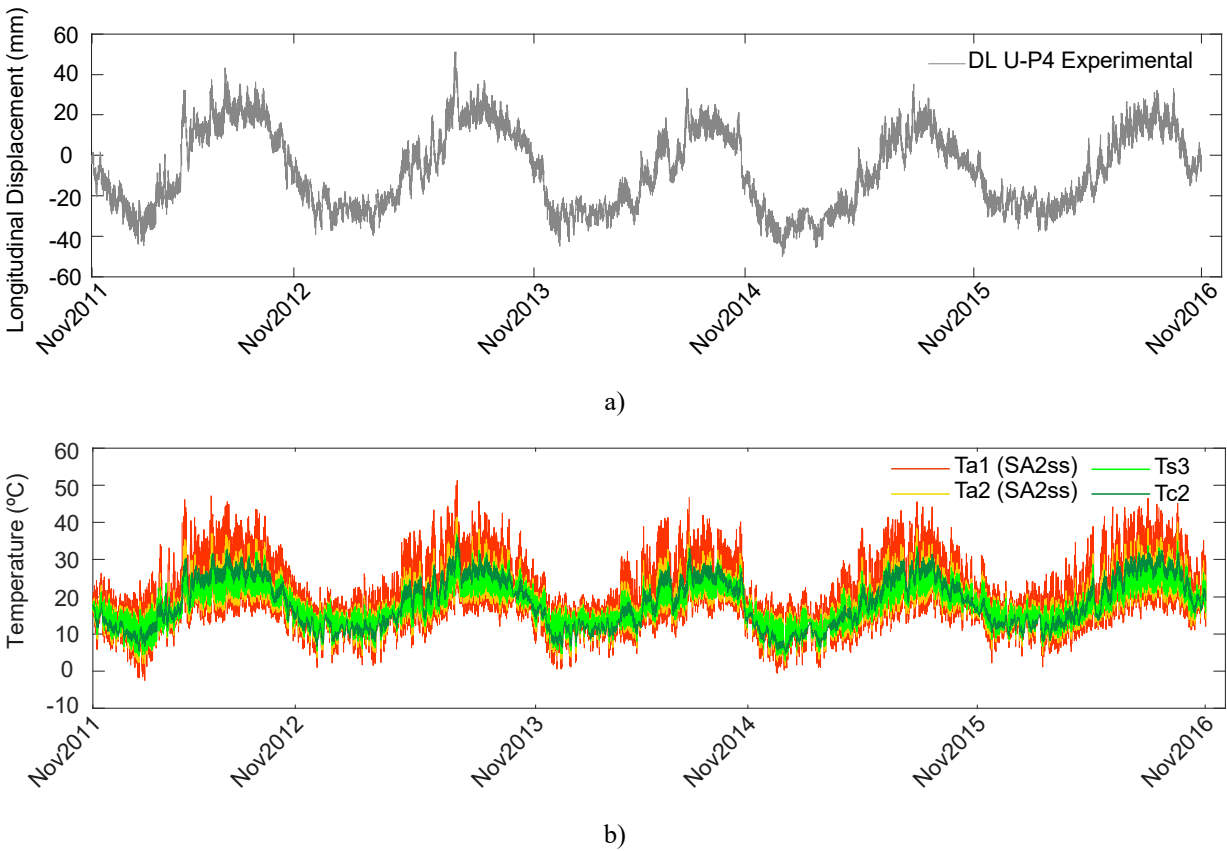
Figure 3.19 - Data acquired between November 2011 and November 2016: a) longitudinal displacements of the upstream bearing located on pier P4 and b) temperature measurements on the middle arch (Ta1 and Ta2), steel box (Ts3) and concrete slab (Tc2).

Although visual inspections suggested changes in the behaviour of the bearing devices, it was not possible to estimate their exact time frame. Therefore, these observations led to the conclusion that more sensors needed to be installed, specifically in the bearings that presented structural changes, and, above all, that the migration from static to dynamic monitoring is of the utmost importance in order to take advantage of the excitation induced by the several trains that cross the bridge every day.

3.3.4 Dynamic monitoring

3.3.4.1 Description of the sensors network

In 2017 an additional set of transducers was installed on the bridge over the Sado River (Figure 3.20a), mainly for the dynamic measurement of accelerations. This new set included two pairs of optical sensors, model E3SAT31, at both ends of the bridge, to capture the speed of the trains and carry out the detection of the axles and four longitudinal MEMS DC accelerometers, model PCB 3711E112G, on the piers between the bearings (Figure 3.20b). The set of sensors also comprised one vertical piezoelectric accelerometer, model PCB 393A03, fixed at mid-span of the concrete slab, two triaxial EpiSensors (ES-T) force balance accelerometers at thirds of the mid-span steel box girder, and twelve vertical EpiSensors (ES-U) force balance accelerometers fixed along each span of the steel box girder (Figure 3.20c). Measurements of the longitudinal displacement transducers were also acquired from sensors adjacent to each of the eight bearing devices (Figure 3.20b).

● Ac: Vertical accelerometer at the concrete slab   ● Al-P: Longitudinal accelerometer between bearings
● AsV: Vertical accelerometer on the steel box   ↔ DLU-P: Upstream longitudinal displacement transducers
● AsT: Triaxial accelerometer on the steel box   ↔ DLD-P: Downstream longitudinal displacement transducers
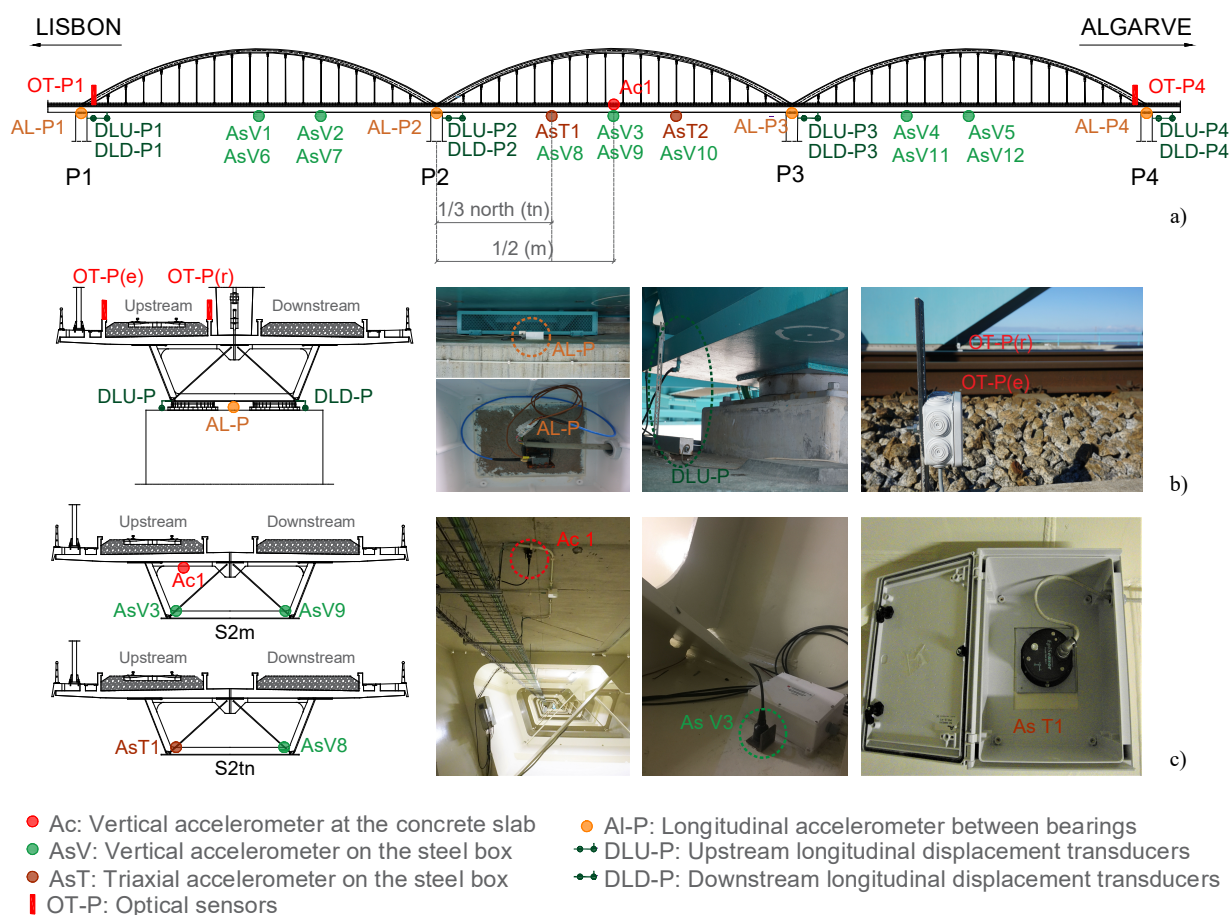❚ OT-P: Optical sensors

Figure 3.20 – Dynamic monitoring system installed in the railway bridge over the Sado River: a) overview, b) longitudinal accelerometer, displacement transducer, and optical sensor, c) triaxial and vertical accelerometers.

Unlike the static data acquisition system, which saves measurements every hour, this system acquires the responses of the bridge continuously, in order to save the time history while the train is crossing the bridge, at a sampling rate between 500 Hz and 2000 Hz depending on the aliasing requisites.

3.3.4.2 Data analysis

In order to assess the evolution of the friction coefficient of the bearings, an analysis of the data acquired continuously on piers P2, P3 and P4 was conducted using longitudinal accelerometers and longitudinal displacement transducers.

Figure 3.21a presents the analysis of the behaviour of the bearings on each pier for a period of 24 hours. The bearing response depends on the combined action of a vertical load (FN) and a horizontal load (FH). For a friction coefficient μ, the bearing will slide if the criteria of yielding (FH = μ|FN|) is verified. The sliding of the bearing varies depending on the temperature and the train-induced vibration applied at a specific instant. The longitudinal accelerations shown in Figure 3.21a allow observing that 17 trains crossed the bridge over the Sado River on December 2, 2016. The amplitude of these responses varies, depending on the type of train. Furthermore, the responses measured by the accelerometer on pier P4 display higher amplitudes, when compared with the ones on piers P2 and P3. A direct correspondence can also be observed between the acceleration measurements for each train that crossed the bridge and the displacement of the upstream bearing on pier P4, highlighted by dashed lines. During the observation period shown in Figure 3.21a, the bearing on pier P4 slides in one direction in the morning, in the opposite direction in the afternoon, and changes direction again during the night. This behaviour is clearly influenced by the variation of the structure's temperature throughout the day. Due to the sun exposure of the bridge, the upper fibre of the arch (Ta1) presents the greatest temperature variation. On the other hand, the transducers located on the bearings of piers P2 and P3 recorded near-null longitudinal displacements during the passage of all trains.

Each plot of Figure 3.21a comprises a dashed window highlighting the responses acquired between 9 and 10 am, shown in Figure 3.21b. Over the course of this one-hour window, all longitudinal accelerometers recorded amplified responses during the passage of 2 trains. The upstream bearing on pier P4 systematically slides when a train is passing, always in the same direction but with different amplitudes. It is not possible to observe the influence of temperature on the behaviour of the bearing here, but it is easier to identify the bearing displacement caused

by a passing train. However, the bearings on piers P2 and P3 show near-null values during the passage of the same trains, which corroborates the conclusions obtained in the visual inspections. In addition, it can be observed that during this hour the temperatures in the steel box (Ts3), in the concrete slab (Tc2) and in the middle arch (Ta1-upper fibre and Ta2 - bottom fibre) are practically stable.
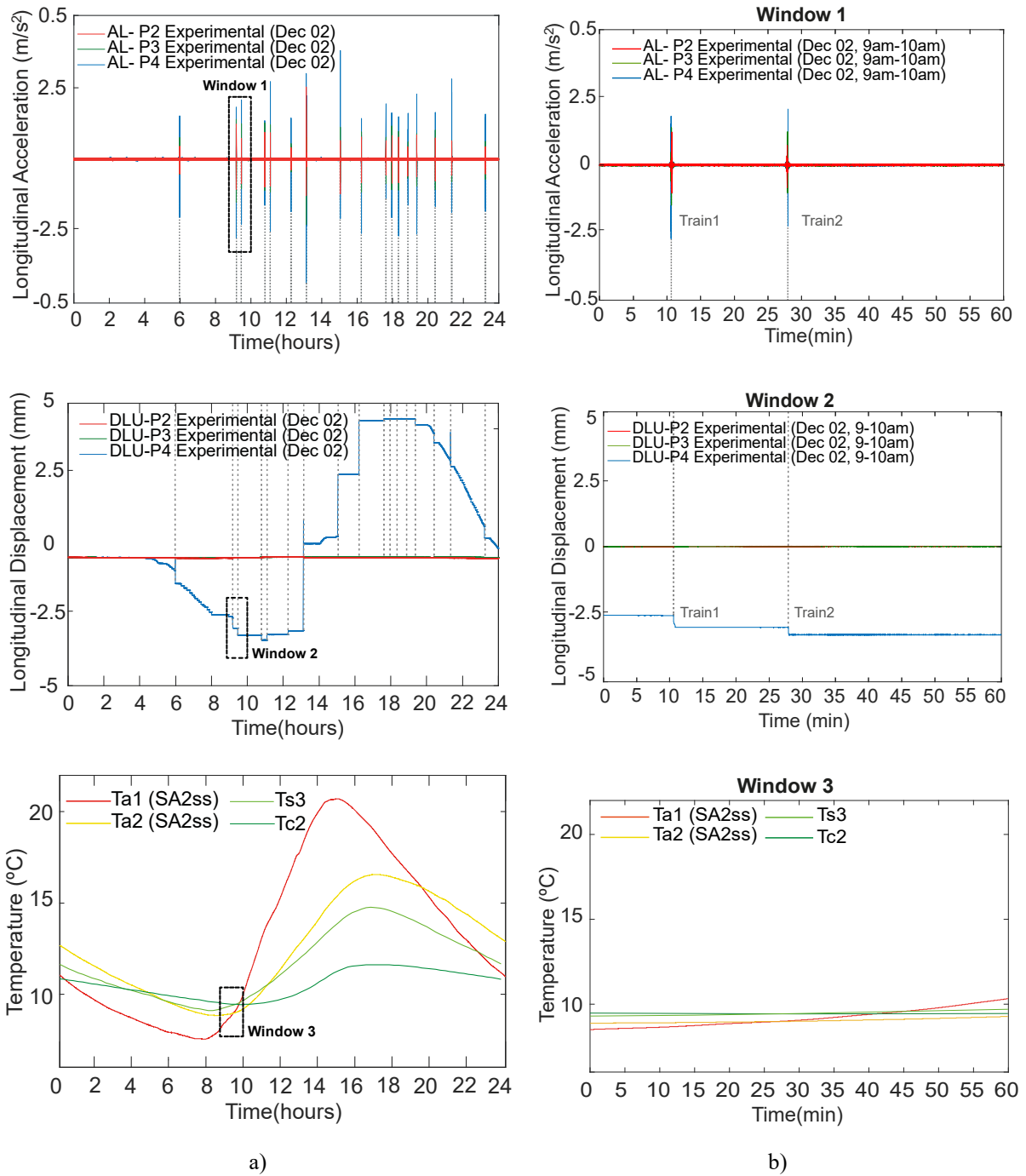

a)

b)

Figure 3.21 - Analysis of the longitudinal accelerations and displacements on piers P2, P3 and P4, and the temperature of the structure measured on December 2, 2016: a) for 24 hours and b) for 1 hour.

This analysis allowed observing the combined actions of temperature and train-induced vibration in the bearing devices. It is possible to conclude that the static deformation imposed to the bearing devices by the temperature is more preponderant than the dynamic longitudinal displacement inflicted by a passage of a train. The degradation of the friction coefficient alters the behaviour of the bearing, which can lead to the full restraint of its movements, as verified in piers P2 and P3. It was found that a dynamic monitoring system has the advantage of detecting bearing defects based on the excitation induced by passing trains. With the passage of several trains, the diagnosis can be validated, and false positives can be dismissed in a short period of time.

3.4 CONCLUDING REMARKS

This chapter presented the case study used throughout this work and addressed the implementation of a progressively phased in-situ structural monitoring system. The case study is the long-span bowstring-arch railway bridge over the Sado River comprising an extensive network of sensors, which have provided a diverse set of data streams ranging from static and dynamic responses to the measurement of environmental and operational traffic loads.

By analysing experimental data from the ambient vibration test and static monitoring, it was possible to estimate the modal parameters, as well as the responses to important slow actions, such as temperature. However, the experimental information alone did not enable the identification of changes in the behaviour of the bearing devices, which were suggested by visual inspection.

On the other hand, it was concluded that a continuous dynamic monitoring based on the analysis of traffic loading allowed the identification of changes in the structural responses and pointed out the existence of restraints in the movements of the bearing devices on piers P2 and P3.

Using the comprehensive set of sensors that result from this operational evaluation and data acquisition, the structural health condition of the railway bridge over the Sado River can be continuously monitored and, the traffic-induced responses can be used to implement a damage identification methodology.

Chapter 4

NUMERICAL MODEL VALIDATION OF A BOWSTRING-ARCH RAILWAY BRIDGE[*]

4.1 INTRODUCTION

To obtain different damage scenarios in civil engineering structures, especially bridges, that allow to test and validate the damage identification methodologies developed, is particularly difficult. Since, also in this case study, it was not possible to obtain such conditions experimentally, a digital twin of the bridge over the Sado River was implemented.

This chapter presents a progressive numerical model validation of the bowstring-arch railway bridge over the Sado River based on the analysis of experimental data from different structural response measurements, namely, static deformations under environmental actions, modal vibrations, and transient dynamic responses under traffic loads. This chapter also addresses an integrated approach that uses SHM measurements in combination with finite element (FE) modelling to understand the structural behaviour of a long-span complex bridge.

The first phase consists of defining a detailed baseline FE model of the bridge, envisaging the initial condition of the structure immediately after construction, and its validation using

modal parameters (natural frequencies and mode shapes) derived from the AVT. Since overall in-service deflections in general do not exercise the non-linear regime of the bridge response, the second phase focuses on the analysis of static response data and temperature measurements to validate the non-linear behaviour of the structural system, particularly at the bearing devices, under slow actions. The third and final phase addresses the dynamic analysis under traffic actions, which provides greater sensitivity in the detection of non-linear behaviour due to the effects of high amplitude actions induced by regular train loading profiles. To guarantee the accuracy of the baseline numerical model, particularly under temperature and traffic actions, it was necessary to use contact restrictions in some specific bearing devices. This improvement is in line with the structural changes detected in some bearing devices through visual inspections.

As a result, an updated numerical model capable of reproducing the modal, static, and dynamic structural responses was achieved. This progressively stepped validation will increase the reliability of the numerical model, envisaging further uses, such as condition assessment, simulations under extreme loading scenarios, evaluation of safety and serviceability or risk analysis. Such capabilities ultimately begin to realize the concept of a digital twin for the structure.

After the introduction, section 4.2 describes the numerical model and explains the details of the non-linear analyses. Afterwards, in section 4.3, the validation of the numerical model is presented with the simulation of the responses to ambient vibration, environmental actions and traffic loads, considering abnormal restrains observed in the bearing devices of the bridge. Finally, section 4.4 lists the concluding remarks obtained with the work from the present chapter, along with the main achievements.

4.2 NUMERICAL MODELLING

4.2.1 Description

A 3D finite element numerical model of the bridge was developed in the ANSYS (2016) software. The deck, hangers and arches were previously modelled by Albuquerque et al. (2015). The assessment of the structural changes discussed in Chapter 3 led to the need to develop a numerical model that accurately simulates the longitudinal response of the bridge and the non-linear behaviour of the bearings. For that purpose, the upgraded numerical model developed

in the present study also includes the track, the bearing devices, the piers and the foundations, as shown in Figure 4.1.

a)

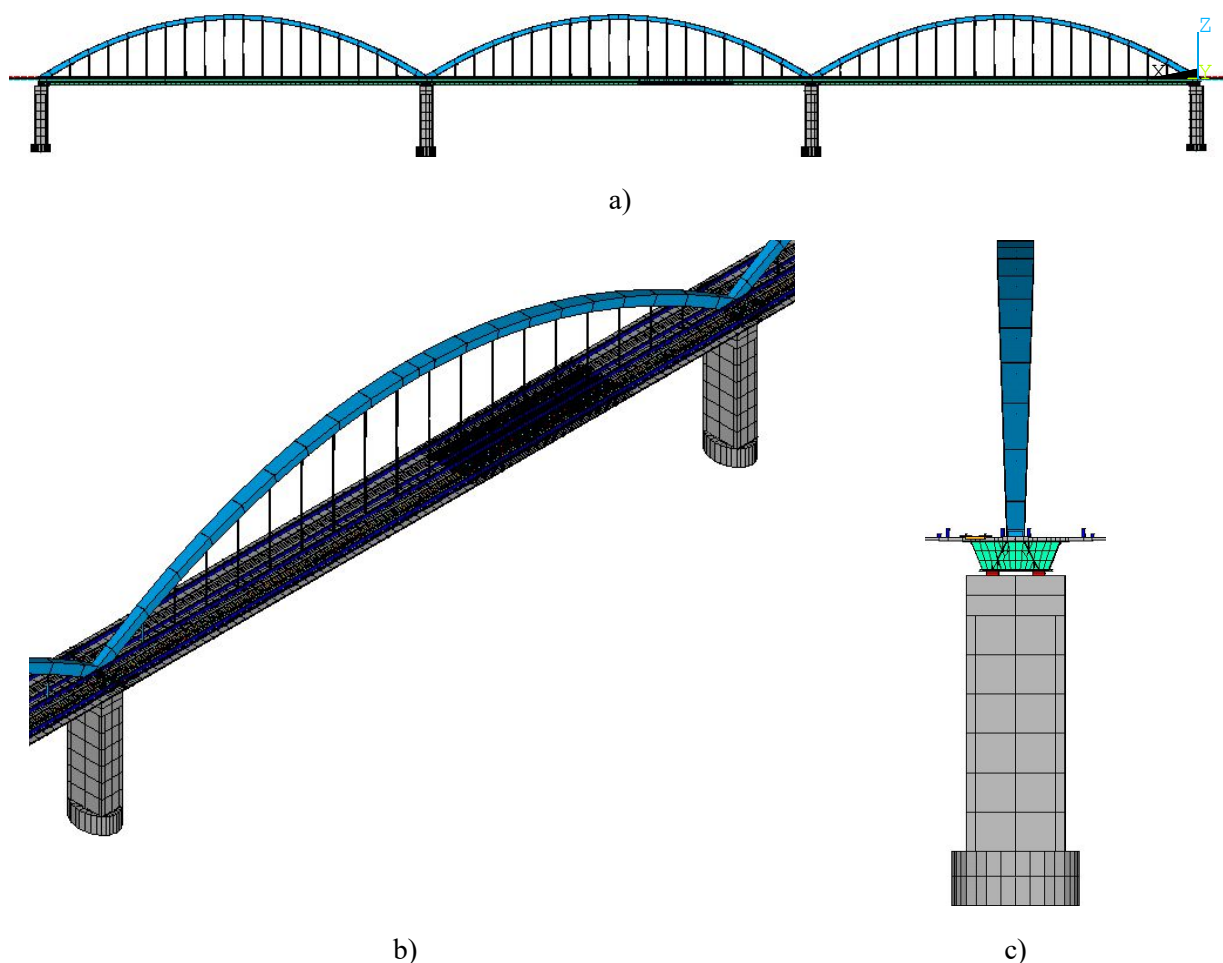b)   c)

Figure 4.1 - 3D numerical model of the railway bridge over the Sado River: a) lateral view, b) middle span detail, c) front view.

Among the modelled structural elements, those defined as beam finite elements consist of piers, sleepers, ballast-containing beams, rails, arches, hangers, transverse stiffeners, diaphragms and diagonals. Shell elements were used to model the concrete slab and the steel box girder, while the pads, the ballast layer and the foundations were modelled using linear spring-dashpot assemblies. The mass of the non-structural elements and the ballast layer was distributed along the concrete slab. Concentrated mass elements were used to reproduce the mass of the arches' diaphragms and the mass of the sleepers, which were simply positioned at their extremities. The connection between the concrete slab and the upper flanges of the steel box girder, as well as the connection between the deck and the track, were performed using rigid links. Special attention was paid to the bearing devices, as they can strongly influence the performance of the bridge. Hence, in order to simulate the sliding behaviour of the bearings,

non-linear contact elements were applied. Moreover, constraint elements located between the bearings were used to restrict the transversal movement in each pier, and the longitudinal and transversal movements in the case of the first pier. It is worth mentioning that the seismic dampers were not modelled, as they are not activated during serviceability loads, such as the ones caused by passing trains or environmental actions. Figure 4.2 illustrates a schematic representation of the numerical model highlighting the different types of finite elements that were used.
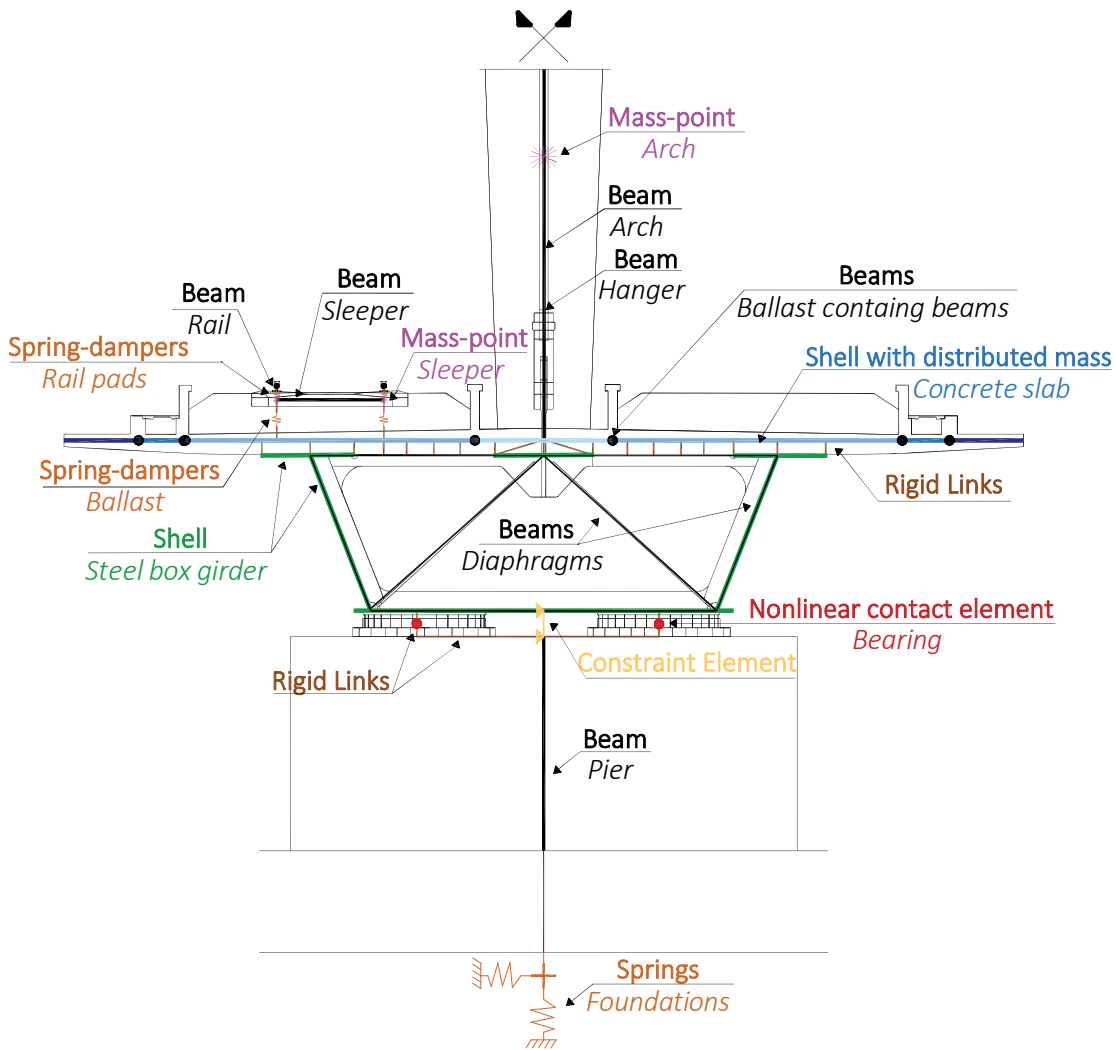
Figure 4.2 - Schematic cross-section representation of the FE numerical model.

A mesh of elements with a discretization of less than 2 m in the longitudinal direction was adopted for most of the deck. However, a more refined mesh was defined at the central third of the central span for a more precise characterization of the dynamic responses under traffic loads (Figure 4.3b). To ensure a correct representation of the transition zones between the structure and the embankment, an extension of the track and sleepers, spaced 0.6 m, was modelled at both

ends of the bridge (Figure 4.3a). The numerical model of the bridge includes 25924 nodes and 38620 finite elements.

a)　　　　　　　　　　　　　　　　　　　　　b)

Figure 4.3 - Details of the numerical model: a) transition zone, b) refined mesh in the second span.
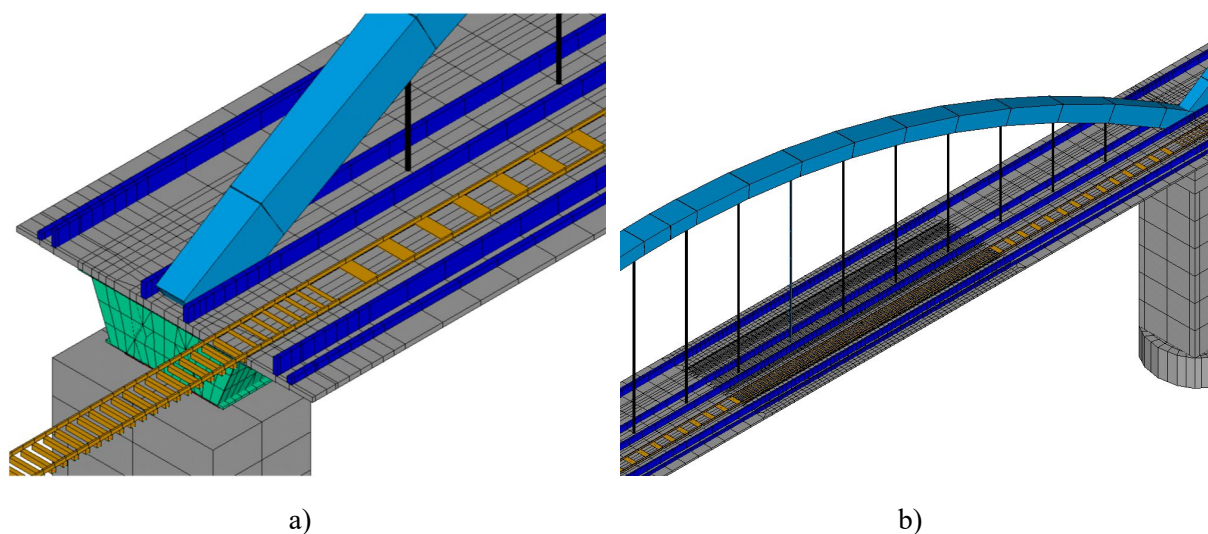
4.2.2　Geometrical and mechanical properties

The following subsections present a detailed explanation of the main geometrical and mechanical parameters of the different structural components of the numerical model.
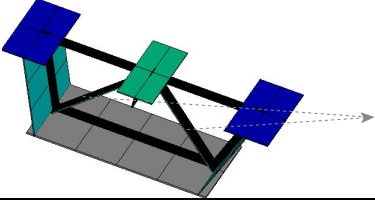
4.2.2.1　Superstructure
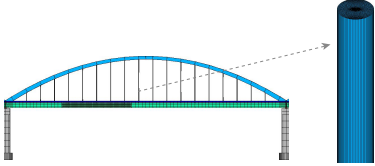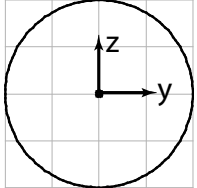
The steel of the deck was defined with a modulus of elasticity of 210 GPa, a Poisson's ratio of 0.3 and a density of 7850 kg/m^3, while the concrete slab was defined with a density of 2500 kg/m^3, a Poisson's ratio of 0.15 and a modulus of elasticity of 43 GPa, based on the updated model presented by Albuquerque et al. (2015).

The mass of the non-structural elements and of the track ballast is distributed in the sections of the concrete slab emphasized in Figure 4.2. The values considered in each section are summarized in Table 4.1. The diagonal elements located in each diaphragm have the geometrical properties specified in Table 4.2. The arches were composed of variable cross-sections, with varying thickness, width and height, both of flanges and webs. Their geometric and mechanical characteristics were reproduced in the numerical model along with the nodal masses added to the hanger-to-arch connections, which replicate the diaphragms built in those locations. Regarding the hangers, their cross-sections consist of a circumference with a 200 mm diameter and the properties presented in Table 4.2. Both the arches and the hangers were modelled in steel with the same characteristics as the one used in the deck box girder.

Table 4.1 - Distributed mass regarding the track ballast and non-structural elements of the deck's slab.

SECTION	MASS (kg/m³)	DESCRIPTION
	190	Concrete slab covering (waterproofing, light concrete and screed)
	1121	Track ballast and concrete slab covering
	77	Prefabricated concrete slab
	735	Lightweight concrete and metallic bridge-rail

Table 4.2 - Geometrical parameters of the diagonals of the diaphragms and hangers.

NUMERICAL MODEL DETAIL	CROSS-SECTION	GEOMETRICAL PROPERTIES
		$A = 0.035 \times 0.60 = 0.021$ m² $I_y = 0.214\text{E-}05$ m⁴ $I_z = 0.630\text{E-}03$ m⁴ $J = 0.828\text{E-}05$ m⁴
		$A = 3.14\text{E-}02$ m² $I_y = 7.85\text{E-}05$ m⁴ $I_z = 7.85\text{E-}05$ m⁴ $J = 1.57\text{E-}04$ m⁴

4.2.2.2 Bearings

The bearing devices were modelled using non-linear contact elements CONTA178 (ANSYS, 2016). These elements allow contact and sliding between any pair of nodes, and are able to withstand compression forces normal to their plane and friction forces along the tangential directions based on the Coulomb model. Their friction coefficient µ was defined as 1.5% during the numerical analysis, based on the specifications of the design (REFER, 2010).

As observed in Figure 4.4, the force deflection relationships for the contact element were separated in the normal and tangential (sliding) directions. In the normal direction, when the normal force (FN) is negative, the contact status remains closed. In this circumstance, in the tangential direction, if the absolute value of the tangential force (FS) is below µ|FN|, the contact element works as a linear spring; otherwise, if FS = µ|FN|, sliding will occur. As FN becomes positive, the contact is broken and no force is transmitted (FN = 0, FS = 0). This non-linear contact problem is solved by the Penalty method (Mijar & Arora, 2000).
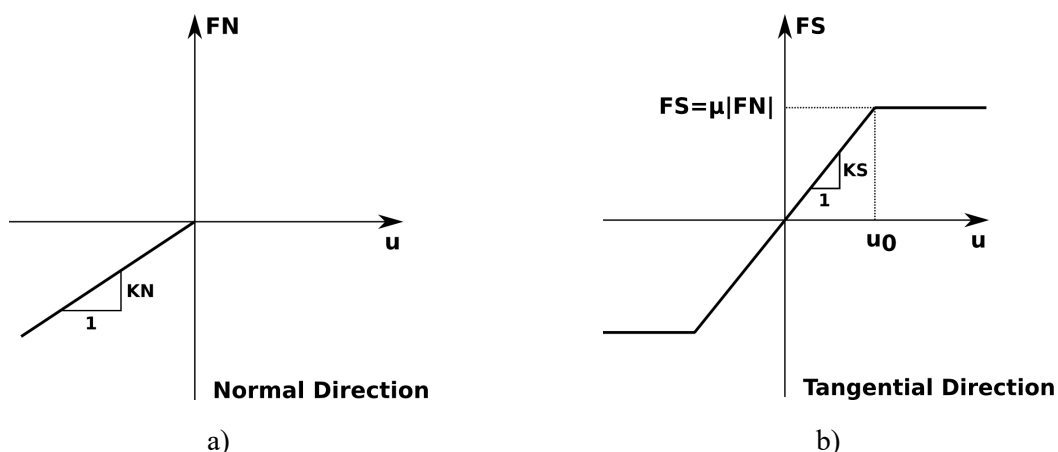
Figure 4.4 - Force-deflection relationship of the contact element: a) normal direction, b) tangential direction.

4.2.2.3 Substructure

The piers are composed of three different types of reinforced concrete cross-sections, namely, a solid rectangular section, a rectangular hollow-section, and an elliptical hollow-section. The geometric properties of each section are presented in Table 4.3. The two central piers were modelled with the same height (25.72 m), while the first and fourth are slightly shorter (23.10 m and 23.68 m, respectively). The piers were modelled using a concrete with a density of 2500 kg/m^3, a Poisson's ratio of 0.15 and a modulus of elasticity of 43 GPa.

Table 4.3 - Geometrical properties of the piers.

NUMERICAL MODEL DETAIL	CROSS-SECTION	GEOMETRICAL PROPERTIES
		A = 44.20 m^2 I_y = 99.60 m^4 I_z = 266.12 m^4 J = 250.81 m^4
		A = 19.36 m^2 I_y = 72.77 m^4 I_z = 167.57 m^4 J = 164.50 m^4
		A = 42.74 m^2 I_y = 234.78 m^4 I_z = 406.44 m^4 J = 560.07 m^4

The boundary conditions were modelled using the results obtained from *in-situ* geotechnical tests conducted during the construction of the bridge (REFER, 2010). The Standard Penetration

Test (SPT) was done twice on each pier, while the Crosshole Test was specifically conducted on pier P3. Table 4.4 summarizes the *N-values* of the SPT and the shear wave velocity of the soil (V_s) obtained from the *in-situ* tests previously mentioned, together with the classification of the soil resulting from the laboratory analyses of the samples collected during the same tests.

Table 4.4 – Geotechnical properties at each pier location.

Depth (m)	P1 Soil Classif.	P1 N (SPT)	P1 $K_{average}$ (kN/m)	P2 Soil Classif.	P2 N (SPT)	P2 $K_{average}$ (kN/m)	P3 Soil Classif.	P3 N (SPT)	P3 Vs (m/s) CrossHole	P3 $K_{average}$ (kN/m)	P4 Soil Classif.	P4 N (SPT)	P4 $K_{average}$ (kN/m)
2		0			0			0	58			0	
3		0			0			0	58			0	
4		0			0			0	59			0	
5		0			0			0	59			0	
6		0			0			0	63			0	
7		0			0			0	61			0	
8		0			0			0	64		OH	0	6.83E+03
9		0		OH	0	7.22E+03		0	64			0	
10	OH	0	7.75E+03		0		OH	0	63	6.22E+03		0	
11		0			0			0	64			0	
12		0			0			0	66			0	
13		0			0			0	66			0	
14		0			0			0	67			0	
15		0			1			0	67			0	
16		0			1			0	68			32	
17		0			20			0	67			32	
18		6			24			0	65		SP	19	5.18E+04
19	SP	30	5.51E+04		24			0	66			19	
20		30		SP	26	5.84E+04		3	156			6	
21	CH	30	5.51E+04		21		SP	13	157	4.44E+04		11	
22		30			21			13	132			11	
23		60			58			9	169			11	
24		60			52			60	158		CH	11	4.49E+04
25		60			37			60	181			14	
26		60			37			38	167			14	
27		60			48			60	168			52	
28		60			48			60	184			52	
29		60	7.21E+04		42			60	185	7.02E+04		52	
30		60			42	6.77E+04		60	188			31	
31		60			42			60	185			31	7.75E+04
32	SM	60			48		SM	60	148			60	
33		60		SM	50			60	152			60	
34		60			51			60	149		SM	60	
35		60			60			60	143			60	
36		60			60			60	400			60	
37		60			60			60	674			60	
38		60	1.05E+06		60	1.05E+06		60	704	1.07E+06		60	1.05E+06
39		60			60			60	740			60	
40		60			60			60	743			60	
41		60			60			60	824			60	

OH — Organic silty clays   SP — Poorly graded sands, gravelly sands, little or no fines   CH — Silts and Clays   SM — Silty sand

The flowchart presented in Figure 4.5 illustrates the several steps taken to obtain an equivalent soil stiffness in each direction, which was later included in the numerical model of the bridge using spring elements. The equivalent soil stiffness (k_{trans} and k_{rot}) computed on each pier is indicated in Table 4.5.
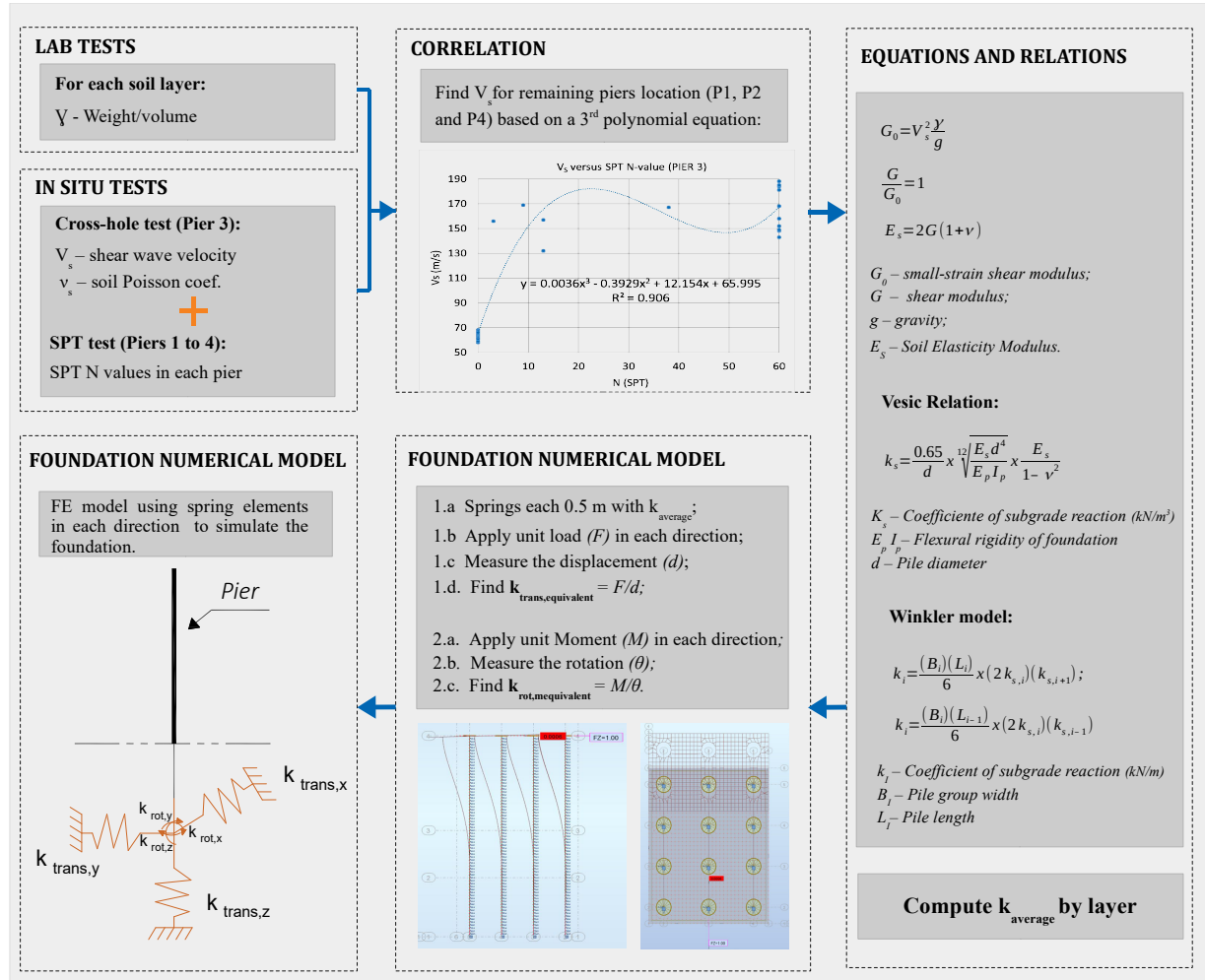

Figure 4.5 - Flowchart describing the simulation of the soil stiffness.

Table 4.5 - Equivalent soil stiffness considered on each pier.

PARAMETER	P1	P2	P3	P4	UNITS
$k_{trans,x}$	1.11E+06	1.43E+06	1.25E+06	1.00E+06	kN/m
$k_{trans,y}$	1.11E+06	1.67E+06	1.25E+06	1.00E+06	kN/m
$k_{trans,z}$	1.00E+12	1.00E+12	1.00E+12	1.00E+12	kN/m
$k_{rot,x}$	1.33E+09	2.09E+09	2.09E+09	1.19E+09	kN/m
$k_{rot,y}$	1.33E+09	1.61E+09	1.61E+09	1.19E+09	kN/m
$k_{rot,z}$	1.93E+09	3.70E+09	3.70E+09	1.72E+09	kN/m

4.2.2.4 Railway track

The geometric and mechanical properties of the UIC60 rail were adopted following the guidelines of the EN 13674-1(2007) and UIC 861-3 (E) (1969) standards. The modulus of elasticity, density weight and Poisson's ratio of the steel were considered equal to 210 GPa, 7850 kg/m^3 and 0.30, respectively. The main properties of the track, such as the stiffness and damping of the ballast and rail pads, were adopted from the literature or from previous research works and summarized in Table 4.6. It is worth pointing out that the ballast mass was distributed over the slab and that the inertia and geometry of these elements were corrected to consider the different mesh discretization adopted along the deck.

Table 4.6 - Mechanical properties of the numerical model of the track.

	DESIGNATION	PARAMETER	VALUE	UNITS	REFERENCE
Ballast	Longitudinal stiffness	$K_{bal,l}$	30	MN/m/m	(UIC 774-3-R, 2001)
	Transversal stiffness	$K_{bal,t}$	7.5	MN/m/m	(ERRI D 202/RP 11, 1999)
	Vertical stiffness	$K_{bal,v}$	100	MN/m/m	
	Damping (3 directions)	C_{bal}	50	kN.s/m/m	(Wu, & Yang, 2003)
Rail pads	Longitudinal stiffness	$K_{fas,l}$	20	MN/m	(Zhai, et al., 2009)
	Transversal stiffness	$K_{fas,t}$	20	MN/m	
	Vertical stiffness	$K_{fas,v}$	160	MN/m	(Paixão, et al., 2014)
	Rotational stiffness	$K_{fas,r}$	45	kN.m/rad	(ERRI D 202/RP 11, 1999)
	Longitudinal damping	$C_{fas,l}$	50	kN.s/m	(Zhai, et al., 2009)
	Transversal damping	$C_{fas,t}$	50	kN.s/m	
	Vertical damping	$C_{fas,v}$	17	kN.s/m	(Paixão, et al., 2014)
Concrete sleeper	Modulus of elasticity	$E_{c,sleeper}$	30	GPa	(Paixão, et al., 2014)
	Poisson's ratio	$v_{c,sleeper}$	0.25	-	

4.2.3 Non-linear numerical analyses

4.2.3.1 Static analysis

The structural static behaviour of the bridge was simulated in the FE model by running a time-history analysis using experimental data as input, as described in Figure 4.6. The simulation procedure consisted of using the temperatures acquired every hour on site over the course of one year, some of which are shown in Figure 4.7, as input for the numerical simulations, and obtaining the corresponding output, composed of time-series of displacements and deformations. Each time series used in the numerical simulation consists of over 8400 data points, spanning over a period of 12 months (between November 2015 and November 2016). Figure 4.7 also shows a lateral view and a section detail of the numerical model, including the experimental temperatures from one hour of a day in November. A clustering strategy was

considered regarding the input of the experimentally acquired temperatures. As it is possible to observe, the steel box was divided into four clusters (Ts1, Ts2, Ts3 and Ts4), the concrete slab was divided into three (Tc1, Tc2 and Tc3), and each arch was also divided into three clusters (SA2sn, SA2m and SA2ss), with the temperature being introduced in the upper (Ta1) and bottom (Ta2) part of the arch section. A reference temperature of 30º C was considered in the simulations, according to the average seasonal temperature at the time the bridge construction was completed.
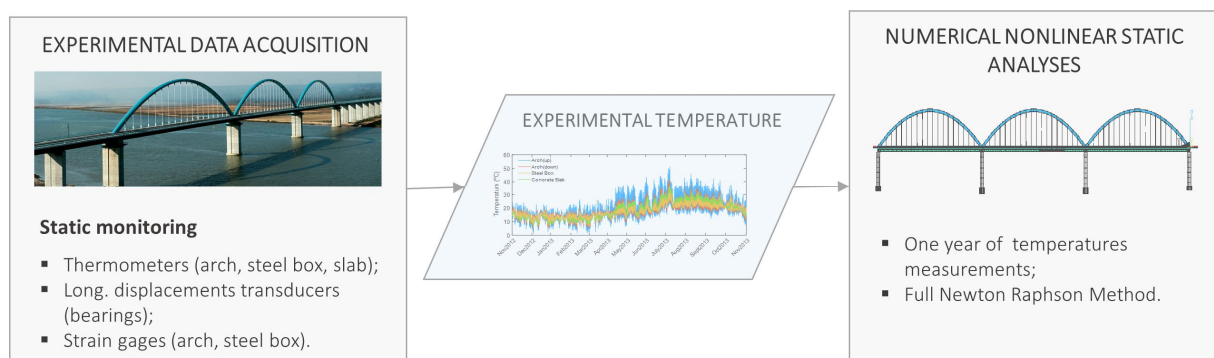

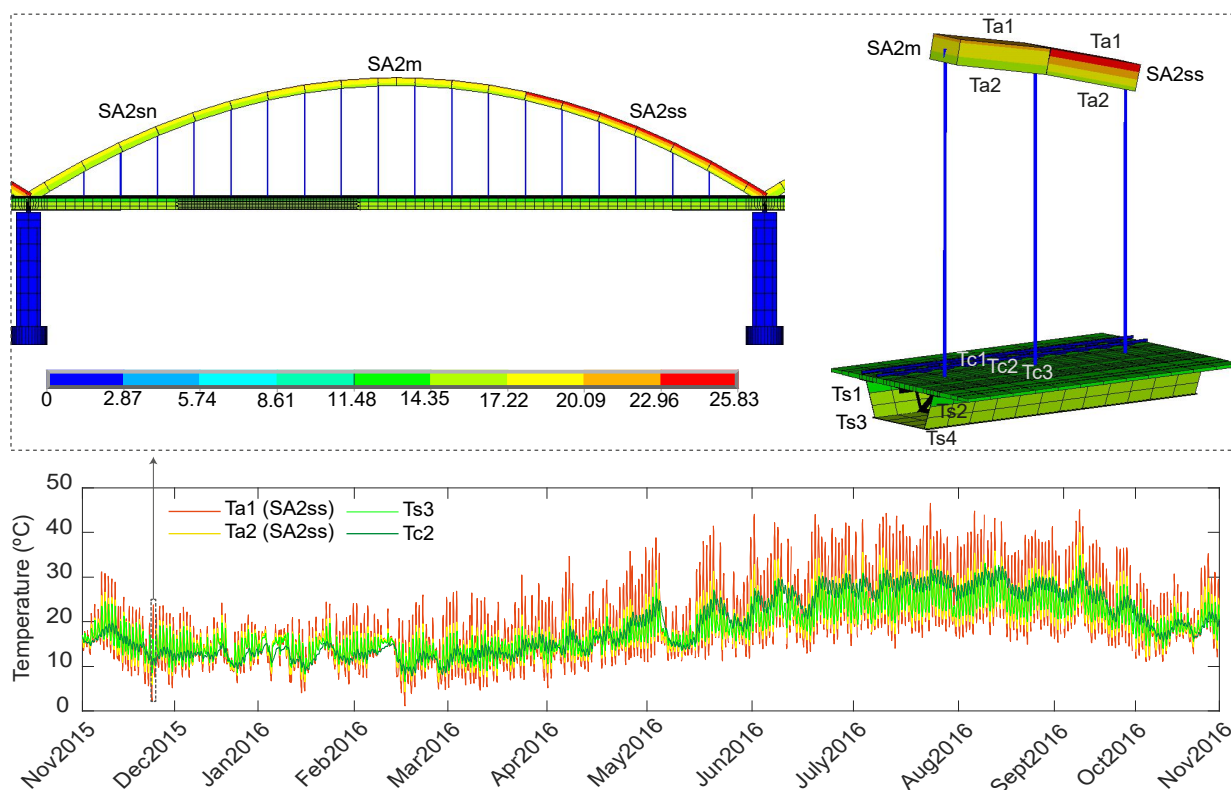Figure 4.6 – Steps to simulate the static response of the bridge under thermal loads.

Figure 4.7 - Experimental temperatures used as input for the numerical time history simulation.

To ensure that the numerical model accurately describes the structural behaviour of the bridge during the numerical analysis, the non-linear contact elements simulating the bearings were

activated. The Full Newton-Raphson Method implemented in the ANSYS software was used to solve the non-linear problem.

4.2.3.2 Dynamic analysis

Dynamic numerical simulations were conducted in order to reproduce the structural quantities that were measured in the exact locations of the real sensors, installed on site. To faithfully reproduce these structural responses, the action of the measured temperature (from the sensors mentioned in Chapter 3) precisely during each train passage, the train speed and geometry, as well as the Rayleigh damping are introduced as inputs in the numerical model (Figure 4.8).
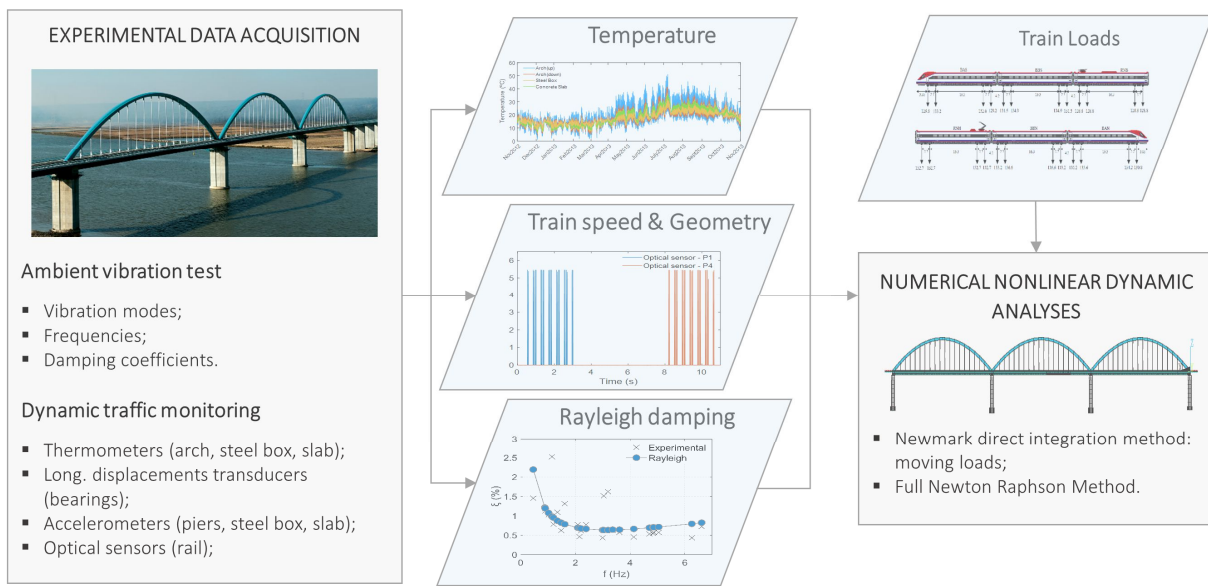

Figure 4.8 - Steps to simulate the dynamic response of the bridge under traffic loads.

Using the measurements of the optical sensors setup installed at both ends of the bridge, it is possible to compute the speed of the train and identify the type of train, according to its geometry. Figure 4.9 shows an example of the optical sensors' response when an Alfa Pendular (AP) train crosses the bridge over the Sado River. Each peak in the response of the optical sensors is generated by the passage of an axle through the optical beam. Given that the axles are easily identified, and knowing the distance (d) between the two synchronously logged optical sensors setup, as well as the time interval (t) in which each axle crosses the laser, the train speed (V) can be seamlessly obtained as d/t.
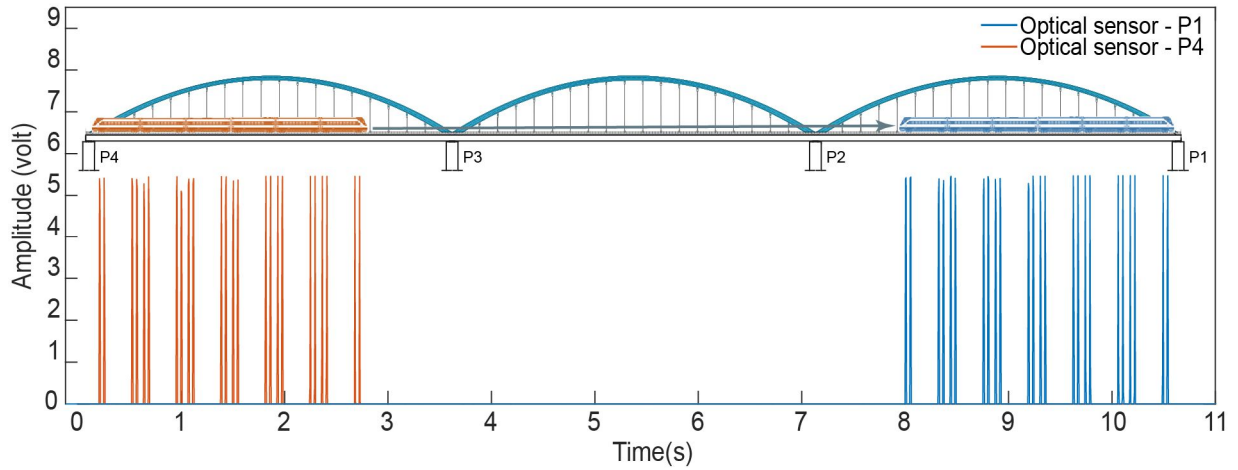
Figure 4.9 - Axle detection based on measurements from the optical sensors during the passage of an AP train.

All the dynamic analyses mentioned hereinafter in this chapter were carried out for the AP train, which has a total length of approximately 150 m comprising four motor vehicles (BAS, BBS, BBN and BAN) and two hauled vehicles (RNB and RNH) (Ribeiro et al., 2013). The axle loads considered during the dynamic analysis vary between 128.8 kN and 138.4 kN, according to the loading scheme presented in Figure 4.10a. Usually, the AP train crosses the bridge near its maximum speed, which is 220 km/h. Figure 4.10b shows the dynamic signature of the train, which characterizes the dynamic excitation imposed by the train on the infrastructure, for a wavelength range of 4 m to 30 m, as well as the corresponding frequency response, in the range of DC to 14 Hz, for a train speed of 216 km/h. The dynamic signature depends on the axle load values and the distances between axles, and is given by the following expression (ERRI D 202/RP 11, 1999):

$$S_0(\lambda) = \max_{i=1,N-1} \sqrt{\left[\sum_{k=0}^{i} P_k \cos\left(\frac{2\pi x_k}{\lambda}\right) \right]^2 + \left[\sum_{k=0}^{i} P_k \sin\left(\frac{2\pi x_k}{\lambda}\right) \right]^2} \qquad (4.1)$$

where i is the number of axles of the train, P_k is the static load of axle k, x_k is the distance between axle k and the first axle of the train, and λ is the wavelength of excitation. In Figure 4.10b, the most important dynamic component of this train's action is highlighted, with a wavelength of 25.9 m, associated with a regular distance between groups of four axles and a frequency of 2.362 Hz for an AP train at a speed of 216 km/h.
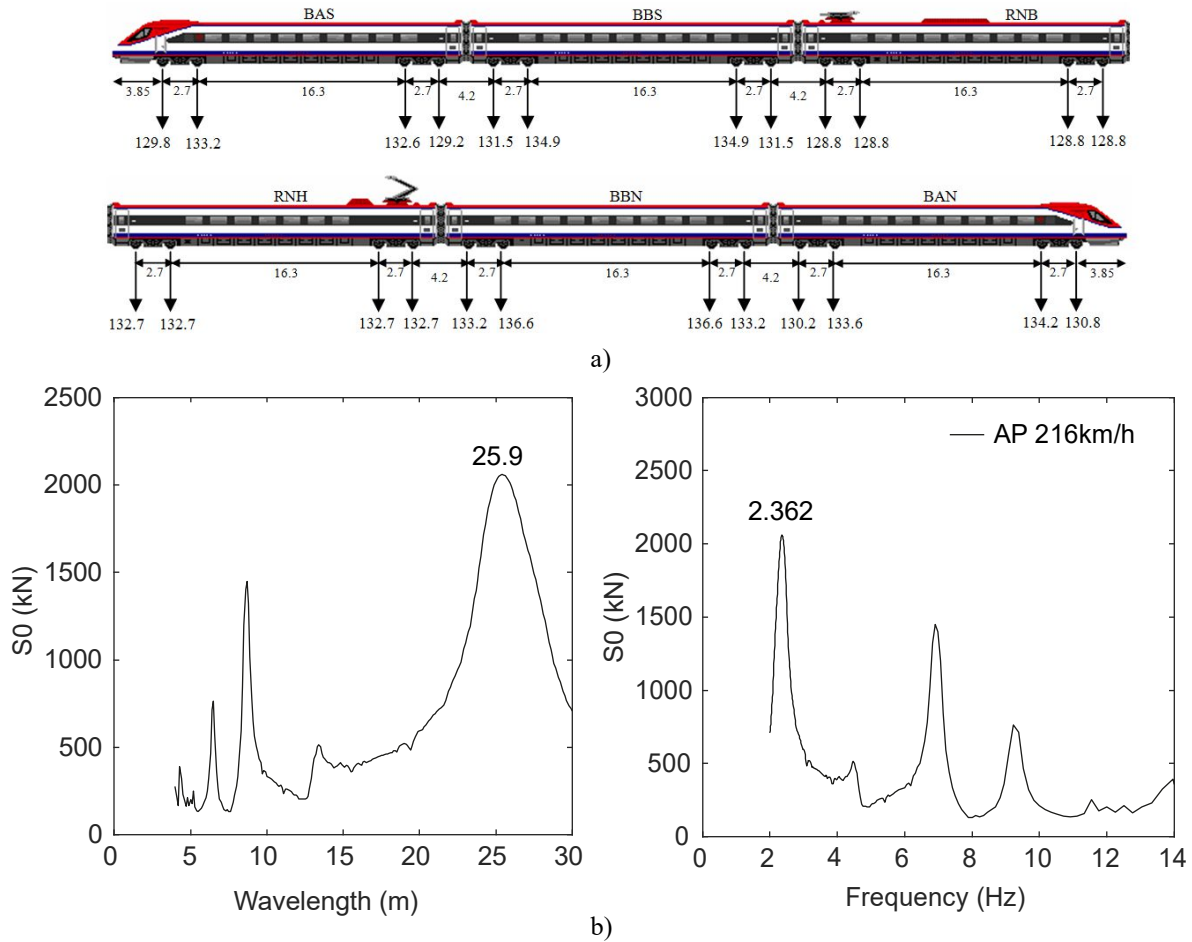
Figure 4.10 - AP train: a) load scheme, b) dynamic signatures.

In order to perform the necessary dynamic analysis to predict the response of the bridge subjected to a moving train, the damping was considered using a Rayleigh damping matrix (C), which assumes the linear combination of the mass (M) and stiffness (K) matrices:

$$C = c_1 M + c_2 K \tag{4.2}$$

where c_1 and c_2 are the mass and stiffness proportional damping coefficients, which can be obtained by applying the least-squares method, using the following expression, that implies the prior knowledge of frequency and damping coefficient values identified in the AVT (Figure 3.13) (Calçada, 2001):

$$\xi = \frac{c_1}{2\omega} + c_2 \frac{\omega}{2} \tag{4.3}$$

The least-squares method finds the optimal values of the coefficients (c_1 and c_2) by minimizing the sum (S) of squared residuals, e.g., the difference between the experimental (ξ_i) and numerical (ξ_i^c) damping values of the considered mode shapes:

$$S = \sum_{i=1}^{N}(\xi_i - \xi_i^c)^2 = \sum_{i=1}^{N}\left(\xi_i - \frac{c_1}{4\pi f_i} - c_2\pi f_i\right)^2 \tag{4.4}$$

The minimum value of the sum of squares was found by setting the gradient functions to zero:

$$\begin{cases} \dfrac{\partial S}{\partial c_1} = 0 \\[2mm] \dfrac{\partial S}{\partial c_2} = 0 \end{cases} \tag{4.5}$$

which leads to the following system of equations:

$$\begin{cases} \dfrac{1}{4\pi}\sum_{i=1}^{N}\dfrac{1}{f_i^2}c_1 + N\pi c_2 = \sum_{i=1}^{N}\dfrac{\xi_i}{f_i} \\[4mm] \dfrac{N}{4\pi}c_1 + \pi\sum_{i=1}^{N}f_i^2\, c_2 = \sum_{i=1}^{N}\xi_i f_i \end{cases} \tag{4.6}$$

The obtained Rayleigh damping curve is illustrated in Figure 4.11.
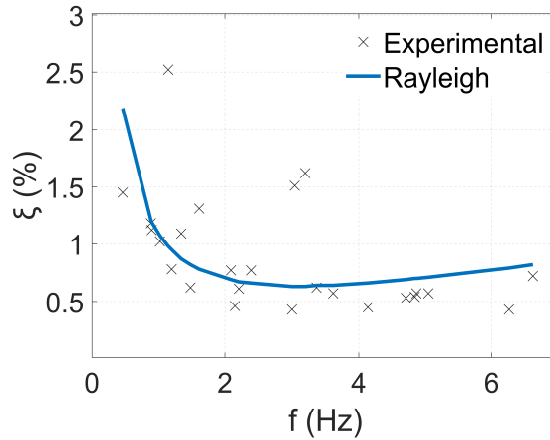

Figure 4.11 - Relation between the damping ratio and the natural frequencies identified in the AVT.

Once again, the contact elements simulating the bearings were activated, hence, the non-linear problem was solved based on the Full Newton-Raphson method, while the dynamic analyses were performed by the Newmark direct integration method, using a moving loads methodology (Ribeiro et al., 2012). The integration time step (Δt) used in the analyses was 0.005 s. The analyses were concluded two seconds after the vehicle crossed the viaduct to take into account the period of free vibration of the structure.

4.3 EXPERIMENTAL VALIDATION

4.3.1 Validation based on ambient vibration

To validate the accuracy of the baseline numerical model in replicating the stiffness and mass distribution across the geometry of the bridge, the numerical modal properties of the bridge over the Sado River were compared with those experimentally identified in the AVT described in section 3.3.2. Table 4.7 presents the experimental and numerical frequencies and the MAC (Modal Assurance Criterion) values for 10 of the 22 vibration modes experimentally identified. The frequency Fitting Error (FE) was defined as:

$$FE_i = (f_{i,exp} - f_{i,num})/f_{i,exp} \times 100 \ (\%) \tag{4.7}$$

where $f_{i,exp}$ and $f_{i,num}$ are the experimental and numerical frequencies obtained for mode i. The average value of the fitting error, across the identified mode shapes, is equal to 2.01%, whereas the average MAC value obtained is 0.94. Figure 4.12 shows a very high coefficient of determination ($R^2 = 0.9993$) between the 22 numerical and experimental frequencies. The mode shapes corresponding to 10 of the 22 frequencies identified in the experimental and numerical modal analysis are plotted in Figure 4.13. The numerical vibration modes were identified using the materials and geometric properties defined in the design and construction phases, with the exception of the modulus of elasticity of the concrete slab, previously updated by Albuquerque et al. (2015). No abnormal behaviour or structural change needed be considered to update the numerical model. However, it is important to note that during the numerical modal analysis, the non-linear contact elements simulating the behaviour of the bearings were inactive, since they are not mobilized in an ambient vibration test.

Table 4.7 - Natural frequencies and MAC values.

MODE NUMBER	EXPERIMENTAL FREQ (Hz)	NUMERICAL FREQ (Hz)	FE (%)	MAC	MODE TYPE
1	0.462	0.466	0.87%	0.95	1st LA
2	0.886	0.847	4.40%	0.95	1st V
3	0.898	0.867	3.45%	0.98	1st LAD
4	1.023	0.989	3.32%	0.90	2nd V
5	1.146	1.146	0.00%	0.99	1st L
6	1.198	1.178	1.67%	0.98	3rd V
7	1.343	1.316	2.01%	0.98	2nd LA
8	1.482	1.493	-0.74%	0.91	4th V
9	1.612	1.536	4.71%	0.86	5th V
10	2.090	2.081	0.43%	0.93	6th V

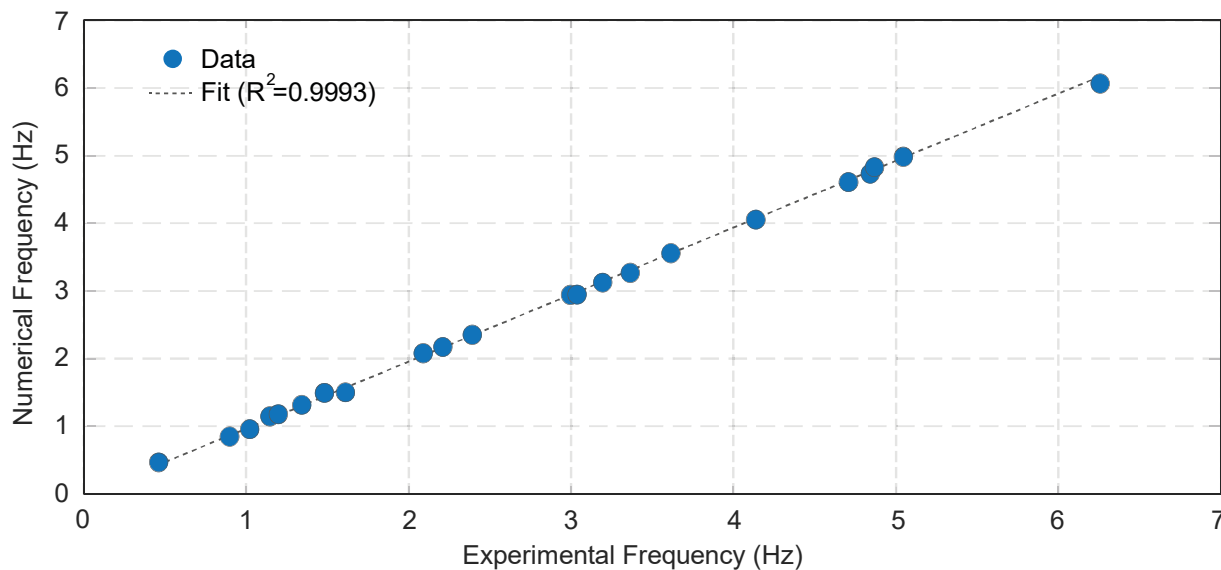LA – Lateral Arches; V – Vertical, LAD – Lateral Arch & Deck coupled, L – Longitudinal.

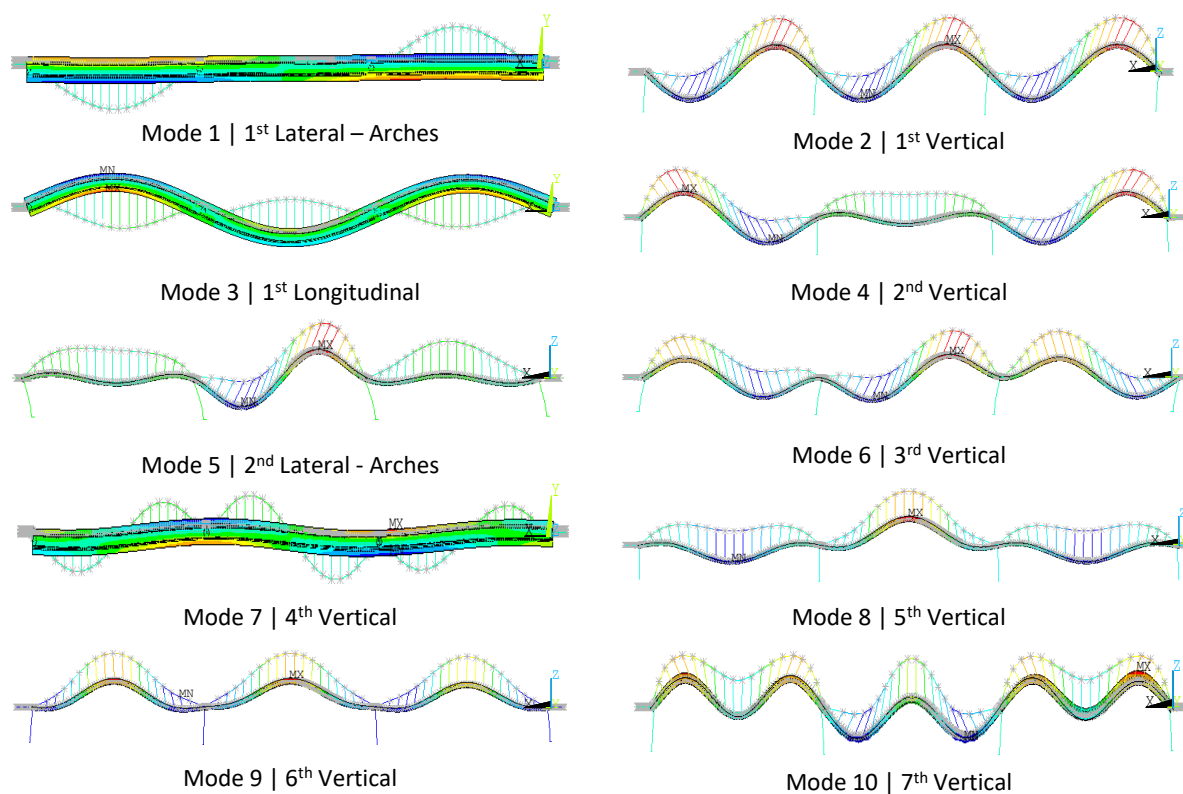Figure 4.12 - Agreement between numerical and experimental modal frequencies.

Mode 1 | 1st Lateral – Arches

Mode 2 | 1st Vertical

Mode 3 | 1st Longitudinal

Mode 4 | 2nd Vertical

Mode 5 | 2nd Lateral - Arches

Mode 6 | 3rd Vertical

Mode 7 | 4th Vertical

Mode 8 | 5th Vertical

Mode 9 | 6th Vertical

Mode 10 | 7th Vertical

Figure 4.13 - Numerical mode shapes.

4.3.2 Validation using the response to environmental loading

Validation based on environmental loading was conducted using two distinct numerical models. The first, the baseline model, was defined considering partially restrained displacements between piers P2, P3 and P4 and the deck, assuming the non-linear behaviour of the bearings

and a friction coefficient equal to 1.5%, according to the data from the bearing manufacturer. The second, the updated model, was considered with fully restrained movements between piers P2 and P3 and the deck, based on the conclusions obtained in visual inspections and dynamic monitoring.

The comparison between the numerical responses (baseline and updated models) and the experimental time-history responses of the bridge over a year of thermal loads, acquired between November 2015 and November 2016, is illustrated in Figure 4.14 to Figure 4.16. Figure 4.14a,b show that the baseline numerical model overestimated the longitudinal displacements of the upstream bearing on pier P4. The difference between numerical and experimental data is particularly relevant during the summer months, as the temperature variability doubles that observed during winter. When conducting the same comparison using the results of non-linear static analyses performed in the updated model, a much greater correlation was obtained between numerical and experimental static responses (Figure 4.14). This outcome allows concluding that the longitudinal displacements of the bearings on pier P4 are influenced by the restrictions imposed on those installed on piers P2 and P3. This conclusion would hardly be obtained by analysing the experimental longitudinal displacements of P4 alone, whereas the comparison with the numerical simulation responses obtained using the environmental conditions measured on site allows the direct observation of the differences induced by structural changes.

Regarding the deformations of the steel box girder and the arch, Figure 4.15 and Figure 4.16 show that these elements are not significantly influenced by the defects of the bearings, since the responses obtained with the baseline numerical model are identical to those obtained with the updated numerical model. This observation allows concluding that the consequences of the restraints in the bearings on the global stresses of the arch and deck are very small. Nevertheless, a good correlation in terms of arch deformations and steel box deformations can be observed, particularly in the 1-month time-series shown in each of these figures.

The scatter plots shown in these figures for each structural response confirm the high correlation between the responses of the updated numerical model and the experimental measurements, wherein the coefficients of determination (R^2) show values of 0.981 for longitudinal displacements, 0.936 for steel box deformations and 0.903 for arch deformations.
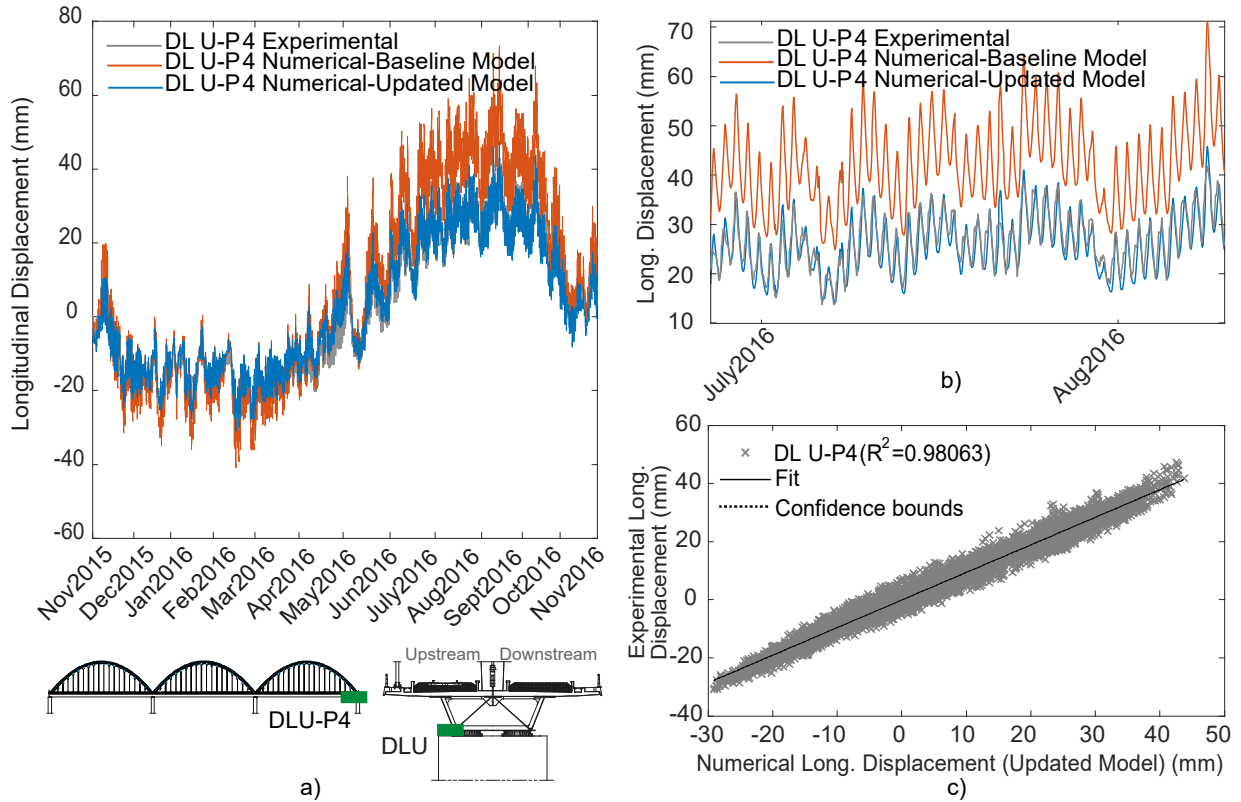
Figure 4.14 - Numerical and experimental longitudinal displacements of the bearing on the upstream side of pier P4: a) time-history comparison, b) detail of the time-history, c) scatter plot and R^2.
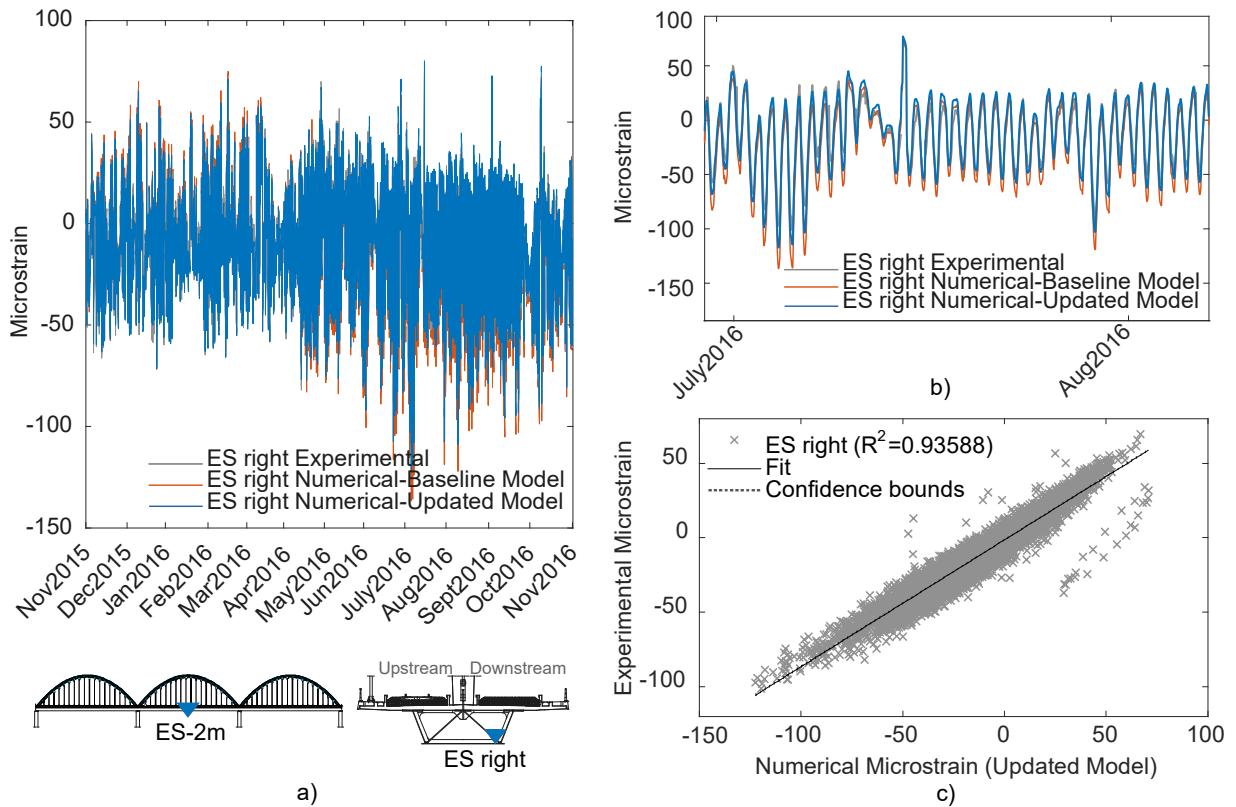

Figure 4.15 - Numerical and experimental deformations of the steel box on the downstream side of the central deck at the mid-span section of the bridge: a) time-history comparison, b) detail of the time-history, c) scatter plot and R^2.
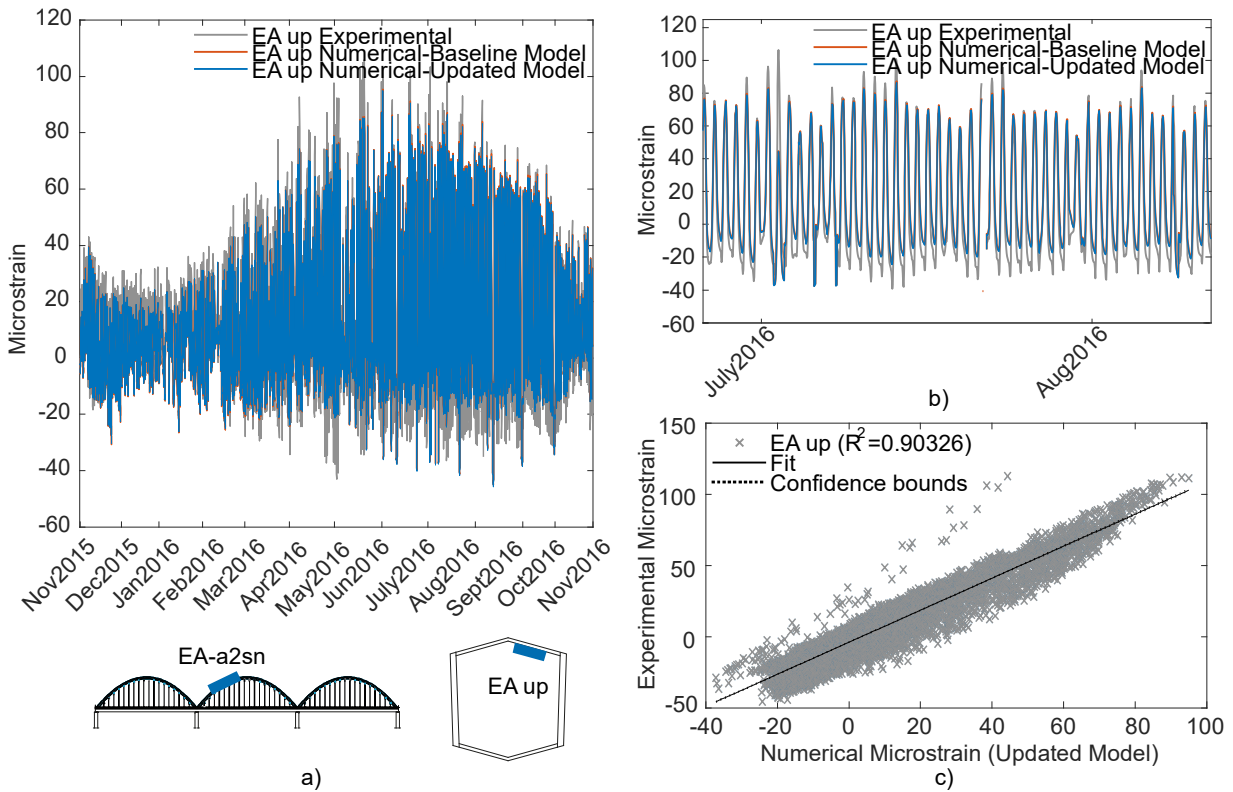
79

Figure 4.16 - Numerical and experimental deformations on the upper fiber at 1/6 of the central arch section: a) time-history comparison, b) detail of the time-history, c) scatter plot and R^2.

4.3.3   Validation based on train induced dynamic responses

The analysis discussed in section 3.3.4 showed that the use of acceleration signals analysed in the time-domain during the passage of trains is more sensitive to slight structural changes, and, therefore, should result in a more precise validation of the model.

Numerical simulations were conducted considering the AP train as a set of moving loads (Ribeiro et al., 2012) crossing the bridge over the Sado River at 216 km/h. With this approach, in addition to considering environmental effects, as explained in the previous section, operational effects are considered.

4.3.3.1 Analysis of displacement data

Regarding the validation of longitudinal displacements under train loads, a comparison was made between the numerical responses (baseline and updated models) and the experimental displacement time-history responses of the bridge (Figure 4.17 to Figure 4.19). As for the validation under environmental loading, the baseline numerical model was considered with partially restrained movements between piers P2, P3, P4 and the deck, assuming the non-linear

behaviour of the bearings, and the updated numerical model was considered with fully restrained movements between the piers P2 and P3 and the deck.

As expected, Figure 4.17a, Figure 4.18a and Figure 4.19a, obtained for piers P2, P3 and P4, respectively, show a significant difference between numerical and experimental responses, since the experimental bearing displacements identified on piers P2 and P3 show near-null values during the passage of trains, while the numerical ones do not. Regarding pier P4, the experimental bearing displacements seem to be influenced by the restriction imposed on those installed on piers P2 and P3, as previously observed in the displacements obtained under environmental loading.

The results shown in Figure 4.17b, Figure 4.18b and Figure 4.19b were obtained through non-linear dynamic analyses performed in the updated model but using the same experimental input data. In these plots, a very high correlation between numerical and experimental responses was achieved, not only for the near-null displacements observed on piers P2 and P3, but also, and more importantly, for the case of pier P4, where no specific model updating took place. A maximum displacement of 1.28 mm was obtained for the bearings located on pier P4 for an AP train crossing the bridge over the Sado River at 216 km/h. In a scenario in which all bearing displacements would be unrestricted, the maximum displacement on pier P4 would be approximately 2 mm, as shown in Figure 4.19a. It should be noted that no comparison was made for the bearings located on pier P1, since, as previously mentioned, these are mechanically fixed, according to the bridge design.
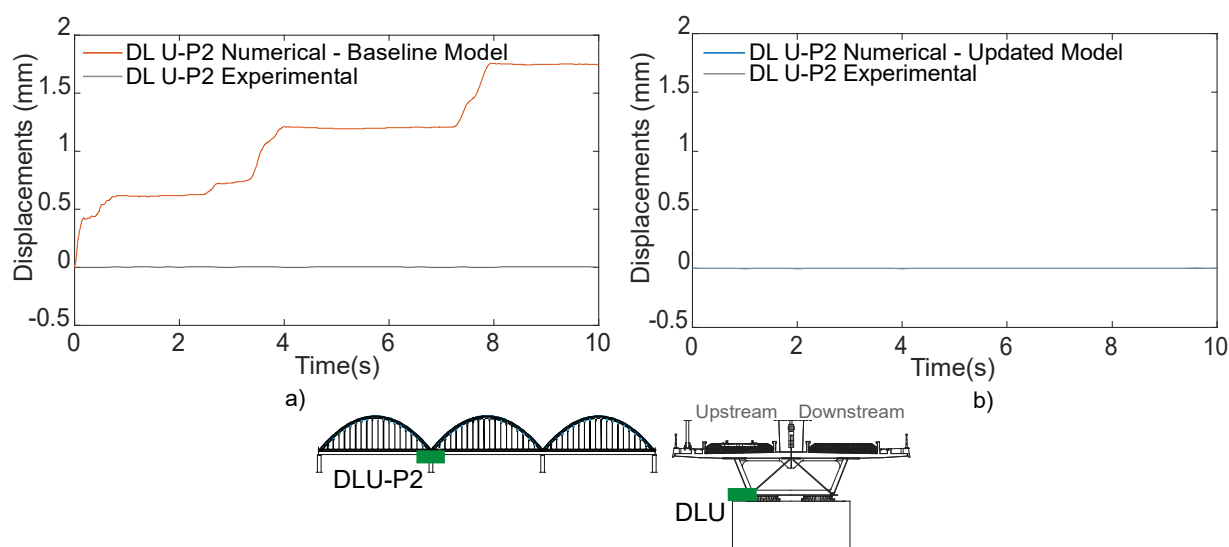

Figure 4.17 - Numerical and experimental longitudinal displacements of the bearing on the upstream side of pier P2, with the AP train crossing the bridge at 216 km/h: a) baseline model, b) updated model.

Figure 4.18 - Numerical and experimental longitudinal displacements of the bearing on the upstream side of pier P3, with the AP train crossing the bridge at 216 km/h: a) baseline model, b) updated model.

Figure 4.19 - Numerical and experimental longitudinal displacements of the bearing on the upstream side of pier P4, with the AP train crossing the bridge at 216 km/h: a) baseline model, b) updated model.
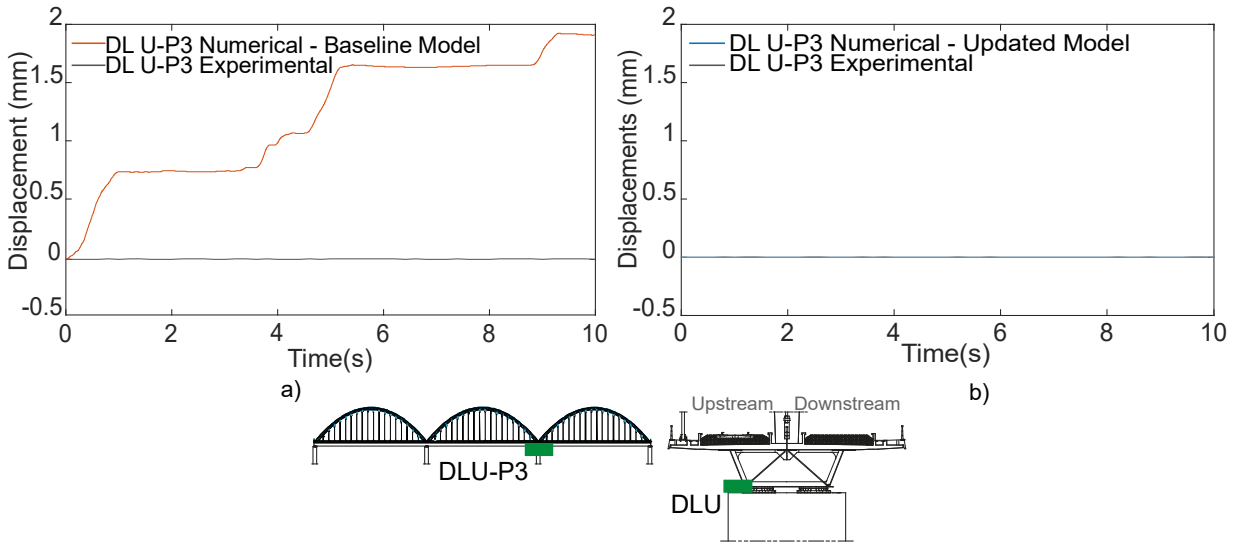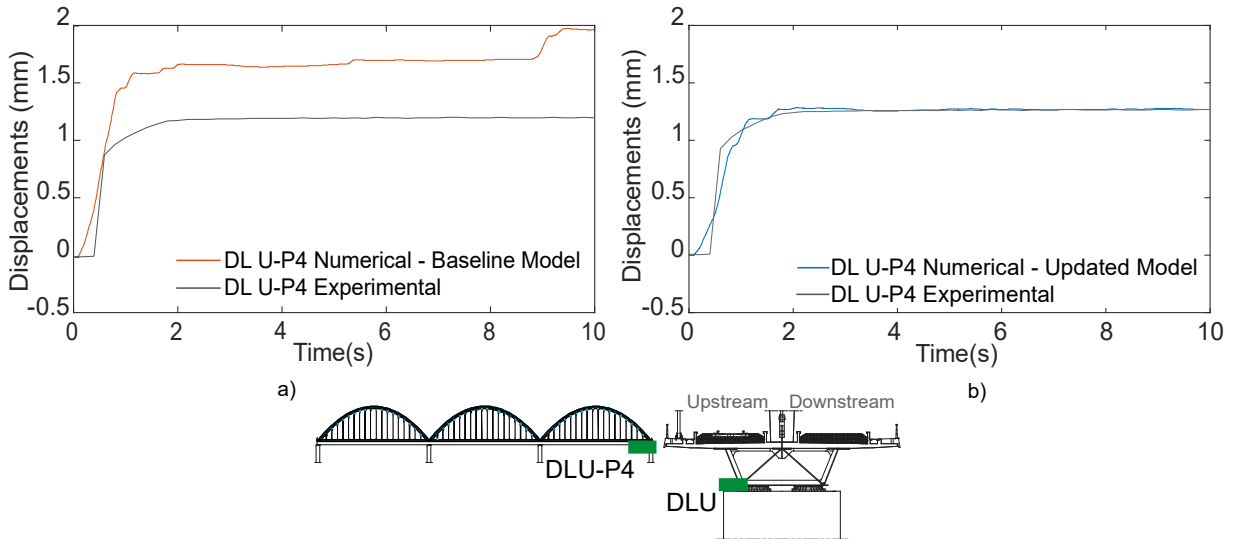
4.3.3.2 Analysis of acceleration data

In addition to the validation of the longitudinal displacements measured at each bearing device, the longitudinal accelerations measured on top of each pier were also computed for the same baseline and updated numerical models. Figure 4.20 to Figure 4.23 illustrate the comparison between numerical and experimental longitudinal accelerations on piers P1, P2, P3 and P4, respectively, considering the numerical models in the baseline (a) and updated (b) conditions. The records were filtered using a low-pass digital filter with a cut-off frequency of 15 Hz.

In general, with the restraining of the bearings located on piers P2 and P3, a visible improvement was achieved, both in the time and frequency domains, as observed in the standard deviation values of the differences between numerical and experimental responses, shown in these figures. As expected, the longitudinal accelerations acquired on piers P2 and P3 were the ones that showed the greatest differences between the responses measured in the baseline and updated models, with a decrease in the standard deviation values of 21% and 11%, respectively. In contrast, those computed for the measurements on pier P1 decreased by only 0.68%, since the deck is fixed to this pier. The bearings on pier P4 appear to be working correctly, and, as a result, the standard deviation of the differences between the numerical and experimental accelerations measured on pier P4 decreased 1.28%, considerably less than on piers P2 and P3.

Regarding the auto-spectra resulting from the longitudinal accelerations measured at each pier (Figure 4.20 to Figure 4.23), the main frequency is repeatedly 2.3 Hz, which illustrates a clear correspondence with the main peak of the dynamic signatures of the trains (Figure 4.10b), for both numerical models comprising unrestrained and restrained bearing devices.
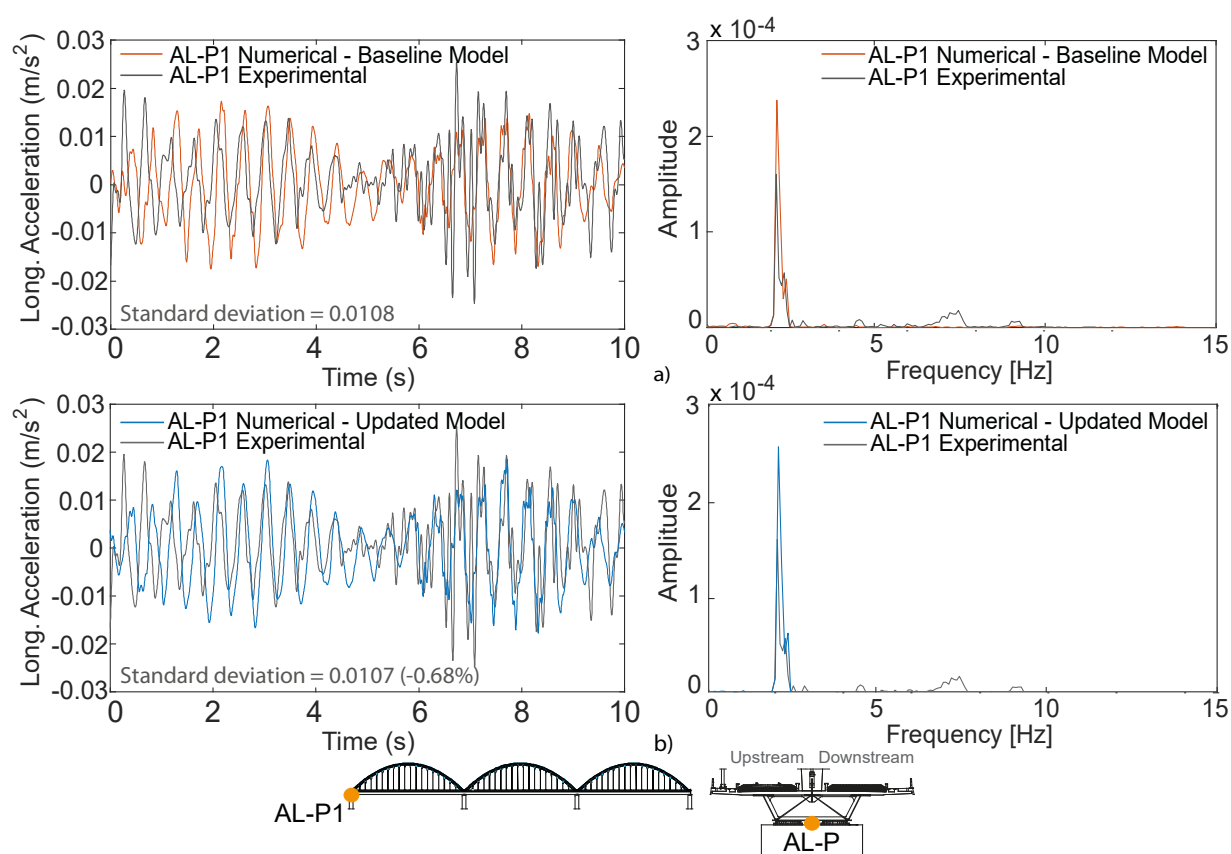

Figure 4.20 - Numerical and experimental longitudinal accelerations and corresponding auto-spectra measured between the bearings of pier P1, with the AP train at 216 km/h: a) baseline model, b) updated model.
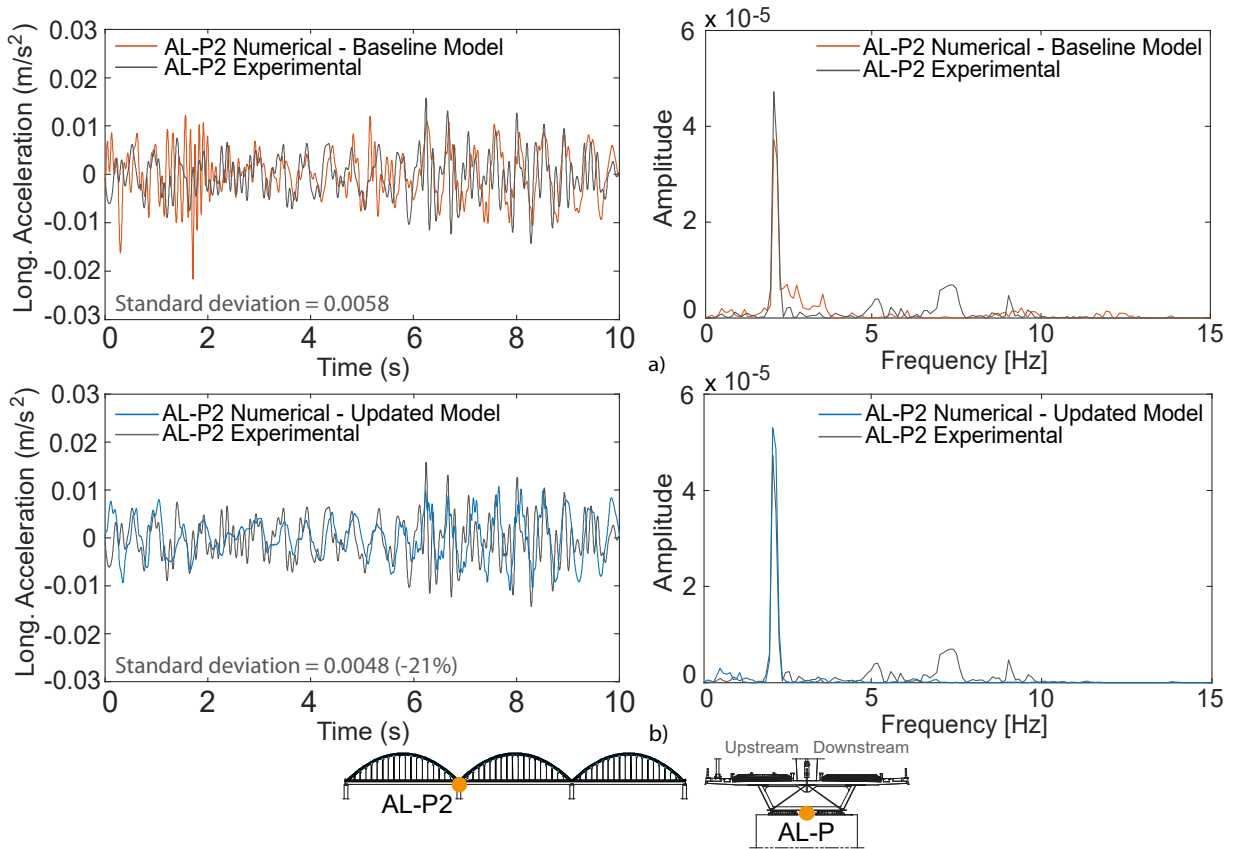
Figure 4.21 - Numerical and experimental longitudinal accelerations and corresponding auto-spectra measured between the bearings of pier P2, with the AP train at 216 km/h: a) baseline model, b) updated model.

Figure 4.22 - Numerical and experimental longitudinal accelerations and corresponding auto-spectra measured between the bearings of pier P3, with the AP train at 216 km/h: a) baseline model, b) updated model.
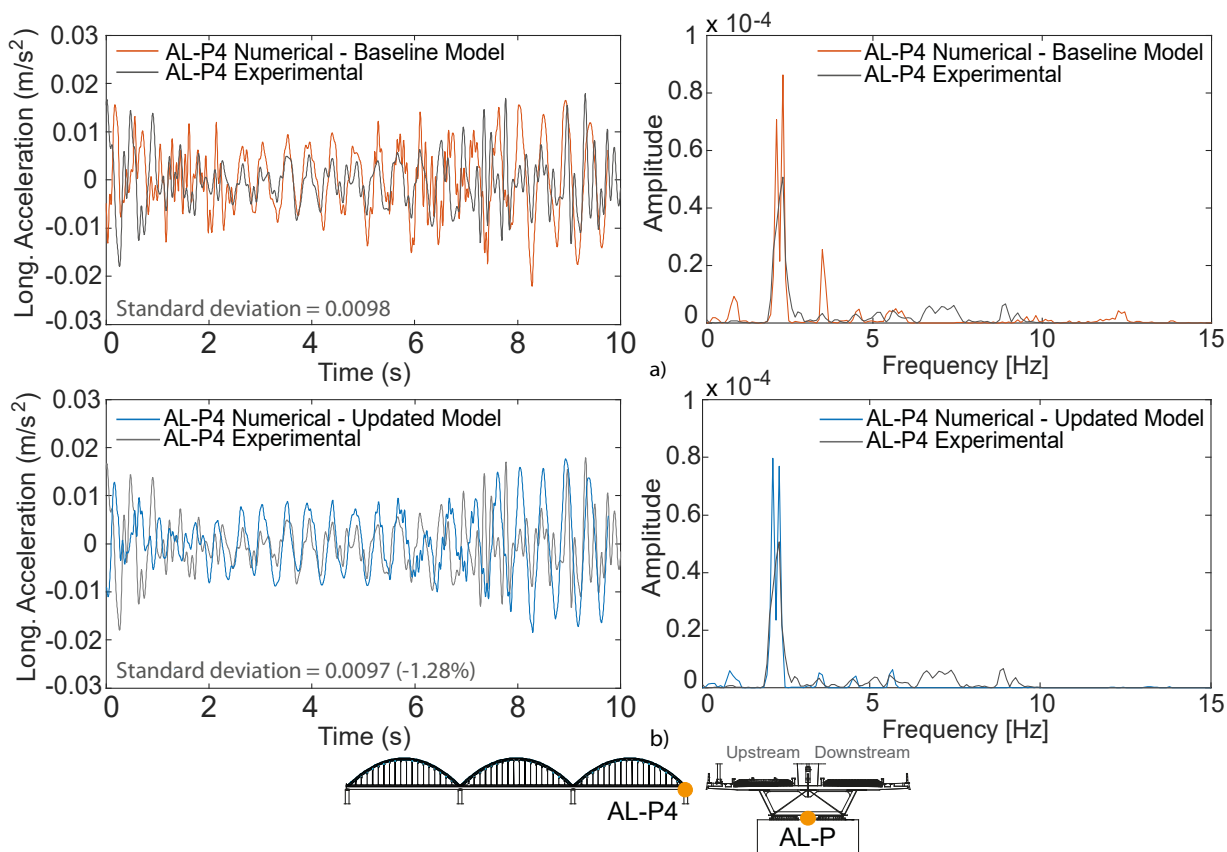
Figure 4.23 - Numerical and experimental longitudinal accelerations and corresponding auto-spectra measured between the bearings of pier P4, with the AP train at 216 km/h: a) baseline model, b) updated model.
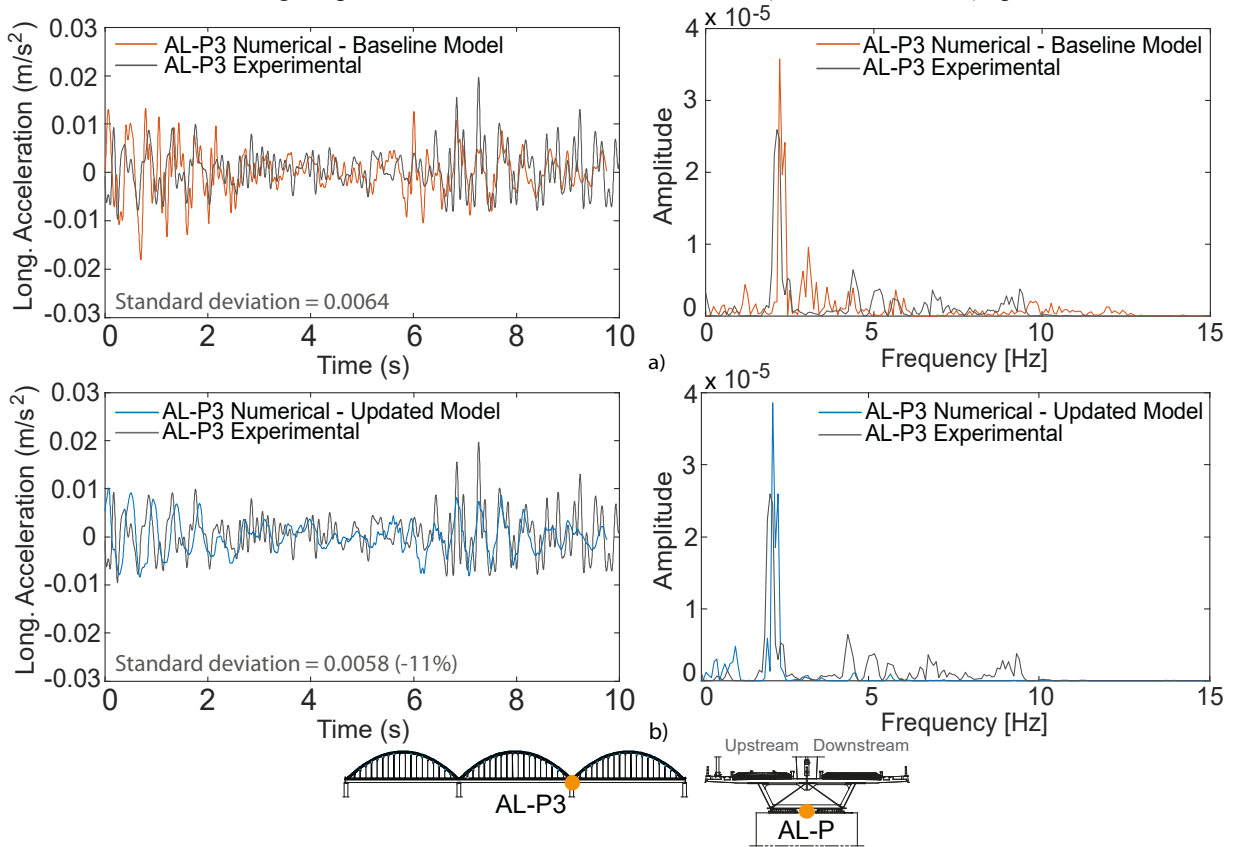
While the accelerometers installed on the piers are influenced by structural changes in the bearing devices, those installed on the bridge deck appear to be not as sensitive, since the responses obtained with the baseline numerical model coincide with those obtained with the updated numerical model (Figure 4.24 and Figure 4.25).

Figure 4.24 - Numerical and experimental vertical accelerations and corresponding auto-spectra measured on the concrete slab in the mid-span section, with the AP train at 216 km/h.
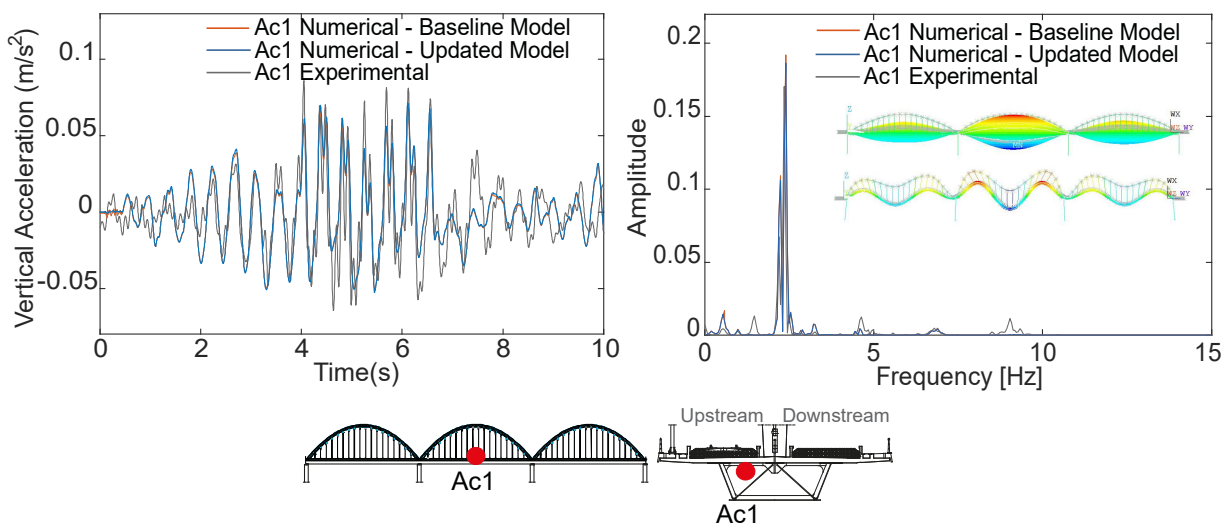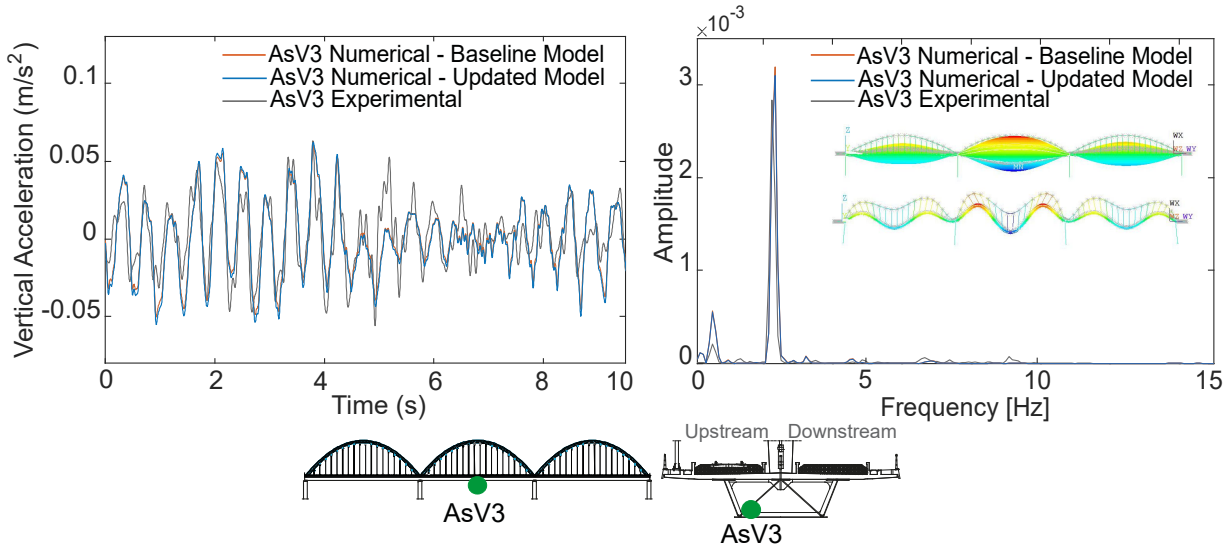
Figure 4.25 - Numerical and experimental vertical accelerations and corresponding auto-spectra measured on the steel box girder in the mid-span section, with the AP train at 216 km/h.

In Figure 4.24 and in Figure 4.25 it is possible to observe the auto-spectra resulting from the vertical accelerations measured in the concrete slab and the steel box girder, respectively, where the frequencies around 2.3 Hz are related to the main vibration modes of the structure, namely, torsion and bending modes. The preponderance of these modes is to be expected since the train loading is eccentric to the single-plane bowstring-arch structure.

The comparison between the experimental and numerical records of vertical acceleration measured on the concrete slab (Figure 4.24) and on the steel box girder (Figure 4.25) in the mid-span section shows a very good agreement, both in the time and frequency domains.

4.4 CONCLUDING REMARKS

The present chapter addressed the progressive numerical validation of the complex non-linear FE model of the bridge over the Sado River using the measurements from the monitoring system installed on site and performing modal analysis under ambient vibration, static analysis based on temperature loading and dynamic analysis based on traffic loading. One of the main outcomes was a fully validated numerical model that will be used, in the next chapters, as a tool for generate several scenarios (undamaged and damaged) to validate the damage identification methodology.

The validation of the numerical model based on ambient vibration and modal analysis, revealed to be adequate to define the baseline numerical model. However, it is insufficient to

perform SHM or identify structural changes, since it does not mobilize mechanical devices such as bearings (or joints).

The static validation approach based on environmental loading provided a step forward in the accuracy of the model validation, when compared to the ambient vibration analysis, due to the imposition of greater displacements on the structural elements. Based on a correlation analysis between experimental and numerical results, the restraints of the bearing devices on piers P2 and P3 were clearly identified, which is in line with the structural changes detected through visual inspections. Without the support of a numerical model, these changes would not be easily identified using the data from the installed static monitoring system, which did not include the measurement of the displacements of these specific bearings. This is, in fact, another main outcome of this chapter, to illustrate the combined use of measurements and modelling, and the need to adapt both components over the course of a project to better understand the structural behaviour of the bridge.

The validation of the model based on dynamic monitoring under traffic loads was carried out in order to take advantage of the large displacements and vibrations imposed by this type of operational action. The model allowed analysing the influence that the restraints of the bearing devices impose on the longitudinal behaviour (displacements and accelerations) of the piers, and to the vertical accelerations of the deck. It was shown that the use of numerical modelling and its validation by comparison with the monitoring data, allows the detection of the restraint to the movements of the bearing devices on piers P2 and P3 without the need to measure the longitudinal displacements in the bearings. Instead, longitudinal accelerations on top of the piers, where the bearings are located, can be measured using low-cost sensors.

Based on this fully validated numerical model, the following chapters will consider the simulation of damage scenarios with different levels of severity and at several locations on the bridge. The damage identification methodology will be implemented, tested and validated to prove capable of automatically extracting meaningful information related to the structural condition of railway bridges.

Chapter 5

MACHINE LEARNING STRATEGY FOR EARLY DAMAGE IDENTIFICATION BASED ON TRAIN INDUCED DYNAMIC RESPONSES[*]

5.1 INTRODUCTION

This chapter presents a machine learning strategy consisting of a hybrid combination of time-series analysis methods and multivariate statistical techniques. Different combinations of techniques are implemented and tested in order to achieve the most robust, generic and effective one. The choices made regarding the techniques implemented within each step are explained and justified throughout the chapter.

Damage-sensitive features of train induced responses are extracted and allow taking advantage, not only of the repeatability of the loading, but also, and more importantly, of its great magnitude, thus enhancing the sensitivity to small-magnitude structural changes. A comparison between the performance obtained from AR and autoregressive with exogenous input (ARX) models as feature extractors is conducted. The use of a regression-based method

---

such as MLR or a latent-variable method such as PCA grants the strategy the ability to remove EOVs and proves the importance of feature modelling. Feature discrimination is addressed by evaluating the performance of outlier analysis and clustering algorithms. The ability to identify early damage, imperceptible in the original signals, while avoiding observable changes induced by variations in train speed or temperature, is achieved by carefully defining the modelling and fusion sequence of the information.

The effectiveness of the proposed strategy is demonstrated in the railway bridge over the Sado River. The experimentally validated finite element model presented in Chapter 4 was used, along with experimental values of temperature, noise, and train loadings and speeds, to realistically simulate baseline and damage scenarios.

After the introduction, section 5.2 gives an overview of the machine learning strategy implemented during the chapter. Section 5.3 explains the simulation of realistic damage scenarios, necessary because such conditions could not be experimentally measure. In sections 5.4 to 5.7 the several steps of the proposed strategy, namely feature extraction, feature modelling, data fusion and feature discrimination, respectively, are implemented. Finally, section 5.8 draws the main concluding remarks from the work presented in this chapter, along with the main achievements.

5.2 OVERVIEW

The unsupervised data-driven SHM strategy implemented in this chapter for identifying damage in bridges, based on traffic-induced dynamic responses, aims at being robust and generic enough to be applied to any type of bridge, and entails the four operations shown in Figure 5.1: i) damage-sensitive feature extraction from the acquired structural responses, ii) feature modelling to remove EOVs, iii) data fusion to merge multi-sensor features without losing damage-related information, and, iv) feature discrimination to classify the extracted features in two categories, healthy or damaged.

Feature extraction is addressed in this chapter by comparing the performance of AR and ARX models. The AR/ARX models are fitted to the acceleration responses of the monitored structure, and their parameters are extracted resulting in as many sets of multivariate data as the number of sensors installed.

Afterwards, the suppression of thermal and operational variations is conducted following two alternative approaches, one based on structural response measurements alone and the other based on both actions and structural response measurements. This is accomplished through the parallel implementation of two multivariate statistical tools: the latent-variable method PCA for the first approach using AR or ARX-based features, and the regression-based method MLR for the second approach using AR-based features.

In order to improve sensitivity, a Mahalanobis distance is implemented to the modelled features, allowing for an effective fusion, first of the AR or ARX-based features from each sensor and, in a second stage, of the multi-sensor information only for AR-based features. In case of AR-based features, the data fusion step is performed either for features based on actions and structural responses measurements or for features based only on structural responses measurements. The data fusion of the ARX-based features is performed using only structural responses measurements.

The outcome after implementing the data fusion step to the AR-based features is a damage index, DI, for each train crossing. In the last stage, an outlier analysis is implemented to automatically discriminate each DI into healthy or damaged, using a statistical confidence boundary, CB, based on the Gaussian inverse cumulative distribution function. In case of ARX-based features, a cluster analysis is performed to the multi-sensor features using the iterative k-means algorithm. The goal is to separate the healthy features and the damaged features into different clusters.

Although this methodology comprises a set of baseline features to define the CB, it is considered unsupervised, since the responses acquired to build this baseline regard the state condition of the bridge at the time it begins to be monitored, which does not necessarily correspond to an undamaged state. For either existing or new bridges, regardless of their geometry, the only data needed to implement this methodology is the train crossing signals for one or more types of trains at their different operating speeds and for several temperatures. As a consequence, structural changes signalled by the methodology comprise progressive damages in relation to the condition defined during the baseline. In addition, and more importantly, one of the great advantages of the methodology is the speed at which the baseline can be defined. It can be promptly established during one day for several types of trains with different loads crossing the bridge. The environmental effects can also be considered since the weather (temperature and wind) varies according to the time of day.
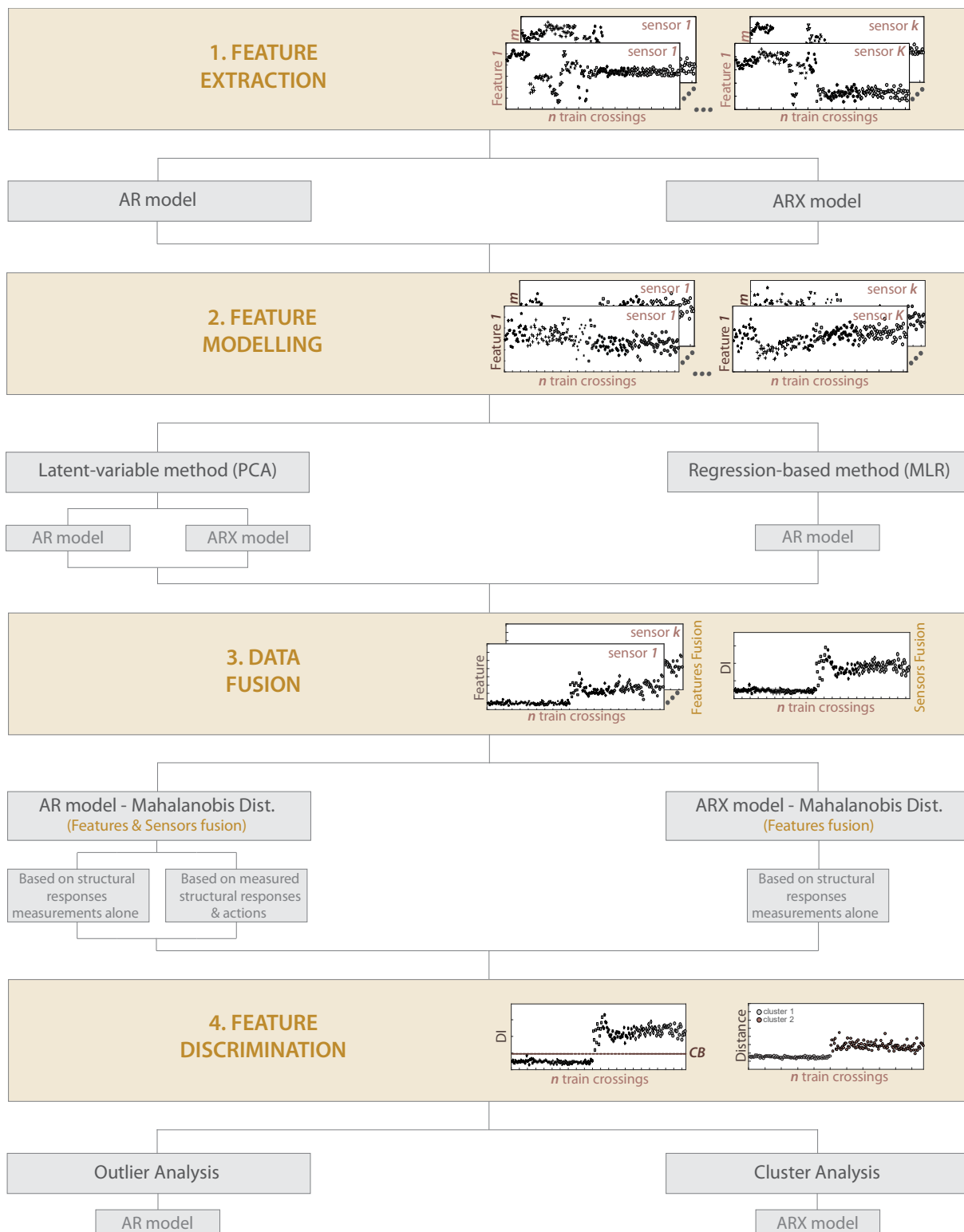
Figure 5.1 – Flowchart of different techniques implemented in the damage identification machine learning strategy.

5.3 SIMULATION OF BASELINE AND DAMAGE SCENARIOS

A realistic simulation of baseline (healthy) and damage scenarios was conducted using the reliable digital twin of the railway bridge over the Sado River, in order to test and validate the strategy proposed herein, since it is not possible to obtain such conditions experimentally in operating infrastructures of high expenditure values, such as the one being addresses herein. After a successfully numerical validation of the methodology, it can be applied directly to experimental data from different types of bridges.

5.3.1 Baseline scenarios

Different combinations for the baseline condition, that aim at reproducing the bridge responses considering the variability of train type, speed, temperature actions, and loads, are summarized in Figure 5.2. These baseline scenarios compose the training dictionary and do not include any damage on any location.
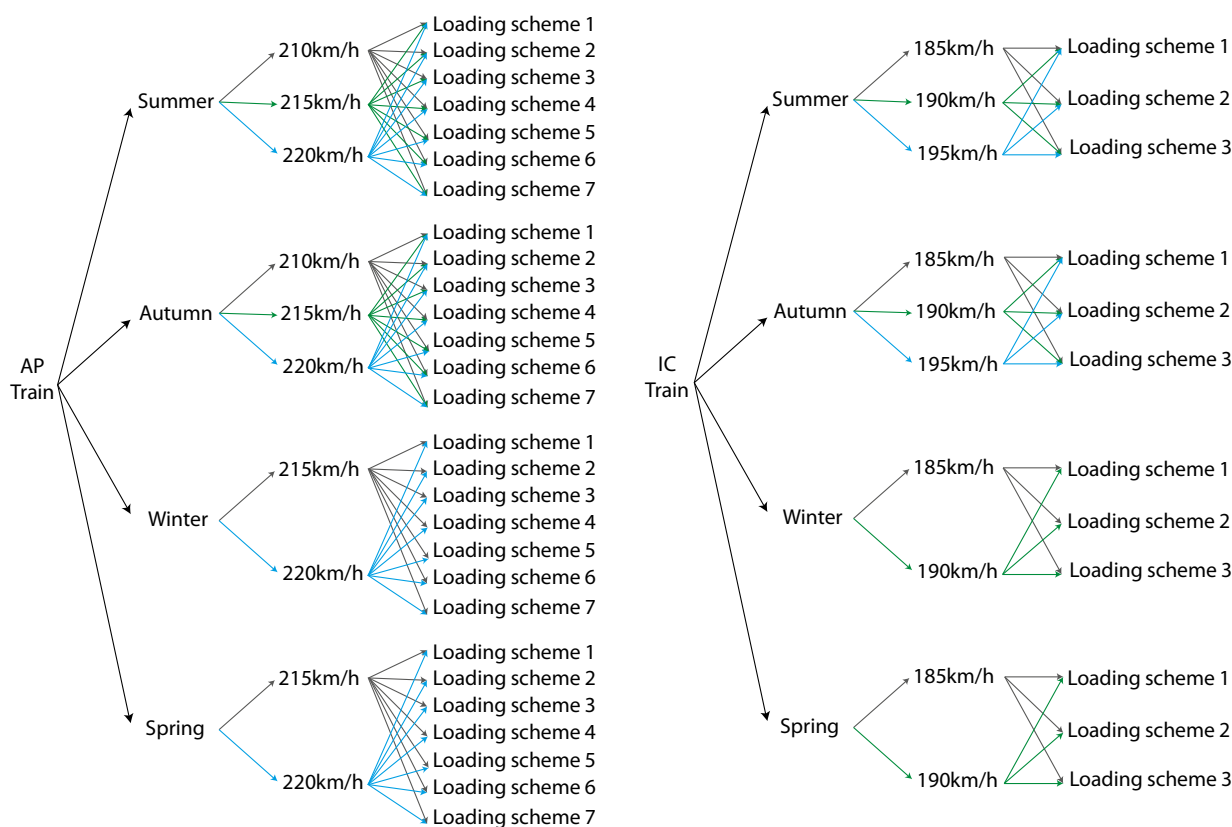

Figure 5.2 – Combination of 100 simulations for the baseline (undamaged) condition.

During each simulation, real temperatures measured by the SHM system precisely during each train crossing were introduced as input to the numerical elements. The average values for each season were 30ºC for summer, 16ºC for autumn, 10ºC for winter and 21ºC for spring, but

the dispersion across the structure was considered by measuring and using temperature values in all elements of the bridge. The simulations included passages of two of the passenger trains that normally cross the bridge over the Sado River, namely, the AP and the Intercity (IC) trains. Their common speeds on the bridge are 220 km/h for the AP train and 190 km/h for the IC train. The average axle loads of the AP train were presented in Figure 4.10a and of the IC train are illustrated in Figure 5.3. A total of ten different loading schemes were taken, according to the experimental observations previously made by Pimentel et al. (2008). Three train speeds were considered for each type of train, as observed in Figure 5.2, resulting in 100 dynamic simulations for the baseline condition, each taking approximately 10 hours of calculation time on a 4.2 GHz Quad-Core desktop with 32.0 GB of RAM.
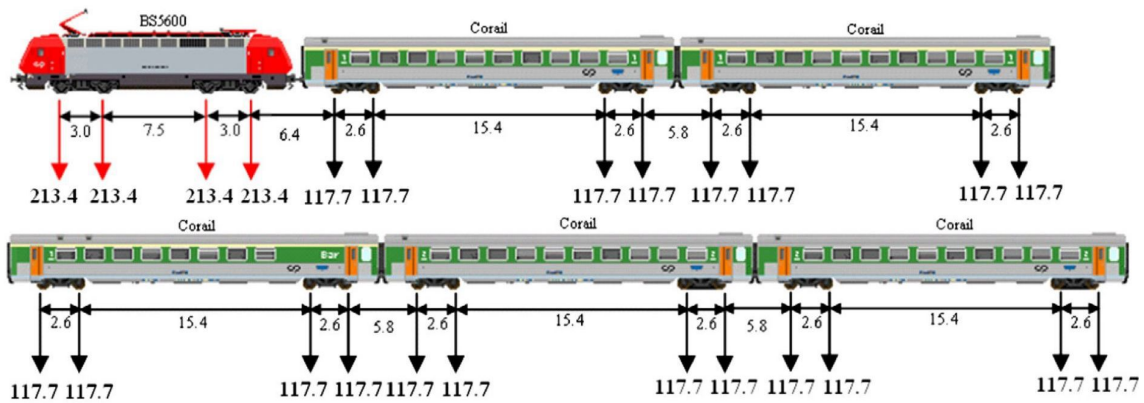
Figure 5.3 – IC train and corresponding loading scheme.

5.3.2 Damage scenarios

The damage scenarios were chosen based on possible vulnerabilities identified for the type of structural system, taking into account its materials, connections, behaviour and loadings (Santos, 2014). Among the several scenarios that can be considered, those related to friction increments in mechanical moving elements of the structural system (such as bearing devices), and those associated with corrosion in structural and reinforcing steel as well as cracking of concrete, were assumed as the most likely (Akesson, 2008; Khan, 2010; Santos, 2014; Wardhana et al., 2003) and therefore simulated to validate the techniques presented herein. While friction increments were simulated in all bearing devices, cracking and corrosion were considered in several sections across the structure to ensure representativeness. Hence, damage scenarios were simulated, along with dynamic traffic loading, according to four different classes:

i)   damage in the bearing devices (type D1);

ii)   damage in the concrete slab (type D2);

iii)   damage in the diaphragms (type D3);

iv)   damage in the arches (type D4).

The locations of each type of damage are illustrated in Figure 5.4, where different codes were assigned to each location depending on the damage type. For instance, D2:m1 is a damage in the concrete slab located in the first mid-span. Each scenario was simulated considering only one damage location. Nevertheless, if, by any chance, two or more damage scenarios in different locations are observed at the same time, the effects from multiple damage locations are expected to superimpose, and the influence on the features extracted from the data will be greater. Therefore, multiple damage scenario will be more observable in the features, when compared to single scenarios. For this reason, only single-scenario damages were simulated to test the proposed methodology under the most challenging conditions.
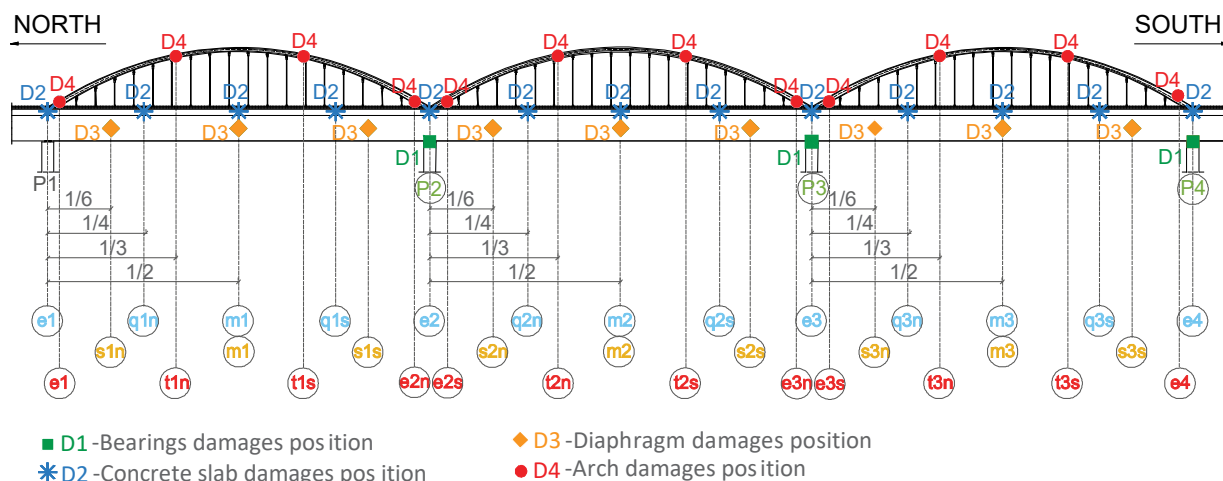
Figure 5.4 – Types of damages and their location on the bridge over Sado River.

Regarding damages of type D1, discrete damages comprising four severities were simulated, namely increases of the friction coefficient from a reference value of 1.5% to 1.8%, 2.4%, 3.0% as well as to the full restraint of the movements between the pier and the deck. The remaining damage scenarios were simulated as 5%, 10% and 20% stiffness reductions in the chosen sections of the bridge (Figure 5.4). The damage type D2 consisted of a stiffness reduction in the cross section of the concrete slab, 2 m long along the bridge's longitudinal axis, and a damage-to-span length ratio of 1.25%. The damage type D3 was simulated as local stiffness reductions in single diaphragms, which consist of sections of the deck directly suspended by each hanger. For each location of the damage type D4, a stiffness reduction was applied in an arch extension of 8 m, which represents 4.7% of the arc length. These structural changes were simulated by reducing the modulus of elasticity of the concrete (damage type D2) and of the

steel (damage types D3 and D4). Thus, a total of 114 damage scenarios were simulated for AP train crossings at 220 km/h, using the loading scheme presented in Figure 4.10a and adding as input the temperatures measured on site. Additional damage scenarios could have been simulated for different combinations of EOVs. However, as it will be discussed in section 5.5, the proposed methodology is effective in removing these effects and keeping only those generated by structural changes.

5.3.3   Noise distribution

To obtain the most similar and reliable reproduction of the real SHM data, the noise measured on site by each accelerometer was added to the corresponding numerical output. These noise distributions were acquired while no trains were travelling over the bridge and under different ambient conditions. Each simulation was corrupted with different noise signals acquired at different days, thus ensuring the most representative validation for the techniques developed herein. Figure 5.5 presents an example of a vertical acceleration bridge response at the central mid-span of the concrete slab for an AP train crossing, before and after being corrupted. The noise distribution applied to the response, which was measured by accelerometer Ac1 of the SHM system, is also shown.
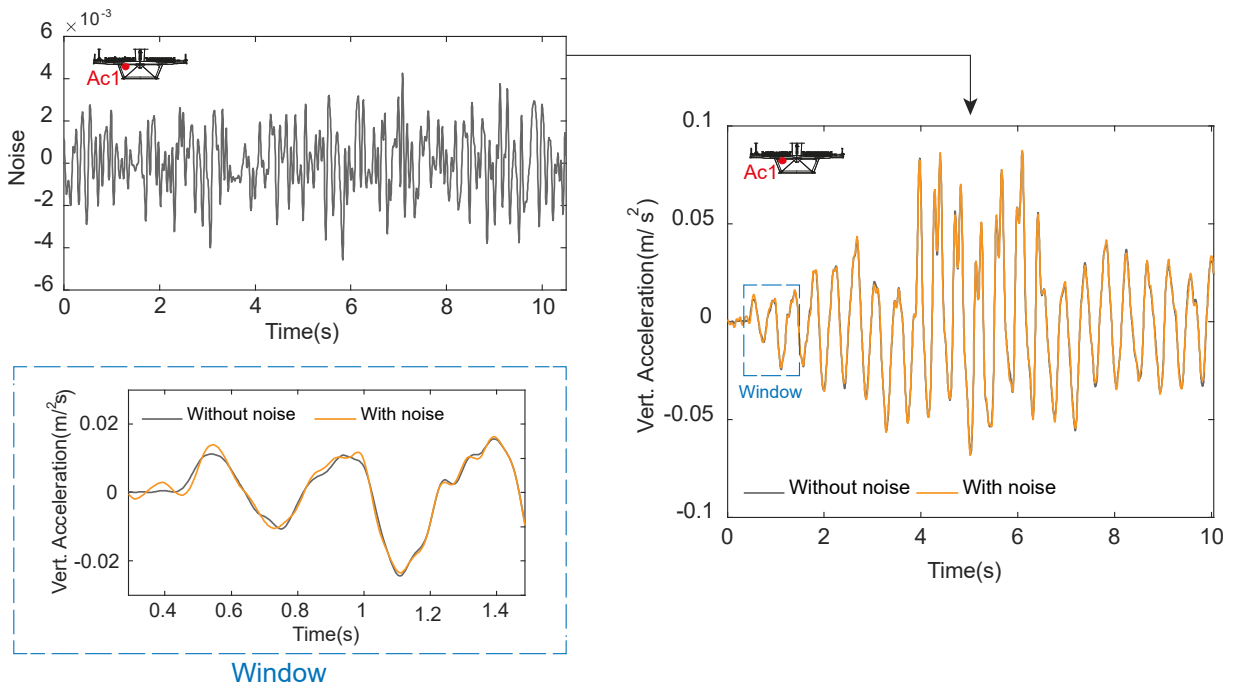
Figure 5.5 – Noise distribution and vertical acceleration bridge response before and after being corrupted.

5.3.4 Numerical simulation

The dynamic numerical simulations conducted in the present work aimed at reproducing the structural quantities measured in the exact locations of the 23 accelerometers installed on site (Figure 3.20a), when a train crosses the bridge. The numerical simulations implemented to obtain responses describing damaged and undamaged structural conditions followed the procedure described in section 4.2.3.2, using different train loading configurations at different speeds (according to Figure 5.2), as well as temperature data acquired on site (Figure 3.14) as input. The acceleration responses were then 'corrupted' with the noise distributions measured on site, as shown in the previous section.

The time-series illustrated in Figure 5.6 are examples of simulated responses for undamaged baseline conditions, acquired from the accelerometer located at the central mid-span of the concrete slab (Ac1). The variations associated with different train types, loading schemes, train speed and temperature actions are shown in this figure.
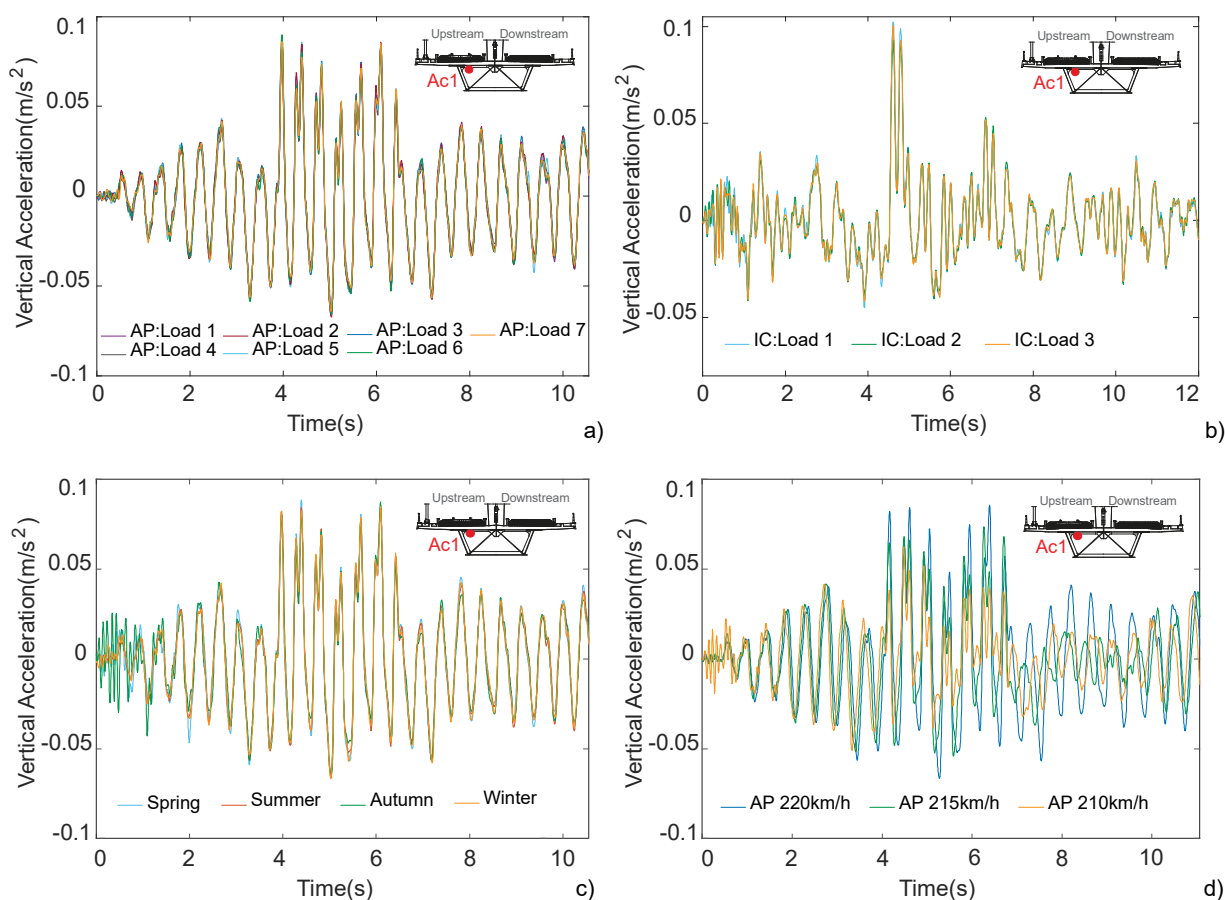
Figure 5.6 – Baseline time-series simulations of sensor Ac1: a) using different loading schemes of the AP train at 220 km/h, b) using different loading schemes of the IC train at 190 km/h, c) using temperature measurements from different seasons, d) with the AP train traveling at different speeds.

A clear distinction between the bridge responses to the crossings of the AP train (Figure 5.6a) and the IC train (Figure 5.6b) can be observed, showing the need of considering different train types for the development of damage identification strategies. Conversely, the same plots allow observing that different loading schemes, representing the variability between identical trains, generate smaller changes in the dynamic responses. Temperature action and train speed also influence the structural response imposed by trains crossing the bridge, as it can be readily observed in Figure 5.6c and Figure 5.6d for AP train crossings.

Figure 5.7 shows examples of simulated responses of the Ac1 accelerometer for damaged scenarios in the concrete slab (D2: m2) and in the bearing devices on pier P2 (D1: P2), during a summer day and with the AP train crossing the bridge at 220 km/h.

Figure 5.7 – Time-series obtained in a summer day for the AP train at 220 km/h: a) stiffness reduction D2:m2 and vertical acceleration from sensor Ac1, b) stiffness reduction D2:m2 and vertical acceleration from sensor AsV3 and c) friction increase D1:P2 and vertical acceleration from sensor Ac1.

The influence of damage scenarios on the signal obtained for train crossings appears to be much smaller than that observed for changes in temperature actions, train type an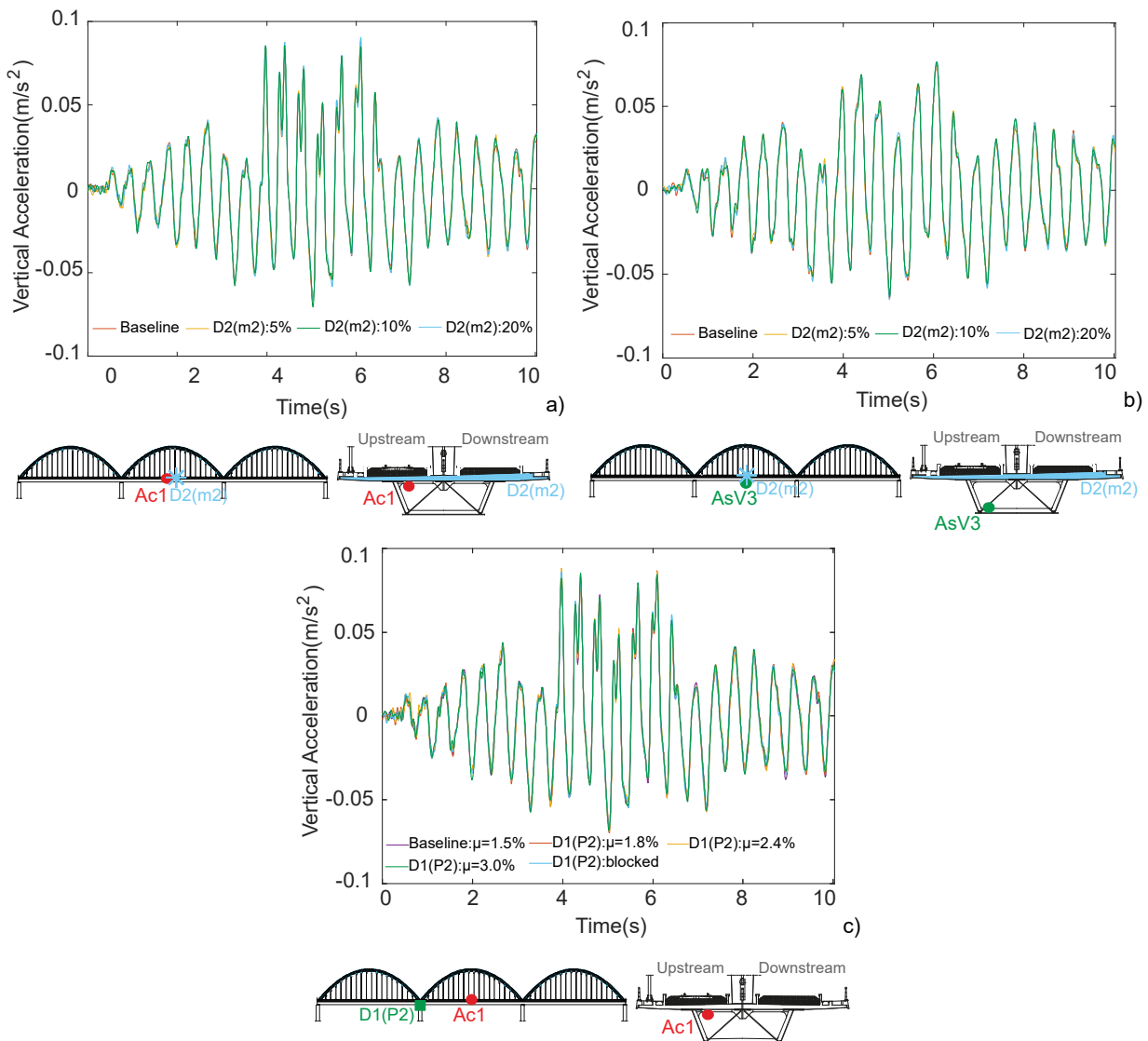d train speed, even when analysing sensors adjacent to the damages and for the largest magnitudes considered (20% stiffness reduction and full restraint of the bearing). This conclusion can be easily derived from Figure 5.7, where the high overlapping of the time-series obtained from the baseline condition and the remaining ones puts in evidence the small magnitude of the simulated damage scenarios, which can be considered as early damage.

5.4   FEATURE EXTRACTION

Feature extraction is addressed in this section by implementing AR models and ARX models to the acceleration responses measured by the railway bridge over the Sado River to the train crossings for several structural conditions, as synthetized in Figure 5.8. The features obtained from each approach are compared and an evaluation of the performance of both models is conducted.
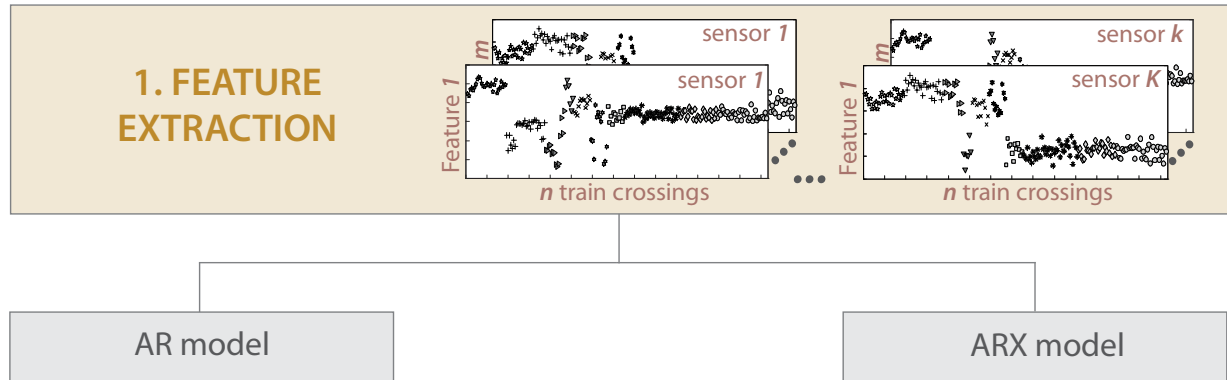
Figure 5.8 – Schematic representation summarising the portion of the machine learning strategy implemented in section 5.4.

5.4.1   Theoretical background

Features are extracted from a statistical time series analysis. In this section, a brief discussion about the autoregressive model with exogenous inputs (ARX) and the autoregressive (AR) model is presented. The ARX model regresses the current measurement upon finite measurements of its past and upon an exogenous input series:

$$y_j = \sum_{i=1}^{n_a} a_i y_{j-i} + \sum_{k=1}^{n_b} b_k x_{j-k} + \varepsilon_j \tag{5.1}$$

where y_j, x_j, and ε_j are output, input, and error terms of the model at the signal value j, respectively. On the other hand, n_a, n_b and a_i, b_k represent the orders and the parameters of the output and input data, respectively. The ARX model can be simplified to the AR model if n_b is set to zero:

$$y_j = \sum_{i=1}^{n_a} a_i y_{j-i} + \varepsilon_j \tag{5.2}$$

The process of extracting the AR/ARX parameters, a_i and b_k, is based on fitting the AR/ARX models to vibration time-domain responses, acquired from different sensors, in the undamaged and damaged conditions. The vectors of the AR/ARX model parameters in the baseline and damaged state conditions are used as the damage-sensitive features, which depend on sensors from multiple locations. Typical time-series lead to an overdetermined set of equations that must be solved to obtain optimal estimates of the AR and ARX coefficients. There are several methods that can be used to solve the coefficients; the least-squares method was the one applied in this study (Box & Jenkins, 1976).

Regarding the ARX model, the accelerometer located at the central mid-span of the concrete slab (Ac1 – Figure 3.20), named as the reference channel, was defined as output, y_j, since it is located in a central point of the bridge and is representative of its global behaviour. Each of the other installed accelerometers was defined as the input signal, x_j.

5.4.2 Model order

The AR/ARX model orders should be rationally determined considering the data characteristics. This is a key issue, since a higher-order model may better match the data, but may not be generalized to other data sets. On the other hand, if one selects a low-order model, it will not necessarily capture the underlying response of the physical system (Farrar & Worden, 2013). The Akaike Information Criterion (AIC) has been reported as one of the most efficient techniques for order optimization (Bishop 1995; Figueiredo et al., 2010). The AIC is a measure of the goodness-of-fit of an estimated statistical model that is based on the trade-off between fitting accuracy and number of estimated parameters. In the context of ARX models this criterion assume the form

$$AIC = N_t \, ln \, \varepsilon + 2N_p \tag{5.3}$$

where N_p is the number of estimated parameters, N_t the number of predicted data points, and $\varepsilon = SSR/N_t$ the average sum-of-square residual (SSR) errors. To find out an optimum order, one should examine a wide range of orders and choose a number with the minimum AIC value.

With the purpose of establishing a common appropriate order, analyses of the AIC values were performed for twenty-two independent ARX (n_a, n_b) models of increasing order ($n_a = n_b = 1, 2, \ldots, 50$). Figure 5.9a shows the average AIC function resulting from analyses carried out on the 100 baseline time-series. As observed, after the model order 30 the AIC values tend to stabilize indicating that higher orders do not provide relevant information for the construction of the model.

Herein, the Normalized Root Mean Square Error (NRMSE) fitness value (Eq. 5.4) was also used to quantify the model accuracy according to the ARX order defined.

$$NRMSE = 1 - \frac{\sum_{i=1}^{n}(y_i - \hat{y}_i)^2}{\sum_{i=1}^{n}(y_i - \bar{y})^2} \tag{5.4}$$

where, y_i is the measured data, $\hat{y}_i$ is the simulated data through the ARX model, and $\bar{y}$ is the mean of the measured dataset. For each baseline structural condition, the parameters were estimated using the least squares technique applied to time-series from all twenty-three accelerometers, and the NRMSE values were computed for ARX models of increasing order. Figure 5.9b plots the average NRMSE values, which represent the difference between the actual data and the ARX model predicted data. It is possible to observe that the accuracy of the ARX model gradually increases with the ARX model order and appears to stabilize close to 30, whereby both the input and output orders of the ARX model were set to 30. The same output order was adopted for the AR model.
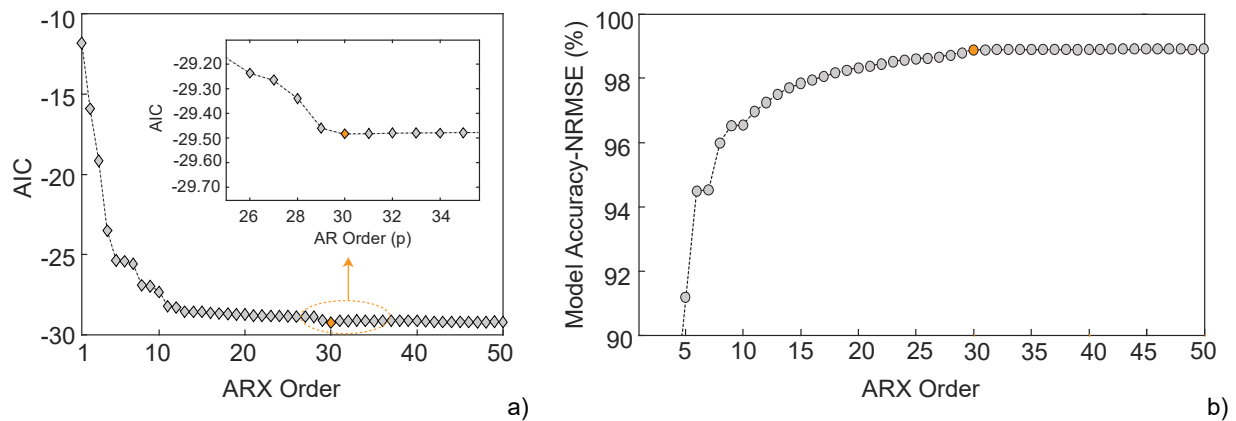
Figure 5.9 – Model order definition: a) average AIC function for twenty-two independent ARX (n_a, n_b) models of increasing order using the 100 baseline time series and b) model accuracy according to the ARX model order.

Based on these assessments, for each structural condition and for each accelerometer, individual AR (30) and ARX (30, 30) models were implemented to fit the corresponding time-series and their parameters were used as damage-sensitive features.

5.4.3 AR models

Thirty AR parameters extracted for each of the 100 simulations of the baseline condition and 114 simulations of the damaged condition, using the measurements from the accelerometer located at the central mid-span of the concrete slab (Ac1), are shown in Figure 5.10.
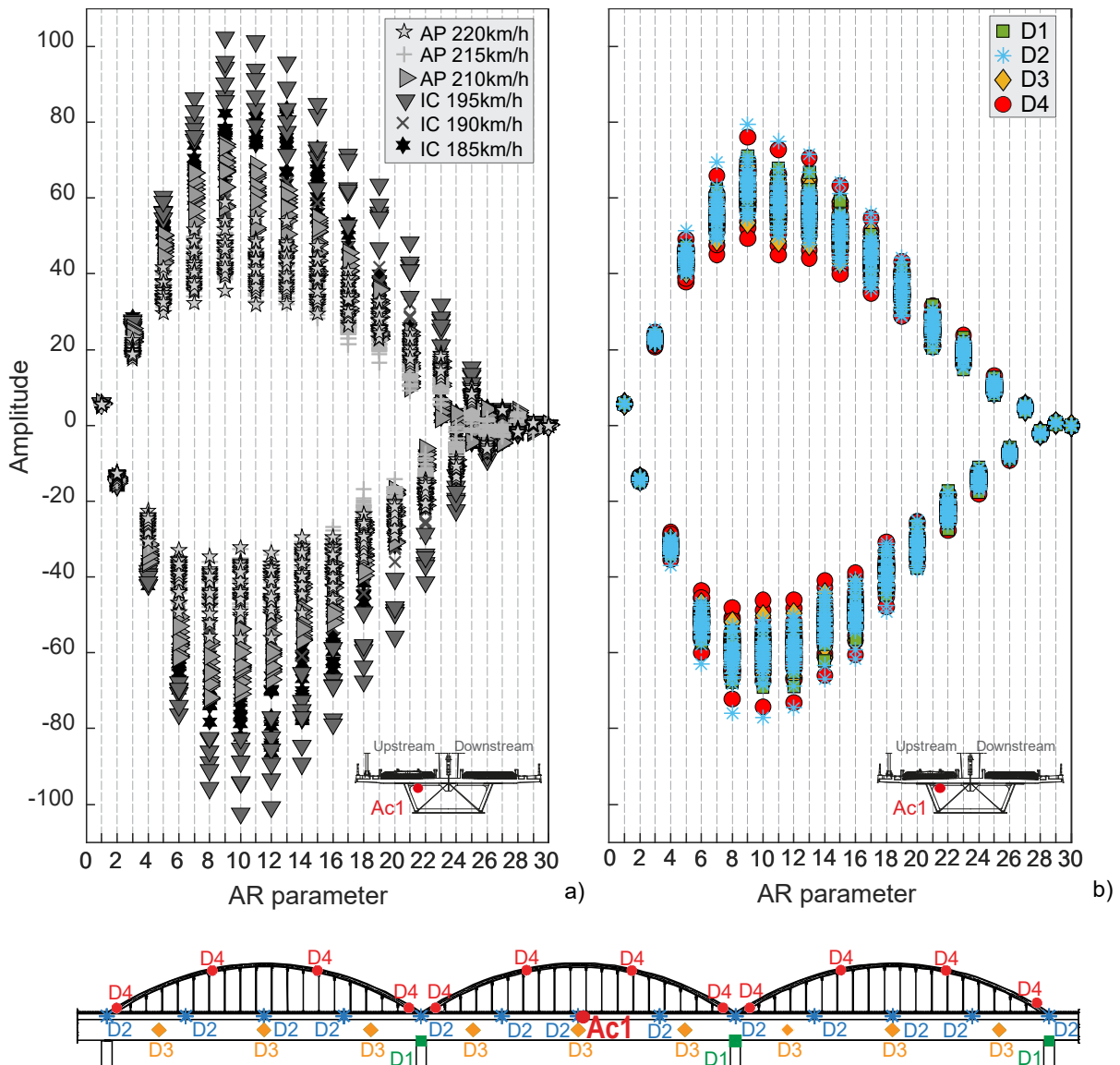
Figure 5.10 – AR features obtained from the accelerations responses in the mid-span section of the concrete slab (Ac1): a) for each of the 100 simulations of the baseline (undamaged) condition, b) for each of the 114 damage scenarios.

A comparison of the features' amplitude between scenarios allows observing a higher variability of the AR parameters for EOVs (Figure 5.10a) than for damages (Figure 5.10b). Additional damage-sensitive features were extracted likewise from each one of the remaining 22 accelerometers installed on site comprising time-series with 2112 measurements, which resulted in a three-dimensional feature matrix of *214-by-30-by-23* elements. In this sense, the AR model proved to be also an effective data fusion tool by transforming 2112 points into 30 features.

To illustrate the feature extraction procedure, Figure 5.11 details four AR parameters (AR1, AR10, AR15 and AR20) obtained for sensor Ac1, as well as all the thirty AR parameters represented by box-and-whisker plots. The features are divided into two major groups according to the structural condition: baseline (first 100 simulations) and damaged (114 subsequent simulations).

In the plots shown in Figure 5.11a, for each baseline condition, the seven identical symbols in a row (regarding shape and colour), in the case of the AP train, and the three symbols in a row, in the case of the IC train, represent the different loading schemes considered for each train type and speed, and for each temperature. For each damage location (codes from Figure 5.4), a sequence of three or four symbols represents different levels of severity (low to high from left to right), according to the magnitude choices described in 5.3.2. A comparison between the values of the AR1, AR10, AR15 and AR20 parameters across all 214 scenarios allows concluding that each feature is describing distinct trends of the analysed data. The main changes in the amplitudes of these parameters are induced by the type and speed of the train. In addition, for each value of train speed, the observed changes in the amplitude of these parameters are generated by variations in the values of structural temperature (spanning all four seasonal average temperatures). The loading schemes are the operational influencing parameter with the least impact on the parameter variability in the baseline simulations, as previously observed.

Figure 5.11b confirms that the distributions of all thirty AR parameters from damage scenarios vary significantly less when compared to the distributions of baseline conditions, which leads to a preponderance of EOVs, regardless of the type of damage as well as its location and severity.
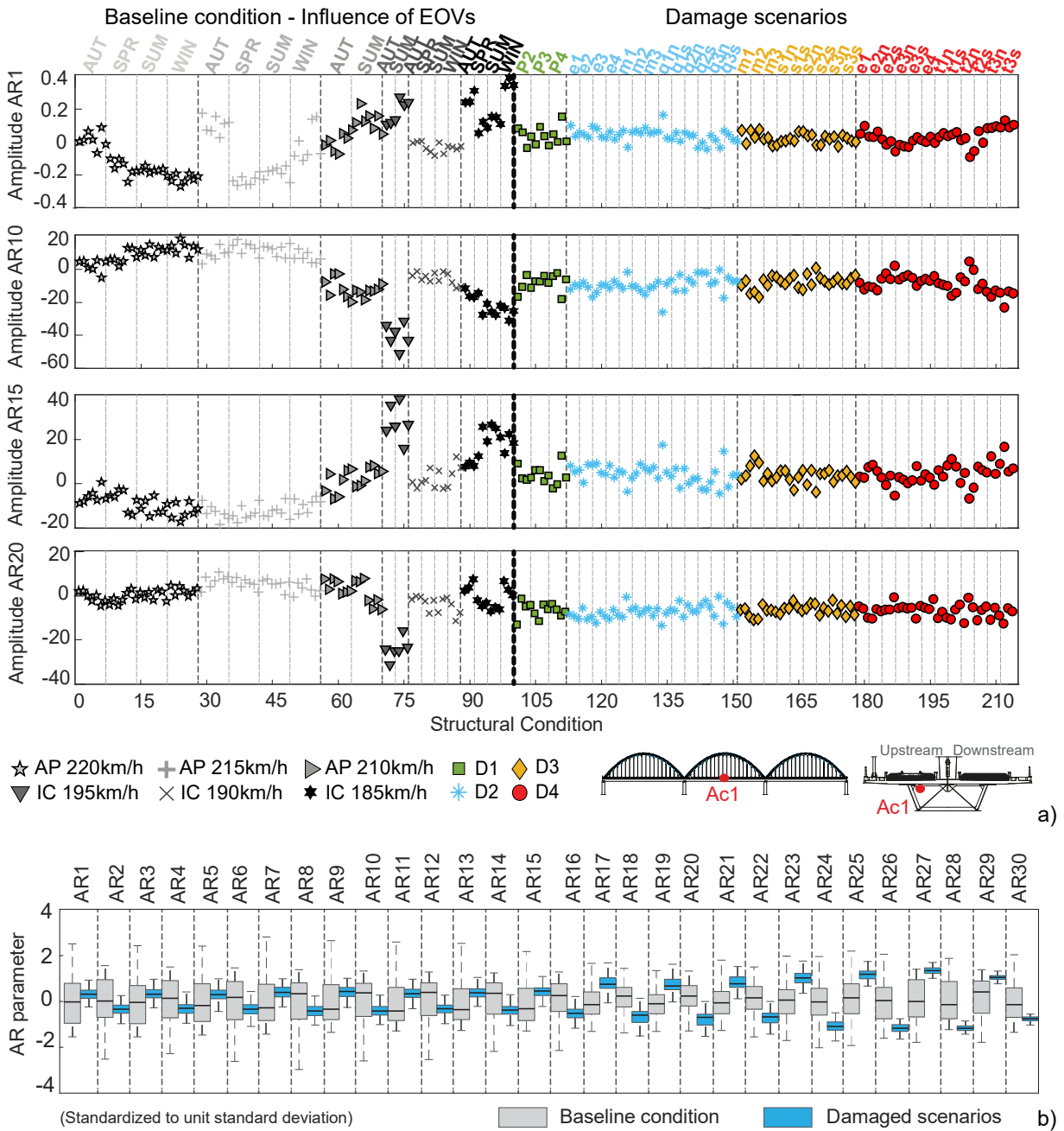
Figure 5.11 – For all 214 structural conditions considering the responses of accelerometer Ac1: a) amplitude of four of the thirty AR parameters, b) box-and-whiskers plots representing the thirty AR parameters.

The importance of a disperse sensors network can be observed in Figure 5.12 where the AR features are extracted from different sensors, namely, sensor Ac1 (Figure 5.12a), sensor AL-P3 (Figure 5.12b) and sensor AsT$_t$2 (Figure 5.12c). It illustrates the features obtained from two simulations of the baseline condition:

a) AP|220km/h|SUM: the AP train crossing the bridge at 220 km/h in a summer day;

b) AP|210km/h|AUT: the AP train crossing the bridge at 210 km/h during an autumn day.

The features extracted from the following four damage scenarios are also shown:

a) D1 (P3: restrained), the full restraint of the bearing devices at pier P3;

b) D2 (m2:20%), the 20% stiffness reduction in the central mid-span of the concrete slab;

c) D3 (m2:20%), the 20% stiffness reduction at the diaphragm, also in the central mid-span;

d) D4 (t2s:20%), the 20% stiffness reduction in the arch at one-third south of the central span.

The bar charts presented in Figure 5.12 were drawn from the sum of the differences between the amplitude of the parameters from each of these scenarios and the amplitude of the parameters from the baseline condition AP|220km/h|SUM.
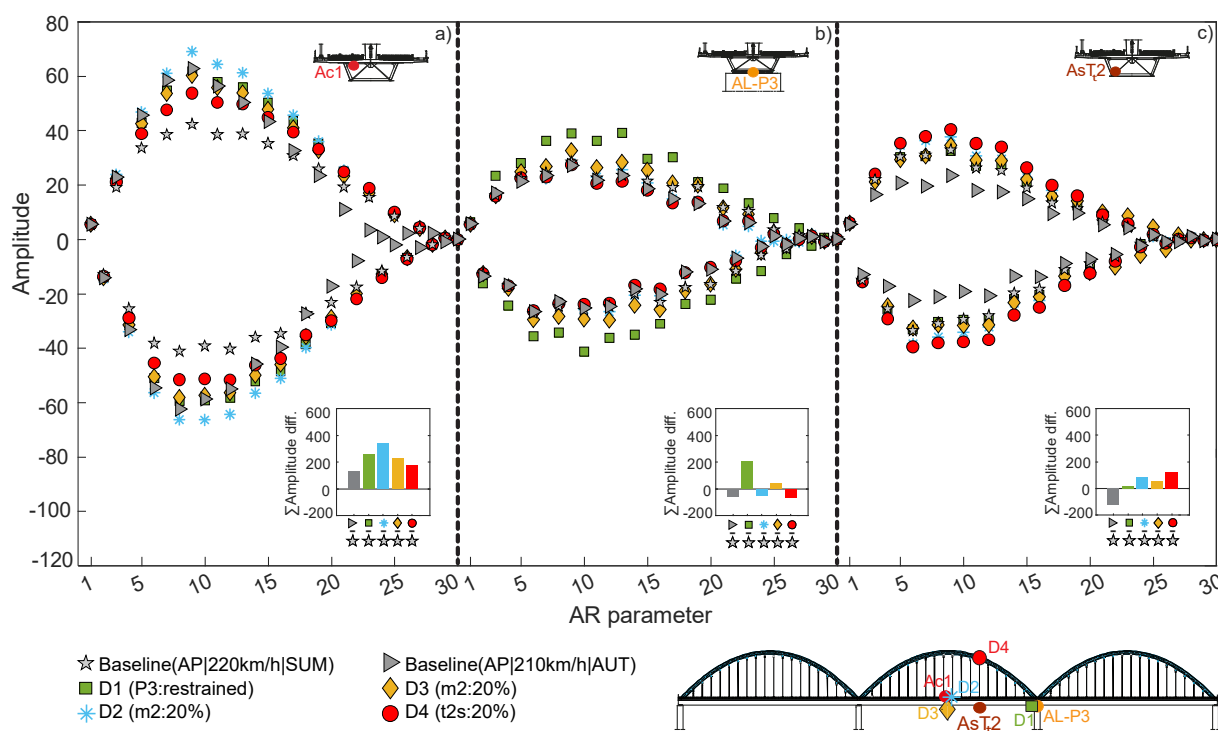
Figure 5.12 – AR features obtained from the accelerations responses measured by three sensors regarding two baseline and four damaged structural conditions: a) Ac1, b) AL-P3 and c) AsTt2.

The plots show that the parameters' amplitudes for sensor Ac1 (Figure 5.12a), located at mid-span, are those with the most significant changes from one of the baseline scenarios, especially for the damage condition adjacent to this sensor - D2 (m2:20%). Regarding the sensor AL-P3, the features with higher amplitude were observed for the parameters of the damage scenario D1 (P3: restrained), which is the closest to this sensor (Figure 5.12b). The AR parameters extracted from the transversal accelerometer AsT_t2, located in the steel-box girder at the southern third of the central span (Figure 5.12c), show more sensitivity to a damage

105

simulated in the same section but in the arch – D4 (t2s:20%) and to a damage in the mid-span of the concrete slab – D2 (m2:20%).

5.4.4   ARX models

Sixty ARX damage-sensitive features extracted for baseline and damaged conditions, considering as output the measurements from the accelerometer located at the central mid-span of the concrete slab (Ac1), and as input the measurements of the accelerometer located at the central mid-span of the steel box girder (AsV3), are shown in Figure 5.13.

As observed with the AR parameters, comparing the undamaged (Figure 5.13a) and the damaged features (Figure 5.13b), the ARX parameters present a higher variability in the presence of a range of EOVs, compared to a range of damage scenarios. The outcome after implementing the ARX model to each structural condition and to each of the remaining 21 accelerometers was a 3D feature matrix of *214-by-60-by-22* elements.

Figure 5.14 details two ARX output parameters (ARX1 and ARX10) and two ARX input parameters (ARX50 and ARX60) obtained considering the output sensor Ac1 and the input sensor AsV3, as well as all the sixty ARX parameters (ARX1 to ARX60) represented by box-and-whisker plots.

In Figure 5.14a, a comparison between the values of the ARX1 and ARX10 output parameters across all 214 scenarios allows concluding that each feature is describing distinct inner relationships of the analysed data and that the features from the baseline condition have a much higher amplitude variation than the features from damage scenarios. However, the input parameters ARX50 and ARX60 exhibit a completely different behaviour, since for them, the influence of EOVs (baseline) is not as predominant when compared to the influence of damage, as it is in the other two parameters (ARX1 and ARX10). Instead, the amplitude of the features has an identical magnitude in all 214 structural conditions.

This trend can also be observed in the box-and-whisker plots presented in Figure 5.14b. For the output parameters (ARX1 to ARX30), there is an increased importance of the distributions of baseline conditions, and, consequently, of EOVs, in relation to the distributions of damage scenarios, while, for the input parameters (ARX31 to ARX60) these distributions are more similar, which denotes an increase in the damage preponderance.
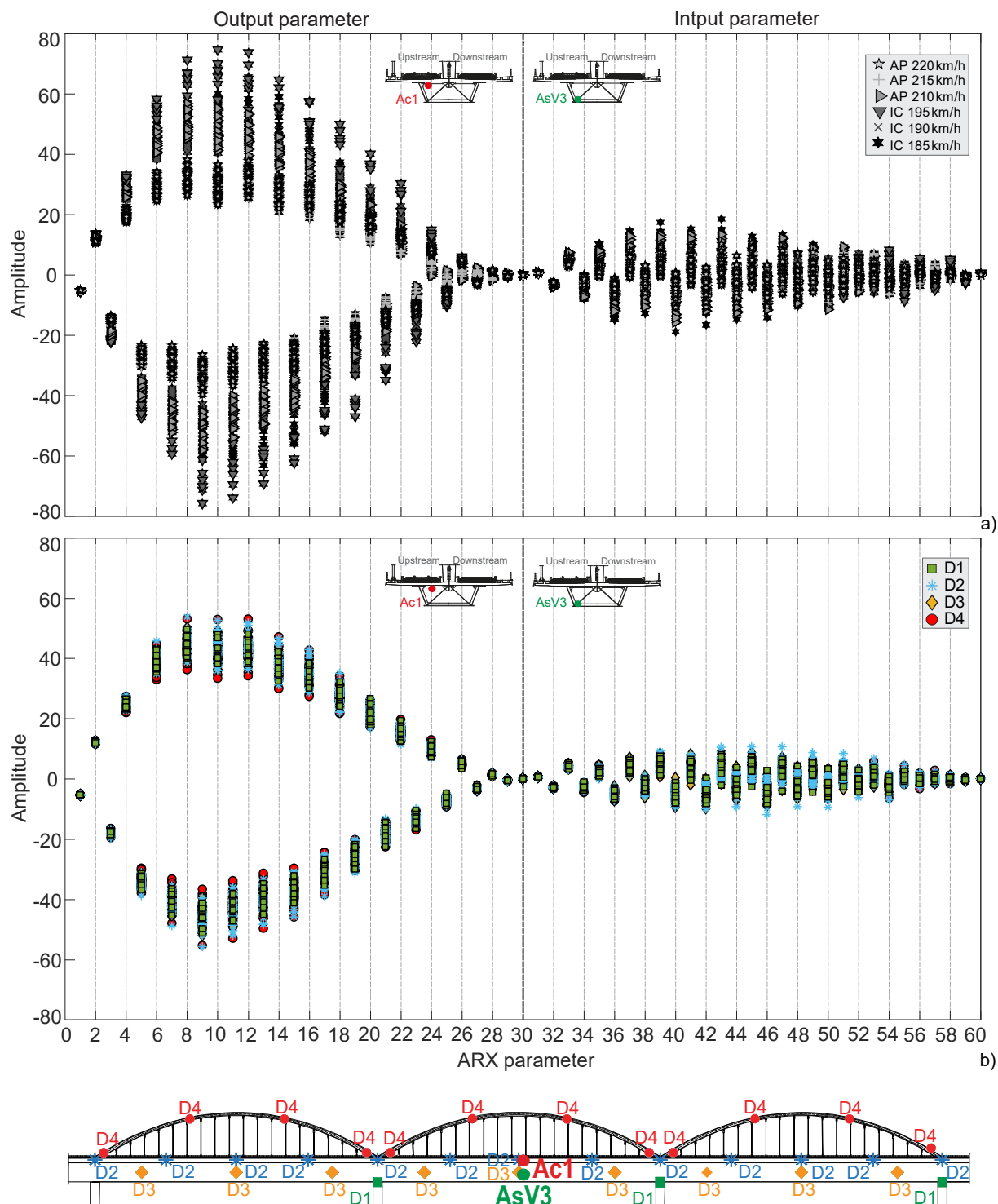
Figure 5.13 – ARX features obtained from the accelerations responses in the mid-span section of the concrete slab (Ac1) and steel-box girder (AsV3): a) for each of the 100 simulations of the baseline (undamaged) condition, b) for each of the 114 damage scenarios.
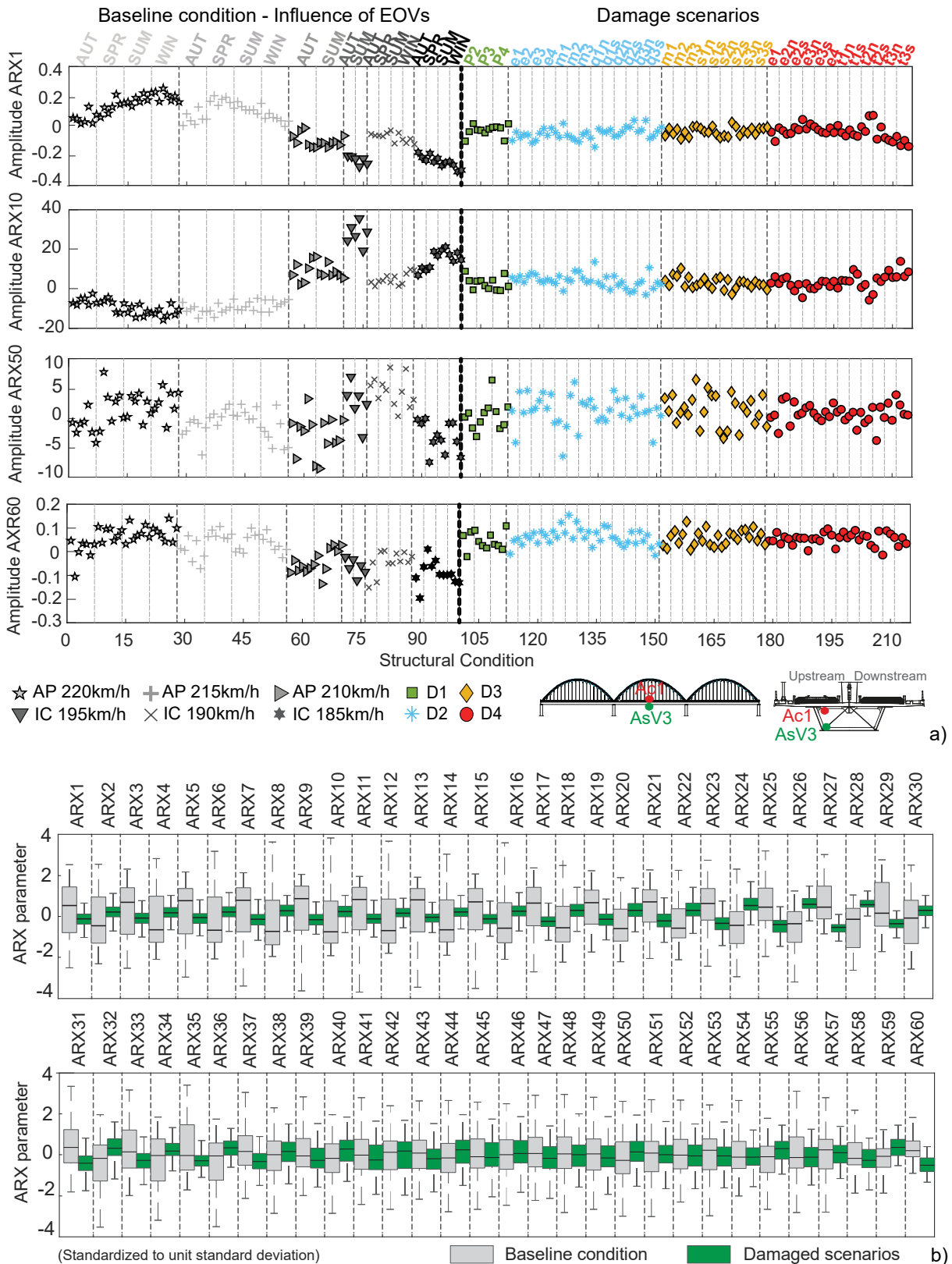
Figure 5.14 – For all 214 structural conditions, considering the responses of accelerometer Ac1 as output and sensor AsV3 as input: a) amplitude of four of the sixty ARX parameters, b) box-and-whiskers plots representing the sixty ARX parameters.

Figure 5.15 shows that ARX features extracted for different state conditions represent very distinct distributions depending on the input sensor. In this figure, the signal obtained from sensor Ac1 was taken as the output and each one of the sensors AsV3 (Figure 5.15a), AL-P3 (Figure 5.15b) and AsT$_t$2 (Figure 5.15c) as the input. As for the study conducted with the AR model in Figure 5.12, Figure 5.15 illustrates the ARX features extracted from two simulations of the baseline condition: AP|220km/h|SUM and AP|210km/h|AUT; and from four damage scenarios: D1 (P3: restrained), D2 (m2:20%), D3 (m2:20%), and D4 (t2s:20%). The bar charts presented in this figure were also drawn from the sum of the differences between the amplitude of the parameters from each of these scenarios and the amplitude of the parameters from the baseline condition AP|220km/h|SUM.
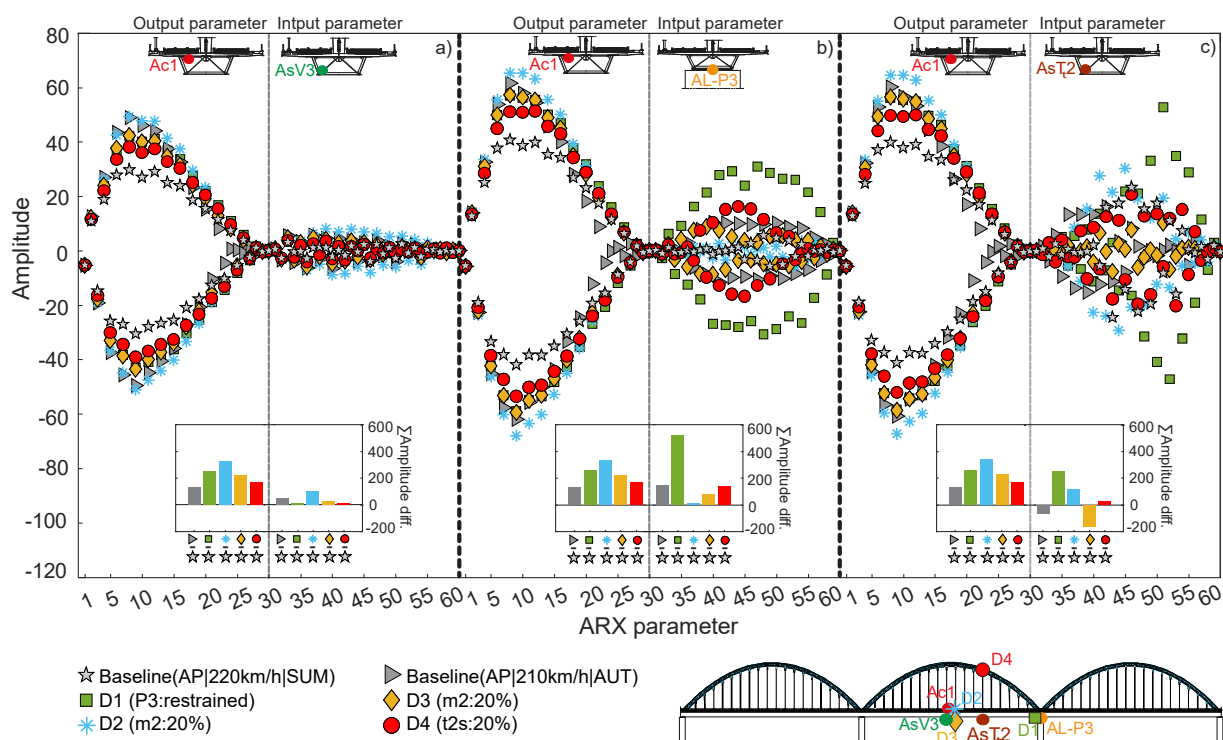
Figure 5.15 – ARX features obtained for the accelerations responses from one output sensor and three different input sensors regarding two baseline and four damaged structural conditions: a) Ac1 and AsV3, b) Ac1 and AL-P3, c) Ac1 and AsTt2.

The ARX parameters' amplitudes obtained from the output sensor Ac1 are higher than those extracted from the input sensors, especially for the damage scenario closest to this sensor - D2 (m2:20%). As expected, comparing the bar charts of Figure 5.15a, b and c, there is a consistency in terms of the relative amplitude of the parameters from the output sensor Ac1, regardless of the input sensor. On the other hand, the features from the sensor AsV3 (Figure 5.15a) have the lowest amplitude, which can be justified by the fact that this is the input sensor closest to the output sensor Ac1. The bar chart in Figure 5.15a shows that the ARX parameters from this input

sensor are more sensitive to damage scenario D2 (m2:20%), which is adjacent to this sensor. A comparison between the bar charts between Figure 5.12a and Figure 5.15 indicates a similarity in the relative amplitude obtained when using the signal from sensor Ac1 as output in both the AR and ARX models. Regarding the input sensor AL-P3 (Figure 5.15b), the features with the highest amplitude are those of the parameters of the damage scenario D1 (P3: restrained), which is also the closest to this sensor, as can be clearly confirmed in the bar chart of Figure 5.15b. By comparing these results with those obtained with the AR model (Figure 5.12b), a considerable increase in the relative amplitude of the features is observed in the bar chart of Figure 5.15b. This bar chart also shows the importance of considering and modelling EOVs, since the input parameters from the baseline condition AP|210km/h|AUT present an equal or higher relative amplitude than the damage scenarios D2, D3 and D4. Figure 5.15c presents the ARX input parameters extracted from sensor AsT$_t$2, which are highly sensitive to damage D1 (P3: restrained) and damage D2 (m2:20%). Its corresponding bar chart allows observing that, in this case, the ARX input parameters from the damage scenario D3 (m2:20%) and the baseline scenario AP|210km/h|AUT have less sensitivity than those extracted from the baseline scenario AP|220km/h|SUM.

As a result from this study, the clear advantage of crossing information between sensors has shown that ARX models allow for an improvement in terms of the knowledge extracted from the features, which may lead to greater sensitivity, when compared to AR models.

5.5   FEATURE MODELLING

The analysis of the AR/ARX parameters shown in sections 5.4.3 and 5.4.4, as well as the time series presented in section 5.3.4, allow drawing some conclusions about the difficulty in distinguishing damage and undamaged scenarios, since changes in environmental and operational actions generally result in larger changes in the parameters. Therefore, it is necessary to adequately model these parameters to remove the changes generated by EOVs and highlight those generated by damage. As summarized in Figure 5.16, in this section, feature modelling is performed to the AR parameters using regression-based and latent-variable methods, while the ARX parameters are normalized implementing only a latent-variable method. A comparison between both types of methods to model features is conducted, as well as the study of the performance obtained when using AR or ARX-based features.
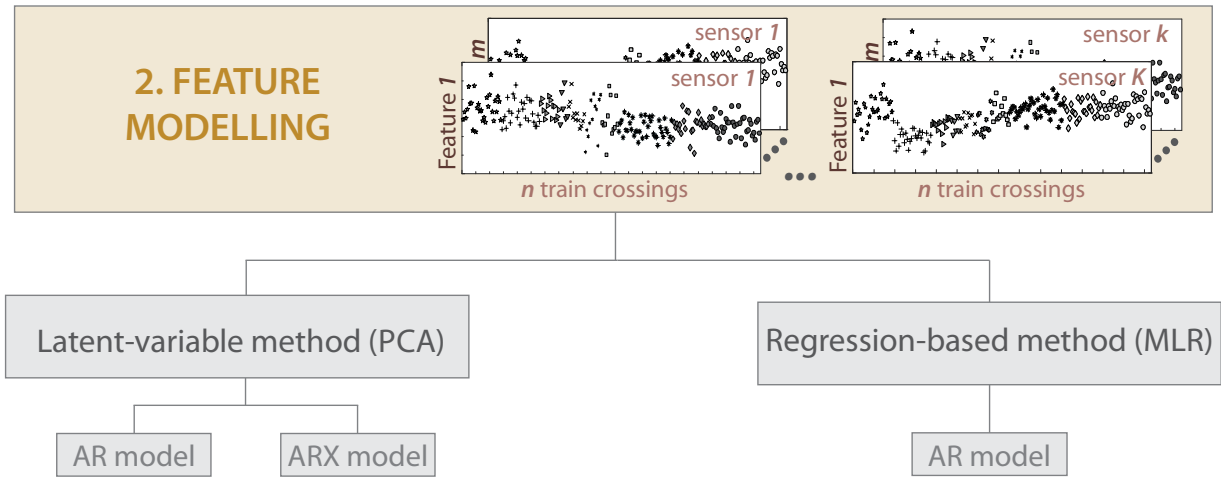
Figure 5.16 – Schematic representation summarising the portion of the machine learning strategy implemented in section 5.5.

5.5.1 Latent-variable method

5.5.1.1 Theoretical background

One of the main obstacles in implementing vibration-based SHM systems in operational conditions is the challenge in separating (assumed unmeasured) environmental and operational effects from the dynamic responses in order to obtain features that are primarily sensitive to damage. To overcome this problem, a latent-variable method as the principal components analysis (PCA) (Yan et al., 2005) is used here for feature modelling. PCA is a multivariate statistical method that produces a set of linearly uncorrelated vectors called principal components or scores, from a multivariate set of vector data. Assuming that environmental conditions have a linear effect on the identified parameters, PCA of continuous monitoring results may efficiently remove EOVs (Yan et al., 2005; Hu et al., 2012; Ribeiro et al., 2021). Considering an *n-by-m* matrix X with the original features extracted from the dynamic responses, where m is the number of ARX/AR parameters and n is the number of simulations for the baseline condition, a transformation to another set of m parameters, Y, designated principal components or scores, can be achieved by the following equation:

$$Y = X \cdot T \tag{5.5}$$

where T is an *m-by-m* orthonormal linear transformation matrix that applies a rotation to the original coordinate system. The covariance matrix of the ARX/AR parameters in the baseline condition, Σ, is related to the covariance matrix of the scores, Λ, as follows:

$$\Sigma = T \cdot \Lambda \cdot T^T \tag{5.6}$$

in which T and Λ are matrixes obtained by the singular value decomposition of the covariance matrix Σ of the ARX/AR parameters. The columns of T are the eigenvectors and the diagonal matrix Λ comprises the eigenvalues of the matrix Σ in descending order. Hence, the eigenvalues stored in Λ are the variances of the components of Y and express the relative importance of each principal component in the entire data set variation (Yan et al., 2005).

As demonstrated by Santos et al. (2013), the PCA is able to retain meaningful information related to environmental and operational effects in the first components, whereas variations related to other effects, especially those of small-magnitude, such as early-damage, may be summarized in latter components. Since the aim of the present work is to detect damage, which has generally a local effect, the feature modelling procedure consists of removing the most significant principal components from the features and retaining the rest for subsequent statistical analysis. With this in mind, the matrix Λ can be divided into a matrix with the first p eigenvalues and a matrix with the remaining $m\text{-}p$ eigenvalues. Defining the number of p components remains an open question with regard to the representation of the multivariate data; although several approaches have been proposed, there is still no definitive answer (Härdle & Simar, 2015). In this work, the value of p (or the number of principal components to discard) is determined based on a rule of thumb in which the cumulative percentage of the variance reaches 80% (Härdle & Simar, 2015; Jolliffe, 2002). After choosing p, the $m\text{-}p$ components of the matrix Y can be obtained using Equation (5.5) and a transformation matrix $\hat{T}$ built with the remaining $m\text{-}p$ columns of T. Those $m\text{-}p$ components can be remapped to the original space using the following:

$$F_{PCA} = X \cdot \hat{T} \cdot \hat{T}^T \qquad (5.7)$$

where F_{PCA} is the *n-by-m* matrix of PCA-based features, expected to be less sensitive to EOVs and to be more sensitive to the damage cases. This procedure is then repeated for each sensor.

5.5.1.2 AR-PCA-based features

PCA-based modelling, as described in the previous section, was applied to the AR parameters, and a *23-by-30* matrix with PCA-based features was obtained for each train crossing. The important advantage of fitting a latent-variable method, instead of a regression-based method, is the ability to remove the influence of temperature and train speed without having to measure them. Since the cumulative percentage of variance of the first principal component (PC)

was greater than 80% for different structural conditions, this PC was the only one discarded during the modelling process (i.e. $p = 1$).

Figure 5.17 shows the four AR parameters for accelerometer Ac1, obtained after implementing the PCA-based modelling, and the thirty box-and-whiskers plots for the thirty AR-PCA-based features. The comparison of these plots with those shown in Figure 5.11a shows an evident suppression of the changes generated by EOVs, which can be corroborated for all parameters by the distributions shown in Figure 5.17b.

Figure 5.17 – For all 214 structural conditions considering the responses of accelerometer Ac1: a) amplitude of four of the thirty AR-PCA-based features, b) box-and-whiskers plots representing the thirty AR-PCA-based features.

5.5.1.3 ARX-PCA-based features

The implementation of the PCA modelling to the ARX parameters resulted in a *22-by-60* matrix with PCA-based features for each train crossing. Since the cumulative percentage of the variance of the sum of the first three principal components was higher than 80% for different structural conditions, these three PCs were discarded during the modelling process (i.e., $p = 3$). Figure 5.18a shows four series of parameters, across the 214 scenarios, obtained for an ARX model comprising accelerometer Ac1 (output) and accelerometer AsV3 (input), after the application of the PCA. Figure 5.18b shows the boxplots obtained from the 60 ARX-PCA-based features.

The direct comparison of these action-free ARX parameters (Figure 5.18) with those shown before applying PCA (Figure 5.14) shows that, in fact, feature modelling allowed minimizing the differences generated by the effects of train type and speed and by temperature, shown in grey box-and-whiskers plots, which significantly reduce from one figure to the other. The same is not observed in the features from damage cases, represented in green box-and-whiskers plots, which remain identical or even increase.
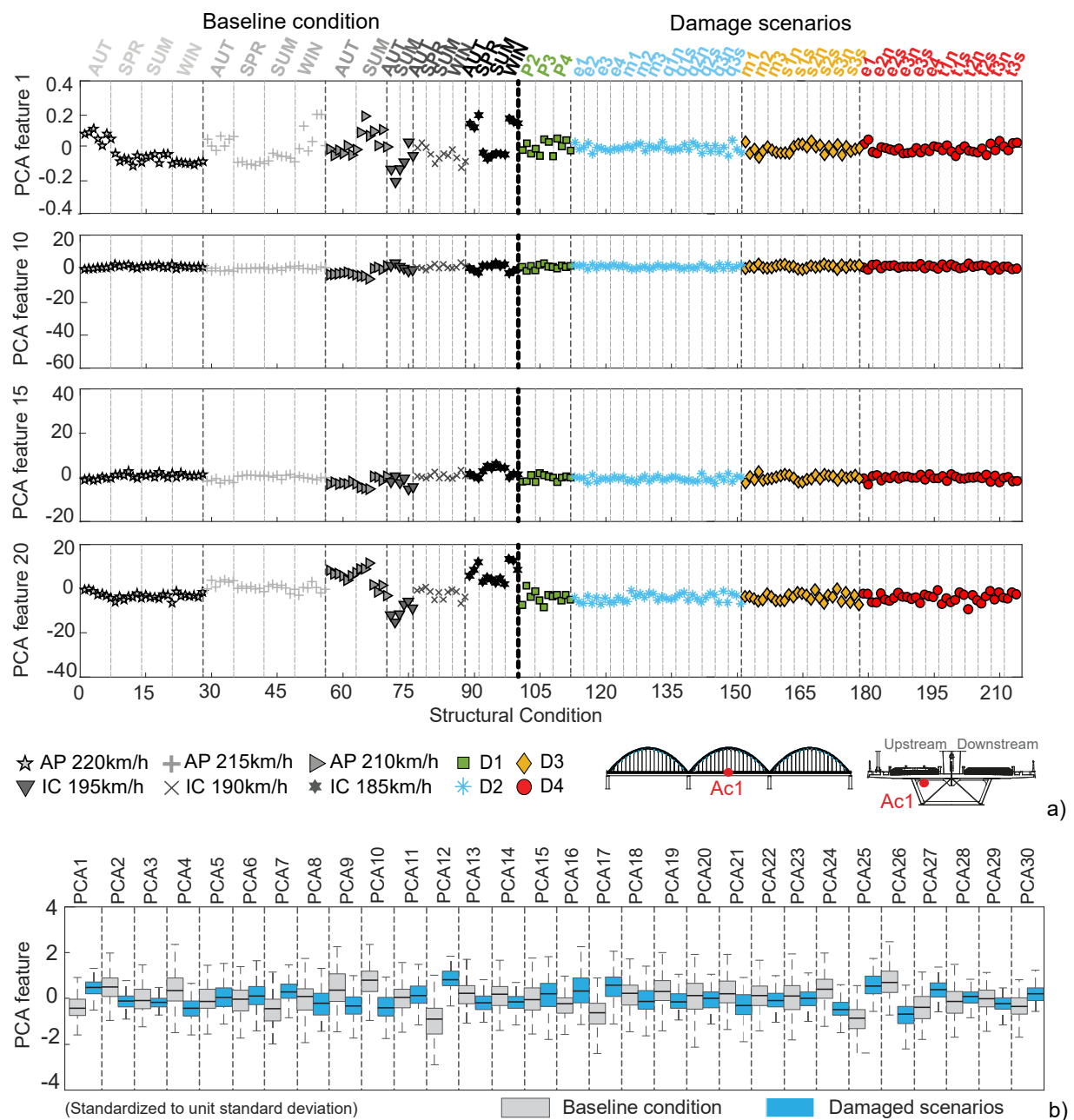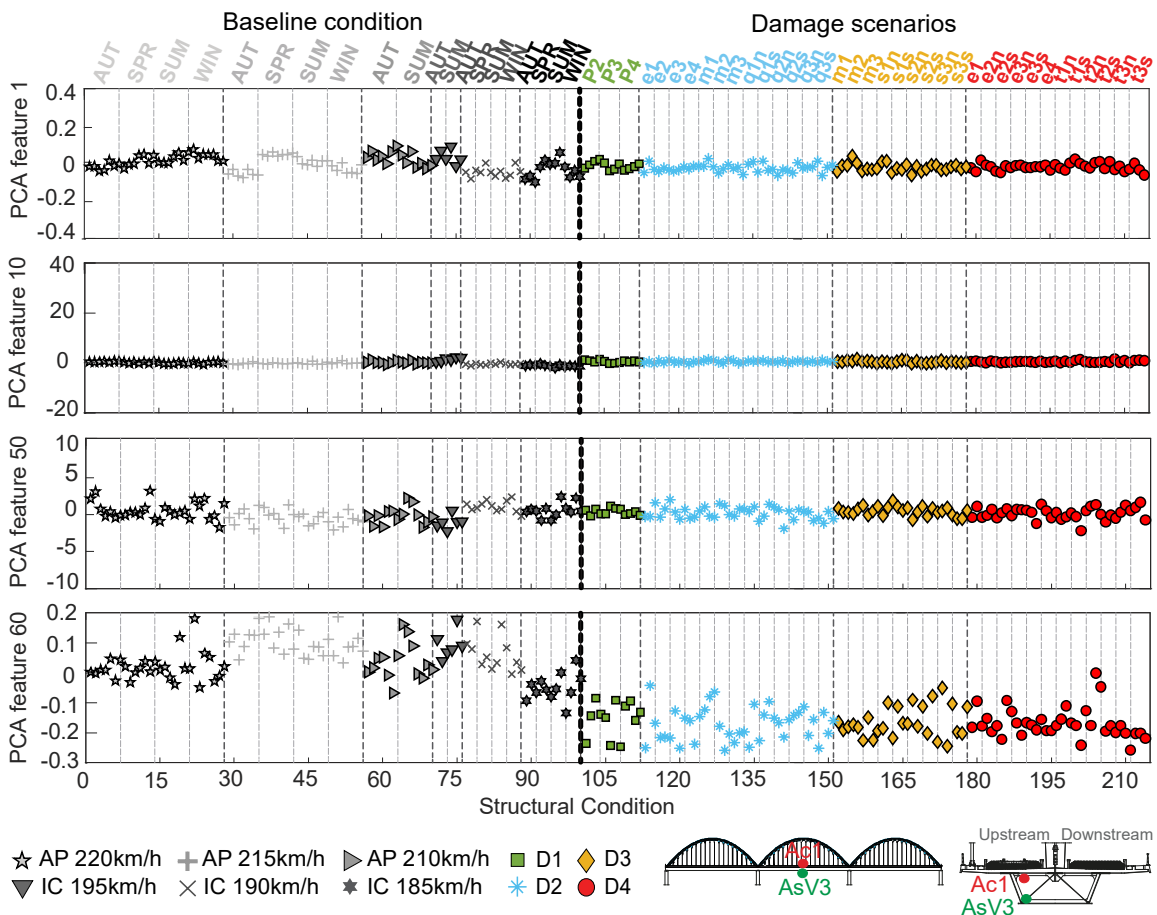
Figure 5.18 – For all 214 structural conditions considering the responses of accelerometer Ac1: a) amplitude of four of the sixty ARX-PCA-based features, b) box-and-whiskers plots representing the sixty ARX-PCA-based features.

As corroborated by Figure 5.18b, the EOVs were mitigated and a clear improvement is obtained, especially for the first thirty parameters (the output), which after feature modelling reveal distributions that are similar to those from the thirty input parameters (ARX31-ARX60). Also, comparing the AR-PCA-based features (Figure 5.17b) with the ARX-PCA-based features (Figure 5.18b), the second ones show a bigger improvement between the distributions of the baseline simulations and the damage scenarios.

5.5.2 Regression-based method

Given the results obtained with the PCA in the modelling of the AR features were not as good as when modelling the ARX features, MLR model was applied only to the AR features in order to improve sensitivity.

5.5.2.1 Theoretical background

In this work, the MLR model uses a set of measured train speeds and bridge temperatures as inputs and delivers a matrix output that represents the estimated (or predicted) AR parameters. Given m AR parameters, n baseline simulations and s operational / environmental actions, the multivariate regression model is expressed by the following (Johnson & Wichern, 2013):

$$Y = X \cdot \widehat{w} + \varepsilon_{MLR} \tag{5.8}$$

where X is the *n-by-(s+1)* input temperature and speed matrix, $\widehat{w}$ is a *(s+1)-by-m* matrix of coefficients that weights each environmental / operational input, ε_{MLR} is the *n-by-m* regression error and Y is an *n-by-m* output matrix of predicted AR parameters. The coefficients of the model parameters $\widehat{w}$ are obtained through the least squares method and given by the following equation:

$$\widehat{w} = (X^T \cdot X)^{-1} \cdot X^T \cdot Y \tag{5.9}$$

Once the model is calibrated, i.e., the optimal weights are evaluated, new data can be used as input ($\widehat{X}$) and the residual error matrix $\widehat{\varepsilon}_{MLR}$, which corresponds to the damage-sensitive features from which the environmental and operational effects are removed, is denoted by:

$$\widehat{\varepsilon}_{MLR} = Y - \widehat{X} \cdot \widehat{w} \tag{5.10}$$

This procedure is repeated for the parameters of each sensor.

5.5.2.2 AR-MLR-based features

The regression models were fitted to the AR parameters to obtain, for each of the 214 train crossings, a new matrix of AR parameters of the same size (*30-by-23)*, which is assumed to be independent (as much as possible, given the error associated with modelling) from environmental and operational effects. Regressions were applied using the AR parameters as dependent, or predicted, variables (Y in Eq.(5.8)), and temperature measurements and train speeds as explanatory variables (X in Eq.(5.8)).

Figure 5.19a shows the series of four parameters across the 214 scenarios obtained for the Ac1 accelerometer, after the application of the MLR. The direct comparison of these action-free AR parameters with those shown before the feature modelling (Figure 5.11a) allows observing that, in fact, the feature modelling enabled removing the effects generated by the type and speed of the train and by temperature, but not those generated by damage.

As shown in Figure 5.19b, not only have the effects of the EOVs been mitigated, but an important improvement can be observed in the distinction between simulations of baseline and damage conditions in all thirty parameters. More importantly, a clear upgrading when compared with AR-PCA-based features (Figure 5.17) is achieved.
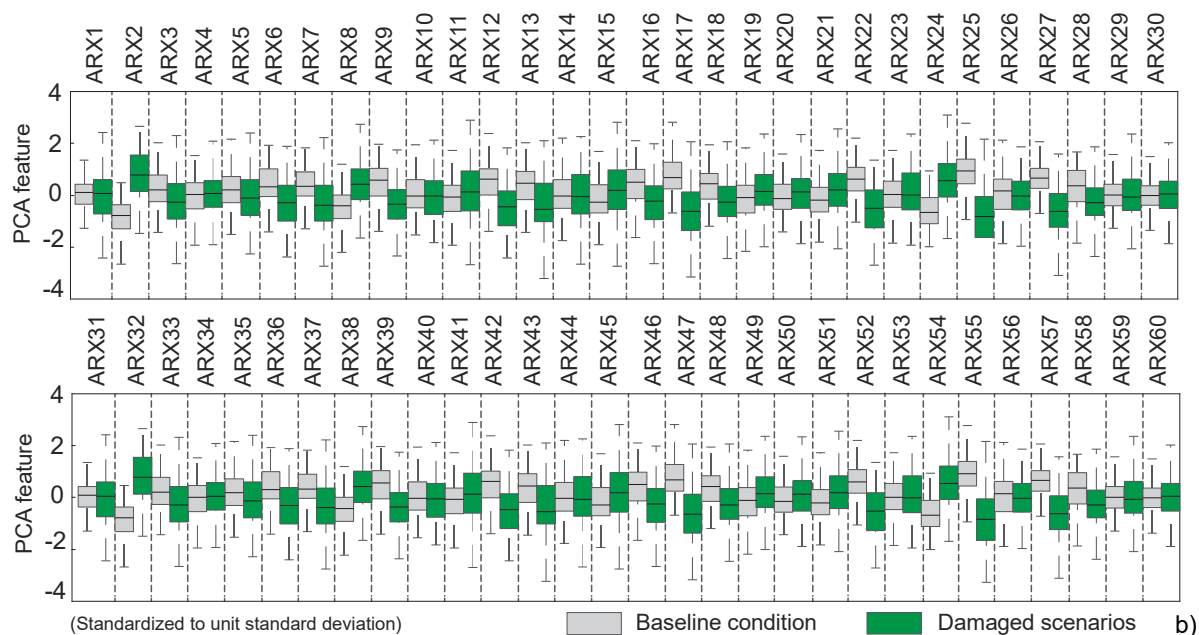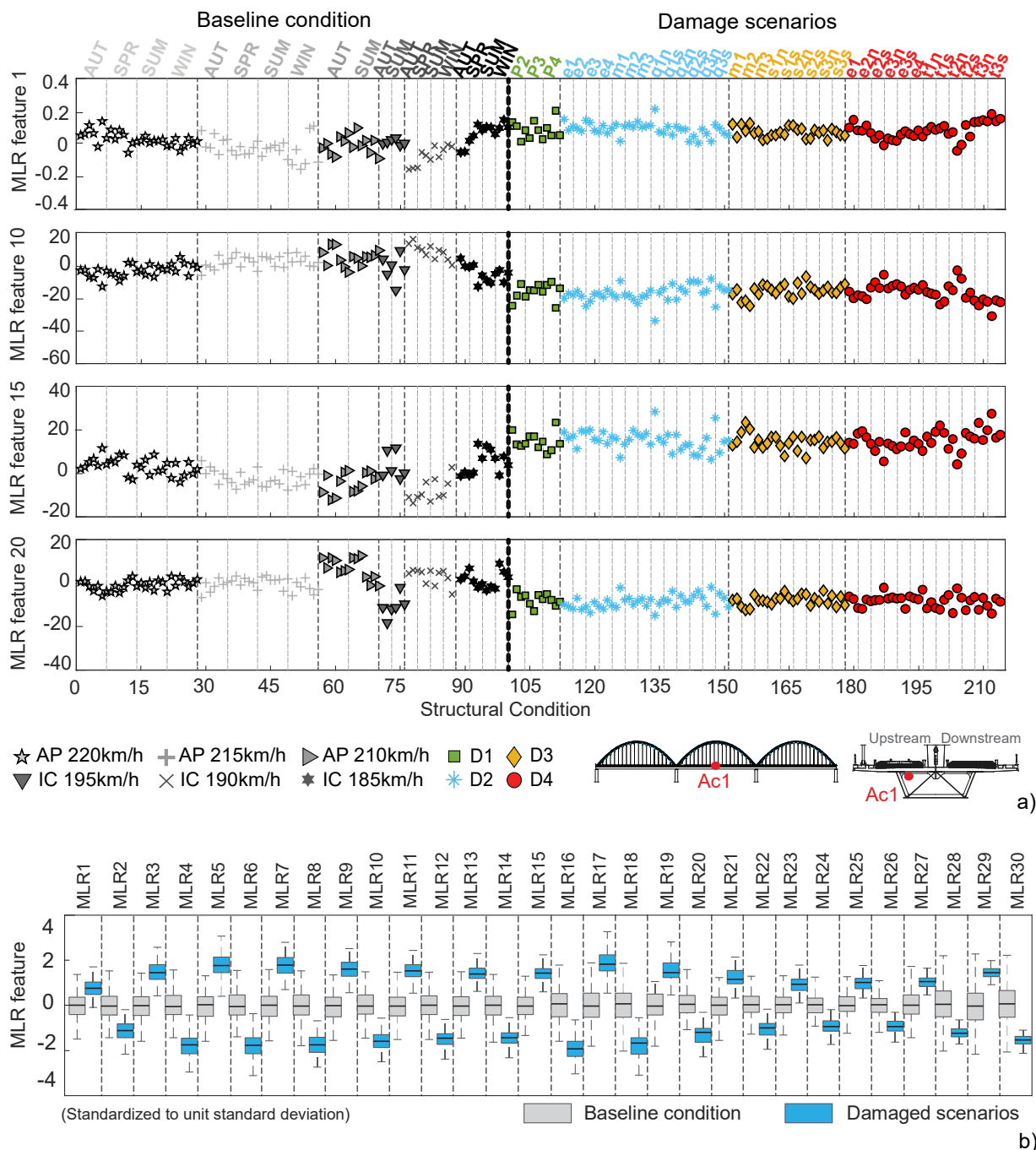
Figure 5.19 – For all 214 structural conditions considering the responses of the Ac1 accelerometer: a) amplitude of four of the thirty AR-MLR-based features, b) box-and-whiskers plots representing the thirty AR-MLR-based features.

5.6 DATA FUSION

The steps performed in the present section are summarised in Figure 5.20. To fuse the data obtained from all AR-based features, a Mahalanobis distance (MD) measure was implemented on the estimation errors based on structural responses measurements alone (PCA), and on the estimation errors based on both actions and structural responses measurements (MLR). In this

case, the 30 AR-based features are first merged into one for each sensor and, afterwards, the information from all sensors is also merged in order to achieve a univariate damage indicator. In the case of the ARX-PCA-based features, the Mahalanobis distance is applied only to merge the 60 features from each sensor.
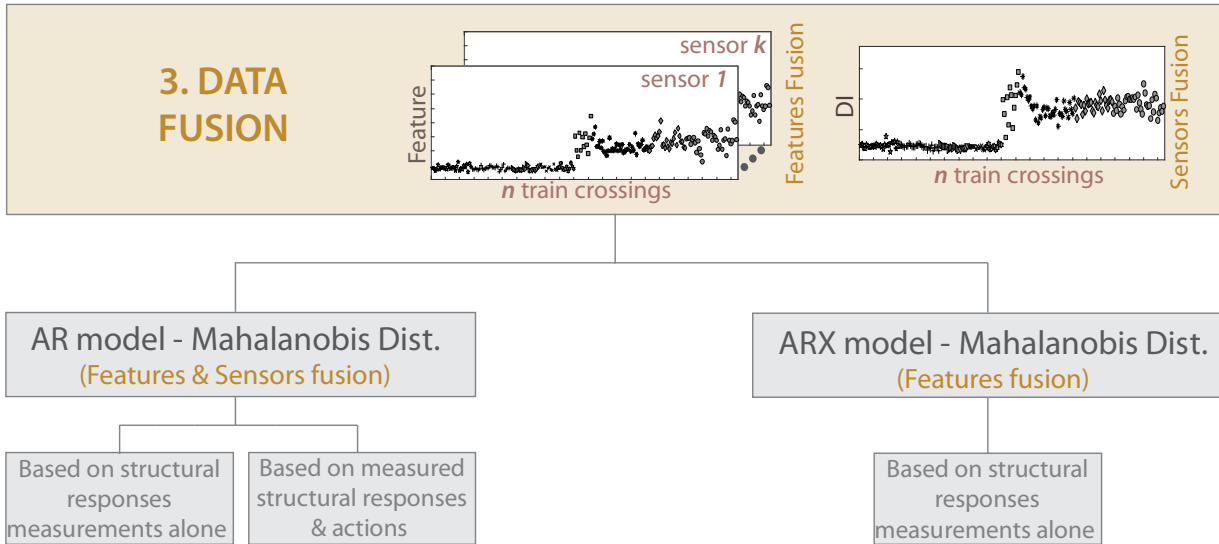
Figure 5.20 – Schematic representation summarising the portion of the machine learning strategy implemented in section 5.6.

5.6.1 Theoretical Background

The MD was selected since it is based on the AR/ARX parameters' centre and covariance, therefore enabling additional sensitivity if these quantities are computed using only the AR/ARX parameters extracted from the baseline conditions. With this approach, the MD measures the distance between the representative baseline and each set of features extracted from a train crossing. Smaller MD values represent greater similarities with the representative baseline, while higher values reveal greater differences, and, therefore, more dissimilar structural conditions. The analytical expression of MD for each simulation i is given by:

$$MD_i = \sqrt{(x_i - \bar{x}) \cdot S_x^{-1} \cdot (x_i - \bar{x})^T} \tag{5.11}$$

where x_i is a vector of m features representing the potential damage/outlier, $\bar{x}$ is the matrix of the means of the features estimated on baseline simulations, and S_x is the covariance matrix of the baseline simulations.

The MD can be applied in two different stages:

a) stage 1: to merge features;

b) stage 2: to merge sensors.

In the first stage, the MD is computed for each simulation and each sensor resulting in a matrix with n Mahalanobis distances for k sensors, where n is the total number of simulations. In the second case, a new MD can be applied to the *n-by-k* matrix in order to obtain a vector *n-by-1* merging the information from all the sensors and providing a damage index (*DI*) for each simulation. When data from a structural state that differs from the baseline is tested, the *DI* value is expected to increase substantially. The first stage was applied to both AR and ARX features, while the second stage was applied only to the AR damage-sensitive features.

5.6.2   Fusion of AR-based features

5.6.2.1   Based on structural response measurements alone

With the objective of merging all the AR parameters obtained for each acceleration sensor, the Mahalanobis distance was implemented to the PCA-based features as shown in Figure 5.21a for the Ac1, AL-P3, and AsT$_t$2 sensors. The MD allowed transforming, for each sensor and train crossing, the 30 AR parameters into one single feature (a distance in the feature space), which exhibits higher values for different structural conditions and nominal values for identical structural scenarios. The outcome of this procedure is a vector of *214-by-1,* of distances, one for each of the 23 sensors.

The three plots in Figure 5.21a show the difference in sensitivity for different sensors in each structural condition. The accelerometer located at the central mid-span of the concrete slab (Ac1) exhibits an important global sensitivity to damage, since there is a distinction between the baseline simulations and the damage scenarios, but it is not efficient in distinguish the different types of simulated damages. Conversely, the longitudinal accelerometer on pier P3 (AL-P3) is more sensitive to damages on piers P3 and P4, with special emphasis on the damage related to the full restrain of the bearing devices on pier P3. The transversal accelerometer located in the steel box at one-third south of the central span (AsT$_t$2) also allows distinguishing between certain specific types and magnitudes of damage. Figure 5.21b allows observing the distribution obtained from each accelerometer (presented in Figure 3.20a) and its improved sensitivity to distinguish baseline and damage conditions.

Figure 5.21 – Mahalanobis distance of the AR-PCA-based features for all 214 structural conditions: a) considering the responses from accelerometers Ac1, AL-P3 and AsT$_t$2, b) box-and-whiskers plots for each sensor combination.

In order to detect all damage scenarios, a data fusion of the PCA-based features of the 23 sensors located on the bridge was also performed. It consisted of implementing the MD to the 23 distances representing each sensor, thus resulting in a single *DI 214-by-1* vector that represents all the data acquired through the 23 sensors. As a result, a clearer distinction between simulations of the baseline condition and damage scenarios was achieved, as presented in Figure 5.22, with the important advantage of not having to accurately measure temperature, nor identify the type and speed of the train. Merging the information from all sensors, it is clear that the damages related to the restrain of the bearing devices and the stiffness reduction of the concrete slab near the piers (e1 and e2) are those to which the sensing system appears to be more sensitive.

Figure 5.22 – DI values obtained with AR-PCA-based features for all 214 structural conditions considering the responses from all sensors.

5.6.2.2 Based on measured actions and structural responses

The same procedure, as the one detailed in the previous section, was implemented to the 30 AR-MLR-based features, which also resulted in a *214-by-1* vector of distances for each sensor. Figure 5.23a shows an important sensitivity increment of each sensor in distinguish baseline from damaged conditions, when compared with the features before fusion from Figure 5.19, especially when observing the box-and-whiskers distributions in Figure 5.23b.

Using the MLR-based damage-sensitive features of all 23 sensors, the single series of *DI* values presented in Figure 5.24 was accomplished. With this fusion of the sensors information, it is possible to clearly distinguish baseline from damage conditions and a clear improvement is verified in relation to the results obtained with the AR-PCA-based features after fusion (Figure 5.22). This improvement is achieved due to the actions measurements (temperature and train speed), which allowed for a more precise removal of the EOVs' influence and, consequently, a more efficient detection of damage. The combination of the information retained in this feature describing the data from all sensors also shows that the sensing system is more sensitive to damages on the bearing devices of Pier P4 (illustrated by green squares in Figure 5.24), and on the concrete slab near the piers (e1 and e2, represented by blue asterisks), since these damages have the higher *DI* values.
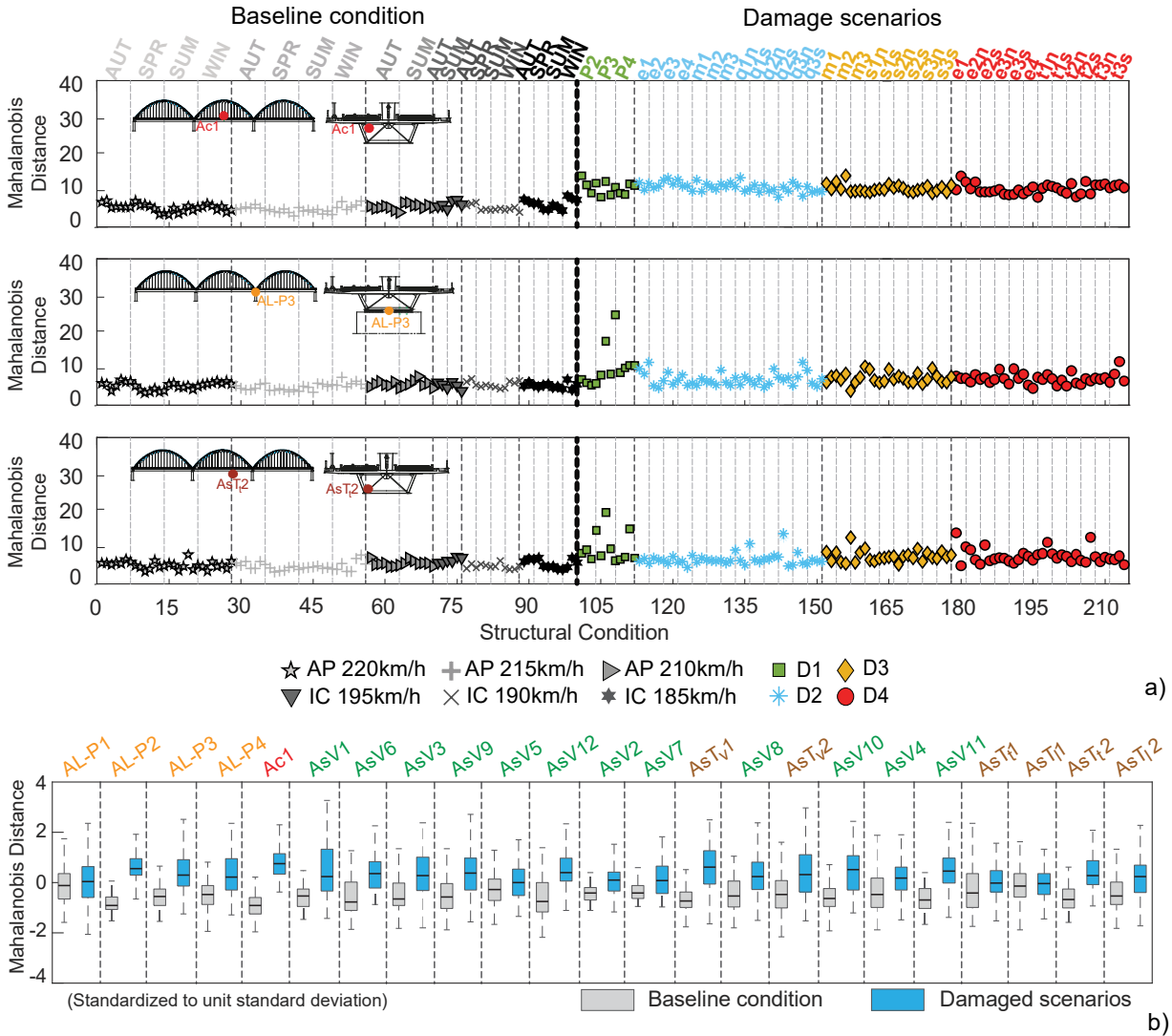
Figure 5.23 – Mahalanobis distance of the AR-MLR-based features for all 214 structural conditions: a) considering the responses from accelerometers Ac1, AL-P3 and AsT_t2, b) box-and-whiskers plots for each sensor combination.
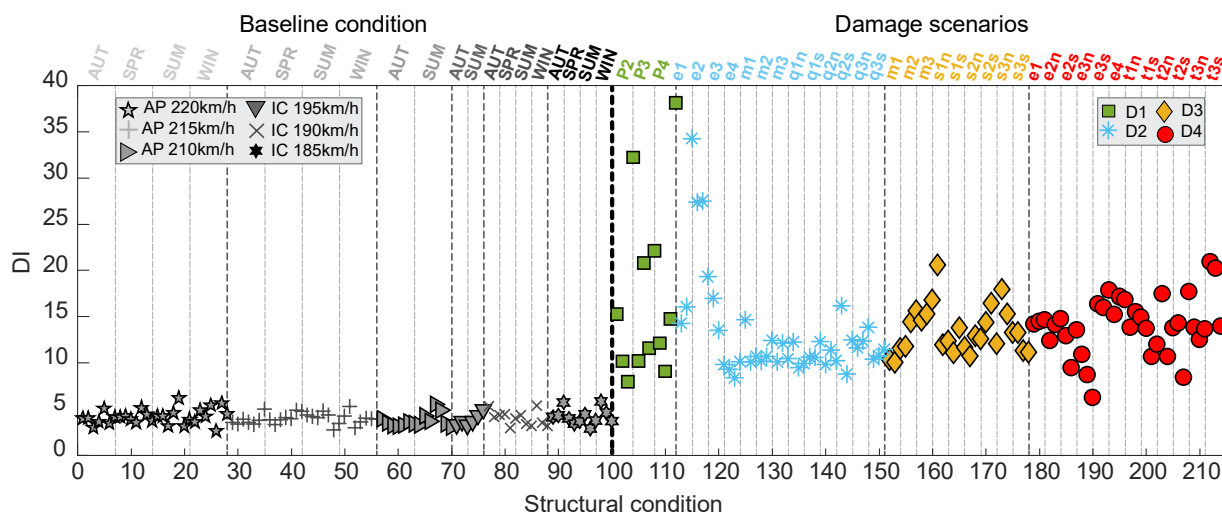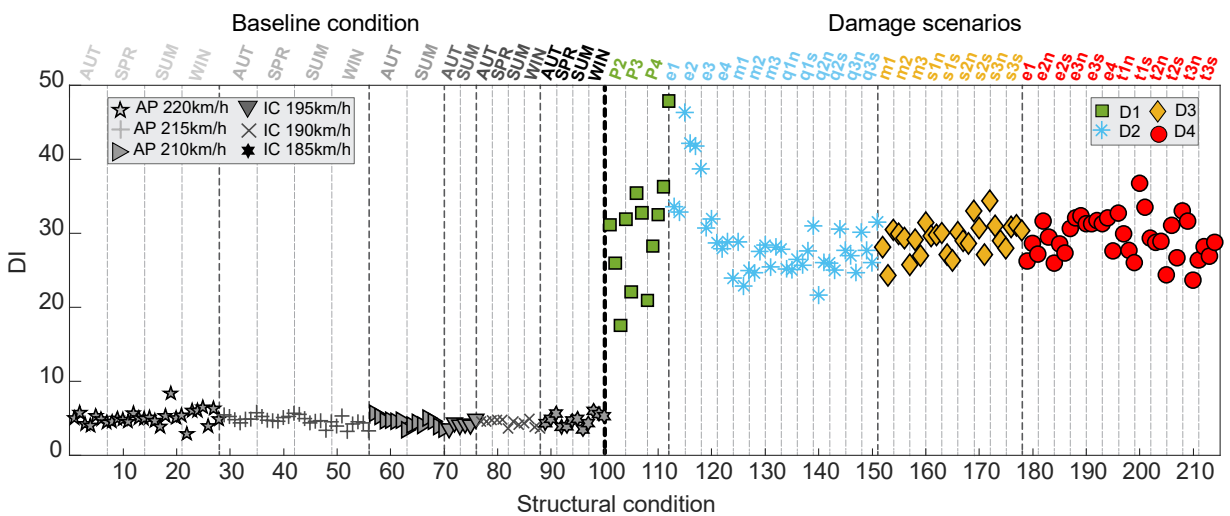

Figure 5.24 – DI values obtained with AR-MLR-based features for all 214 structural conditions considering the responses from all sensors.

5.6.3 Fusion of ARX-based features

As with the AR damage-sensitive features, the MD allows transforming, for each sensor and for each train crossing, the 60 ARX-PCA-based parameters into one single distance-based feature. The outcome of this procedure is a 214-by-1 vector of distances for each sensor. The three plots from Figure 5.25a clearly show a sensitivity improvement for sensors' cluster Ac1+AsV3, Ac1+AL-P3, and Ac1+AsTt2 to each structural condition. Figure 5.25b shows the distribution obtained from each of the twenty-two sensors' clusters (with the locations presented in Figure 3.20a), which suggests an evident separation between the simulations of the baseline condition and the damage scenarios.
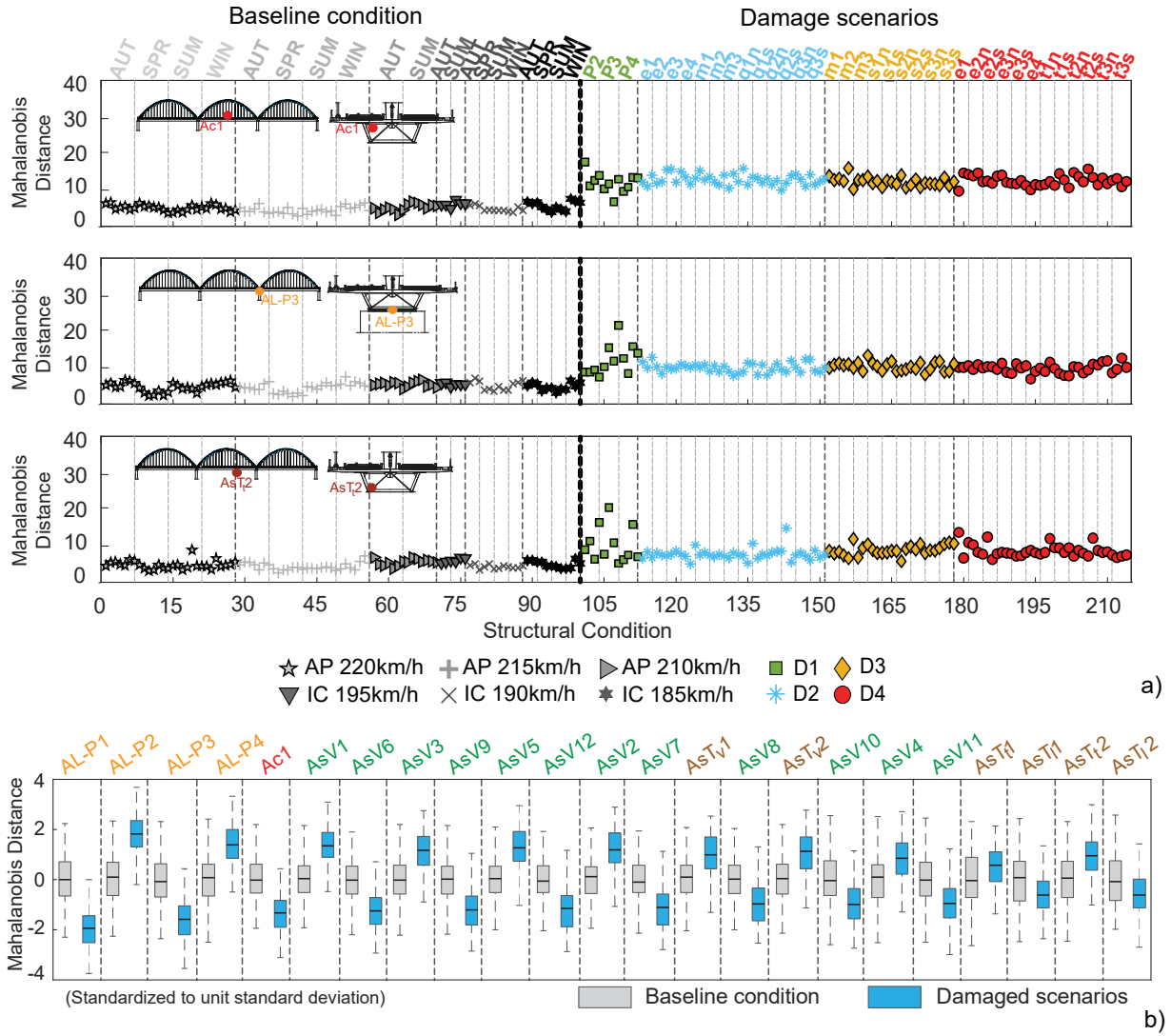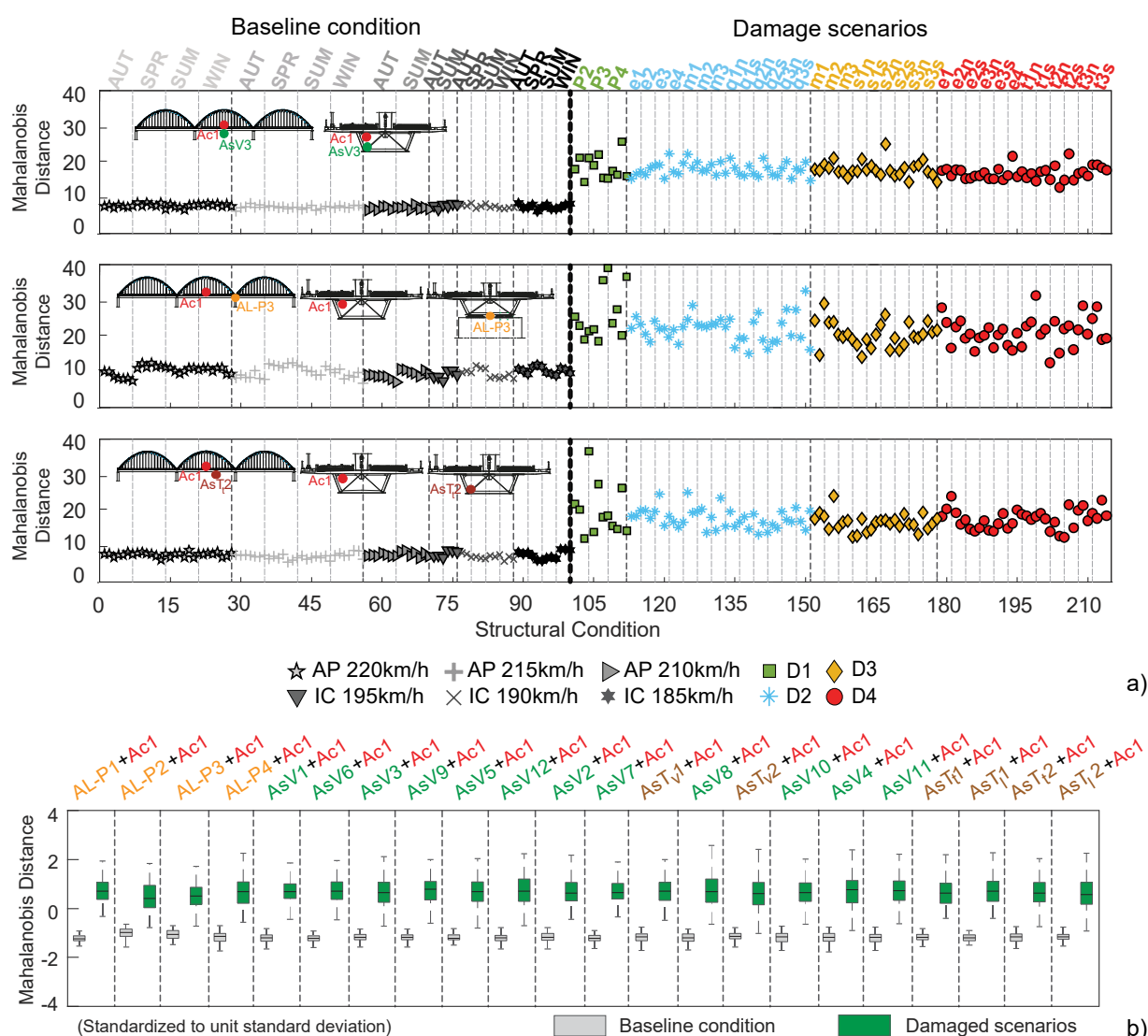

Figure 5.25 – Mahalanobis distance of the ARX-PCA-based features for all 214 structural conditions: a) considering the responses from accelerometers Ac1+AsV3, Ac1+AL-P3 and Ac1+AsT$_t$2, b) box-and-whiskers plots for each sensor combination.

There is an undeniable superior performance of the ARX model in relation to the AR model when comparing the MD outcomes (Figure 5.21, Figure 5.23 and Figure 5.25) as noted earlier. For this reason, the sensors' information from the ARX features were not merged using the Mahalanobis distance and different approaches were implemented for AR and ARX features discrimination, as detailed in the following section.

5.7 FEATURE DISCRIMINATION

Time-series analysis and distance measures can help perform data analysis and suggest the existence of different structural behaviours within a data set, as shown in the previous sections. However, the development of online SHM strategies should resort to machine learning algorithms that can autonomously decide whether one or more distinct structural behaviours are being observed from patterns in the features. Hence, feature discrimination is addressed herein using unsupervised discrimination algorithms.

As illustrated in Figure 5.26, outlier analysis is performed to the AR-based features, while cluster analysis is implemented using the ARX-based features. A comparison between approaches is conducted and the best combination of methods to be included in the machine learning strategy used to conduct online unsupervised damage identification is chosen.
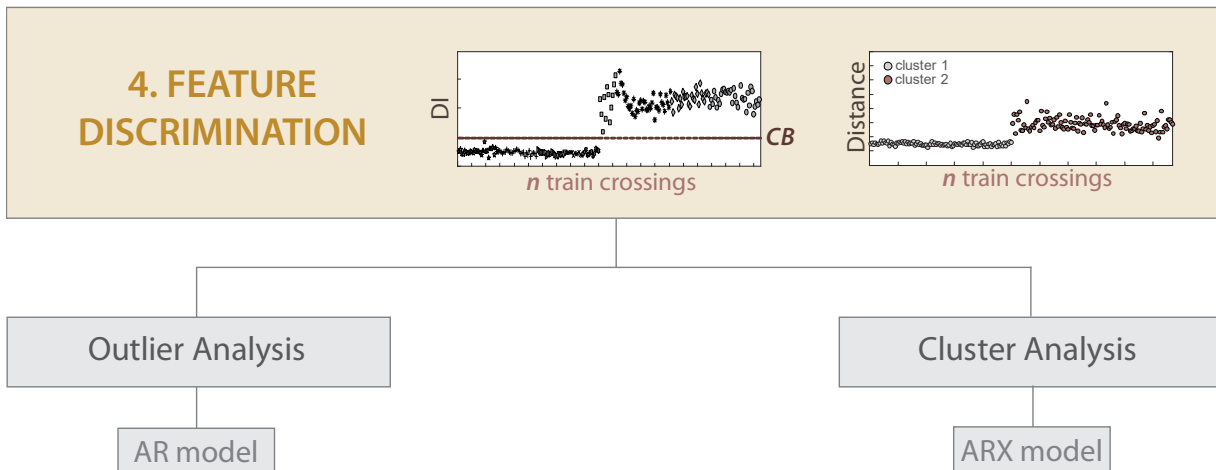
Figure 5.26 – Schematic representation summarising the portion of the machine learning strategy implemented in section 5.7.

5.7.1 Outlier analysis

5.7.1.1 Theoretical background

Generally, the literature assumes that the Mahalanobis squared distance can be approximated by a chi-squared distribution in *n*-dimensional space, thus the Mahalanobis distance can be approximated by a normal (or Gaussian) distribution and an outlier analysis can be performed based on a statistical threshold (Datteo et al., 2018; Worden et al., 2002; Yeager et al., 2019). Under this hypothesis, a confidence boundary to detect a DI that constitutes an outlier can be estimated by the Gaussian inverse cumulative distribution function (ICDF) considering a mean $\bar{\mu}$ and standard deviation σ of the baseline feature vector, and for a level of significance α. The inverse function can be defined in terms of the Gaussian cumulative distribution function (CDF) as follows:

$$CB = invF(1 - \alpha) \tag{5.12}$$

where,

$$F(x|\bar{\mu}, \sigma) = \frac{1}{\sigma\sqrt{2\pi}} \int_{-\infty}^{x} e^{-\frac{1}{2}\left(\frac{x-\bar{\mu}}{\sigma}\right)^2} dy, for\ x\epsilon\mathbb{R} \tag{5.13}$$

Thus, a feature is considered to be an outlier when its DI is equal or greater than CB. It is important to note that the selection of α carries a trade-off between the Type I error (*false-positive* indication of damage) and the Type II error (*false-negative* indication of damage) (Farrar & Worden, 2013).

5.7.1.2 AR-statistical-based automatic damage detection

The automatic detection of damages based on a CB computed using the Gaussian ICDF is presented in this section using the AR damage-sensitive features after modelling and fusion. A significance level of 1% was defined, as it is commonly observed in several SHM works addressing damage identification (Farrar & Worden, 2013; Santos et al., 2015; Tomé et al., 2020). Figure 5.27 allows observing the effectiveness of the methodology which, both for the features based on measured actions and structural responses (MLR-based), and for those based only on measured structural responses (PCA-based), allows distinguishing baseline from damage scenarios. The approach based on an output-only method (Figure 5.27a) exhibits one (0.88%) Type II error concerning a stiffness reduction in the arch of the second span in a section near pier P3 (e3n). On the other hand, the approach that uses an input-output method for feature

modelling exhibits one (1%) Type I error, regarding the crossing of an AP train at 220 km/h on a summer day with a loading scheme 5 (Figure 5.27b).
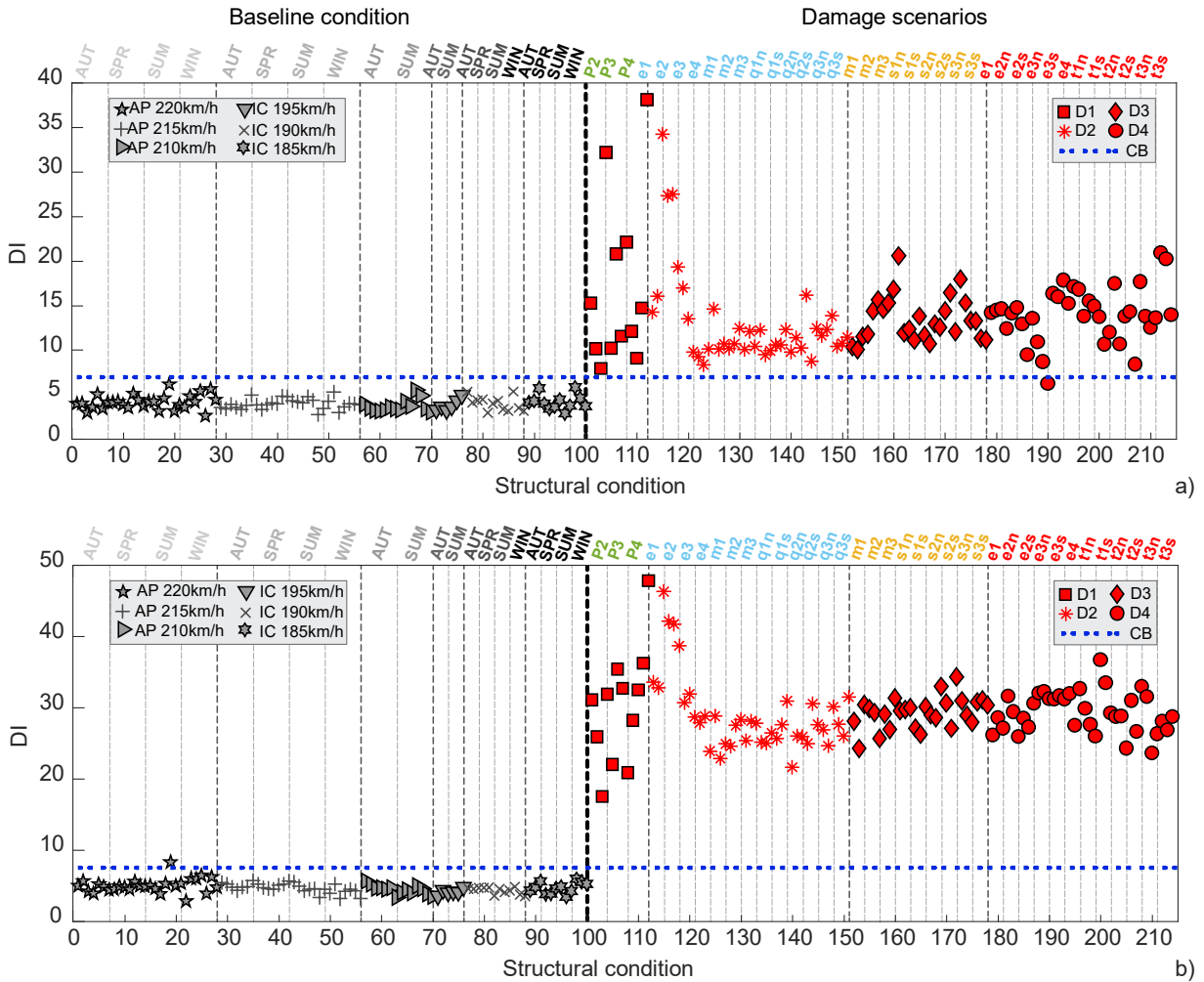
Figure 5.27 – Automatic damage detection using *DI* values for all 214 structural conditions considering the responses from all sensors and a CB determined for a significance level of 1%: a) PCA-based features, b) MLR-based features.

5.7.2 Cluster analysis

5.7.2.1 Theoretical background

The aim of the clustering process is to divide a dataset into groups, which must be as compact and separate as possible (Rendón, et al., 2011). This can be mathematically posed as an attempt to minimize the dissimilarity between features assigned to the same cluster (within-cluster distance), which, consequently, maximizes the dissimilarity between the features assigned to different clusters (between-cluster distance) (Cury & Cremona, 2010). Considering a given

partition containing K clusters, $P_k = \{C_1, \dots, C_k\}$, the overall within-cluster dissimilarity $W(P_k)$ and the overall dissimilarity OD can be defined as:

$$W(P_k) = \frac{1}{2} \sum_{k=1}^{K} \sum_{c(i)=k} \sum_{c(j)=k} d_{ij} \tag{5.14}$$

$$OD = \frac{1}{2} \sum_{i=1}^{N} \sum_{j=1}^{N} d_{ij} \tag{5.15}$$

in which the between-cluster dissimilarity is given by the subtraction $B(P_k) = OD - W(P_k)$. Here, N is the total number of features and $c(i)$ is a many-to-one allocation rule that assigns feature i to cluster k, based on a dissimilarity measure d_{ij} defined between each pair of features i and j (Marian Ralbovsky et al., 2014). The best-known clustering algorithm is iterative and called k-means (Hastie et al., 2011). The k-means requires that the number of $K < N$ clusters be initially defined along with a randomly defined set of K clusters' prototypes. This task is called initialization. Afterwards, each iteration starts by allocating the features to the clusters according to an allocation rule, $c(i)$, that assigns each feature to the least dissimilar (closest) cluster prototype. The second step of each k-means' iteration is called representation and consists of defining the centroids of the K clusters as their prototypes and assuming that each feature belongs to the cluster whose prototype is closest. These two steps, allocation and representation, are subsequently repeated until an objective function, which depends on the compactness and separation of the cluster, reaches its global minimum value. The k-means considers the squared within-cluster dissimilarity measured across the K clusters as an objective function (Hastie et al., 2011). Clusters' dissimilarities are generally defined as distance metrics. Among these, the Euclidean (square root of the sum-of-squares) is used here.

5.7.2.2 *ARX-clustering-based automatic damage detection*

Using the ARX-PCA-based features after fusion, shown in Figure 5.25, for each sensor cluster, the dissimilarities between undamaged and damaged conditions can be computed and represented in distance matrices. Figure 5.28a presents the matrix for baseline conditions, while Figure 5.28b shows the matrix considering baseline and damaged structural conditions, where dark blue represents the null distance (identical features) and yellow represents the most dissimilar features of the analysed sample set (maximum distance). A straightforward observation of Figure 5.28b allows conclusions to be drawn regarding the existence of two

compact groups of samples: darker regions within the matrix separated by lighter regions of the same matrix. These two groups correspond unmistakably to the two distinct structural conditions simulated: damaged and undamaged (baseline). It can also be observed that the baseline group of features is much more compact than the set of damage-related features, since the first consists of a darker blue colour, while the second exhibits greener areas since it is composed of numerous distinct structural conditions. Conversely, Figure 5.28a reveals a uniform distribution of colours throughout the entire sample set, suggesting that no changes occurred in the structure during those train crossings.
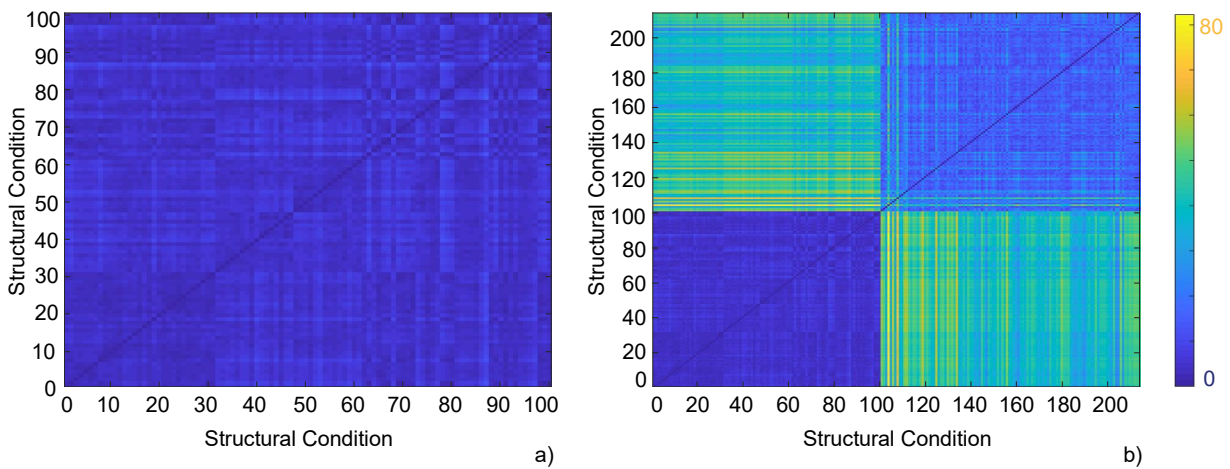
Figure 5.28 – Dissimilarity matrices obtained from: a) baseline conditions, b) undamaged and damaged conditions (dark blue=identical features, yellow=most dissimilar ones).

As previously mentioned, the k-means clustering method requires that the number of clusters be defined in advance and provided as input (in the initialization phase). For damage detection, there is no way of knowing this number in advance (Santos et al., 2016), which requires that multiple partitions, comprising different numbers of clusters, be tested and their outcomes analysed using cluster validity indices (Hastie et al., 2011). Numerous validity indices have been proposed and tested, not only in specific literature but also in SHM applications. Herein, the global silhouette index (SIL) is used, since it revealed a superior performance in previous studies (Santos et al., 2015, 2016), in which its formulation is carefully described.

The application of the k-means along with the SIL index is exemplified here using the features extracted from the sample time-series. For the present work, it is important to note that, among the *K* tested, the partition that generates the highest SIL value is the one that is expected to best describe the analysed feature set (Rendón et al., 2011), and should, therefore, be considered for SHM purposes. Using the ARX-PCA-based features after fusion, shown in Figure 5.25, the SIL indices extracted from five cluster partitions, shown with 'o' marks in Figure 5.29a, exhibit a

maximum for $k = 2$ clusters. The corresponding features' allocations were automatically generated by the k-means method and are shown in Figure 5.29b for four of the twenty-two sensor clusters: i) AL-P2 + Ac1, ii) AsV1 + Ac1, iii) AsT$_t$2+Ac1, and v) AsV3+Ac1. These plots demonstrate that the clustering method is capable of dividing the features without any human interaction or input. In Figure 5.29b can be observed the dissimilarity between the two centroids of six different combinations of sensors, while the plots in the diagonal of this figure show that the two clusters found for each couple of sensors are compact over time and separated when the simulated damages start. This result undeniably shows that the k-means method is capable of analysing the feature set and, in a fully automated manner, separating it according to the structural conditions observed on site. Also, it is demonstrated that the clusters have the advantage of allowing a multidimensional representation of the features, unlike the Mahalanobis distance, which is unidimensional.
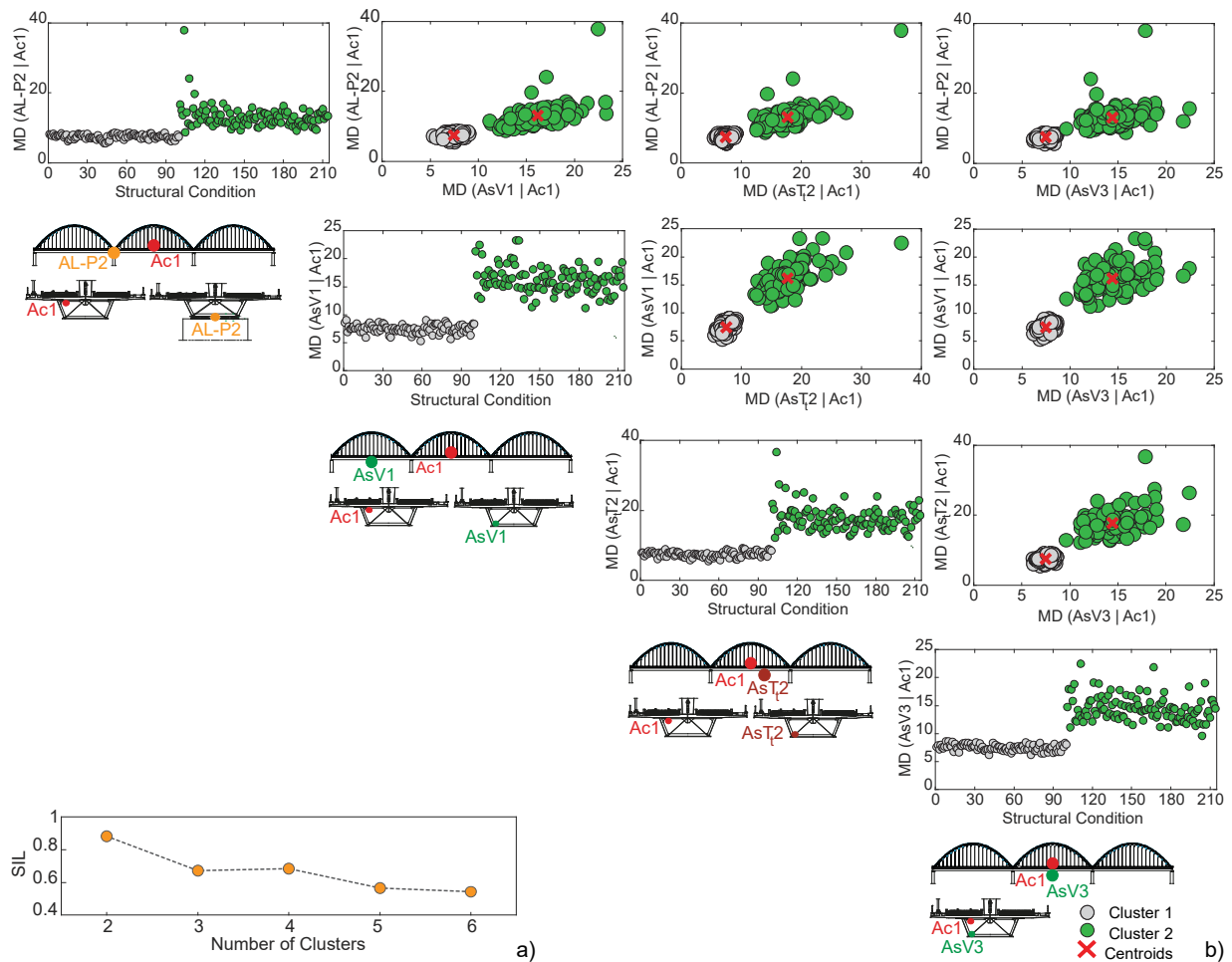

Figure 5.29 – Allocation of damage-sensitive features into clusters: a) silhouette index (SIL), b) clusters defined for all structural conditions and their centroids for four of the twenty-two sensors couples.

5.8 CONCLUDING REMARKS

This chapter presents a novel SHM machine learning strategy for conducting unsupervised damage detection on railway bridges based on traffic-induced responses, applying time series analysis and multivariate statistics algorithms. The proposed strategy consists of fusing sets of acceleration measurements to improve sensitivity and combines different techniques:

i)   AR or ARX models for features extraction;

ii)   PCA or MLR for feature modelling;

iii)   Mahalanobis distance for data fusion;

iv)   outlier analysis or cluster analysis for feature discrimination.

The effectiveness of the proposed strategy was tested using the validated digital twin of the bridge over the Sado River and experimental data acquired with the SHM system installed on site. Dynamic numerical simulations of several structural conditions (undamaged and damaged) using only experimentally obtained actions as input, namely temperature, noise, train loadings and speeds were conducted. To obtain the most similar and reliable reproduction of the real SHM data, each simulation was polluted with different noise signals acquired on site by each accelerometer, on different days, thus ensuring the most appropriate validation of the methodology developed herein. Damage severities of 5%, 10% and 20% of stiffness reductions in the concrete slab, diaphragm and arches were simulated, as well as friction increases in the movements of the bearing devices from a reference value of 1.5% to 1.8%, 2.4%, 3.0% and the full restraint of these elements.

The damage-sensitive features were extracted by fitting AR (30) and ARX (30,30) models to the bridge accelerations induced by train crossings in different locations along the bridge. The study of the AR/ARX parameters obtained from different structural conditions, allowed drawing conclusions about the superiority of the EOVs when compared with damage, proving the importance of feature modelling. On the other hand, the analysis of the AR/ARX parameters from different sensors showed that the information stored for each type of damage is different. Also, this type of time-series analysis proved capable of accurately generalizing the information present in data, while performing significant compressive fusion (thirty features in case of AR model and sixty features in case of ARX model are extracted from 2112 measurement points). A comparison between the performance obtained from AR and ARX models as feature extractors was conducted, and it was concluded that ARX models lead to increased sensitivity

to damage due to their ability to capture cross information between the sensors (the input and the output). These linear models proved sufficiently robust to extract features from responses that result of slightly nonlinear systems, such as the train-bridge system.

To overcome the challenge of EOV events corrupting the raw data obtained in operational conditions, both MLR and PCA were implemented to study the trade-off between modelling the features using latent-variable (output-only) or regression-based (input-output) methods. Both approaches were applied using features extracted with AR models and allowed for an undeniable reduction in the effects of EOVs, although the features obtained with MLR allowed for a clearer distinction between undamaged and damaged AR-based features. The PCA was also applied to the ARX-based features and proved its importance and effectiveness in removing observable changes induced by variations in train speed or temperature without the need to measure them. It was shown that the EOVs can be more effectively normalized using ARX models rather than AR models.

To describe the variability present in the modelled features, a Mahalanobis distance was implemented to the thirty AR-based features and sixty ARX-based features obtained from each sensor. It was possible to verify that different sensors have greater or lesser sensitivity, depending on the location of the damage. As noted earlier, the performance of the ARX-based features was considerably superior to the AR-based features. To enhance sensitivity of the AR-based features, the information from all the sensors was merged and a single damage index for each train crossing was defined and obtained. This step proved to be crucial to achieve the highest possible level of information fusion and to obtain a clear distinction between undamaged and damaged conditions for AR-MLR-based and AR-PCA-based features. Notwithstanding, the damage indicator values obtained with AR-MLR-based features proved to be more sensitive than those obtained with AR-PCA-based features.

In order to automatically detect the presence of damage, an outlier analysis was performed in the AR-based features using a CB computed for a significance level of 1%. The robustness and effectiveness of the proposed strategy was demonstrated by automatically detecting the damage scenarios as different from those belonging to the undamaged baseline. Using features modelled based on measured actions and structural responses (MLR-based), only one false-positive was exhibited (1% incidence), while with features modelled based on structural response measurements alone (PCA-based), only one false-negative was obtained (0.88% incidence). Further performance enhancement was achieved by performing a cluster analysis using the

ARX-based features. This step allowed to effectively separate, in a fully automated manner and without human intervention, the features according to the structural conditions observed on site.

In short, the strategy that considers ARX models for feature extraction, PCA for feature modelling and a cluster analysis for feature discrimination proved to be the most efficient and sensitive hybrid combination of techniques. The results showed that even when using an SHM system without the ability of measuring environmental and operational effects, it is possible to successfully detect different types of damage using the bridge's responses to train crossings. This strategy also has the advantages of minimizing the number of sensors that need to be installed and, consequently, the cost of the SHM system, as well as allowing for a more automatic and straightforward implementation.

Based on this robust and effective machine learning strategy, an online unsupervised procedure for damage identification in real-time and without user intervention was developed, implemented, and validated, as detailed in the next chapter.

Chapter 6

ONLINE UNSUPERVISED PROCEDURE FOR EARLY
DAMAGE IDENTIFICATION BASED ON TRAIN INDUCED
DYNAMIC RESPONSES [*]

6.1 INTRODUCTION

This chapter proposes an online unsupervised data-driven procedure for early damage identification based on train induced dynamic bridge responses. The machine learning methodology implemented herein also includes a novel approach to define an adaptive confidence boundary that successfully detects new damage in bridges already showing structural changes. To ensure a real-time continuous assessment and avoid false detections, a hybrid combination of ARX models, PCA, and clustering algorithms is sequentially applied to the monitoring data, in a moving window process.

The efficiency of the developed methodology is tested and validated, using the digital twin of the bridge over the Sado River tuned with experimental data acquired from the SHM system installed on site. The robustness of the methodology to false detections is demonstrated for a comprehensive set of damage scenarios, as well as its sensitivity to smaller damage levels

---

[*] This chapter is based on the paper:
Meixedo, A., Santos, J., Ribeiro, D., Calçada, R., Todd, M. (2021). *Online unsupervised detection of structural changes using train-induced dynamic responses*. Mechanical Systems and Signal Processing [submitted and revised].

(earlier in life), even when it consists of small stiffness reductions that do not impair structural safety and are imperceptible in the original signals.

After the introduction, section 6.2 describes the online unsupervised procedure for damage identification. In section 6.3 a sensitivity analysis is performed to different damage locations. Section 6.4 assesses the most robust window lengths and section 6.5 studies the effectiveness of smaller sensor networks. In section 6.6 an adaptive confidence boundary capable of automatically adapting to detect new damages after the occurrence of previous ones is implemented and validated. Finally, section 6.7 draws the main concluding remarks from the present chapter.

6.2   ONLINE METHODOLOGY DEVELOPED

In Chapter 5, it was demonstrated that the combination of the ARX model, PCA, and data fusion is the most effective in extracting and modelling features and detecting damage under a variety of confounding environmental and operational conditions. It was also observed that the cluster analysis is capable of automatically distinguishing between baseline and damaged conditions. However, the output of cluster analysis requires user intervention to assess whether clusters are compact or dispersed over time, and therefore difficult to apply in automated online SHM. To circumvent this limitation, instead of relying on the allocation of features to clusters over time, the average dissimilarity between clusters, DC, is implemented (Santos et al., 2015):

$$DC = \frac{1}{K(K-1)} \sum_{k=1}^{K} \sum_{\substack{c=1 \\ c \neq k}}^{K} d_{ck} \tag{6.1}$$

where K is the number of clusters belonging to the partition with the highest SIL, c and k are two of the K clusters, and d_{ck} is the dissimilarity measured between their centroids. If no damage occurs and the structural behaviour remains unchanged (as in Figure 5.28a), the clusters generated by the k-means are similar and will generate small DC values. Conversely, if damage is observed, the k-means generates dissimilar and separate clusters (as in Figure 5.28b) and, consequently, large DC values.

The online methodology developed aims to provide continuous binary information of the type TRUE/FALSE regarding the existence of damage. It consists of successively extracting parameters from time series, statistically modelling the features, and classifying the structural response, using the algorithms described in Chapter 5, within moving windows of SHM data to

obtain a set of DC values. These windows are defined with a fixed number of train crossings. Due to the fact that the DC value does not provide TRUE/FALSE information on its own, the proposed methodology requires an additional step. It consists of statistically testing the DC values obtained within each window's length. The statistical testing of each set of DC values results in the definition of a CB, which is exceeded only if the target structural system exhibits changes. The CBs are defined by statistically testing the DC distribution, under the premise that residual errors obtained from unchanged structures are only influenced by random effects. This premise is commonly used in SHM works addressing damage detection (Glaser & Tolman, 2008, Posenato et al., 2010) and is generally associated with the use of the Gaussian statistical distribution. Under this hypothesis, a CB to detect a DC that constitutes an outlier can be estimated by the Gaussian ICDF (Eq. 5.12 and Eq. 5.13), considering a mean $\bar{\mu}$ and standard deviation σ of the baseline DC vector, and for a level of significance α.

The moving windows online procedure proposed is detailed in the flowchart of Figure 6.1 and is divided into two main stages: i) the baseline and CB build and ii) the online damage identification.

After the initialization, which consists of defining the total number of trains crossings, j, that compose the baseline (Figure 6.1a), as well as the number of trains crossings within each window (Figure 6.1b), the machine learning strategy described in Chapter 5, which combines ARX models, PCA, MD and clustering techniques, is applied to the responses measured during the passage of the trains within each window i. During the first stage, after extracting the baseline ARX features (Figure 6.1c), the coefficients of PCA (Figure 6.1d) and the covariance and mean matrices (Figure 6.1e) of the baseline features are obtained. At the end of this stage, the baseline DC vector (Figure 6.1f) is achieved and used to estimate the CB (Figure 6.1g).

During the second stage, the moving windows process is implemented in real time, and the machine learning strategy is implemented in each window i (Figure 6.1h). Here, after extracting the ARX parameters from the window's time series (Figure 6.1i), the baseline PCA transformation is obtained (Figure 6.1j), and the baseline covariance and mean matrices are used for MD-based feature fusion (Figure 6.1k). The corresponding damage-sensitive distances are used as inputs for clustering. The outcome of the windowing process consists of one DC value per window i (Figure 6.1l), and the detection is based on comparing each of these values with the CB (Figure 6.1m). An average distance between clusters, DC, lower than CB suggests that the changes measured during the corresponding window i were generated by EOVs and,

consequently that the structure may be assumed to be unchanged during that window (Figure 6.1n). Conversely, a DC higher than the CB suggests the occurrence of damage during the same period (Figure 6.1o). In the case of damage identification, after j train crossings a new baseline may be defined, which will allow to identify when a new type of damage occur.
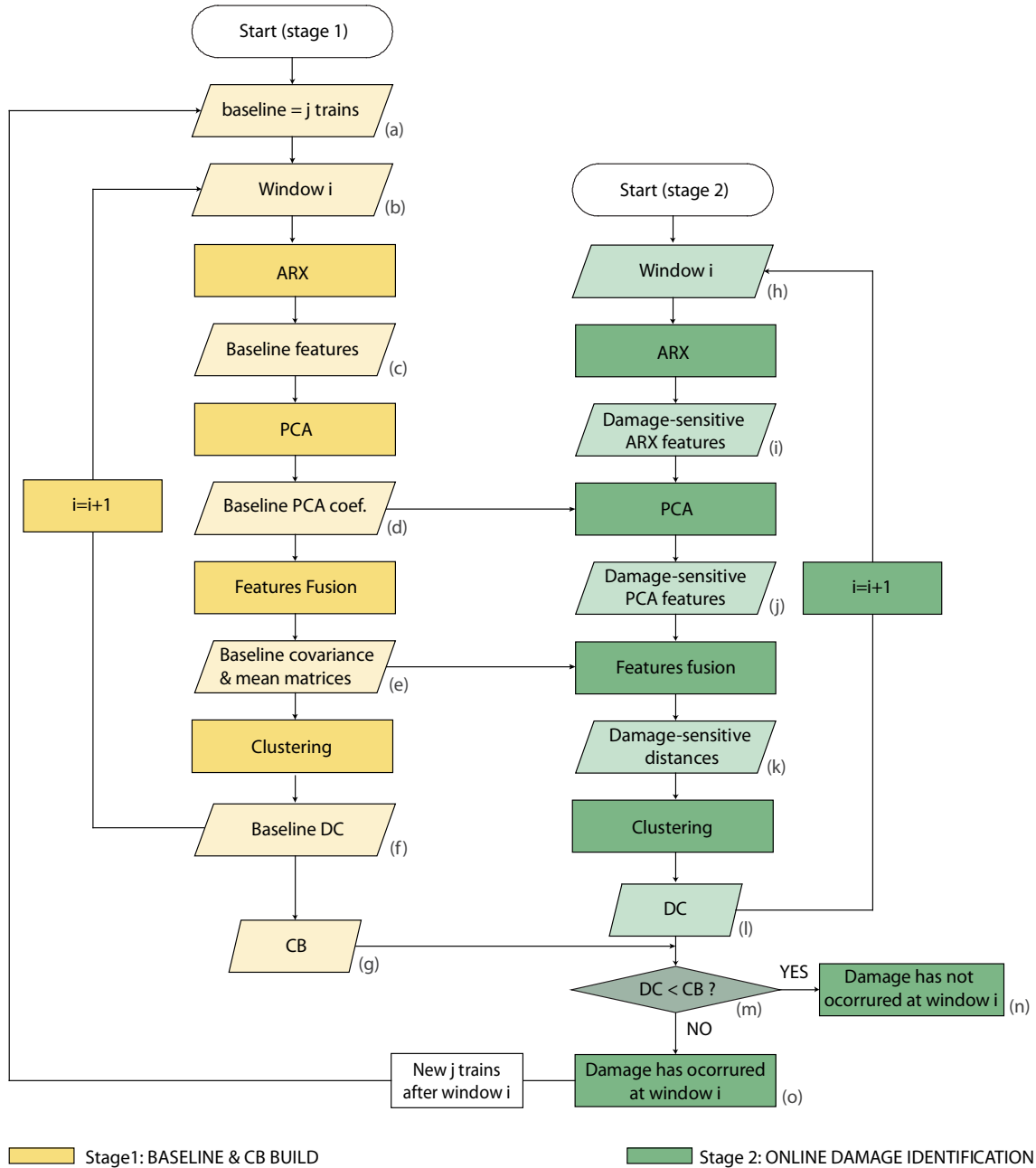
Figure 6.1 – Flowchart of online damage identification methodology based on moving windows.

The first stage of the methodology (Figure 6.1a-g), which concerns defining the CB, was implemented for a significance level of 1% and for $j = 100$ trains. Figure 6.2 shows the CB defined for undamaged structural responses under different environmental and operational conditions. The DC series shown in Figure 6.3 as examples were obtained during the

implementation of the second stage (Figure 6.1h-o) for one hundred healthy structural conditions and for four types of damage:

    i)   D1 located in pier P4;

    ii) D2 located in the first mid-span of the concrete slab (m1);

    iii) D3 located in the diaphragm at 1/6 north of the third span (s3n);

    iv) D4 located in the arch at 1/3 south of the second span (t2s).

   For both stage 1 and stage 2, moving windows with 15 trains and the responses of all sensors installed on site were considered.
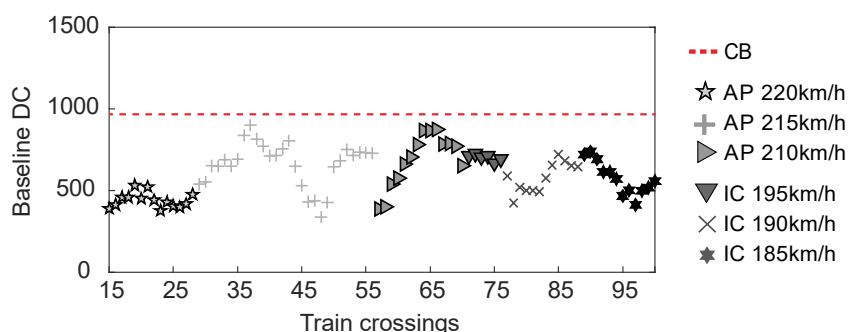
Figure 6.2 – Stage 1 of the methodology: CB defined for a significance level of 1% and for $j = 100$ trains.
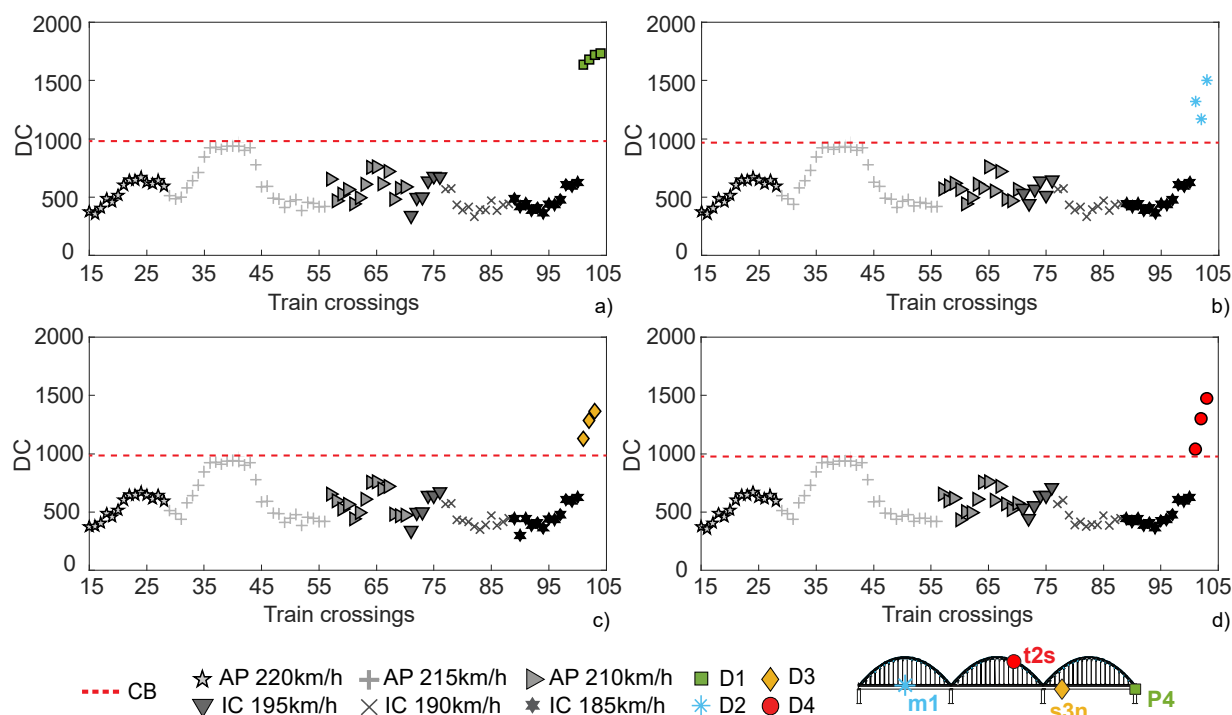
Figure 6.3 – Stage 2 of the methodology: DC values obtained for one hundred healthy scenarios and four types of damages with different severities: a) D1-P4: μ=1.8%, μ=2.4%, μ=3.0%, μ=full restrain, b) D2-m1: 5%, 10%, 20%, c) D3-s3n: 5%, 10%, 20% and d) D4-t2s: 5%, 10%, 20%.

The effectiveness of the online procedure to detect different types of damage with different severities is shown in Figure 6.3, since for each type of damage, each symbol represents a different severity, increasing from left to right (μ=1.8%, μ=2.4%, μ=3.0%, μ=full restrain for D1; 5%, 10% and 20% for D2, D3 and D4). It can be observed that, with the exception of damage D2, the value of DC increases with the severity.

Bearing in mind the small severity of the damages simulated and the realistic character of the numerical simulations conducted (Section 5.3), which include the effects of noise, temperature, and train loading measured on site, it can be observed that the developed methodology is highly sensitive to damage because it allows detecting stiffness reductions as small as 5%. Furthermore, among the one hundred undamaged scenarios tested in stage 2, no false positives were detected.

6.3   SENSITIVITY TO DIFFERENT DAMAGE LOCATIONS

To evaluate whether the results achieved so far may be generalized to different damage states, a more extensive sample of structural conditions (described in section 5.3 in the locations shown in Figure 5.4) was tested and applied to the same damage detection methodology.

The 114 online analyses conducted herein comprised 10.146 windows, each with 15 trains. Several unchanged structural conditions were already evaluated in Figure 6.3, and no false positives were obtained; only the sensitivity to new damage scenarios was evaluated using the same window size and the DC values extracted immediately after a damage incidence. These DC values are presented in Figure 6.4, as well as the corresponding CB.

The results show that, even if the single-valued DC represents the responses acquired from multiple sensors, it is sufficiently sensitive to highlight small magnitude damage with local character and in different structural elements. Only five false negatives were observed in a total span of 114 very different damage scenarios, namely, two in the concrete slab, one in the diaphragm and two in the arches, all with a stiffness reduction of only 5%. These results strongly suggest that the proposed methodology is, in fact, robust and may be used for damage identification throughout the entire structural system.
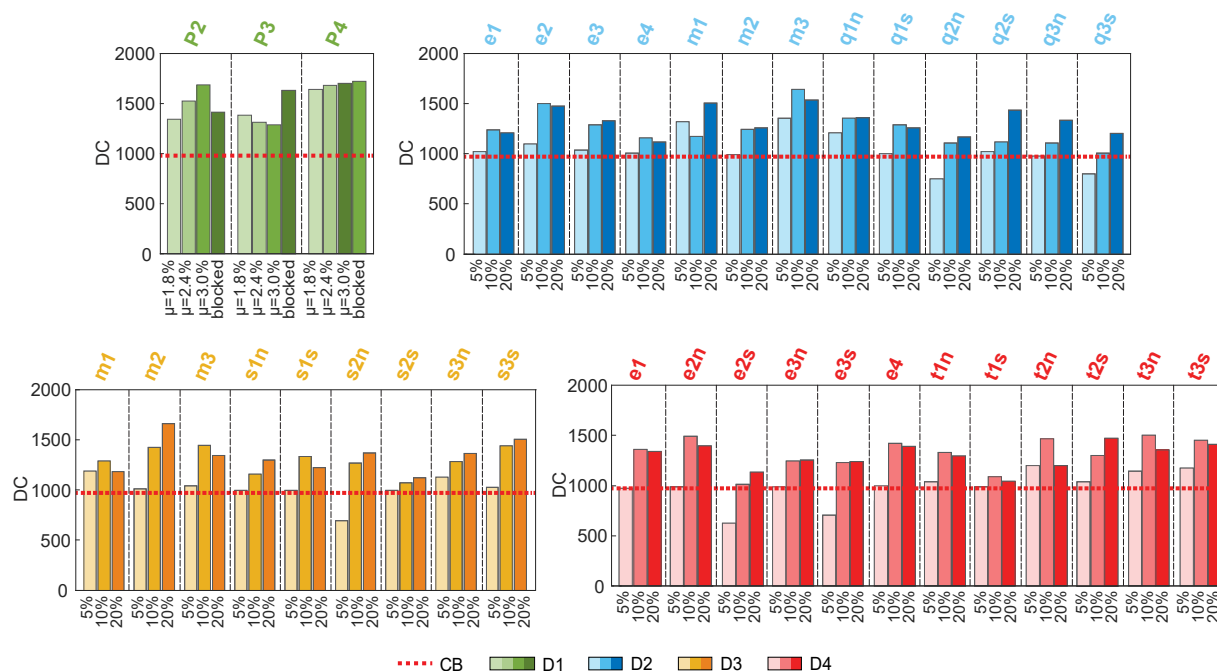
Figure 6.4 – DC values obtained considering four types of damage (D1, D2, D3 and D4) with different severities (D1: μ=1.8%, μ=2.4%, μ=3.0%, μ=full restrain, D2 to D4: 5%, 10%, 20%) in all the locations shown in Figure 5.4.

6.4 ASSESSING THE MOST ROBUST WINDOW LENGTHS

The example presented in section 6.3 showed that the proposed methodology was capable of detecting a 5% to 20% stiffness reduction, as well as different bearing restraints, in four types of damage (D1, D2, D3, D4) and in different locations, with a low number of false detections. This performance is, however, affected by the number of trains per window. The trade-off between detection rapidity and robustness is next studied by applying the damage detection procedure using windows with different lengths, i.e., with a varying number of trains per window between six and twenty.

As in Figure 6.4, the simulated responses of all accelerometers deployed on site were considered and a total of 1.710 DC vectors (114 different damages and 15 different windows lengths) were obtained from 155.610 independent windows. The results achieved with this analysis are summarized in Figure 6.5, where the percentage of false detections, taken as the incidence of false positives (false damage alerts) and false negative occurrences (true damage states that were not detected by the method), depending on the length of the window, is presented. The bars in this chart show that important amounts of false detections are obtained for window lengths between 6 and 13 trains, both for undamaged and damaged scenarios. Also, it is shown that most of the false detections are related to damage in the concrete slab (D2) and

in the arch (D4). This can be associated with the sensor locations, since no sensor has been installed in the arches, and the concrete slab has only one sensor located in the central mid-span. With a window length of 14 trains, false detection reduces to 6%, but it is with a window of 15 trains that only 2% of false detections are reached, which corresponds to a most robust detection process. As presented in Figure 6.4, these 2% are associated with damages with a severity of only 5%. The analysis was also performed for windows including 16 to 20 trains, but the improvement in terms of false detections was residual, if not null, which suggests that a substantial number of additional trains would be needed to achieve a 0% of false detections. It can also be observed that the percentage of false positives is zero with window lengths of 15 or more trains.
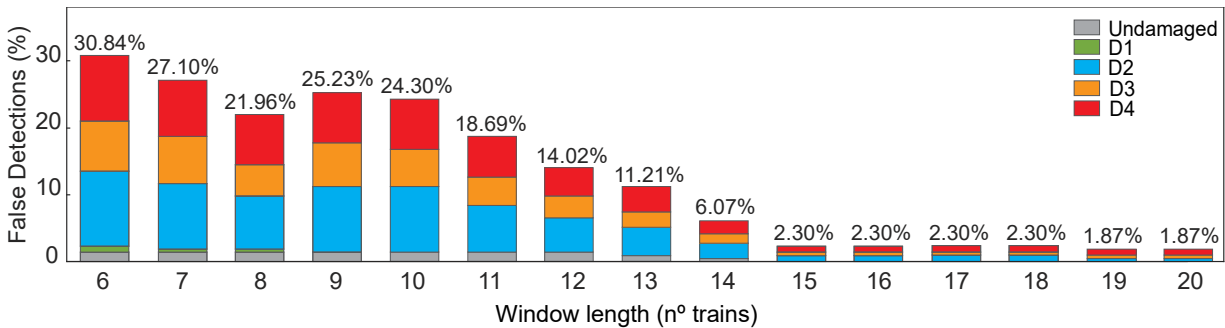
Figure 6.5 – Percentage of false detection incidences depending on the window length.

6.5 STUDYING THE EFFECTIVENESS OF DIFFERENT SENSOR SETUPS

To assess whether the number of sensors used to detect different types of damage may be optimized, a study on the false detection incidences as a function of the monitoring system configuration is considered. For all structural conditions mentioned in the previous sections, the online damage identification procedure was implemented with a window length of 15 trains, but considering the responses obtained with four possible configurations of an SHM system progressively adjusted for smaller numbers of sensors than those installed on site.

Figure 6.6 shows the percentage of false detections got for each configuration, with the lowest value (2%) achieved with the 23 accelerometers currently installed on site. If the vertical accelerometers installed on the downstream side of the steel box-girder were removed, there would be a 2% increase in false detections. The third SHM system configuration also excludes the vertical accelerometers located at 1/3 of the first and third spans and leads to an increase of 1% in the false detections. Finally, if only seven sensors remained, namely, the longitudinal accelerometers on the four piers, the vertical accelerometer on the second mid-span of the

concrete slab, and the vertical accelerometers in the steel box girder at each mid-span, 7% false detections would be observed.

It is worth noticing that among the four configurations, the increment of false detections with the reduction of the number of sensors only happens for damage cases with a 5% severity. The scenarios comprising higher severities are always flawlessly detected.
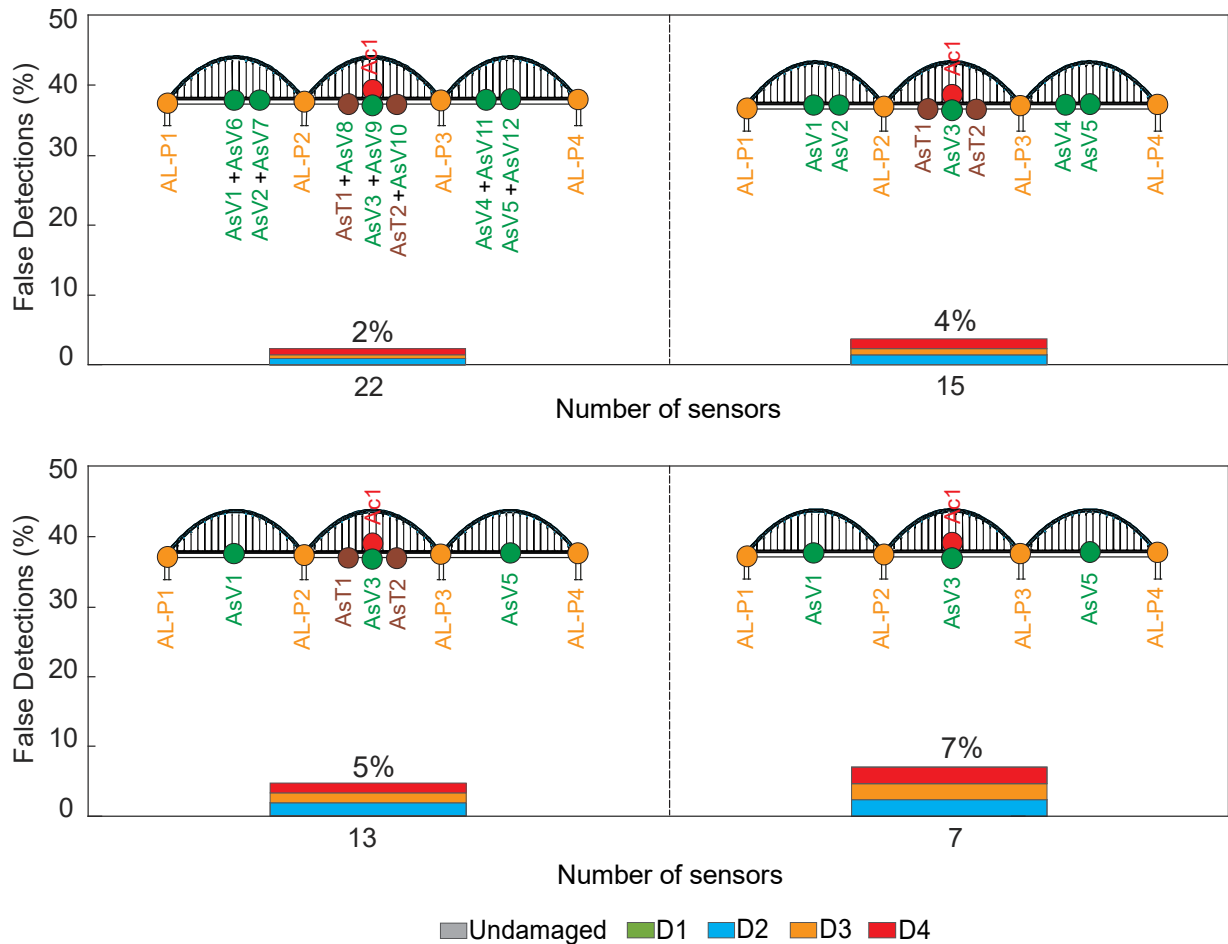
Figure 6.6 – Percentage of false detection incidences depending on the number of sensors.

6.6 DEFINING AN ADAPTIVE CONFIDENCE BOUNDARY

Thus far, the proposed online damage identification methodology was applied considering a single CB build based on responses from unchanged structural conditions. However, in case a specific type of damage occurs, it is desirable for the CB to adapt in order to identify future damage that may arise over time. Figure 6.7 shows an application of CB progression, where additional damage scenarios (types D1, D2, D3 and D4) were simulated to implement this procedure.
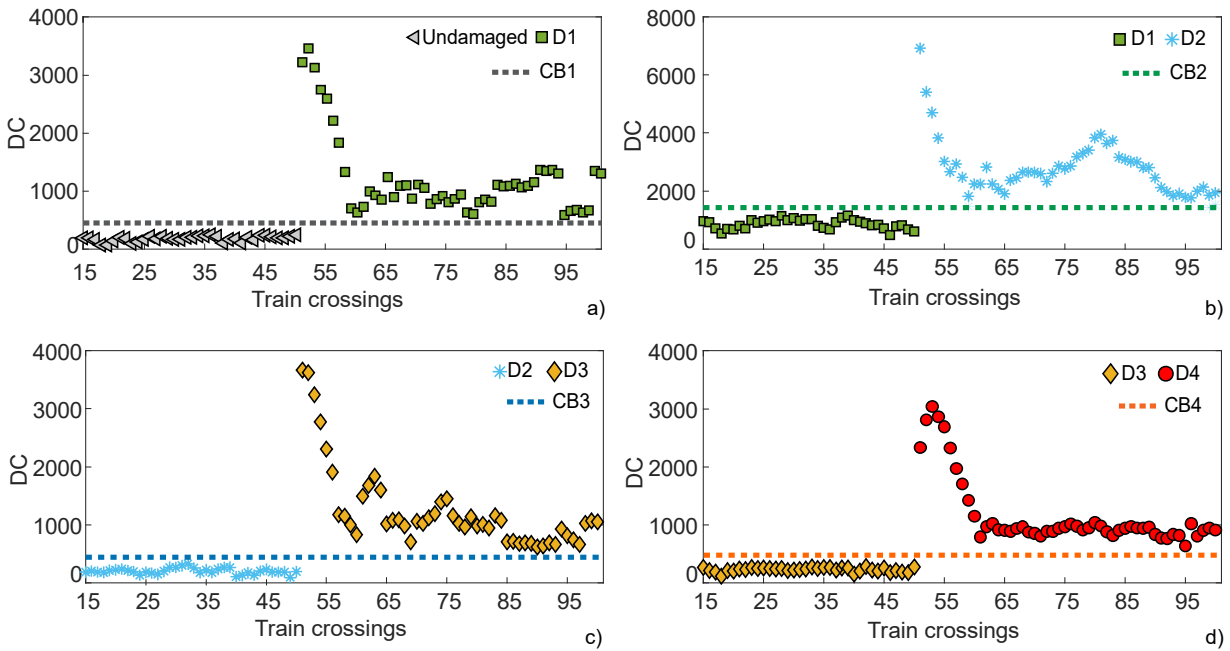
Figure 6.7 – Adaptive CB for different types of damage.

In Figure 6.7a, the CB1 was defined, as in the previous sections, for the baseline (undamaged) condition using $j = 50$ trains crossings and a time window of 15 trains. The implementation of the damage identification online procedure proposed lead to the substantial increase of the DC values and exceedance of the CB1, when a train crosses the bridge with a damage in the bearing of pier P4 (D1). The DC values progressively decrease as the windows contain more trains from a damaged structure than for a baseline condition.

In Figure 6.7b, a new baseline and confidence boundary (CB2) were defined using the bridge response from the 50 train crossings simulated with damage in the bearing of pier P4 (D1). This new baseline containing not only PCA coefficients, but also Mahalanobis distances with the new covariance and mean matrices, acquired from the bridge responses with damage D1, allowed defining a new confidence boundary (CB2) and, subsequently, detecting the new type of damage that occurred in the concrete slab (D2).

Afterwards, the CB3 was built considering new 50 train crossings simulated with the structure damaged on the concrete slab (D2), resulting in the detection of a damage on the diaphragm (D3), as shown in Figure 6.7c.

The same strategy was applied to detect a damage on the arch (D4) after a damage on the diaphragm (D3) has occurred (Figure 6.7d).

This analysis has shown the effectiveness of the proposed adaptive CB in automatically detecting new types of damage. The procedure herein implemented proved be successful, not only regarding the detection of damage, but also, on preventing false damage alerts.

6.7   CONCLUDING REMARKS

This chapter presented a comprehensive SHM methodology for conducting continuous online damage identification, using train induced responses, integrating several algorithms that address detection, EOVs, and online, autonomous classification. This methodology included the sequential implementation of ARX models, PCA transformation, and clustering algorithms to the observed data, using a moving window procedure. The unsupervised machine learning strategy proposed herein also includes an innovative approach to define an adaptive confidence boundary, which can be automatically updated to detect new damage that would progressively occur.

To assess whether the online procedure was reliable for different damage scenarios, the proposed methodology was applied to a representative set of simulated stiffness reductions (5%, 10% and 20%) in the concrete slab, diaphragm and arches, as well as friction increases in the movements of the bearing devices. This analysis allowed observing that changes as small as 5% of stiffness reduction may be detected in the vast majority of scenarios, using a simple system composed of a few sensors installed on a long-span bridge, while all the remaining severities and friction increments can be detected without false detections.

To study the trade-off between robustness and detection swiftness, a parametric analysis was conducted on the window lengths and on the number of sensors used by the SHM monitoring system. From this analysis it was shown that small stiffness reductions can be reliably detected with negligible false detection incidences (taken as the sum of "false alerts" and missed true detections) of 2% or less if the moving windows comprise 15 or more trains. Smaller windows lead to larger false detection rates. The detection can be achieved once the first train crosses the bridge after the damage occurrence.

The low percentage of false detections is accomplished considering the simple monitoring system currently installed on site. The effectiveness and performance of the proposed approach for damage identification with a smaller number of sensors was also investigated. The results demonstrate that if the number of sensors were reduced from twenty-three to just seven, on a 480 m long bridge, the proposed methodology could be effectively used, but an increase of 5%

in false detections would be observed. Nonetheless, it should be noted that the damage cases that would not be detected are only those with the lowest severity (5% of stiffness reduction).

Finally, using several train induced responses from the bridge comprising progressively different types of damage, the effectiveness of an original adaptive CB in detecting new structural changes that may occur in a structure already damaged was also successfully demonstrated.

Chapter 7

CONCLUSIONS AND FUTURE DEVELOPMENTS

7.1 CONCLUSIONS

The present thesis is focus on exploit unsupervised data-driven SHM in order to propose a continuous online procedure for damage identification based on train induced dynamic bridge responses. This procedure also includes a novel approach to define an adaptive confidence boundary that successfully detects new damage in bridges already showing structural changes. To achieve these goals a machine learning methodology was developed, implemented and validated with a complex case study.

In Chapter 2, an historical overview of the studies carried out in the field of vibration-based SHM, with special focus on bridges, was presented. The main definitions and concepts related to structural health monitoring and damage identification approaches are given. The main goals and components of an SHM system were defined and a literature review on damage identification was conducted. Finally, the strategy followed in this thesis for damage identification using structural health monitoring was also presented.

In Chapter 3, the railway bridge over the Sado River, used as case study in this thesis, was presented. The implementation of a progressively phased in-situ structural monitoring system was described. Immediately after construction, the modal properties of the long-span railway bridge, namely its natural frequencies, mode shapes and damping coefficients were assessed through an ambient vibration test. In addition, the structural health condition of the bridge over

the Sado River was monitored through periodic visual inspections, and using a comprehensive structural monitoring system defined with the objective of controlling the global stiffness of the bridge and the global longitudinal internal forces, as well as the behaviour of its special devices, such as the bearings, to the important actions of temperature and railway traffic. As this is a single-plane bowstring-arch structure, the important torsional effect resulting from train loading on only one side of the girder was also considered, insofar as the sensors were eccentrically positioned in order to monitor not only the effects due to bending but also the torsion of the structure. Between 2011 and 2016, the system consisted of static measurements of strain, temperature, and displacement, whose responses were acquired and evaluated every hour. In 2017 an upgrade of the monitoring system was implemented to allow for a better characterization of the dynamic response of the bridge and the behaviour of the bearing devices. This upgrade consisted mainly of additional dynamic measurements using accelerometers located on the top of each pier and along the deck, to take advantage of the excitation induced by the several trains that cross the bridge every day.

By analysing experimental data from the ambient vibration test and static monitoring, it was possible to estimate the modal parameters, as well as the responses to important slow actions, such as temperature. However, the experimental information alone did not enable the identification of changes in the behaviour of the bearing devices, which were suggested by visual inspection. On the other hand, it was concluded that a continuous dynamic monitoring based on the analysis of traffic loading allowed the identification of changes in the structural responses and pointed out the existence of restraints in the movements of the bearing devices on piers P2 and P3. It was found that a dynamic monitoring system has the advantage of detecting bearing defects based on the train induced responses. With the passage of several trains, the diagnosis can be validated, and false positives can be dismissed in a short period of time.

Chapter 4 addressed the progressive validation of a complex non-linear FE model of the bridge over the Sado River using the measurements from the monitoring system installed on site and performing modal analysis under ambient vibration, static analysis based on temperature loading and dynamic analysis based on traffic loading. One of the main outcomes was a reliable digital twin used as a tool for generate realistic simulations of healthy and damage scenarios, in order to test and validate the machine learning strategy developed herein, since it was not possible to obtain such conditions experimentally.

The validation of the numerical model based on ambient vibration and modal analysis, revealed appropriate to define the baseline numerical model. However, it was concluded that this type of numerical model is insufficient to perform SHM or identify structural changes, since it does not mobilize mechanical devices such as bearings (or joints).

When compared to the ambient vibration analysis, the static validation approach based on environmental loading allowed concluding that the imposition of greater displacements on the structural elements provides a step forward in the accuracy of the model validation. Based on correlation analysis between experimental and numerical results, the restraints of the bearing devices on piers P2 and P3 were clearly identified, which is in line with the structural changes detected through visual inspections. Without the support of a numerical model, these changes would not be easily identified using the data from the installed static monitoring system, which did not include the measurement of the displacements of these specific bearings. This is, in fact, another main outcome of Chapter 4, to illustrate the combined use of measurements and modelling, and the need to adapt both components over the course of a project to better understand the structural behaviour of the bridge.

The validation of the model based on dynamic monitoring under traffic loads was carried out to take advantage of the large displacements and vibrations imposed by this type of operational action. The model allowed analysing the influence that the restraints of the bearing devices impose on the longitudinal behaviour (displacements and accelerations) of the piers, and to the vertical accelerations of the deck. It was concluded that the use of numerical modelling and its validation by comparison with SHM data, allows the detection of the restraint to the movements of the bearing devices on piers P2 and P3 without the need to measure the longitudinal displacements in the bearings. Instead, longitudinal accelerations on top of the piers, where the bearings are located, can be measured using low-cost sensors.

The results achieved in Chapter 4 allowed concluding that a dynamic traffic-based monitoring system is capable of detecting structural changes that would not be easily detected by an ambient vibration or static monitoring. It also has the advantages of allowing data to be collected in a very short period of time thus reducing the influence of noise, sensor drifts and other external effects.

In Chapter 5, a novel SHM machine learning strategy for conducting unsupervised damage identification in railway bridges based on traffic induced dynamic responses, comprising time series analysis and multivariate statistics algorithms, was presented and implemented. The

developed strategy consists of fusing sets of acceleration measurements to improve sensitivity and combines different techniques: i) AR or ARX models for features extraction, ii) PCA or MLR for feature modelling, iii) Mahalanobis distance for data fusion and iv) outlier analysis or cluster analysis for feature discrimination. The signals resulting from train crossings correspond to an important mass travelling at significant speeds, thus generating features that can hide those associated with damage. The study of the performance of different combinations of techniques aimed at removing all the train-related features to expose, with high sensitivity, those generated by damage.

The effectiveness of the proposed strategy was tested using the fully validated numerical model of the bridge over the Sado River and experimental data acquired with the structural monitoring system installed on site. Dynamic numerical simulations of several structural conditions (undamaged and damaged) using only experimentally obtained actions as input, namely temperature, noise, train loadings and speeds were conducted. After a successfully validation of the methodology, it can be applied directly to experimental data from different types of bridges.

To obtain the most similar and reliable reproduction of the real SHM data, the responses obtained with the simulations were collected on the exact locations of the accelerometers installed on site. Furthermore, each simulation was polluted with different noise signals acquired on site by each accelerometer, on different days, thus ensuring the most appropriate validation of the methodology developed herein. Damage severities of 5%, 10% and 20% of stiffness reductions in the concrete slab, diaphragm and arches were simulated, as well as friction increases in the movements of the bearing devices from a reference value of 1.5% to 1.8%, 2.4%, 3.0% and the full restraint of these elements.

The damage-sensitive features were extracted by fitting AR (30) and ARX (30, 30) models to the bridge accelerations induced by train crossings in different locations along the bridge. The study of the AR/ARX parameters obtained from different structural conditions, allowed drawing conclusions about the superior influence of the EOVs when compared with damage, proving the importance of feature modelling. On the other hand, the analysis of the AR/ARX parameters from different sensors allowed concluding that the information stored for each type of damage is different. Besides, this type of time-series analysis proved capable of accurately generalizing the information present in data, while performing significant compressive fusion (thirty features in case of AR model and sixty features in case of ARX model are extracted from 2112

measurement points). A comparison between the performance obtained from AR and ARX models as feature extractors was conducted, and it was concluded that ARX models lead to increased sensitivity to damage due to their ability to capture cross information between the sensors (the input and the output). These linear models proved to be sufficiently robust to extract features from responses that result of slightly nonlinear systems, such as the train-bridge system.

To overcome the challenge of EOV events corrupting the raw data obtained in operational conditions, both MLR and PCA were implemented to study the trade-off between modelling the features using latent-variable (output-only) or regression-based (input-output) methods. Both approaches were developed using features extracted with AR models and allowed for an undeniable reduction in the effects of EOVs, although it was concluded that the features obtained with MLR enable a clearer distinction between undamaged and damaged AR-based features. The PCA was also applied to the ARX-based features and proved its importance and effectiveness in removing observable changes induced by variations in train speed or temperature without the need to measure them. It was also concluded that the EOVs can be more effectively normalized using ARX models rather than AR models.

To describe the variability present in the modelled features, a Mahalanobis distance was implemented to the thirty AR-based features and sixty ARX-based features of each sensor. This implementation allowed concluding that different sensors have greater or lesser sensitivity, depending on the location of the damage. Moreover, this step allowed corroborating the conclusion that the performance of the ARX-based features is considerably superior to the AR-based features.

To enhance sensitivity of the AR-based features, the information from all the sensors was merged and a single damage indicator for each train crossing was defined and obtained. This step proved to be crucial to achieve the highest possible level of information fusion and to obtain a clear distinction between undamaged and damaged conditions for AR-MLR-based and AR-PCA-based features. Notwithstanding, it was concluded that the damage indicator values obtained with AR-MLR-based features are more sensitive than those obtained with AR-PCA-based features.

To automatically detect the presence of damage, an outlier analysis was performed in the AR-based features using a statistical CB implemented for a significance level of 1%. The robustness and effectiveness of the developed strategy was demonstrated by automatically detecting the damage scenarios as different from those belonging to the undamaged baseline.

Using features modelled based on measured actions and structural responses (MLR-based), only one false-positive was exhibited (1% incidence), while with features modelled based on structural response measurements alone (PCA-based), only one false-negative was obtained (0.88% incidence). In view of these outcomes, it can be concluded that a strategy comprising the PCA for modelling the AR features is not only effective, but also advantageous, since it does not require the measurement of the actions.

However, further performance enhancement was achieved by implementing a cluster analysis to the ARX-based features. This step allowed to effectively separate, in a fully automated manner, the features according to the structural conditions observed on site. Moreover, since the clusters have de advantage of allowing a multidimensional representation of the features, unlike the Mahalanobis distance that is unidimensional, it was concluded that the information retained is more accurate, thus improving sensitivity to damage.

Therefore, the machine learning strategy comprising ARX models for feature extraction, PCA for feature modelling and a cluster analysis for feature discrimination proved to be the most effective and sensitive hybrid combination of techniques. An additional important conclusion obtained from this work is that, even with an SHM system not capable of measuring environmental and operational effects, it is possible to successfully detect different types of damage using the bridge's responses to train crossings. This achievement renders the strategy the ability to be less dependent on spatial actions very difficult to characterize, thus contributing for the normalization of SHM procedures. This strategy also has the advantages of minimizing the number of sensors that need to be installed and, consequently, the cost of the SHM system, as well as allowing for a more automatic and straightforward implementation.

Given the main goal of developing a fully online unsupervised damage identification methodology, Chapter 6 presented a comprehensive SHM procedure for conducting continuous real-time autonomous classification. This methodology includes the sequential implementation of ARX models, PCA transformation, and clustering algorithms to the observed data, using a moving window procedure. The machine learning strategy developed also includes an innovative approach to define an adaptive confidence boundary, which can be automatically updated to detect new damage that would progressively occur. Throughout Chapter 6 the robustness and the effectiveness of the methodology was tested.

To assess whether the online procedure was reliable for different damage scenarios, the proposed methodology was applied to the representative set of simulated structural conditions

(undamaged and damaged). This analysis allowed concluding that, for the global SHM system installed, changes as small as 5% of stiffness reduction may be detected in most damage scenarios and locations, using a simple system composed of a few sensors installed on a long-span bridge, while all the remaining severities and friction increments can be detected without false detections.

To study the trade-off between robustness and detection swiftness, a parametric analysis was conducted on the window lengths and on the number of sensors used by the SHM monitoring system. From this analysis, it was concluded that small stiffness reductions can be reliably detected with negligible false detection incidences (taken as the sum of "false alerts" and missed true detections) of 2% or less if the moving window comprises 15 or more trains. Smaller windows lead to larger false detection rates. Additionally, it was concluded that the percentage of false positives is zero with window lengths of 15 or more trains. In line with this outcome, using a different case study the window length may be set based on the number of false positives. It was also possible to conclude that the detection can be achieved once the first train crosses the bridge after the damage occurrence, which guarantees the real-time assessment.

The low percentage of false detections is accomplished considering the simple monitoring system currently installed on site. The effectiveness and performance of the proposed approach for damage identification with a smaller number of sensors was also investigated. The results allowed concluding that if the number of sensors were reduced from twenty-three to just seven, on a 480 m long bridge, the proposed methodology could be effectively used, but an increase of 5% in false detections would be observed. Nonetheless, it should be noted that the damage cases that would not be detected are only those with the lowest severity (5% of stiffness reduction).

Finally, using several train-induced responses from the bridge comprising progressively different types of damage, an original adaptive CB to detect new structural changes that may occur in a structure already damaged was developed and tested. The procedure implemented allowed concluding about the effectiveness of the adaptive CB not only in detecting new damage, but also in avoiding false damage alerts. It is worth noting that one of the great advantages of the methodology developed is the speed at which the baseline and the CB can be defined. It can be promptly established during one day for several types of trains with different loads crossing the bridge. The environmental effects can also be considered since the weather (temperature and wind) varies according to the time of day.

7.2 FUTURE DEVELOPMENTS

The work described throughout the present dissertation focuses on developing an online unsupervised methodology for the identification of damage based on train-induced dynamic responses. However, the course of this research raised several topics, issues and additional objectives that were not addressed. In this context, some topics requiring further analysis are referred in the following paragraphs:

a) Since the train-bridge system may exhibit a nonlinear behaviour, the use of an alternative non-linear feature extractor, such as the nonlinear autoregressive exogenous (NARX) neural network model, may result in a sensitivity improvement for damage identification, and is considered as a very interesting future development.

b) The most natural future development for the work conducted in the present dissertation consists in locating the damage. The potential of the ARX model was clearly proved during this dissertation, and their sensitivity to sensors located in different positions along the bridge was also demonstrated, which gives a good indication about the possible success on implementing a step for damage localization. In the sequence of the previous research recommendation, the combination of the NARX as feature extractors with the application of cluster analysis for feature discrimination can result in the ability to locate damage. The idea is to use the SHM system already installed on site and define different clusters of sensors along the bridge that will be the input and output parameters of the NARX model. As near the damage a specific cluster of sensors is, more sensitive the NARX parameters from this cluster are expected to be, and consequently, the damage indicator will also be higher for this cluster of sensors than for the remaining ones.

c) An important issue to be addressed is the definition of different alert levels. As shown in Chapter 6, the DC values tend to increase as the damage increases. In this sense, alert levels can be defined, for instance, using probabilistic methods applied to the DC values gathered over time. To choose these alert levels, additional simulations of damage scenarios with increasing severities using the digital twin of the structure can be implemented. The correspondent corrective measures and immediate actions, to take after the trigger of a certain alert, should be defined in collaboration with the bridge manager.

d) It would be interesting to apply the methodology proposed using only experimental data. In fact, as reported in Chapter 3, structural changes were found in the bearing devices of piers P2 and P3 of the bridge over the Sado River. However, in that moment, only the static monitoring system was installed, so the data acquired could not be used to apply the methodology. The structural changes observed in the bearing devices may, over time, induce changes in the structural behaviour of the bridge, which are expected to be detected with the developed methodology for additional validation of its effectiveness, robustness and sensitivity.

e) During the work presented in this thesis the focus was always to develop a robust and generic unsupervised methodology to detect damages based on traffic induced responses in order to give significant contribution for the transition of SHM from academia to industry. Even though the developed methodology analysed several damage scenarios, in different locations and with different severities, was limited to a single case study. It would be interesting to investigate how the proposed procedure behave when applied to a different structure.

f) A further validation of the applicability of the methodology, to demonstrate their versatility and confirm their robustness and efficiency, would be to exploit the detection of completely different types of damages, such as wheel defects, using sensors installed on the rail track.

g) The implementation of the methodology to detect damages in railway bridges based on responses measured by sensors installed on the train is another interesting and ambitious future development. The ability of detecting damages based on the responses of the train would have the tremendous advantage of monitoring daily several structures using a single sensors' network.

h) Civil structures tend to be one-of-a-kind, large capital assets, that are generally kept in good condition by the managers with appropriate inspection and maintenance actions. As such, bridge data acquired under damaged conditions is generally scarce. Therefore, the effectiveness of the methodologies such as the one implemented herein tend to be validated using digital twins, with a reliable description of the structure's stiffness, mass, and boundary conditions, as well as its response to environmental and operational actions. In this sense, it is important to evolve towards the development of digital twins for different types of railway bridges.

REFERENCES

A

Akesson, B. (2008). *Understanding Bridge Collapses* (1st ed.). London, UK: Taylor & Francis.

Albuquerque, C., Silva, A. L. L., Jesus, A. M. P. De, & Calçada, R. (2015). An efficient methodology for fatigue damage assessment of bridge details using modal superposition of stress intensity factors. *International Journal of Fatigue*, *81*, 61–77. https://doi.org/10.1016/j.ijfatigue.2015.07.002

Alvandi, A., & Cremona, C. (2006). Assessment of vibration-based damage identification techniques. *Journal of Sound and Vibration*, *292*, 179–202. https://doi.org/10.1016/j.jsv.2005.07.036

Alves, V., Meixedo, A., Ribeiro, D., Calçada, R., & Cury, A. (2015). Evaluation of the performance of different damage indicators in railway bridges. *Procedia Engineering*, *114*, 746–753. https://doi.org/10.1016/j.proeng.2015.08.020

ANSYS. (2016). Academic Research. Release 17.1. Canonsburg, PA, USA: ANSYS Inc.

Appleton, J. (2005). *Inspecção e reabilitação de pontes*. Instituto Superior Técnico, Lisbon, Portugal.

Armando Rito Engenharia. (2016). http://www.arito.com.pt/.

Azim, R., & Gül, M. (2019). Damage detection of steel girder railway bridges utilizing operational vibration response. *Structural Control and Health Monitoring*, (August), 1–15. https://doi.org/10.1002/stc.2447

B

Barthorpe, R. (2011). *On model- and data-based approaches to structural health monitoring*. PhD Thesis, Department of Mechanical Engineering, University of Sheffield.

Bedworth, M., & O'Brien, J. (1991). The Omnibus Model: A New Model of Data Fusion. Malvern, UK: Defence Evaluation and Research Agency.

Bishop, C. (1995). *Neural Networks for Pattern Recognition*. Oxford, UK: Oxford University Press.

Box, G., & Jenkins, G. (1976). *Time Series Analysis: Forecasting and Control*. Englewood Cliffs, NJ: Prentice Hall.

C

Calçada, R. A. B. (2001). *Avaliação Experimental e Numérica de Efeitos Dinâmicos de Cargas de Tráfego em Pontes Rodoviárias*. University of Porto, Faculty of Engineering. [Portuguese]

Cantero, D., & González, A. (2015). Bridge Damage Detection Using Weigh-in-Motion Technology. *Journal of Bridge Engineering*, *20*(5), 04014078–1 to 04014078–10. https://doi.org/10.1061/(ASCE)BE.1943-5592.0000674

Carey, C. H., O'Brien, E. J., & Keenahan, J. (2013). Investigating the Use of Moving Force Identification Theory in Bridge Damage Detection. *Key Engineering Materials*, *569–570*(January 2016), 215–222. https://doi.org/10.4028/www.scientific.net/KEM.569-570.215

Cavadas, F. (2008). *Comportamento de pontes metálicas antigas – A ponte Eiffel*. Master Thesis, FEUP, Porto, Portugal.

Cavadas, F., Smith, I. F. C., & Figueiras, J. (2013). Damage detection using data-driven methods

applied to moving-load responses. *Mechanical Systems and Signal Processing*, *39*(1–2), 409–425. https://doi.org/10.1016/j.ymssp.2013.02.019

Colombo, L., Sbarufatti, C., & Giglio, M. (2019). Definition of a load adaptive baseline by inverse finite element method for structural damage identification. *Mechanical Systems and Signal Processing*, *120*, 584–607. https://doi.org/10.1016/j.ymssp.2018.10.041

Cury, A. (2010). *Téchniques D'Anormalité Appliquées a la Surveillance de Santé Structurale*. Université Paris-Est.

Cury, A., & Cremona, C. (2010). Novelty detection based on symbolic data analysis applied to structural health monitoring. *Bridge Maintenance, Safety and Management - IABMAS'10*, 172–182.

Cury, A., & Cremona, C. (2012). Assignment of structural behaviours in long-term monitoring : Application to a strengthened railway bridge. *Structural Health Monitoring*, *11*(4), 422–441. https://doi.org/10.1177/1475921711434858

Cury, A., Cremona, C., & Dumoulin, J. (2012). Long-term monitoring of a PSC box girder bridge: Operational modal analysis, data normalization and structural modification assessment. *Mechanical Systems and Signal Processing*, *33*, 13–37. https://doi.org/10.1016/j.ymssp.2012.07.005

D

Datteo, A., Busca, G., Quattromani, G., & Cigada, A. (2018). On the use of AR models for SHM: A global sensitivity and uncertainty analysis framework. *Reliability Engineering and System Safety*, *170*, 99–115. https://doi.org/10.1016/j.ress.2017.10.017

Doebling, S. W., Farrar, C. R., Prime, M. B., & Shevitz, D. W. (1996). *Damage Identification and Health Monitoring of Structural and Mechanical Systems from Changes in Their Vibration Characteristics: A Literature Review*. Report: LA.

E

EN 13674-1:2003. (2007). *Railway applications — Track — Rail* (Vol. 3).

Entezami, A., & Shariatmadar, H. (2017). An unsupervised learning approach by novel damage indices in structural health monitoring for damage localization and quantification. *Structural Health Monitoring*, *I–21*. https://doi.org/10.1177/1475921717693572

Entezami, A., Shariatmadar, H., & Mariani, S. (2019). Fast unsupervised learning methods for structural health monitoring with large vibration data from dense sensor networks. *Structural Health Monitoring*, *I–26*. https://doi.org/10.1177/1475921719894186

ERRI D 202/RP 11. (1999). *Improved knowledge of forces in CWR track (including switches): Parametric study and sensivity analysis of CWERRI*. Utrecht: European Rail Research Institute.

F

Farrar, C. R. & James, G. H. (1997). System identification from ambient vibration measurements on a bridge. *Journal of Sound and Vibration*, *205*(1), 1–18. https://doi.org/10.1006/jsvi.1997.0977

Farrar, C., & Worden, K. (2013). *Structural Health Monitoring: a machine learning perspective*. Wiley.

Farrar, C., Doebling, S. W., & Nix, D. A. (2001). Vibration-based structural damage identification. *Philosophical Transactions of the Royal Society A: Mathematical, Physical and Engineering Sciences*, *359*(1778), 131–149. https://doi.org/10.1098/rsta.2000.0717

Farrar, C., Sohn, H., & Worden, K. (2001). Data Normalization : A Key For Structural Health Monitoring. *Technical Report, Los Alamos National Laboratory*, *836*(LA-UR-01-4).

Farrar, C., & Worden, K. (2013). *Structural Health Monitoring: a machine learning perspective*. Wiley.

Farrar, C., Doebling, S. W., & Nix, D. (2001). Vibration–based structural damage identification. *Philosophical Transactions of the Royal Society of London A: Mathematical, Physical and Engineering Sciences*, *359*(1778), 131–149. https://doi.org/10.1098/rsta.2000.0717

Farrar, C., & Worden, K. (2007). An introduction to structural health monitoring. *Philosophical Transactions of the Royal Society A: Mathematical, Physical and Engineering Sciences*,

365(1851), 303–315. https://doi.org/10.1098/rsta.2006.1928

Figueiredo, E, Moldovan, I., & Barata Marques, M. (2013). *Condition Assessment of Bridges : Past , Present and Future A Complementary Approach*.

Figueiredo, E., Park, G., Farrar, C. R., Worden, K., & Figueiras, J. (2010). Machine learning algorithms for damage detection under operational and environmental variability. *Structural Health Monitoring*, *10(6)*, 559–572. https://doi.org/10.1177/1475921710388971

Figueiredo, Elói. (2010). *Damage Identification in Civil Engineering Infrastructure under Operational and Environmental Conditions*. Faculty of Engineering of the University of Porto [Portuguese].

Friswell, M. I. (2008). *Damage identification using inverse methods, in Dynamic Methods for Damage Detection in Structures*. New York: Springer Wien.

Fujino, Y., & Siringoringo, D. M. (2008). Structural health monitoring of bridges in Japan : an overview of the current trend. *Fourth International Conference on FRP Composites in Civil Engineering (CICE2008)*, 22–24.

G

Glaser, S. D., & Tolman, A. (2008). Sense of Sensing: From Data to Informed Decisions for the Built Environment. *Journal of Infrastructure Systems*, *14*(1), 4–14. https://doi.org/10.1061/(ASCE)1076-0342(2008)14:1(4)

Gonzalez, I., & Karoumi, R. (2015). BWIM aided damage detection in bridges using machine learning. *Journal of Civil Structural Health Monitoring*, *5*(5), 715–725. https://doi.org/10.1007/s13349-015-0137-4

GRID, GREISH, BEG, & FERBRITAS. (2006). Variante de Alcácer: Projecto de Execução do travessamento do Rio Sado. REFER.

H

Härdle, W. K., & Simar, L. (2015). *Applied Multivariate Statistical Analysis* (4th ed.). Springer.

Hastie, T., Tibshirani, R., & Friedman, J. (2011). *The Elements of Statistical Learning, Data Miningm Inference, and Prediction* (2nd ed.). Stanford, USA: Springer.

Hu, W. H., Moutinho, C., Caetano, E., Magalhes, F., & Cunha, L. (2012). Continuous dynamic monitoring of a lively footbridge for serviceability assessment and damage detection. *Mechanical Systems and Signal Processing*, *33*, 38–55. https://doi.org/10.1016/j.ymssp.2012.05.012

Huang, Q., Gardoni, P., & Hurlebaus, S. (2012). A probabilistic damage detection approach using vibration-based nondestructive testing. *Structural Safety*, *38*, 11–21. https://doi.org/10.1016/j.strusafe.2012.01.004

J

Johnson, R. A., & Wichern, D. W. (2013). *Applied Multivariate Statistical Analysis* (6th ed.). Harlow: Pearson.

Jolliffe, I. T. (2002). *Principal Component Analysis* (2nd ed.). New York: Springer.

K

Khan., A. Mohiuddin (2010). *Bridge and Highway. Structure Rehabilitation and Repair* (1st ed.). New York, USA: McGraw-Hill.

Kong, X., Cai, C. S., & Kong, B. (2015). Damage Detection Based on Transmissibility of a Vehicle and Bridge Coupled System. *Journal of Engineering Mechanics*, *141*, 1–17. https://doi.org/10.1061/(ASCE)EM.1943-7889.0000821.

L

Lautour, O. R. De, & Omenzetter, P. (2010). Damage classification and estimation in experimental structures using time series analysis and pattern recognition. *Mechanical Systems and Signal Processing*, *24*, 1556–1569. https://doi.org/10.1016/j.ymssp.2009.12.008

Li, H., Li, S., Ou, J., & Li, H. (2010). Modal identification of bridges under varying

environmental conditions : Temperature and wind effects. *Structural Control and Health Monitoring*, (17), 495–512. https://doi.org/10.1002/stc

M

Magalhães, F., Cunha, A., & Caetano, E. (2011). Vibration based structural health monitoring of an arch bridge : From automated OMA to damage detection. *Mechanical Systems and Signal Processing Journal*. https://doi.org/10.1016/j.ymssp.2011.06.011

Magalhães, F., Cunha, A., & Caetano, E. (2012). Vibration based structural health monitoring of an arch bridge : From automated OMA to damage detection. *Mechanical Systems and Signal Processing*, *28*, 212–228. https://doi.org/10.1016/j.ymssp.2011.06.011

Marian Ralbovsky, Santos, J. P., Kwapisz, M., Dallinger, S., & Catarino, J. (2014). Damage detection based on structural response to Temperature changes and model updating. In *EWSHM - European Workshop of Structural Health Monitoring* (pp. 427–434). Nantes, France.

Meixedo, A, Ribeiro, D., Calçada, R., & Delgado, R. (2014). Global and Local Dynamic Effects on a Railway Viaduct with Precast Deck. In *Civil-Comp Proceedings of the Second International Conference on Railway Technology: Research, Development and Maintenance* (pp. 1–13).

Meixedo, A, Alves, V., Ribeiro, D., & Calçada, R. (2016). Selection of Sensitive Features for Damage Identification in a Railway Bridge. In *Selection of Sensitive Features for Damage Identification in a Railway Bridge* (pp. 1–15).

Meixedo, A., Alves, V., Ribeiro, D., Cury, A., & Calçada, R. (2016). Damage identification of a railway bridge based on genetic algorithms. In *Maintenance, Monitoring, Safety, Risk and Resilience of Bridges and Bridge Networks - Proceedings of the 8th International Conference on Bridge Maintenance, Safety and Management, IABMAS 2016* (pp. 998–1005). Foz do Iguaçu; Brazil.

Meixedo, A., Ribeiro, D., Santos, J., & Calçada, R. (2019). Assessment of the dynamic behavior of the railway bridge over the Sado River based on a monitoring system. In *Proceedings of the 7th International Conference on Structural Engineering, Mechanics and Computation* (pp. 1805–1809). Cape Town, South Africa. https://doi.org/10.1201/9780429426506-311

Meruane, V., & Heylen, W. (2011). Structural damage assessment under varying temperature conditions, *11*(3), 345–357. https://doi.org/10.1177/1475921711419995

Mijar, A. R., & Arora, J. S. (2000). Review of formulations for elastostatic frictional contact problems. *Structural and Multidisciplinary Optimization*, *20*(3), 167–189.

Min, X., & Santos, L. (2011). *Ensaios dinâmicos da ponte ferroviária sobre o rio sado na variante de alcácer*. Lisboa [Portuguese].

N

National Transportation Safety Board. (2008). *Collapse of I-35W Highway Bridge*. Minneapolis, Minnesota.

Neves, A C, González, I., Leander, J., & Karoumi, R. (2017). Structural health monitoring of bridges : a model-free ANN-based approach to damage detection. *Journal of Civil Structural Health Monitoring*, (7), 689–702. https://doi.org/10.1007/s13349-017-0252-5

Neves, Ana C, GonzaLez, I., Karoumi, R., & Leander, J. (2020). The influence of frequency content on the performance of artificial neural network – based damage detection systems tested on numerical and experimental bridge data. *Structural Health Monitoring*, *I–17*. https://doi.org/10.1177/1475921720924320

Ni, Y. Q., Zhou, H. F., & Ko, J. M. (2009). Generalization Capability of Neural Network Models for Temperature-Frequency Correlation Using Monitoring Data. *Journal of Structural Engineering*, *135*(10), 1290–1300.

Nie, Z., Guo, E., Li, J., Hao, H., Ma, H., & Jiang, H. (2020). Bridge condition monitoring using fixed moving principal component analysis. *Structural Control and Health Monitoring*, (February), 1–29. https://doi.org/10.1002/stc.2535

P

Paixão, A., Fortunato, E., & Calçada, R. (2014). Transition zones to railway bridges: Track measurements and numerical modelling. *Engineering Structures*, *80*, 435–443. https://doi.org/10.1016/j.engstruct.2014.09.024

Park, G., Overly, T. G., & Farinholt, K. M. (2008). Experimental investigation of wireless active-sensor nodes using impedance-based structural health monitoring. In *Proceedings of 15th SPIE Conference on Smart Structures and Non-destructive Evaluation*. San Diego, CA, SPIE.

Peeters, B., & Roeck, G. de. (2001). One-year monitoring of the Z24 Bridge environmental effects versus damage events. *Earthquake Engineering and Structure Dynamics*, *30*(2), 149–171.

Pimentel, R., Barbosa, M., Costa, N., Ribeiro, D., Ferreira, L., Araújo, F., & Calçada, R. (2008). Hybrid Fiber-Optic / Electrical Measurement System for Characterization of Railway Traffic and Its Effects on a Short Span Bridge. *IEEE SENSORS JOURNAL*, *8*(7), 1243–1249. https://doi.org/10.1109/JSEN.2008.926519

Posenato, D., Kripakaran, P., & Smith, I. F. C. (2010). Methodologies for model-free data interpretation of civil engineering structures. *Computers & Structures*, *88(7-8)*, 467–482. https://doi.org/10.1016/j.compstruc.2010.01.001

Posenato, Daniele, Lanata, F., Inaudi, D., & Smith, I. F. C. (2008). Model-free data interpretation for continuous monitoring of complex structures. *Advanced Engineering Informatics 22*, *22*, 135–144. https://doi.org/10.1016/j.aei.2007.02.002

R

REFER. (2010). Variante de Alcácer. Lisboa: REFER.

Rendón, E., Abundez, I., Arizmendi, A., & Quiroz, E. M. (2011). Internal versus External cluster validation indexes. *International Journal of Computers and Communications*, *5*(1).

Ribeiro, D., Calçada, R., Delgado, R., Brehm, M., & Zabel, V. (2012). Finite element model updating of a bowstring-arch railway bridge based on experimental modal parameters. *Engineering Structures*, *40*, 413–435. https://doi.org/10.1016/j.engstruct.2012.03.013

Ribeiro, D., Calçada, R., Delgado, R., Brehm, M., & Zabel, V. (2013). Finite-element model calibration of a railway vehicle based on experimental modal parameters. Vehicle System Dynamics, Taylor & Francis, 51(6), 821–856. https://doi.org/10.1080/00423114.2013.778416

Ribeiro, D., Leite, J., Meixedo, A., Pinto, N., Calçada, R., & Todd, M. (2021). Statistical

methodologies for removing the operational effects from the dynamic responses of a high-rise telecommunications tower. *Structural Control and Health Monitoring*. https://doi.org/10.1002/stc.2700

Rytter, A. (1993). *Vibrational Based Inspection of Civil Engineering Structures*. Aalborg: Dept. of Building Technology and Structural Engineering, Aalborg University.

S

Santos, J. (2014). *Smart Structural Health Monitoring Techniques for Novelty Identification in Civil Engineering Structures*. PhD Thesis. Instituto Superior Técnico - University of Lisbon.

Santos, J. P., Crémona, C., Calado, L., Silveira, P., & Orcesi, A. D. (2015). On-line unsupervised detection of early damage. *Structural Control and Health Monitoring*. https://doi.org/10.1002/stc

Santos, J., Crémona, C., & Calado, L. (2016). Real-time damage detection based on pattern recognition. *Structural Concrete 17*, *17*(3), 338–354. https://doi.org/10.1002/suco.201500092

Santos, João Pedro, Crémona, C., Orcesi, A. D., & Silveira, P. (2013). Multivariate statistical analysis for early damage detection. *Engineering Structures*, *56*, 273–285. https://doi.org/10.1016/j.engstruct.2013.05.022

Silva, R. D. (2016). http://expresso.sapo.pt/sociedade/2016-03-04-Entre-os-Rios-15-anos-nao-e-tempo-suficiente.

Silva, S., Júnior, M., Junior, V., & J.Brennan, M. (2008). Structural damage detection by fuzzy clustering. *Mechanical Systems and Signal Processing*, *22*(7), 1636–1649.

Sohn, H. (2007). Effects of environmental and operational variability on structural health monitoring. *Philosophical Transactions. Series A, Mathematical, Physical, and Engineering Sciences*, *365*(1851), 539–560. https://doi.org/10.1098/rsta.2006.1935

Sohn, H., & Law, K. H. (2000). Bayesian probabilistic damage detection of a reinforced-concrete bridge column. *Earthquake Engineering and Structure Dynamics*, *29*(June 1998), 1131–1152.

Sohn, H., Czarnecki, C. R. F. F. M. H., Shunk, D. D., Stinemates, D. W., Nadler, B. R., & Czarnecki, J. J. (2004). *A Review of Structural Health Monitoring Literature : 1996 – 2001*.

Structural Health Monitoring. Los Alamos (USA).

Sohn, H., Worden, K., & Farrar, C. R. (2002). Statistical Damage Classification Under Changing Environmental and Operational Conditions. *Journal of Intelligent Material Systems and Structures*, *13*, 561–574. https://doi.org/10.1106/104538902030904

SVS. (2005). ARTeMIS Extractor Handy. *Denmark: Structural Vibration Solution*, (Release 3.5).

T

Theodoridis, S. Koutroumbas, K. (2009). *Pattern Recognition* (4th ed.). London, UK: Elsevier.

Tomé, E., Pimentel, M., & Figueiras, J. (2020). Damage detection under environmental and operational effects using cointegration analysis – Application to experimental data from a cable-stayed bridge. *Mechanical Systems and Signal Processing*, *135*, 4–8.

U

UIC 774-3-R. (2001). *Track/bridge interaction - Recommendations for calculation*. (International Union of Railways (UIC), Ed.) (2nd ed.). Paris.

UIC 861-3 (E). (1969). *Standard 60 Kg/m Rail Profiles - Types UIC 60 and 60E* (3rd ed.).

W

Wardhana, K., Hadipriono, F. C., & Asce, F. (2003). Analysis of Recent Bridge Failures in the United States. *Journal of Performance of Constructed Facilities*, *17*(3), 144–150.

Wenzel, H. (2009). *Health Monitoring of Bridges*. Wiley.

White, F. E. J. (1990). Joint Directors of Laboratories Data Fusion Subpanel Report: SIGINT Session. In *Technical Proceedings of the Joint Service Data Fusion Symposium* (pp. 469–484).

Worden, K, & Dulieu-Barton, J. M. (2004). An Overview of Intelligent Fault Detection in Systems and Structures. *International Journal of Structural Health Monitoring*, *3*(1), 85–98.

Worden, K., Sohn, H., & Farrar, C. R. (2002). Novelty detection in a changing environment: regression and interpolation approaches. *Journal of Sound and Vibration*, *258*(4), 741–761. https://doi.org/10.1006/jsvi.2002.5148

Worden, Keith, Staszewski, W. J., & Hensman, J. J. (2011). Natural computing for mechanical systems research : A tutorial overview. *Mechanical Systems and Signal Processing*, *25*, 4–111. https://doi.org/10.1016/j.ymssp.2010.07.013

WordPress. (2016). https://comesatime.wordpress.com/category/i-35w/.

Wu, Y. S., & Yang, Y. Bin. (2003). Steady-state response and riding comfort of trains moving over a series of simply supported bridges. *Engineering Structures*, *25*(2), 251–265. https://doi.org/10.1016/S0141-0296(02)00147-5

Y

Yan, A., Kerschen, G., Boe, P. De, & Golinval, J. (2005a). Structural damage diagnosis under varying environmental conditions — Part I : A linear analysis. *Mechanical Systems and Signal Processing*, *19*, 847–864. https://doi.org/10.1016/j.ymssp.2004.12.002

Yan, A., Kerschen, G., Boe, P. De, & Golinval, J. (2005b). Structural damage diagnosis under varying environmental conditions — part II : local PCA for non-linear cases. *Mechanical Systems and Signal Processing*, *19*, 865–880. https://doi.org/10.1016/j.ymssp.2004.12.003

Yeager, M., Gregory, B., Key, C., & Todd, M. (2019). On using robust Mahalanobis distance estimations for feature discrimination in a damage detection scenario. *Structural Health Monitoring*, *18*(1), 245–253. https://doi.org/10.1177/1475921717748878

Z

Zennaro, L. (2019). https://www.theguardian.com/cities/2019/feb/26/what-caused-the-genoa-morandi-bridge-collapse-and-the-end-of-an-italian-national-myth.

Zhai, W., Wang, K., & Cai, C. (2009). Fundamentals of vehicle-track coupled dynamics. Vehicle System Dynamics, 47(11), 1349–1376. https://doi.org/10.1080/00423110802621561

Zhang, W., Li, J., Hao, H., & Ma, H. (2017). Damage detection in bridge structures under moving loads with phase trajectory change of multi-type vibration measurements. *Mechanical Systems and Signal Processing*, *87* (November 2016), 410–425. https://doi.org/10.1016/j.ymssp.2016.10.035

Zhou, H. F., Ni, Y. Q., & Ko, J. M. (2010). Constructing input to neural networks for modeling temperature-caused modal variability : Mean temperatures , effective temperatures , and principal components of temperatures. *Engineering Structures*, *32*(6), 1747–1759. https://doi.org/10.1016/j.engstruct.2010.02.026